The Development of a Simulation Technique for the Analysis of Helicopter Offshore Operations

by

Christopher Taylor, B. Eng.

Dissertation Submitted to the Faculty of Engineering, University of Glasgow, for the Degree of Doctor of Philosophy.

ProQuest LLC.
789 East Eisenhower Parkway
P.O. Box 1346
Ann Arbor, MI 48106 – 1346

Contents

Figures

Acknowledgements

The author wishes to express sincere gratitude to the following individuals: Dr. Douglas Thomson and Professor Roy Bradley for their considerable guidance and encouragement whilst supervising this project.

Thanks are also extended to Mr. Nigel Talbot and Mr. Robin Ablett for their support and enthusiasm during the course of the research programme and Mrs Christine Taylor who proof read this manuscript.

This work has been funded by a Civil Aviation Authority Airworthy Requirements Board Fellowship.

Abstract

The helicopter has been accepted as being the only form of transport that can serve reliably and rapidly the routine operational needs of oilrig platforms. The role of unmanned simulation studies in this field is important, since it can provide a positive and immediate contribution towards the safety issues associated with helicopter operations in this environment. Previous theoretical simulation studies have been of limited scope due to the lack of emphasis placed on pilot strategy and the simplified rotorcraft models employed. In this research programme, a conceptually novel simulation technique (HIFIS) that includes the ability to model pilot reaction time has been developed.

A helicopter operating in the proximity of an oil rig is often required to fly in flight regimes that are unique to the offshore environment. As a result, the helicopter mathematical model employed must be able to accurately replicate these conditions if the correct aircraft behaviour is to be portrayed. Consequently much research effort has been attributed to the rotorcraft model employed to ensure that it did not impose any limitations on the investigative programme.

In this research programme, knowledge of the manoeuvres performed in the offshore environment has been provided mostly in terms of a narrative description of the corresponding pilot strategy. For this investigation, a mathematical model of the manoeuvre trajectory is required to drive the HIFIS simulation algorithm. In order to formulate such models, a generic method that transforms the narrative of the pilot strategy into validated expressions of the aircraft trajectory has been developed.

One of the most significant aspects of helicopter offshore operations is the possibility of an engine failure in the proximity of the oilrig platform. The task of directly simulating such a failure is difficult as the original manoeuvre as intended by the pilot may be unflyable due to the limited power available. In order to portray this feature, a specialised simulation technique has been developed that allows the pilot strategy in response to a failure to be accurately determined.

The HIFIS simulation technique has been demonstrated by its application to the investigation of rotorcraft safety related topics during takeoff of landing manoeuvres. During the course of this investigation, the ability of the rotorcraft to perform a manoeuvre has been explored in terms of the key parameters that would be available to a pilot in practice.

Nomenclature

List of Symbols

a	peak gust intensity	(m/s)
a_0	blade lift curve slope	(1/rad)
$a_{x_{bl}}$, $a_{y_{bl}}$, $a_{z_{bl}}$	components of rotor blade translational acceleration	(m/s^2)
a_x, a_y, a_z	components of body axes translational acceleration	(m/s^2)
b	number of rotor blades	
c	rotor blade chord	(m)
C_L	rotor aerodynamic rolling coefficient	
C_{Lw}	rotor aerodynamic rolling coefficient in wind - hub axes	
C_M	rotor aerodynamic pitching coefficient	
C_{Mw}	rotor aerodynamic pitching coefficient in wind - hub axes	
C_T	main rotor thrust coefficient	
C_{Tw}	main rotor thrust coefficient in wind - hub axes	
d	drag per unit span of blade	(N/m)
e	length of main rotor root cut out as fraction of total span	
f	frequency of gust stream	(H_z)
F	fraction of new gusts with zero intensity	
g	acceleration due to gravity	(m/s^2)
g_{c0}, g_{c1}	collective channel gearing constants	(rad)
g_{ls0}, g_{ls1}, g_{sc0}, g_{sc1}	longitudinal channel gearing constants	(rad)
g_{ct0}, g_{t0}, g_{t1}	pedal channel gearing constants	(rad)
g_{lc0}, g_{lc1},	lateral channel gearing constants	(rad)
G_{TR}	ratio of main to tail rotor angular velocity	
I_{TR}	main rotor and transmission moment of inertia	(kg m^2)
I_{xx}, I_{yy}, I_{zz}	helicopter moments of inertia	(kg m^2)
I_{xz}	helicopter product of inertia about centre of gravity	(kg m^2)
k_g	normal accelerometer feedback gain	(rad)
k_θ, k_ϕ, k_ψ	proportional pitch attitude feedback gain	
k_p, k_q, k_r	derivative action feedback gain	(s)
k_{1c}, k_{1s}	stick feed forward gain	(rad)
k	upper vortex ring boundary constant	
K	vortex ring model scaling constant	
K_{e1}	gain associated with changes in rotor speed	(kg/rad)
K_{e2}	gain associated with changes in engine torque	(Nms/kg)

K_3	overall engine governor gain (= K_{e1} K_{e2})	(Nm/rad/s)
l	lift per unit span of blade	(N/m)
l_{Fin}	distance of fin behind rotor hub	(m)
l_{TP}	distance of tailplane behind rotor hub	(m)
l_{TR}	distance of tail rotor behind main rotor hub	(m)
L, M, N	components of external moments on helicopter	(Nm)
l_1, ..., n_3	direction cosines for Euler transformation	
$\underline{\mathbf{L}}_{nl}$	nonlinear inflow gain matrix	
m	mass of helicopter	(kg)
m	integer intervals of simulation frame time (= T/τ)	
m_b	mass of rotor blade	(kg)
m_0	blade mass per unit length	(kg/m)
M_β	blade mass distribution	(kg m)
$\underline{\mathbf{M}}$	apparent mass matrix	
N_r	rotor speed	(%)
n_β	blade inertia number	
p, q, r	vehicle rotational velocities about centre of gravity	(rad/s)
p_H, q_H, r_H	rotor hub angular velocities about hub axes	(rad/s)
p(x)	probability density function	
P(x)	probability function	
Q_E	engine torque ouput	(Nm)
$Q_{E_{IDLE}}$	engine torque output at idle (= 0)	(Nm)
$Q_{E_{LIM}}$	limiting engine torque output (= $\frac{1}{2}$ $Q_{E_{MAX}}$)	(Nm)
$Q_{E_{MAX}}$	maximum engine torque output	(Nm)
Q_R	rotor torque	(Nm)
Q_{TR}	tail rotor torque	(Nm)
R	rotor radius	(m)
R_{TR}	tail rotor radius	(m)
r_b	blade element radius	(m)
s	rotor solidity	
S_{Fin}	fin area	(m^2)
S_{TP}	tailplane area	(m^2)
s_{TR}	tail rotor solidity	
T	gust rise time	(s)
$\underline{\mathbf{T}}_{hub_w}$	transformation matrix from hub to wind axes	
u, v, w	vehicle translational velocities referred to body axis	(m/s)
u_H, v_H, w_H	rotor hub velocity components	(m/s)
U_T, U_P	tangential and normal components of airflow at blade	(m/s)

	element	
$\bar{U}_T$, $\bar{U}_P$	non-dimensionalised tangential and normal components of airflow at blade element	
v_{1sw}, v_{1cw}	harmonic components of induced velocity in wind axes	(m/s)
v_i	rotor induced velocity	(m/s)
V_f	flight path velocity	(m/s)
v_{xbl}, v_{ybl}, v_{zbl}	components of velocity of a main rotor blade element	(m/s)
V	velocity	(m/s)
$V_{core_{des}}$	descent velocity of vortex cores	(m/s)
V_{crit}	critical descent velocity of vortex core	(m/s)
V_M	nondimensionalised weighted velocity component	
V_T	resultant nondimensionalised velocity through rotor disc	
$\underline{V}$	mass flow parameter matrix	
w_f	fuel flow rate	(kg/s)
w_f^*	scaled fuel flow rate	(rad/s)
$w_{f_{IDLE}}$	fuel flow rate at flight idle	(kg/s)
X, Y, Z	components of external forces of helicopter	(N)
x_{cg}	position of centre of gravity behind rotor hub	(m)

Greek Symbols

α_{bl}	angle of incidence of blade element	(rad)
α_{tp}	angle of incidence of tailplane	(rad)
β	blade flap angle	(rad)
β_0	rotor coning angle	(rad)
β_{1c}, β_{1s}	rotor longitudinal and lateral flapping	(rad)
β_{Fin}	fixed sideslip angle of fin	(rad)
β_{Fus}	fuselage sideslip angle	(rad)
χ	rotor wake angle	(rad)
δ	blade profile drag coefficient	
$\bar{\delta}$	nondimensionalised residual velocity	
ϕ	blade inflow angle	(rad)
ϕ	power spectral density	$((m/s)^2/cycle/m)$
γ	rotor droop factor	
γ_s	rotor shaft inclination	(rad)
η_{1c}	lateral cyclic stick position	
η_{1s}	longitudinal cyclic stick position	
η_c	pilot collective lever position	

η_{ct}	cable length	
η_p	pedal position	
$\lambda_0, \lambda_{1c}, \lambda_{1s}$	main rotor inflow components	
$\lambda_{1cw}, \lambda_{1sw}$	harmonic inflow components in wind - hub axes	
λ_β	main rotor flap frequency ratio	
λ_m	mean nondimensionalised flow through rotor	
μ	normalised in plane rotor hub velocity	
μ_x, μ_y, μ_z	normalised rotor hub velocity components	
θ	blade pitch angle	(rad)
θ, ϕ, ψ	fuselage pitch, roll and yaw angles	(rad)
θ_0	main rotor blade collective angle	(rad)
$\theta_{0_a}, \theta_{0tr_a}$	autostab contribution to main and tailrotor collective pitch angles	(rad)
$\theta_{0_p}, \theta_{0tr_p}$	pilot contribution to main and tailrotor collective angles	(rad)
θ_{0tr}	tailrotor blade collective pitch angle	(rad)
θ_{1c}	main rotor blade lateral cyclic pitch angle	(rad)
θ_{1s}	main rotor blade longitudinal cyclic pitch angle	(rad)
$\theta_{1s_a}, \theta_{1c_a}$	autostab contribution to cyclic pitch	(rad)
$\theta_{1s_p}, \theta_{1c_p}$	pilot contribution to cyclic pitch	(rad)
θ_{tw}	main rotor blade twist slope	(rad/m)
θ_{twtr}	tailrotor blade twist slope	(rad/m)
ρ	local air density	(kg/m^3)
τ	simulation frame time	(s)
τ_{c1}, τ_{c2}, τ_{c3}, τ_{c4}	time constants associated with flight control actuators	(s)
$\tau_{e1}, \tau_{e2}, \tau_{e3}$	engine governor and rotor speed time constants	(s)
Ω	angular velocity of main rotor	(rad/s)
Ω_{IDLE}	rotor angular velocity at idle	(rad/s)
Ω_{TR}	tailrotor angular velocity	(rad/s)
ψ	blade azimuthal position	(rad)
ψ_{TR}	tail rotor azimuthal position	(rad)
ψ_w	rotor sideslip angle	(rad)

Acronyms

AEO	All Engines Operating
ARB	Airworthiness Requirements Board
BCAR	British Civil Aviation Requirements

BLSS	Baulked Landing Safety Speed
CAA	Civil Aviation Authority
CTO	Continued Takeoff
FAA	Federal Aviation Authority
FAR	Federal Aviation Requirements
GAR	Civil Aviation Standard of Former Soviet Union
HARP	Helicopter Airworthiness Review Panel
HGS	Helicopter Generic Simulation
ICV	Inter-Component Volume
JAR	Joint Aviation Requirements
LDP	Landing Decision Point
MTE	Mission Task Element
OEI	One Engine Inoperative
PSD	Power Spectral density
RAE	Royal Aircraft Establishement
RTO	Rejected Takeoff
SAS	Stability Augmentation System
SDG	Statistical Discrete Gust
TDP	Takeoff Decision Point
TOSS	Takeoff Safety Speed
WAT	Weight and Temperature

Subscripts

b	body fixed axes set
bl	blade axes set
BLSS	baulked landing safety speed
C	centre of gravity
e	Earth fixed axes
FLR	flare
Fus	fuselage
h	main rotor hub fixed axes set
H	main rotor hub
I	inertial
I, M	individual or multi-blade representation of blade flapping
LDP	landing decision point
P	general point on blade
R	main rotor
s	shaft axes set

TDP	takeoff decision point
TP	tail plane
TR	tailrotor
trbl	tailrotor blade
trh	axes fixed in tailrotor hub
TRH	tailrotor hub
w	hub wind axes set

Note: Vector quantities are written in bold.
Matrix quantities are written in bold and are underscored.

Sign Conventions

Fuselage Attitude

Pitch	+ve	nose up
Roll	+ve	bank to right
Yaw	+ve	yaw to right

Control Deflections

Collective Lever	+ve	up	scale, 0 - 100%
Longitudinal Cyclic	+ve	forward	scale, 0 - 100%
Lateral Cyclic	+ve	stick right	scale, 0 - 100%
Pedal	+ve	right pedal forward	scale, 0 - 100%

Chapter 1

Introduction

The aim of the research reported in this thesis is the development of a simulation technique for the investigation of helicopter offshore operations and to demonstrate its application to the analysis of rotorcraft safety related topics appropriate to this environment. The desire is to develop a simulation technique for use by operational pilots, manufacturers and regulatory bodies that is capable of making a positive and timely contribution to rotorcraft safety in offshore operations.

For West European and Scandinavian countries, the mechanism necessary to assess helicopter safety is currently defined by a predetermined, governing framework known as the Joint Aviation Requirements (JAR). Examination of the JAR reveal that there are many factors contributing to rotorcraft safety and some of these are highlighted in Figure 1.0. This research programme, however, will restrict its attention to those issues that have an immediate and repeated impact on the daily operation of the rotorcraft. From Figure 1.0, these are considered to be pilot strategy, rotorcraft design and operational conditions i.e. prevailing wind and turbulence. These safety influences are now discussed in turn in order to place in context the stimulus of the development of the simulation technique presented in this thesis.

i) Pilot Strategy: The term pilot strategy can be defined as the series of control displacements issued by the pilot, necessary for the rotorcraft to achieve a specific positional or performance goal. In the vicinity of the oil rig platform, the correct pilot strategy is particularly important since when manoeuvring in this region there is a risk of the helicopter striking the rig structure. This is evident from recent, highly publicised, incidents (Whidborne, 1991 & 1993) that have highlighted the risks associated with rotary wing transport operating in these conditions. This feature is exacerbated by the possibility of engine failure and atmospheric effects such as wind and turbulence. The use of flight tests to investigate pilot strategy in offshore operations, however, is often limited by the range and scope of specialised equipment and personnel required to support such a study. In this light, the development of a simulation tool that can accurately portray pilot strategy is merited since it would provide a positive and immediate impact on rotorcraft safety and be favourable on economic grounds.

ii) Rotorcraft Design: One factor in the design of current rotorcraft is the need to meet in particular the takeoff and landing performance regulations outlined in the relevant governing regulations. As the governing regulations become more stringent in an effort to improve

vehicle safety and reliability, there is a trend towards the development of aircraft such as the Westland/Augusta EH101 and Sikorsky S-92 civil transport aircraft. These rotorcraft have been constructed with the satisfaction of the JAR criteria from the outset of their conception. The time between first flight and certification for a rotorcraft can take up to five years as was found for the Bell 222 (Kaydon, 1992), while certification for fixed wing aircraft is often less than 12 months (e.g 11 months for McDonnell Douglas DC-10). The significantly smaller certification time for fixed wing aircraft underscores the lack of mature technology available to the rotary wing industry in this field. Clearly, a generic simulation technique that possesses the ability to demonstrate the compliance of a rotorcraft configuration during the formative stages of the design concept would be very advantageous in terms of assessing the vehicle safety and expediting the development cycle.

iii) Operational Conditions: A predominant factor supporting the choice of the helicopter in providing transport services to the oil exploration industry is its ability to operate reliably over a wide range of atmospheric conditions. The influence of these external effects on rotorcraft safety is difficult to quantify using traditional flight testing since obtaining repeated atmospheric conditions is unlikely. This difficulty is highlighted in the Joint Aviation Requirements where the wind takeoff and landing regulations appear only in the form of a maximum allowable wind speed. Clearly, a theoretical simulation technique could provide a low-cost mechanism for the investigation of rotorcraft performance in wind and turbulence. The same technique could be used in the preliminary specification of the required safety parameters employed in the Joint Aviation Requirements under these conditions.

Meeting the aims of the research programme as stated has been achieved by a series of major technical developments that comprise three categories. The first group pertains to the simulation of pilot strategy and vehicle behaviour during takeoff and landing procedures. As a result, a conceptually novel, hybrid simulation technique that employs both conventional and inverse simulation has been developed. By introducing matched phases of forward and inverse simulation, it is possible to accurately predict pilot strategy over a wide range of offshore manoeuvres including those where an engine failure has occurred. The well established helicopter inverse simulation algorithm of Thomson (1987) was chosen for this role since it is recognised as being an ideal tool with which to investigate pilot strategies. Furthermore, the helicopter mathematical model employed in the inverse algorithm received a series of enhancements to ensure it did not restrict the range and validity of the investigation. As will become apparent in later sections, central to the investigation is the formulation of a mathematical model of the manoeuvre of interest. Indeed, the validity of the final simulated pilot strategy depends on the accuracy with which the flight path trajectory is modelled. Consequently much research effort has been accrued to the development of the manoeuvre profiles and as a result, a technique has been formed which enables the trajectory to be

determined from only a narrative description of the pilot strategy. This technical development has proven to be a vital step in the research programme since it fully integrates all operational aspects of helicopter offshore operations into a form amenable for theoretical simulation.

The validation of the manoeuvre profiles and pilot strategy has driven the second category of technical achievements. In response, a unique, real-time, computer graphic simulation tool has been developed. Using the manoeuvre flight path and vehicle attitude time histories as input, the simulation tool is an important asset to the research program since the validity and suitability of a strategy can be rapidly assimilated by other specialists.

The application of a simulation technique for the analysis of takeoff and landing safety related topics has stimulated a third and final category of developments. A new approach has been adopted with the emphasis being placed on the judicious manipulation of flight path profile (and therefore the pilot strategy) to meet specific manoeuvre goals. As a result, the key parameters critical to the successful execution of a given manoeuvre strategy are determined with realistic operational behaviour of the rotorcraft ensured.

1.1 Overview of Safety Aspects of Helicopter Offshore Operations and Their Regulation

The offshore oil exploration and production industry requires movement of large amounts of personnel and equipment. It is common for oilrig platforms to be 50 to 150 nautical miles offshore and therefore, to satisfy their logistical needs, the helicopter has proved to be the most expeditious and reliable form of transport. Because of, for example, the strict scheduling of shift changes, and the unexpected requirement for rescue and medical services, it is an absolute requirement that helicopter operations be conducted, regardless of severe weather conditions.

The takeoff and cruise phases of flight from shore based heli-ports are routine, however the final stages of the flight will require the helicopter to manoeuvre close to the oilrig platform. It is during this flight regime, that the physical constraints of the landing platform and other structures can pose a serious hazard. Furthermore, manoeuvring close to the rig often leads to flight that has significant hovering or very low speed portions. This has safety implications as the relatively low kinetic and potential energy of the vehicle limits the options available to the pilot in terms of manoeuvrability in wind, the ability to perform a safe landing in the event of a single engine failure, or the capacity to achieve autorotation in the event of a complete power loss. These problems may be further compounded by turbulence, and other atmospheric effects such as fog and low light levels.

The hazards associated with helicopter offshore operations are demonstrated by two recent, highly publicised incidents. The first emphasises the difficulty of manoeuvring close to the rig structure, when in July 1990, a Sikorsky S61-N collided with the Brent Spar platform in the East Shetland Basin. In this instance, the pilot allowed the helicopter tail rotor to strike a nearby crane structure resulting in the helicopter crashing into the helideck before falling into the sea and sinking. The second incident highlights the importance of the pilot strategy adopted in high winds and involves an AS 332L Super Puma operating near the Cormorant 'A' platform in the East Shetland Basin. In this case, the accident occurred as the rotorcraft performed a down-wind turn after completing a takeoff manoeuvre from a platform. During this manoeuvre, the high prevailing wind led to a rapidly changing relationship between airspeed and ground speed which was uncorrected by the handling pilot and the consequent rapid rate of descent at low altitude caused the helicopter to crash into the sea.

From the discussion above it is clear that the proper regulation of helicopter offshore services is necessary to ensure vehicle, passenger and platform safety. There are essentially three accepted regulatory standards world-wide and these are the airworthiness standards of North America known as the Federal Aviation Regulations (FAR), the Joint Aviation Requirements (JAR) of Europe and Scandinavia and the Civil Aviation Standard of the former Soviet Union (GAR). Practically every other country has adopted one of these standards in its entirety or has developed an alternative regulatory standard based on one or more of these standards.

In Britain, the task of regulating helicopter offshore operations is undertaken by the Civil Aviation Authority (CAA). The JAR regulations were developed from the harmonisation of both the format and contents of most West European and Scandinavian regulatory documents. This effort was undertaken to meet the certification demands of increasingly transnational manufacture and operation of both fixed and rotary wing aircraft. For helicopters of maximum mass exceeding 2722kg (these are described as 'large' rotorcraft in the JAR), the appropriate governing criteria are to be found in JAR part 29. This section is further subdivided into Category A and B requirements. The Category A and B regulations are formed by a series of criteria that encapsulate all aspects of helicopter operations including flight under emergency conditions. The regulations include, for example, detailed and extensive guidelines for piloting procedures during takeoff and landing manoeuvres in the presence and absence of engine failures, performance capabilities, flight characteristics, and control systems. Category A requirements permit flight over areas where no emergency landing sites are available, and therefore provide the stricter of the two categories. Consequently, Category A regulations require the helicopter to be of multi-engine design and have independent engine, fuel and electrical systems, so that no single failure can cause loss of more than one engine. Category B rotorcraft may conform either to the single or multi-engine class, however they are not required

to have the capability to continue flight in the event of an engine failure. For a helicopter to be certified airworthy, it must comply in all respects with the governing requirements of the country in which it is to be operated. It is of interest to note that the FAA permits offshore operations with Category B compliance only, whilst the CAA requires demonstration of Category A capability before extended flight over water is permitted.

Although the JAR regulations provide a strict governing framework for helicopter operations, rotorcraft still exhibit higher fatal accident rates due to airworthiness causes than fixed wing aircraft (Helicopter Airworthiness Review Panel, 1984). This characteristic of helicopter operations has been examined by the Helicopter Airworthiness Review Panel (HARP), a panel formed by the CAA Airworthiness Requirements Board and tasked to identify the shortcomings of current rotorcraft airworthiness requirements in the absence of economic pressure. Consequently, the panel proposed a series of recommendations which provided a comprehensive and detailed plan with which current and future helicopter operational safety could be improved. The first phase of this plan related to the development of improved rotorcraft ditching and survival capabilities and was implemented in 1985, however it was rejected by the operators as being "too much too soon". At that time, these restrictions would make some operational helicopters obsolete. Subsequently, various other recommendations have been applied, although their impact on current helicopter operations has still to be determined.

1.2 Review of Previous Research

In 1960's, the latest generation of civil transport helicopters (Sikorsky S61L and Vertol -107) represented a considerable advancement over their predecessors in terms of passenger capacity, speed, and their takeoff and landing characteristics. The first theoretical investigation to quantify the improved performance associated with rotorcraft with multi-engine configurations can be attributed to Jepson (1962 and 1963). In his first paper Jepson used analytical means to investigate factors effecting the takeoff and landing performance of a helicopter. In particular, he examined the influence of twin and single engine powerplant configurations on the low speed portion of the height - velocity envelope. From this investigation, the author concluded that analytical means with the aid of flight test data can qualitatively predict helicopter performance during vertical descents. Furthermore, he noted that the low speed portion of the height velocity envelope of a twin engine configured helicopter is smaller than the low speed portion envelope of a rotorcraft with equivalent power derived from a single engine. In his second report, Jepson used the helicopter longitudinal equations of motion to predict the takeoff and landing performance of a twin engine rotorcraft after an engine failure. As a consequence of this study, Jepson related his results to heliport size requirements. Jepson concluded that twin engine configured helicopters increase vehicle safety whilst

permitting operation from smaller heliports. Jepson did not consider the influence of pilot strategy on the ability of the rotorcraft to land in either document.

More recent studies of takeoff and landing procedures (Cerbe and Reichert 1989, Tranäpp 1989) have employed rotorcraft simulation models based on a steady state power required data field technique that allows the helicopter power required and flight path to be calculated from basic aircraft properties. For a complete explanation of the evaluation of rotorcraft performance based on data field approximation, the reader is referred to (Cerbe and Reichert 1989). In the context of this thesis however, it is sufficient to say that non - steady flight states that occur for example during takeoff and landing manoeuvres, are evaluated by transforming them into equivalent steady flight conditions. These investigations assumed rotorcraft takeoff and landing operations from shore based heli-ports and primarily examined the influence of wind velocity on power required, however they neglected any influence of piloting procedures.

In order to support civil and military customers, the National Aerospace Laboratory of the Netherlands developed a simulation package capable of investigating longitudinal takeoff and landing procedures (Vodegel and Stevens, 1992). The mathematical model of the helicopter employed was based on an energy balance concept. This technique permits, for example, a single engine failure to occur, and the main rotor speed kinetic energy to be exchanged for helicopter kinetic energy or vice versa, thus ensuring the power required deficit remains within acceptable limits. The control strategy of the helicopter was developed from the actual piloting cues adopted in practice for a specific manoeuvre. This information is then used to continuously specify the vehicle's Earth based longitudinal and vertical translational accelerations. The simulation package developed from this approach was employed in an optimisation algorithm that enabled the maximum permissible operating mass for the helicopter to perform a specific manoeuvre to be determined. Although the study neglected the influence of atmospheric effects, by considering rotorcraft power requirements, the authors were able to identify critical phases of helicopter offshore manoeuvres.

Another approach in the investigation of takeoff and landing procedures utilised a rigid body, longitudinal three degree of freedom mathematical representation of the helicopter (Yoshinori and Kawawachi 1993). The aerodynamic performance of the main rotor was obtained from the combination of blade element formulation and a modified momentum theory that permitted the rotor inflow model to simulate the vortex ring state. The helicopter model was incorporated into a numerical algorithm that allowed optimisation of takeoff and landing manoeuvres with respect to a chosen objective function. In this study, piloting strategy was applied via a series of equality and inequality constraints that governed both the vehicles operating limits and manoeuvre boundary conditions. In this investigation, the authors showed

that optimisation of the takeoff flight path can increase payload by 10%, while required heliport size can be significantly reduced.

It is perhaps evident that previous investigations have been primarily concerned with obtaining rotorcraft performance for a specific manoeuvre and omitted any consideration of piloting strategy. Furthermore, the helicopter simulation packages developed were often employed in numerical optimisation algorithms and therefore to reduce run times, the fidelity of the rotorcraft mathematical model used was frequently compromised. This deficiency is important for two reasons. Firstly the limitations of the helicopter model precludes investigation into important flight regions in which an insight into the dynamics of the helicopter is desirable. Secondly, the accuracy of the helicopter mathematical model relates directly to the final pilot strategy evaluated. Clearly, in flight modes where physical space is limited and pilot strategy precisely defined, these limitations directly influence the success of the study. Finally, the contribution of pilot strategy to vehicle safety is prominent within the FAA and CAA regulations, however, its significance is often lost within an optimisation algorithm.

The above discussion has detailed some of the techniques that have been applied in the analysis of helicopter offshore operations and although they exhibit various degrees of success in extracting information about pilot strategy and rotorcraft performance, their applicability is limited due to issues already discussed. To ensure that this investigation of helicopter takeoff and landing procedures was successful, the limitations exhibited by previous studies were addressed from the outset.

1.3 The Specification of a Simulation Tool for the Analysis of Helicopter Offshore Operations and its Application to Rotorcraft Safety

There are two key conditions that are considered sufficient before the aims of this research programme can be met:

i) The development of a simulation algorithm that allows pilot strategy employed in helicopter offshore operations to be accurately portrayed for a given manoeuvre over a range of operational conditions,

ii) The formulation of an investigation philosophy that ensures the authentic representation of pilot strategy by fully integrating the key performance and regulatory criteria that dictate helicopter operations offshore.

The first step towards resolving condition (i) listed above is to ensure the rotorcraft mathematical model, HGS, is suitable for the analysis of helicopter operations offshore. This has necessitated certain modelling enhancements including the provision of mathematical models of an engine failure, wind, turbulence etc.

The ability of the simulation algorithm to realistically portray pilot strategy over a wide range of operational manoeuvres including those that are accompanied by an engine failure must also be addressed. For this to be possible, there are several important technical challenges which must be met including the development of a technique to incorporate pilot reaction time and a generic method for the formulation and validation of representative models of offshore trajectories.

Having established the simulation tool, the task is then to meet the criteria of the second condition mentioned above, i.e. the formulation of a rationale with which the simulation software it is to be applied. As mentioned in section 1.2, the application of previous simulation methods has been towards determining the maximum helicopter operating mass possible for the vehicle to fly a specific manoeuvre. Although this information is of interest, it reveals little about pilot strategy, prevents investigation of alternative pilot strategies and can generate unrepresentative vehicle operating conditions within the restrictions of the appropriate governing regulations. To overcome the limitations exhibited by previous studies, a new rationale for undertaking case studies must be adopted. It must accurately portray the pilot behaviour whilst fully integrating the crucial regulatory and rotorcraft performance criteria that are common to offshore operations.

To satisfy the requirements of the proposed simulation technique highlighted above, the following research programme has been undertaken.

1.4 Modifications to Helicopter Generic Simulation

A series of modelling enhancements have been made to HGS to ensure its suitability for the investigation of helicopter offshore operations and these are now outlined.

1.4.1 Rotor Inflow Modelling Enhancements

The original induced flow employed in HGS was that developed by Glauert (1926) and although this inflow model is widely used, it fails to portray aerodynamic phenomenon that are important in the context of the current investigation. Therefore, the Glauert model was replaced by a Dynamic Inflow model and the opportunity was also taken at this stage to include the vortex ring state in the simulation.

1.4.1a Addition of Vortex-Ring Model

The vortex ring state is an unsteady aerodynamic phenomenon that occurs in a helicopter main rotor when the vehicle is in a steep descent with low forward airspeed. The vortex ring state is characterised by severe power and thrust fluctuations that are attributable to a large torus shaped mass of air enveloping the rotor disc. Knowledge of the vortex ring is important as it is this flight region that separates the powered and unpowered flight modes known as the normal and windmill brake states. To simulate the vortex ring state and hence enable the helicopter controls during vertical descents to be determined, an empirical function of rotor disc vertical velocity was developed. The reader should note that a helicopter tail rotor can also experience the vortex ring state when the vehicle is in high cross-winds and at low forward airspeed. Consequently, the technique used to represent main rotor operation in the vortex ring, has also been extended to the tail rotor inflow model.

1.4.1b Addition of Dynamic Inflow Model

The Glauert inflow model (1926) assumes that the induced flow reacts instantaneously to changes in rotor thrust, however, in reality the induced velocity takes a finite time to reach its new steady state value in response to changes in flight condition or control perturbation. This aspect of rotor inflow is important in offshore operations as manoeuvres in confined areas often require rapid control deflections. To account for this aerodynamic phenomenon, the dynamic inflow model developed by Peters and HaQuang (1988) was incorporated into HGS.

1.4.2 Engine Modelling Enhancement

The development of the multi-engine mathematical model is crucial to the success of this research, as it permits the investigation of piloting procedures during an engine failure where the limited engine power available and the confines of the rig structure seriously limits the options available to the pilot in terms of his strategy. Consequently, a mathematical model that accurately replicates the behaviour of a helicopter powerplant of the free turbine type has been developed. The mathematical model of the powerplant is based on that developed by Padfield (1981) and can portray single or multiple engine failures whilst ensuring a limited torque output of the remaining serviceable engine.

1.4.3 Inclusion of Stability Augmentation and Flight Control System

The original output from the inverse algorithm was in the form of rotorcraft blade pitch angles, however for this investigation, control displacements in terms of pilot collective lever, cyclic stick and pedal movements are more appropriate. The blade pitch displacements of a

helicopter main and tail rotor are determined by contributions from both the pilot and the stability augmentation system. Consequently, a mathematical model of stability augmentation and flight control system must be included if the pilot control displacements are to be extracted. The model used for this purpose is similar to that quoted by Padfield (1981).

1.4.4 Inclusion of Wind Model

The presence of prevailing wind can significantly effect both the power and control margins of a helicopter and therefore a mathematical model of prevailing wind has been included in HGS. Using this model, it is then possible to investigate the degradation/improvement of vehicle safety associated wind and its contribution to pilot strategy during offshore operations.

1.4.5 Inclusion of Turbulence

Turbulence is an important feature of helicopter offshore operations particularly in confined areas where it can promote a transient increase in pilot work load (Bradley et. al., 1994) and vibration that can seriously degrade vehicle safety. To enable studies of piloting strategies in the presence of this atmospheric effect, a mathematical representation of turbulence has been incorporated in HGS. The model chosen for this role was developed by Tomlinson and Bradley (1980) as it faithfully incorporates many features of turbulence that occur in reality, in particular the large fluctuations in air velocity that are critical close to the oilrig. The generation of turbulence from rig and landing platform structure was considered outwith the scope of this study although its importance is recognised.

1.5 A New Concept in Rotorcraft Simulation

The development of a conceptually new simulation technique has been necessary to portray the piloting strategies and vehicle behaviour suitable for the study of rotorcraft operations offshore. The research effort attributable to the development of the simulation tool has concentrated on two areas; the inclusion of pilot reaction time in response to an external disturbance and a generic, systematic, approach for the formulation representative expressions of offshore manoeuvre profiles.

1.5.1 A Novel, Hybrid, Simulation Algorithm Allowing the Analysis of Pilot Reaction Time

The incorporation of pilot reaction time is an important feature of pilot strategy for two reasons. Firstly, suitable pilot reaction times are emphasised within the regulatory documents (JAR part 29), and the simulation package must reflect this importance. Secondly, the pilot

reaction time will directly influence the subsequent recovery trajectory and hence the rotorcraft's capability to perform a recovery manoeuvre. Using matched, sequential, phases of both conventional and inverse simulation, a conceptually novel, hybrid, simulation technique has been formed that can effectively model the influence of pilot response time. The author is unaware of any comparable method that represents pilot reaction in this manner and consequently this innovative technique represents an important contribution to helicopter simulation studies. For the purposes of this thesis, the software helicopter - inverse - forward - inverse simulation package is known as HIFIS.

1.5.2 A Generic Method for Offshore Manoeuvre Formulation and Validation

The starting point of any work involving inverse simulation is the development of a formal description of the manoeuvre(s) of interest. Previous investigations using inverse simulation have had some knowledge of the flight path profile at the start of the study, (Thomson and Bradley, 1992). In this research programme, however, knowledge of a manoeuvre has been provided solely in terms of a detailed narrative description of the corresponding pilot strategy. As a result of an extensive and comprehensive development process, a generic method that permits the formulation of an authentic mathematical model of the manoeuvre of interest from the description of pilot strategy alone has been developed. In the method, the emphasis is placed on the careful selection of manoeuvre performance related parameters required at key stages during the trajectory, rather than the satisfaction of some geometric criteria at the end of the manoeuvre. A further step has been taken by adopting the techniques similar to those employed by Bradley and Thomson (1993) for the study of Mission Task Elements (MTE), as this has enabled the key elements of the piloting strategy to be more readily incorporated.

An important contribution to the method has been made by the application of real-time computer imaginary. The computer graphic software is particularly useful in appreciating the influence of rig proximity on the flight path. However, the real asset of this software lies in its ability to expose the results for validation by other specialists. This is particularly important when it is recalled that the narrative descriptions of the pilot strategy have been provided by a civilian test pilot (Talbot, 1992).

Although the above approach has proved successful, a further technical advancement was required for the analysis of pilot strategy in response to an engine failure. The pilot strategy after an engine failure is often governed by the immediate danger to the helicopter due to the proximity of the rig and the urgency with which the new piloting strategy is to be adopted. Clearly the mathematical model of the recovery trajectory must be constructed in such a way as to permit the realistic portrayal of these important aspects of the pilot strategy. As a

result, a new method of formulating trajectories suitable for use as input to the inverse algorithm has been developed. The approach used employs biased polynomial functions of time and these type of expressions have proved sufficiently flexible to allow a range of recovery manoeuvres to be determined.

1.6 Plan of Thesis

In this chapter, the aims of the investigative programme have been detailed and the adopted approach outlined. Before presenting the research further, it is appropriate to outline a plan of the remainder of this thesis.

The enhancements to the helicopter mathematical model used in this study are described in Chapter 2. These modelling improvements include the addition of a dynamic inflow model and the vortex ring state, a twin engine power plant, a stability augmentation and flight control system, and atmospheric effects such as prevailing wind and turbulence.

A method is presented in Chapter 3 that enables, in the context of inverse simulation, the formulation of representative mathematical models of offshore trajectories. Based on the use of a detailed narrative description of the relevant pilot strategy, the key steps involved in the method are detailed by the application of the technique to a common offshore takeoff strategy.

The rationale and architecture of a novel, hybrid, simulation technique that enables the accurate portrayal of pilot strategy in response to an engine failure or some other external disturbance is shown in section 4.1. The treatment of the recovery flight path in response to an engine failure in detailed in section 4.2. These technical developments are then demonstrated through their application to a typical offshore takeoff manoeuvre in section 4.3. The theoretical pilot strategy is compared to that adopted in practice in section 4.4 where they can be seen to fully vindicate the approach taken.

In Chapter 5, the application of the simulation tools developed in the previous chapters is demonstrated. A new investigative philosophy is adopted and used to study in turn the pilot strategy, design and atmospheric issues outlined in the introduction.

In Chapter 6, the achievements of the research are summarised to note their contribution to rotorcraft safety in offshore operations.

In Chapter 7, a critical review of the technical achievements of the research is given.

1.7 Conclusions

This introductory chapter has stated the aims of the research and the motivation supporting them. The application background has been discussed in order to place in context the specification of the simulation tools developed. The suitability of the inverse algorithm has been addressed to show the central role it plays in the investigation. The technical developments necessary to satisfy the aims of the study have been summarised into three categories. This not only highlights the research programme necessary to achieve the project goals but also puts on record the technical achievements that have been made and their contribution to the field of helicopter offshore operations.

Chapter 2

Mathematical Modelling Enhancements to HGS

The HGS rotorcraft mathematical model was developed initially for the investigation into helicopter Nap-of-the-Earth flight. The rotor model in HGS assumes a multi-blade representation for the evaluation of the rotor forces and moments, with the induced flow calculation being derived from momentum concepts. Look-up tables are employed to determine the fuselage, tailplane and fin forces and moments and a simple engine model portrays the powerplant dynamics. The HGS helicopter model is of central importance in this investigation and consequently is discussed in detail in Appendix 1.

For any investigation, the accuracy of the pilot strategy evaluated from the inverse simulation algorithm is directly related to the validity of helicopter model employed. The performance of the version of the HGS model at the beginning of this study was impaired by several modelling deficiencies, and it was considered wise to address some of the limitations at an early stage. These modifications fall into two categories, the first of which relates to the update of some of the modelling elements that were originally incorporated in HGS. The modelling enhancements consist of the replacement of the momentum inflow model by a dynamic inflow model incorporating the vortex ring state, and the inclusion of a multi-engine representation of the helicopter powerplant. The second group of modifications pertain to modelling features missing in the original version of HGS which are important in the current work. These enhancements include the addition of a model of an automatic flight control system and an atmospheric model containing prevailing wind and turbulence. These modelling enhancements are discussed in the following sections.

2.1 Inflow Modelling

The increase in velocity imparted on a column of air passing through a rotor disc due to the contribution of energy from the rotor is called the induced velocity. The rotor thrust is generated in reaction to the accelerating force applied to the rotor air mass and consequently if the behaviour of the helicopter is to be modelled correctly, then the rotor induced velocity must be accurately determined.

Some of the earliest work on calculating the induced velocity of a rotor can be attributed to Glauert (1928) who assumed that the rotor was uniformly loaded and consisted of an infinite number of blades. Based on momentum considerations Glauert proposed the following formula for the non-dimensionalised rotor induced flow component denoted by λ_i,

$$\lambda_i = \lambda_0 = \frac{C_T}{2\sqrt{\mu^2 + (\mu_z - \lambda_0)^2}}$$

where,

λ_0 is the non-dimensionalised uniform (zeroth) inflow component ($\lambda_0 = v_0 / \Omega R$),

C_T is the rotor thrust coefficient,

μ is the inplane resultant velocity of the rotor hub,

μ_z is the vertical velocity component of the rotor hub.

Glauert acknowledged the limitations of the above expression and appreciated that the rotor induced velocity was far from uniform and consequently modified his momentum approximation by adding additional induced velocity components that were a function of blade radial and azimuthal position. The non-dimensionalised rotor induced velocity, λ_i, can then be determined from,

$$\lambda_i = \lambda_0 + \frac{r_b}{R}(\lambda_{1s} \sin\psi + \lambda_{1c} \cos\psi)$$

where,

λ_{1s} , λ_{1c} are the harmonic inflow components,

r_b is the radial position,

R is the rotor radius.

The main attributes of the Glauert theory are that it is simple to apply and can be readily incorporated into helicopter flight mechanic packages. Furthermore, as noted by Chen (1990), the inflow model predicts with reasonable accuracy the induced velocity over a wide range of flight speeds and consequently the Glauert inflow model has been used to determine the rotor inflow in many rotorcraft simulation models, including HGS. An outline of the Glauert inflow model is presented in Appendix 1. The Glauert model suffers from several inadequacies which limits its use in the current investigation of helicopter offshore operations. It is a quasi-static model that assumes that the rotor induced velocity reacts instantaneously to changes in blade control angles and vehicle flight states. In the real aircraft, however, there is a dynamic lag associated with the build up of induced velocity which is not captured by the Glauert inflow model. This is an important characteristic particularly for helicopters operating near oilrig platforms where the physically restrictive flying environment may require rapid piloting control deflections. Furthermore, the Glauert model neglects the contribution of the aerodynamic

pitching and rolling rotor moments and this has been found to be important when theoretical induced flow is compared with measured test data (Gaonkar and Peters, 1988).

Since the 1920's considerable research has been devoted to the improved theoretical prediction of rotor induced flow models and summary of this work is given by Chen (1990). Part of the research discussed by Chen describes the formulation of the dynamic inflow model of Peters and Haquang (1988). Developed from unsteady actuator disc theory, this model represents the rotor inflow as a three state first order differential equation with time constants included to model the effect of the build up of the induced velocity components. This model incorporates the important features that are missing from the Glauert model and has also been widely validated, (Gaonkar and Peters, 1988).

The dynamic inflow model as quoted by Peters and Haquang has the following form,

$$\underline{\mathbf{M}}\begin{bmatrix}\dot{\lambda}_0\\ \dot{\lambda}_{1s}\\ \dot{\lambda}_{1c}\end{bmatrix}+\underline{\tilde{L}}_{nl}^{-1}\begin{bmatrix}\lambda_0\\ \lambda_{1s}\\ \lambda_{1c}\end{bmatrix}=\begin{bmatrix}C_T\\ -C_L\\ -C_M\end{bmatrix}_{aerodynamic}$$

where $\underline{\mathbf{M}}$ is the apparent mass matrix which associates the dynamic lag with the response of the inflow states to changes in control deflections or changes in flight condition. The matrix $\underline{\tilde{\mathbf{L}}}_{\mathbf{nl}}^{-1}$ relates the inflow states to the rotor thrust coefficient, C_T and the aerodynamic moment coefficients given by C_L and C_M. The formulation of the dynamic inflow model is shown in greater detail in Appendix 3.

The Peters and Haquang inflow model can be solved in the inverse algorithm using a Newton - Raphson iteration scheme similar to that presented in Appendix 2. A more instructive insight into the differences between these two inflow models can be obtained from a conventional forward solution. Some example results are given in Figure 2.0 where a step in collective equivalent to 5% of the blade displacement is applied to the helicopter which starts the simulation in the hover. The simulated uniform induced velocity time histories for both the Glauert and dynamic inflow models is shown in Figure 2.0a. The finite lag associated with the build up of induced velocity in response to changes in collective angle is clearly demonstrated and the rotor inflow reaches its new inflow state after approximately 1 second. A comparison of main rotor thrust coefficients is also shown in Figure 2.0b and it is evident from this plot that the rotor thrust using the inflow components derived from the dynamic inflow model reacts instantaneously to changes in rotor blade pitch. This can be attributed to the fact that the main contribution to the rotor blade angle of attack is determined largely by its geometric pitch angle and not that contributed by the rotor induced velocity.

2.2 Vortex Ring State

In performing steep descents at low airspeeds, helicopters encounter an unsteady aerodynamic flow condition known as the vortex ring state. This state is characterised by severe thrust and torque variations that are attributable to a large torus shaped mass of air that envelopes the rotor disc. The behaviour of the rotor induced velocity between the boundaries of the vortex ring state must be known, as it is this flight region that separates the powered and unpowered flight regimes known as the helicopter and windmill states.

Before proceeding further, it is useful to define the terms 'helicopter state', 'windmill state', and 'vortex ring state' more precisely. In the 'helicopter state', the rotor is imparting energy on the airflow via the induced velocity, whilst in the 'windmill state' the rotor is extracting energy from the free stream by decelerating the flow through the rotor. The 'vortex ring state' can be defined as the condition that occurs when during a steep descent, the downward induced velocity and upward free-steam flow combine to destroy the streamtube that forms around the rotor. Consequently, the momentum concepts underpinning the formulation of equation (A1.22) are no longer valid. A schematic diagram of the flowfield around a rotor operating in the helicopter, windmill and vortex ring states is shown in Figure 2.1.

The practical importance of the vortex ring state phenomenon is highlighted by the crash of an AS332L Super Puma near the Cormorant 'A' platform in the East Shetland Basin which is documented in the air accident report of Whidbourne (1993). Immediately after departing the oilrig platform, the helicopter transitioned forward and performed a downwind turn to the right. The wind at the time of operation was gusting to 55kts, and during the turn the rapidly reducing airspeed was unnoticed by the aircrew. The subsequent rapid rate of descent was unchecked by the pilot and the aircraft crashed into the sea. Investigations carried out by the Air Accident Investigation Branch of the Department of Transport revealed that the piloting difficulties experienced by the aircrew during the accident were consistent with those of a helicopter main rotor operating in the vortex ring state.

It is evident from the above discussion that it is important that the rotor induced flow model can simulate the vortex ring state. Accepting the limitations of the Glauert model concerning the build up of induced velocity discussed earlier, the theory predicts satisfactorily the windmill and helicopter operating states, however it fails in the vortex ring intermediate range. The complex nature of the flowfield through the rotor prohibits a simple theoretical investigation of this phenomenon, and consequently there is little relevant literature concerning the prediction of the vortex ring state. Most investigations have concentrated on the prediction of the onset of the vortex ring state and some of these are now discussed.

A noteworthy study into the prediction of the vortex ring state was carried out by Wolkovitch (1972), who employed momentum theory and actuator disc concepts to predict the boundaries of the vortex ring state. Wolkovitch assumed that the vortex ring state occurs when the velocity of the vortex core relative to the rotor disc falls to zero, or alternatively the rate of descent of the rotor disc is such that the vortex cores no longer move away from the rotor disc. Wolkovitch also studied the lower boundary of the vortex ring state where he appreciated the uncertainty in formulating a criteria for the transition from vortex ring to windmill states. He attributed this to the fact that the accumulation of vorticity and subsequent break down of the slipstream would occur at some unknown position above the rotor disc.

The theory of Wolkovitch exhibits several inconsistencies that were identified by Peters and Chen (1982). In their paper, it was noted that Wolkovitch theory permitted the vortex ring state to develop even in shallow rates of descent, a characteristic which is contrary to actual flight experience and test data. Furthermore the theory predicted that the rotor would enter the windmill state even though it was still operating in helicopter mode. In the light of these deficiencies, Peters and Chen developed a new theory that incorporated the influence of the descent angle. Thus a modified criteria for the onset of the vortex ring state was developed that qualitatively agreed with experience and test data.

One of the first attempts at establishing a complete theory for the aerodynamics of a rotor in steep descent was presented by Shaydakov (1967). This method is based on the assumption of an ideal fluid with a constant induced velocity across the rotor wake (the same assumption as Wolkovitch) and that the rotor imparts no rotational motion on the slipstream. In his first model, it was assumed that the rotor was operating in the windmill state and moved through the air at some angle of attack. A fundamental presupposition of the Shaydakov theory is that the rotor sheds a series of vortex rings that are circulated up a skewed cylinder of diameter equal to that of the rotor. By considering the circulation of the vortices leaving the rotor disc, Shaydakov derived a quartic expression for the rotor induced velocity. Shaydakov extended his theory to flight where power was applied to the rotor and expressed the rotor inflow in terms of a fourth order polynomial function of mean induced velocity.

Although from first impressions the inflow model of Shaydakov would seem ideal for this investigation of helicopter offshore operations and indeed other studies in this field have actually employed this theory to predict the rotor induced velocity (Vodegel and Stevens, 1992), it has been rejected in this study as it can not be readily integrated into the dynamic inflow model.

In the context of the aforementioned discussion, it is perhaps evident that the options available to model the vortex ring using techniques that are suitable for use in the current study

are rather limited. In the absence of any alternative formal means of deriving a vortex ring model, recourse has been made to a more heuristic approach. The next section details a model that enables the key characteristics of the vortex ring state to be quickly determined and is equally applicable to both Glauert and dynamic inflow models.

2.2.1 Model of Vortex Ring State

The momentum equation for the rotor uniform induced velocity can be given as,

$$\lambda_0 = \frac{C_T}{2\sqrt{\mu^2 + (\mu_z - \lambda_0)^2}}$$

This expression is strictly only applicable when the rotor is working in either the helicopter or windmill modes. In the intermediate, vortex ring mode, there are large power fluctuations which are unaccounted for in the simple theory leading to the above expression. Indeed, it can be seen from Figure 2.2 that in the case $\mu = 0$, (vertical motion) there is not a unique solution for λ_0 in terms of μ_z and that a smooth transition through the vortex ring state is not possible.

In order to overcome these difficulties a small residual velocity, δ, is introduced into equation (A1.22) which may then be written in non dimensional form,

$$\bar{\lambda}_0 = \frac{1}{\sqrt{\bar{\mu}^2 + \bar{\delta}^2 + (\bar{\mu}_z - \bar{\lambda}_0)^2}} \qquad (1)$$

where,

$$\bar{\lambda}_0 = \frac{\lambda_0}{\sqrt{C_T/2}} \qquad \bar{\mu} = \frac{\mu}{\sqrt{C_T/2}}$$

$$\bar{\mu}_z = \frac{\mu_z}{\sqrt{C_T/2}} \qquad \bar{\delta} = \frac{\delta}{\sqrt{C_T/2}}$$

The residual velocity is set to zero outside the vortex ring region (which for this purpose is defined as $1 < \bar{\mu}_z < 2.5$); while inside this interval $\bar{\delta}$ is a positive function of $\bar{\mu}_z$ smoothly approaching zero at each end. A suitable definition is,

$$\bar{\delta} = \begin{cases} 0 & 1 \geq \bar{\mu}_z \\ K\, f(\bar{\mu}_z) & 2.5 > \bar{\mu}_z > 1 \\ 0 & \bar{\mu}_z \geq 2.5 \end{cases}$$

where f has been defined as a fourth order polynomial:

$$f(\bar{\mu}_z) = a\,\bar{\mu}_z^{\,4} + b\,\bar{\mu}_z^{\,3} + c\,\bar{\mu}_z^{\,2} + d\,\bar{\mu}_z + e \qquad (2)$$

shown in Figure 2.3 and satisfying,

i) $f(1.0) = f'(1.0) = 0$
ii) $f(1.75) = 1$
iii) $f(2.5) = f'(2.5) = 0$

By applying the listed boundary conditions to equation (2), the coefficients of the polynomial f were found to be:

a=3.160 b=-22.123 c=54.518 d=-55.309 e=19.753

The scaling constant K can be determined by adopting a similar approach to Peters and Chen (1982). Consider equation (1) for the case of vertical motion only. Setting $\bar{\mu} = 0$ and rearranging for $\bar{\mu}_z$, gives,

$$\bar{\mu}_z = \bar{\lambda}_0 \pm \sqrt{\frac{1}{\bar{\lambda}_0^{\,2}} - \bar{\delta}^2} \qquad (3)$$

Figure 2.4 shows the variation of equation (3) for $\bar{\lambda}_0$ where it may be seen there are infact three solutions to the inflow equation for large rates of descent. In reality of course, only one solution is physically realisable, and experiments (Peters and Chen, 1992) have shown this to be the lower case. In this model, the task is to determine the minimum value of $\bar{\delta}$ that permits a single solution to be obtained in the vortex ring region.

Examination of Figure 2.4 reveals that three solutions occur when,

$$\frac{d\bar{\mu}_z}{d\bar{\lambda}_0} = 0$$

Differentiating equation (3) with respect to $\bar{\lambda}_0$ yields,

$$\frac{d\bar{\mu}_z}{d\bar{\lambda}_0} = 1 \pm \frac{1}{\bar{\lambda}_0{}^3 \sqrt{\frac{1}{\bar{\lambda}_0{}^2} - \bar{\delta}^2}}$$

Setting the above expression to zero and rearranging for $\bar{\delta}^2$ gives,

$$\bar{\delta}^2 = \frac{1}{\bar{\lambda}_0{}^2} - \frac{1}{\bar{\lambda}_0{}^6} \tag{4}$$

Substituting the momentum equation into the above expression yields,

$$\bar{\mu}_z = \bar{\lambda}_0 + \frac{1}{\bar{\lambda}_0{}^3} \tag{5}$$

Equations (4) and (5) may be used to plot the region in which the momentum equation yields three roots and this is shown in Figure 2.5. From this diagram , it is evident that for $\bar{\delta} > 0.6204$, multiple roots do not occur and consequently $\bar{\delta}$ may be chosen to take this value. Interestingly, this value of $\bar{\delta}$ is equivalent to a descent angle of $\gamma = \tan^{-1}\left(\frac{1.755}{0.6204}\right) = 70.5^{o}$, i.e. the vortex ring state does not occur for descent angles less that 70.5^{o} which is consistent with the physical mechanism of the aerodynamic phenomenon.

Recalling that the function $f(\bar{\mu}_z)$ has a maximum value of unity, then one can reasonably set K=0.6204.

Using this approach, it is possible to traverse the vortex ring state in a smooth manner and this is shown in Figure 2.6. In order to vindicate this approach, alternative values of K have been shown in this diagram and it can be seen that they are inappropriate.

2.3 Mathematical Modelling of Gas Turbine Powerplants

The original mathematical model of the helicopter utilised in HGS has provision for single operation engine only without either a power limiting structure or capability to simulate multiple or individual engine failures. An example of the response of this model to a step input in engine torque demand is shown in Figure 2.7. Initially the torque demand is 10kNm, and after five seconds, torque required from the engine is increased to 15kNm. This is achieved after 1.5 seconds despite the fact that the engine torque limit was specified to be 12.5kNm.

Clearly, the deficiencies of this engine model must be addressed if pilot strategy is to be accurately portrayed in the current study.

When choosing a new engine model for HGS, however, there are other considerations which must be accounted for and consequently the choice and form of the engine model must not rest solely on its ability to simulate an engine failure. It is important that the engine model adopted exhibits a consistent level of compatibility in the degree of sophistication of the engine and rotor/airframe models. Further, the correct coupling between engine, fuel system, rotor model and airframe must be incorporated if the rotorcraft handling qualities are to be accurately portrayed. This feature of helicopter modelling has been discussed in a report by Kuczynski et. al. (1979), where analytical and experimental studies were used to establish the influence of engine/fuel control design on rotorcraft dynamics. This work stressed the importance of integrated engine, rotor and airframe mathematical model design and highlighted the significant effect an engine governing system can have on helicopter behaviour.

Most helicopters currently in service employ gas turbine based propulsion systems, however, the configurational aspects of these types of powerplants can vary significantly. In some cases the gas turbine is physically linked to the main transmission gearbox as this permits torque demands to be quickly met by the powerplant. Other configurations have the engine isolated from the transmission; in these cases the hot jet efflux of the gas turbine drives a power turbine connected to main rotor gearbox. Although there is a finite lag associated with the build up of torque output from this type of engine layout, its main advantage is that the gas turbine can operate at its most fuel efficient speed for almost all rotorcraft operating conditions. This category of engine layout is known as the free turbine type and is the most common configuration of a helicopter powerplant. A schematic diagram of a free turbine twin engine powerplant is shown in Figure 2.8. There are various techniques and levels of complexity with which this type of powerplant can be modelled and some of these are now discussed.

A relatively simple method of modelling a twin engine gas turbine powerplant is to assume that the independent engines can be considered as a single power source and controlled by two independent hydromechanical governing mechanisms. The resulting equation set is typically in the form of a series of ordinary differential equations. Although this method greatly under represents the physical and thermodynamic concepts of an operating gas turbine, it is very useful as it requires little engine characteristic data and fits easily into current flight mechanic simulation algorithms.

An alternative engine modelling method is that known as 'The Inter Component Volume (ICV) Method'. The ICV method, detailed by Macallum (1992), effectively fragments the gas generator into separate control volumes. Additional storage volumes are provided for the

accumulation of high pressure gases. The physical and thermodynamic attributes of the engine are determined from characteristic tables that relate engine speed, pressure and temperature. Engine model governing can be achieved through either a simulated Full Authority Digital Electronic Control model or by fuel scheduling tables. This approach to gas turbine modelling can be computationally intensive as the solution algorithm is iterative in nature and requires large amounts of data on which the calculation is based. With respect to modelling fidelity, the ICV method is superior to the simpler approach discussed earlier, however the level of sophistication implied by this type of engine model is more akin to a higher level of helicopter mathematical model than that used here.

On consideration of the aforementioned arguments, it was decided to modify the original engine model in HGS by duplicating the engine governing system provided by Padfield (1981). The time constants and gains of the engine governor were retained to ensure the powerplant exhibited the desired power characteristics. The development of this model is now described.

2.3.1 Mathematical Model of Twin Engine Powerplant

To modify the existing engine model for the twin engine case, the first step is to rewrite equation (A1.23) in Appendix 1 as,

$$\dot{\Omega} = (Q_{E_1} + Q_{E_2} - Q_R - G_{TR}\, Q_{TR}) / I_{TR} + \dot{i} \qquad (6)$$

where Q_{E_1} and Q_{E_2} denote the contributions of engine torque output from both engine one and two respectively. The function of varying fuel flow in response to changes in rotor speed in the engine governor is modelled by equation (A1.24). It is convenient to assume that each engine of a twin gas turbine powerplant will consume fuel at half the rate of an equivalent single engine plant, then it is straightforward to write,

$$K_{c1(i)} = \frac{1}{2} K_{c1} \qquad i=1,2$$

where i denotes the i^{th} engine of the powerplant.

Furthermore, the fuel flow module will supply fuel at a sufficient rate to allow any torque demanded to be supplied by the engines and this is demonstrated by Figure 2.7. In a real gas turbine engine, there is only a finite power output available and this is usually specified by the manufacturer as a function of the high pressure turbine inlet temperature. The limiting of

the torque produced by each engine is achieved by setting a limit on the fuel flow rate that the engine governing system can deliver. First, write equation (A1.24) as,

$$\frac{\Delta w_f^*{}_{(i)}}{\Delta\Omega^*} = \frac{1}{1+ \tau_{e1}\, s}$$

or alternatively,

$$\Delta \dot{w}_f^*{}_{(i)} = \frac{-\left(\Delta w_f^*{}_{(i)} - \Delta\Omega^*\right)}{\tau_{e1}} \tag{7}$$

where,

$$\Delta w_f^*{}_{(i)} = \frac{\Delta w_{f(i)}}{K_{e1(i)}} \tag{8}$$

and $\Delta\Omega^*$ represents the difference in rotor speed as defined according to the fuel flow schedule. The construction and implementation of the fuel schedule is discussed later in this section.

Now rewriting equation (A1.25) for the multiple engine case and substitute equation (8) gives,

$$\frac{\Delta Q_{E(i)}}{\Delta w_f^*{}_{(i)}} = K_{3(i)}\left(\frac{1+ \tau_{e2(i)}s}{1+ \tau_{e3(i)}\, s}\right) \tag{9}$$

where the time constants $\tau_{e2(i)}$ and $\tau_{e3(i)}$ are assumed to be linear functions of engine torque and are given by,

$$\tau_{e2(i)} = \tau_{e20} + \tau_{e21}\left(\frac{Q_{E(i)}}{Q_{E\,LIM}}\right)$$

$$\tau_{e3(i)} = \tau_{e30} + \tau_{e31}\left(\frac{Q_{E(i)}}{Q_{E\,LIM}}\right)$$

and $Q_{E\,LIM}$ is the maximum torque output of the powerplant with,

$$K_{3(i)} = K_{e1(i)}\, K_{e2}$$

$$Q_{E\,LIM} = \frac{1}{2} Q_{E\,MAX}$$

Manipulation of equation (9) and remembering $Q_{E_{IDLE}} = 0$, yields,

$$\dot{Q}_{E(i)} = \frac{1}{\tau_{e3(i)}} \left(K_{3(i)} \left(\Delta w_f^*{}_{(i)} + \tau_{e2(i)} \Delta \dot{w}_f^*{}_{(i)} \right) - Q_{E(i)} \right) \qquad (10)$$

It is now assumed that the fuel schedule is a function of the difference in instantaneous and flight idle rotor speed, $\Delta\Omega$. At the condition of maximum torque output from the gas turbine, the fuel flow to the engine will be at a maximum constant level. Furthermore the rotor speed will have dropped below a certain minimum level denoted by, $\Omega_{Q_{MAX}}$, giving $\Delta\Omega^* = \Delta\Omega_{MIN}$ where,

$$\Delta\Omega_{MIN} = \Omega_{Q_{MAX}} - \Omega_{IDLE} \qquad (11)$$

so that $\Delta\Omega_{MIN}$ is naturally a negative quantity. During normal engine torque output operating limits, the fuel schedule is given by,

$$\Delta\Omega^* = \Delta\Omega$$

If rotor speed is greater than the maximum rotor speed denoted by $\Omega_{Q_{MAX}}$, the fuel flow is shut off (so that its value cannot be negative) by setting $\Delta\Omega^*$ to zero. Hence the three operating conditions of the fuel schedule can be written as,

$$\Delta\Omega^* = \begin{cases} \Delta\Omega_{MIN} & \Delta\Omega_{MIN} \geq \Delta\Omega \\ \Delta\Omega & 0 > \Delta\Omega > \Delta\Omega_{MIN} \\ 0 & \Delta\Omega \geq 0 \end{cases}$$

The variation of fuel flow, $\Delta w_f^*{}_{(i)}$, with rotor speed, $\Delta\Omega^*$, is shown graphically in Figure 2.9. It is interesting to note that this type of fuel schedule is very similar to the nonlinear actuator saturation functions used in flight control systems to prevent actuators from exceeding their authority. A description of this technique is given by Stevens and Lewis (1992).

In constructing the fuel schedule, it is necessary to evaluate the minimum rotor speed at which maximum engine torque output is achieved, $\Omega_{Q_{MAX}}$.

Let,

$$\Omega_{Q_{MAX}} = \Omega_{IDLE}\,\gamma \tag{12}$$

where γ denotes a rotor droop factor. Substituting equation (11) into (12) and rearranging for γ gives,

$$\gamma = \frac{\Delta\Omega_{MIN}}{\Omega_{IDLE}} + 1 \tag{13}$$

Under steady conditions equation (A1.26) reduces to,

$$Q_E = K_3\,\Delta\Omega \tag{14}$$

If the power plant is at maximum steady output, then equation (14) can be written as,

$$Q_{E\,MAX} = K_3\,\Delta\Omega_{MIN}$$

and substituting this expression into equation (13) enables the rotor droop factor to be evaluated from,

$$\gamma = \frac{Q_{E\,MAX}}{K_3\,\Omega_{IDLE}} + 1 \tag{15}$$

Therefore equations (6), (10) and (15) represent a twin gas turbine powerplant with a limited power output. An example of the use of this model is shown in Figure 2.10. In this test case, both engines are initially generating 5kNm torque to meet a demand of 10kNm. The maximum available torque from each gas turbine is specified to be 7.5kNm. At t=5s, number two engine is failed and subsequently engine number one begins to increase its torque output to compensate for the reduced net torque output. With the torque required from the powerplant held at 10kNm, it can be seen that the engine governor never permits this torque demand to be met by the remaining engine.

2.4 Model of Helicopter Artificial Stability and Flight Control Systems

The stability characteristics of a helicopter are such that in some conditions maintaining control of the rotorcraft can lead to excessively high pilot workload. For example, a conventional helicopter lacks static stability in hover with respect to changes in attitude as these perturbations produce virtually no aerodynamic restoring moment. Now consider a helicopter

hovering above an oilrig platform, the pilot effort required to perform the hovering task without the aid of a stability augmentation system may be sufficiently large as to detract him from the primary mission goal and/or the safety of the vehicle. Clearly, the role of an artificial stability system in providing effective stabilisation and improved handling characteristics of the rotorcraft is an important one and must be considered. However, compared to a conventional aircraft, the helicopter gives rise to a number of distinctive AFCS problems, namely:

1. The aircraft may be naturally unstable.
2. The vehicle is capable of hovering motion.
3. The pilot can control the major lift generator and the motion about the vehicle body axes.
4. Vehicle motion is highly coupled.

Further difficulties can be identified if a typical helicopter offshore flight is considered. During the transition phase of the flight to the oilrig, extended periods of trimmed flight will be experienced. Perturbations of the trimmed flight state must be stabilised by the flight control system or the advantage of decreased workload will be lost by the pilot continuously monitoring and re-trimming the helicopter. In this instance, it must be accepted that such a system is likely to operate for lengthy periods at large series actuator offsets. Without the presence of an automatic re-trimming facility, an actuator hardover during a crucial phase of the flight may pose significant piloting problems, although this will depend on the dynamics of the vehicle and safety features of the artificial stability system.

From the above discussion, the contribution of an artificial stability system to the behaviour of the helicopter is evident and consequently, a stability augmentation system of the type reported by Padfield (1981) has been included into the HGS mathematical model. The opportunity has also been taken to include a flight control system which defines the relationship between the pilot control inputs and his contribution to the blade pitch angles. This is an important modification to HGS as it permits the inverse simulation output to be expressed in terms of the collective lever, cyclic stick and pedal displacements instead of the blade pitch angles that were previously generated. As in the artificial stability system representation, the model of flight control system is as reported by Padfield (1981) and is shown in Appendix 4.

The influence of the artificial stability system is most conveniently demonstrated by conventional time response simulation. The time histories found in Figure 2.11 were obtained by applying a 5% longitudinal cyclic stick doublet to a helicopter initially in the hover. The results for both the SAS engaged and disengaged are shown. In Figure 2.11a the stabilising effect on pitch attitude clearly shown with the aircraft quickly converging to its original trim

position after 2.5 seconds. The unstabilised aircraft is dynamically unstable and does not recover to its original trim position.

2.5 Atmospheric Disturbance Modelling

The HGS model was modified to enable the influence of wind on the pilot strategy and vehicle behaviour to be evaluated. This modification is particularly important as a prevailing wind can significantly alter the power required and control margins of the helicopter and when operating in confined spaces such as those found in helicopter offshore platforms, can be crucial to the safety of the vehicle. A prevailing wind can also effect pilot strategy, and is particularly important during the low speed phases of a landing manoeuvre where the pilot for example, may find himself applying large degrees of side slip to counteract the influence of a strong cross wind. Finally, wind can increase the opportunity for the vortex ring state to develop particularly in the tail rotor.

2.5.1 Including the Effects of Atmospheric Disturbances into the Equations of Motion

The aerodynamic forces and moments acting on the helicopter are generated by the relative motion of air over the vehicle. In inverse simulation it is usual for the vehicle's trajectory to be expressed with respect to some Earth fixed axes set and previous investigations have assumed that the air surrounding the aircraft does not move relative to this axes set. The velocity time history of the helicopter may then be given by,

$$\mathbf{V}_{\mathbf{h,\,g}} = \mathbf{V}_{\mathbf{h,\,a}} \tag{16}$$

where $\mathbf{V}_{\mathbf{h,\,g}}$ and $\mathbf{V}_{\mathbf{h,\,a}}$ denote the velocity vectors of the helicopter with respect to the ground and air respectively.

Considering the influence of a prevailing wind, it is assumed that the wind velocity field is constant in the region in which the helicopter is immersed. Consequently, there are no significant wind speed variations over the rotorcraft and the helicopter can effectively considered as a point. Let $\mathbf{V}_{\mathbf{a,\,g}}$ denote the velocity vector of the air with respect to the ground, then, equation (16) can be rewritten as,

$$\mathbf{V}_{\mathbf{h,\,g}} = \mathbf{V}_{\mathbf{h,\,a}} + \mathbf{V}_{\mathbf{a,\,g}} \tag{17}$$

As the velocity of the wind with respect to the ground is known, then the velocity of the helicopter with respect to the air can easily be determined from,

$$\mathbf{V_{h,a}} = \mathbf{V_{h,g}} - \mathbf{V_{a,g}} \qquad (18)$$

The specification of the wind velocity is simplified if the horizontal components (in the Earth axes x-y plane) and vertical components are considered separately. The wind velocity in the Earth axes x-y plane is defined in terms of its absolute velocity component, V_{wind} and angle between the inplane velocity vector and the x axis denoted by $\psi_{a,g}$ and this is illustrated in Figure 2.12. The specification of the wind velocity is completed by defining the vertical component of wind, $V_{wind,vert}$ and this is chosen to be positive downwards. Hence, the three wind velocity components of the vector $\mathbf{V_{a,g}}$ can be obtained from,

$$V_{a,g} = \begin{bmatrix} -V_{wind} \sin\psi_{a,g} \\ -V_{wind} \cos\psi_{a,g} \\ V_{wind,vert} \end{bmatrix}$$

Therefore, once the Earth components of wind are known, the velocity of the helicopter with respect to air expressed in Earth axes may be determined from equation (18). It is then a simple matter to transform the resulting velocities through the Euler sequence (ψ, θ, ϕ) to determine the velocity of the airflow with respect to helicopter in vehicle body axes. The aerodynamic components of wind velocity at the rotorcraft centre of gravity u_a, v_a and w_a are the sum of the inertial velocities, u, v, and w, and the wind components $u_{a,g}$, $v_{a,g}$ and $w_{a,g}$. Thus,

$$u_a = u + u_{a,g}$$
$$v_a = v + v_{a,g}$$
$$w_a = w + w_{a,g}$$

The fuselage angle of incidence and side slip used to determine the fuselage forces and moments can be given by,

$$\alpha_{Fus_{aero}} = \tan^{-1}\left(\frac{w_a}{u_a}\right) \qquad \beta_{Fus_{aero}} = \sin^{-1}\left(\frac{v_a}{V_{f_{acro}}}\right)$$

where the aerodynamic flight velocity is given by $V_{f_{acro}} = \sqrt{u_a^2 + v_a^2 + w_a^2}$. Similar expressions can be obtained for the tailplane and fin. Hence, the aerodynamic forces and moments for the complete aircraft may be evaluated in the usual manner as found in Appendix 1.

The influence of wind on power required is demonstrated in Figure 2.13, where a carpet plot with engine torque as a function of wind speed and heading is shown. It should be

noted that each point on this plot represents the helicopter in hovering flight with zero ground speed and constant heading. From this plot, it is evident the presence of wind can result in significant torque increases when the wind has heading 090 or 270 degrees and this can be largely attributed to the dominant profile drag associated with the side planform of the fuselage.

2.6 Inclusion of Turbulence

In turbulent atmospheric conditions, the random nature of the velocity changes of the airflow with respect to the helicopter can lead to large perturbations in the forces and moments acting on the vehicle. Not only is this physically uncomfortable and distracting for the crew, but the subsequent increase in pilot control activity required to manoeuvre the rotorcraft particularly in confined areas can endanger the helicopter. Other important effects of turbulence can be highlighted by considering the helicopter AFCS. For example, a helicopter with an initially high trimmed series actuator offset in the cyclic pitch channel, penetrating a turbulence field. If the turbulence is of sufficient strength, the pitch actuator may reach the limit of its authority and consequently the rotorcraft effectively becomes unstabilised in pitch. This situation is clearly undesirable, especially if the aircraft is naturally unstable.

From the above discussion, turbulence can significantly influence the behaviour and operation of the rotorcraft and consequently the inclusion of this atmospheric effect is essential in this study of pilot strategies. A mathematical model of turbulence has been included into HGS, however, there are several techniques with which a turbulent stream suitable for simulation purposes can be generated and some of these are now discussed.

A relatively simple technique that is inexpensive in computational effort utilises the output of a random number generator with Gaussian properties filtered via a first order lag to generate a turbulent stream. The gain and time constant of the filter are adjusted until the power spectral density of the turbulent stream matches that of either the theoretical Dryden or von Kármán spectra, which are discussed by Hoblit (1988). This simple method allows the for teh efficient generation of a turbulent stream, however, it provides turbulence that is too regular with insufficient provision of large gusts.

An alternative means for the generation of a continuous stochastic turbulence stream can be achieved by reconstructing the random signal from a series of superimposed sinusoids. The gust output as a function of time, y(t), can then be determined from,

$$y(t) = \sum_{m=1}^{\infty} \cos(\omega_m t + \psi_m) \sqrt{\phi(\omega_m)\, \Delta\omega}$$

where,

$\phi(\omega_m)$ denotes the power spectral density of the turbulent signal and can be obtained from the Dryden or von Kármán spectra,
ω_m is the radian frequency of the each sinusoid component,
$\Delta\omega$ is the difference in frequency from stream m to m+1,
ψ_m is the phase angle of each constituent sinusoid signal.

The frequency range is chosen to ensure that the final synthesised turbulent signal contains the correct amplitude and frequency characteristics of actual turbulence relevant to aircraft simulation, while the phase angle is random in the region $(0,2\pi)$ with a white noise (or box car) probability density distribution. This approach of simulating turbulence discussed by Hoblit (1988), suffers from the same inadequacies as the previous method discussed above, in that the turbulent stream is too regular without the 'patchiness' that is a feature of actual turbulence.

The method adopted for the generation of turbulence in this investigation was formulated by Tomlinson and Bradley (1980) and is known as the Statistical Discrete-Gust Model (SDG) of Turbulence. Widely accepted and used in many aircraft simulation packages, the model incorporates the essential features of atmospheric turbulence that occur in reality. The model employs the view that turbulence is not a wholly random process and in fact contains a high degree of inherent order that is formed by an aggregation of simple gusts of basic structure. Thus the turbulence signal is formed from a series of superimposed gust structures that have a velocity profile similar to that of a vortex core. To ensure the correct frequency and amplitude characteristics of the turbulent stream, the velocity gradients and gust intensity are related to the important non-Gaussian features of actual atmospheric turbulence. Furthermore, the actual measured characteristics of turbulence to show a high probability of large and small gusts, with a corresponding low probability of medium intensity gusts is incorporated directly into the model. This feature of turbulence is known as intermittency and can be controlled directly to permit differing kinds of atmospheric turbulence to be calculated. An overview of the mathematical model of turbulence of Tomlinson and Bradley is shown in Appendix 5.

The application of the SDG model to inverse algorithm has been shown in Figure 2.15 where the control time history for a Lynx configured simulation flying at 40kts is shown. For the three component turbulence sample shown in Figure 2.14 employed in the simulation, the fraction of new gusts with zero intensity was set to, F=0.8, whilst the variance of the gust field was selected as, $\sigma = 0.9$. It may be observed from Figure 2.15 that there is a great deal of control activity which is required for rotorcraft to meet the velocity and acceleration profiles of

the manoeuvre. This is unrepresentative of a pilot response adopted in practice, since typically he will only react to those gusts embedded in the turbulence stream that impose an additional workload leaving the remainder to be tolerated as background vibrational discomfort, (Bradley et. al., 1994, Jones, 1971). As noted by Bradley et. al. (1994), the helicopter response to a gust will lie in an intermediate frequency range that separates the high frequency vibrational and low frequency long-period rigid body modes of the rotorcraft.

In addition to the aforementioned comments concerning the pilot strategy in response to a turbulence field, there is another limitation of the use of the SDG model in the context of this investigation of helicopter offshore operations, that merits brief discussion. A fundamental presupposition of the turbulence models given earlier in this section is that the turbulence velocity field is fixed with respect to time and convected past a point in space at the mean wind velocity (Taylor's hypothesis). Accordingly, measurement of the spatial and statistical properties of the turbulence field necessary for SDG model can be achieved using anemometers and wind vanes mounted on a tower or an instrumented aircraft. On account of Taylor's hypothesis, the subsequent measured fluctuations in time can be converted into spatial fluctuations using the relation,

$$f = V_{wind}\, k$$

where f is the frequency in Hz, V_{wind} is the relative velocity of the mean wind speed at a point and k is the spatial frequency in cycles per metre. Using this technique, the SDG model has been found to provide a realistic portrayal of atmospheric turbulence as documented by Jones (1971). An exception to the validity of Taylor's hypothesis, however, arises in the case of turbulence behind bluff bodies such as oilrig platforms. In this instance, large eddies from the rig structure will lead to significant time variations in the turbulence field due to relative movement of the wake and measuring point. In order to derive the correct statistical and spatial properties, a matrix of measurement instruments, situated in the platform wake, would be required to obtain the relevant turbulence spatial gradients. At the time the work was carried out, such information was not available and consequently caution must be employed in deriving conclusions from the application of the SDG model to this investigation.

2.7 Conclusions

A crucial prerequisite to the success of this research programme has been the modification of the HGS helicopter model to ensure that it did not impose any limitations on the range and validity of the final pilot strategy determined from the inverse algorithm. A detailed description of these enhancements has been given in this chapter. The rotor inflow prediction has received considerable attention and includes a model to portray the effect of the build up of

induced velocity in response to changes in blade states and the vortex ring phenomenon. A mathematical model of a twin gas turbine powerplant that realistically predicts the behaviour of an engine failure has also been included. Further, a stability augmentation and flight control system has been provided and this permits pilot collective lever, cyclic stick and pedal displacements to be determined. The influence of wind and turbulence may also be accounted for, however, the pilot control activity in response to the turbulence stream was found to be unrealistic.

These modifications ensure that the HGS helicopter model can be used with confidence in investigating the pilot strategies for offshore takeoff manoeuvres explored in the next chapter.

Chapter 3

A Generic Method For Offshore Manoeuvre Model Formulation and Validation

The use of inverse simulation in any investigation requires a mathematical model of the manoeuvre of interest and naturally the validity of the results will depend to a large degree on the accuracy of the manoeuvre description. The aim of this chapter is to present the development and application of a generic method for the formulation of accurate mathematical representations of offshore trajectories.

In an effort to formulate suitable manoeuvre models, the JAR documents for Category A operations were examined in detail. From this research, it was found that the recommended pilot strategy was defined in terms of both piloting procedure and performance goals at key positions in the manoeuvre. Describing manoeuvres in this way is deliberate, since it provides a degree of flexibility that ensures the recommendations are applicable to as wide a range of rotorcraft types and operating conditions as possible. Furthermore, no additional definitive geometry or trajectory time histories are specified within the governing framework of the Joint Aviation Requirements. This is justified on the grounds that the extra demands made of the pilot to satisfy a series of performance goals in addition to following a precisely defined trajectory would increase his workload to intolerable levels. It is clear from the above description, that although the JAR document provides sufficient guidelines for the pilot to construct a strategy, they are insufficient to allow the manoeuvre to be described in mathematical terms.

It is perhaps evident that an alternative approach is required to formulate a representative model of the flight paths adopted in practice. It is convenient to begin the discussion of this method by considering a pilot performing an arbitrary manoeuvre. The details of his piloting actions may be presented in the form of a narrative description that encapsulates key aspects of his strategy required to perform the manoeuvre. In the context of this research programme, the question arises as to whether it is possible to analyse the narrative of the pilot strategy in such a way as to allow a realistic mathematical description of the manoeuvre trajectory to be developed. The remainder of this chapter contends that the formulation of manoeuvre trajectories from a narrative of pilot strategy alone is possible and the method used to achieved this is now discussed.

As a result of an extensive and comprehensive investigation programme, a method comprising four key steps has been developed. Just as conventional trajectory models rely on

knowledge of the manoeuvre geometric properties, this approach emphasises the importance of an accurate narrative description of pilot strategy. The method is given as:

i) Formulation of Narrative Description of Pilot Strategy. This step has been made feasible with the assistance of N. Talbot of the Civil Aviation Authority. As a test pilot, Mr. Talbot's experience was central to the formulation of the descriptions of pilot strategies employed during takeoff and landing manoeuvres found in Appendix 8. As will become evident in future sections, the breadth and level of detail found in these descriptions provides a high degree of confidence in the fidelity of the final mathematical model of the manoeuvre.

ii) Manoeuvre Modelling. The modelling of trajectory time histories has been achieved using a technique similar to that used by Bradley and Thomson (1993) in their description of Mission Task Elements. In this research programme, the trajectory profile is represented in terms of a series of matched, low order polynomials that are used to portray one or more of the primary events of the manoeuvre. Smoothly connected after each section, these trajectory elements are used to describe the whole flight path and thus it is ensured that all the aspects of the piloting strategy during the manoeuvre are captured.

iii) Theoretical Prediction of Pilot Strategies. The inverse simulation algorithm shown in Appendix 2 has been used for the prediction of pilot strategies using the manoeuvre models mentioned above as input. In this instance, the helicopter mathematical model, HGS, with the enhancements detailed in Chapter 2, was employed to portray the rotorcraft behaviour.

iv) Qualitative Validation of Results. In this phase of the method, the theoretical pilot strategy predicted from part iii) is compared with that adopted in practice, i.e. the strategy found in stage i). A further step in the validation process was achieved by the use of a interactive, three dimensional, bespoke computer graphic software package. In this application, the real-time computer animation allowed rapid validation of the flight path and vehicle response by other specialists. This software was developed on a Silicon Graphics Indigo XS Workstation and is known as HOGS (**H**elicopter **O**ffshore **G**raphical **S**imulation). Written in the 'C' programming language, HOGS makes extensive use of the supporting graphic libraries available within the Silicon Graphics computer. An overview of the HOGS software is discussed in Appendix 9.

The application of the above steps to the analysis of a common offshore takeoff technique is considered a demanding and realistic test of the method and this task is demonstrated in the next section.

3.1 Application of the Method to the Towering Take-off Manoeuvre

Step i) - Formulation of Narrative Description of Pilot Strategy

A detailed description of the pilot strategy for a Towering Takeoff manoeuvre is given in Appendxi 8.1. To underpin the manoeuvre formulation method from concept to validation, the key aspects of the strategy are repeated in situ during the development of the manoeuvre model.

Step ii) - Mathematical Modelling of Manoeuvre

A portrait of the Towering Takeoff flight profile is shown in Figure 3.0 and it is evident that this manoeuvre is defined in terms of four distinct phases. In the following mathematical description the Initial Hover phase as discussed in Appendix 8 is not modelled, partly as this simplifies the overall definition, but also because this is considered as the least critical phase of the manoeuvre. As a consequence of this simplification it is assumed that the manoeuvre is initiated from a hover condition 5m (approximately 15ft) above the helideck. An earth fixed axes set is located at this point with the x-axis pointing North, the y - axis pointing East and the z-axis vertically downwards to complete a right-handed orthogonal frame. The inverse simulation requires time histories of the vehicle's velocity and acceleration throughout the manoeuvre related to this axes set.

On consideration of both the pilot's comments and the regulatory information it was decided that the most fundamental parameters associated with the towering take-off are the helicopter's velocity and climb rate, and hence the model now described is based on knowledge of these parameters. More specifically it is necessary to specify values for the altitude, h_{TDP}, and vertical velocity, v_{TDP}, at the takeoff decision point (TDP), and also the flight velocity, V_E, climb angle, γ_E, and altitude, h_E, at some notional exit point. As will become apparent it is also necessary to supply values for the peak accelerations expected during certain phases of the manoeuvre, and the time it is likely to take for the helicopter to reach these values. These figures are performance related and will depend to a large degree on the take-off mass of the vehicle.

Having specified the vertical velocity and height at the TDP the other two phases (Vertical Climb and Acceleration and Climb) are defined in such a way as to match one another at the TDP to produce a smooth transition.

The Vertical Climb Phase $(0 < t \leq t_{TDP})$

Care has been taken to capture all the principle features prevalent in the pilot strategy for this phase. The key elements of the pilot strategy are given in Appendix 8 as:

"From the initial hover, collective pitch is applied quickly for approximately 2 seconds until an engine or transmission limit is reached or the rate of climb is 500ft/min."

An effective means of incorporating the above strategy is to specify a vertical acceleration profile such as that shown in Figure 3.1a. In this representation it is assumed that from a trimmed hover condition, the application of collective will cause an increasing vertical acceleration up to some maximum value, $\dot{V}_{max}$, (depending on the collective setting). As the required vertical velocity, v_{TDP}, is approached the ideal situation is to reduce the vertical acceleration (by lowering collective) to zero hence giving a constant vertical velocity climb. This climbing phase is completed when the TDP height (h_{TDP}) is reached and the vehicle transitions to forward flight. A piecewise smooth polynomial function of time was used to obtain the profile shown in Figure 3.1a for the vertical acceleration. Its construction is given below:

$$
\begin{aligned}
&0 < t \leq t_1 && \dot{V}(t) = \left[-2\left(\frac{t}{t_1}\right)^3 + 3\left(\frac{t}{t_1}\right)^2 \right] \dot{V}_{max} \\
&t_1 < t \leq t_2 && \dot{V}(t) = \dot{V}_{max} \\
&t_2 < t \leq t_{CP} && \dot{V}(t) = \left[1 - \frac{3}{2}\left(\frac{t - t_2}{t_{CP} - t_2}\right)^2 + \frac{1}{2}\left(\frac{t - t_2}{t_{CP} - t_2}\right)^3 \right] \dot{V}_{max} \\
&t_{CP} < t_{TDP} && \dot{V}(t) = 0 \qquad \text{.....(19)}
\end{aligned}
$$

Cubic polynomial functions were chosen as they have been found to give an adequate degree of continuity whilst being relatively simple to implement. The values of the maximum acceleration, $\dot{V}_{max}$, and the time for the collective pulse, t_{CP}, must be supplied, and it is assumed that the pulse is symmetrical such that

$$t_1 = t_{CP} - t_2.$$

It is then possible to obtain the value for t_2 by enforcing the condition that at $t = t_{CP}$, the constant vertical velocity v_{TDP}, should have been acquired. This is achieved by integration of the acceleration profile :

$$\int_0^{t_{CP}} \dot{V}(t)dt = v_{TDP}$$

Although on completion of this collective pulse the required vertical velocity will have been reached, it is unlikely that a safe altitude will have been gained. It is therefore assumed that the helicopter continues its vertical climb at constant velocity as indicated in Figure 3.1b until the required altitude, h_{TDP}, is reached (at a time t_{TDP}). This time is readily obtained by noting that in a vertical climb,

$$v(t) = \int^t \dot{V}(t)dt$$

and,

$$\int_0^{t_{TDP}} v(t)dt = h_{TDP}.$$

A purely vertical climb from the take-off point is ensured by adding the further constraints that

$$\dot{x}(t) = 0 \quad \text{and} \quad \dot{y}(t) = 0,$$

throughout this phase.

<u>The Acceleration and Climb Phase</u> ($t_{TDP} \leq t < t_m$)

The adopted pilot strategy for this phase is composed of accelerative and climbing constituents. The former is given as:

"At the TDP, the pilot would make a positive nose forward cyclic input to achieve an accelerative attitude. A usual nose down attitude would be 15 degrees,.... after achieving the nose down attitude at the TDP, as speed increases, the pilot allows the nose to rise progressively until it ceases accelerating and it reaches an initial speed of 70kts."

The climb strategy is noted as:

"The collective may require adjustment to keep within engine and transmission limits and to establish a desirable initial rate of climb of 1000ft/min."

The requirement is to obtain some function which gives a realistic geometrical profile for this strategy whilst still satisfying the mathematical constraints imposed by the definition. Consider first the altitude function, this must satisfy the three conditions already imposed at the end of the vertical climb phase (i.e. at $t = t_{TDP}$, $z = -h_{TDP}$, $\dot{z} = -v_{TDP}$ and $\ddot{z} = 0$), whilst also meeting the requirements at the exit. The exit flight state is a constant velocity, V_E, climb at some angle γ_E, whilst at the exit point the altitude should be h_E. This gives the exit conditions

$$t = t_m, \quad z = -h_E, \quad \dot{z} = -V_E \sin\gamma_E, \quad \ddot{z} = 0.$$

The least degree polynomial satisfying these conditions for the altitude profile, z(t) is therefore a fifth order polynomial, Figure 3.1c, where the six constant coefficients are selected to satisfy the six conditions specified above. Note that the choice of a higher order polynomial permits the altitude at the exit point to be directly specified and thereby contributing to the realism of the flight path profile.

The most appropriate way of satisfying the velocity requirement at the exit has proved to be the specification of a longitudinal acceleration profile, $\ddot{x}(t)$. The chosen profile is shown in Figure 3.1d, and is identical in form to that used for the acceleration in the vertical climb phase. Consequently, the functions for $\ddot{x}(t)$ are similar to those given by equation (19). This profile gives a rapid change in acceleration from zero up to a maximum value, $\ddot{x}_{max}$, (as before this value is specified and is related to the performance capabilities of the helicopter) which is maintained until the commanded forward speed is approached and the acceleration is reduced until a constant flight speed is attained. As with the vertical climb, the time taken to achieve maximum acceleration, $(t_3 - t_{TDP})$, and the time taken to establish constant velocity at the exit, $(t_m - t_4)$, must be supplied. It is then possible, given that V_E and γ_E are also known, to obtain a value for the time spent at constant acceleration, $(t_4 - t_3)$, from the expression,

$$\int_{t_{TDP}}^{t_m} \ddot{x}(t)dt = V_E \cos\gamma_E$$

The final condition imposed during the flyaway section is that there should be no lateral motion and hence

$$\dot{y}(t) = 0.$$

The definition of the Towering Take-off is completed by the additional constraint that heading should be maintained constant throughout.

The use of smooth piecewise polynomial representations of manoeuvres may seem an unrealistic over-simplification of the actual situation. Previous work on helicopter nap-of-the-

earth manoeuvres and Mission Task Elements by Bradley and Thomson (1993), including comparison between the actual flight trajectories and the polynomial models, has indicated that this approach can give realistic and valid profiles.

Step iii) and iv) - Inverse Simulation and Validation of Towering Takeoff Manoeuvre

It is necessary to provide only a few basic parameter values to use the definition of the Towering Take-off given above. In the following example the parameter values are

$$h_{TDP} = 10\text{m}, \quad v_{TDP} = 2.5 \text{ m/s } (\equiv 500\text{ft/min}), \quad \dot{V}_{max} = 2 \text{ m/s}^2, \quad t_{CP} = 2 \text{ s}$$
$$\ddot{x}_{max} = 3.5 \text{ m/s}^2, \quad t_3 - t_{TDP} = 2.5\text{s}, \quad t_3 - t_m = 14\text{s}, \quad V_E = 70 \text{ knots}, \quad h_E = 70\text{m},$$
$$\gamma_E = 8 \text{ deg } (\equiv 1000\text{ft/min at } 70 \text{ kts}).$$

These values are representative of those routinely encountered during take-off from offshore installations. Note that the TDP height is referred from the starting height of the climb (5m) and therefore represents an altitude of 15m above the helideck. Time histories of several of the flight path variables are shown in Figure 3.2. The time to reach TDP is 5 seconds and the manoeuvre completion time is approximately 25 seconds. From the vertical acceleration profile, the initial pulse takes 2 seconds (as indicated by the piloting description given in Appendix 8.2(ii)) by which time the vertical velocity is 2.5 m/s. The TDP is reached at about 5 seconds, after which the acceleration and climb phase begins with a rapid increase in forward acceleration, the maximum value being set at 3.5 m/s^2 to be reached after 4 seconds. The velocity increase in conjunction with the relatively slow initial increase in height leads to a rapid decrease in climb angle from 90 degrees at the TDP to a value slightly below the required exit condition of 8 degrees at approximately 15 seconds. Thereafter, as the required constant velocity is approached, and the climb rate begins to increase and the climb angle slowly increases towards its final constant value. The resulting flight path trajectory is also shown in Figure 3.2.

This manoeuvre information may be used to drive the Helinv inverse simulation thereby producing time histories of the helicopter's states and controls. The helicopter configurational data used in this paper is characteristic of a large transport vehicle of the class likely to be employed in offshore operations (based on the Sikorsky S-61). A brief summary of this data is given in Table 1.

Parameter	Value
Aircraft Mass (kg)	8000
Rotor Radius (m)	9.5
Rotor Solidity	0.0363
Flapping Stiffness (kNm/rad)	160
Maximum Power Output (SHP)	2800
Rotor Speed at Flight Idle (rad/s)	22

Table 1 : Leading Parameters for Transport Helicopter Configuration

The inverse simulation results for the transport configuration flying the towering take-off described above are shown in Figure 3.3 The vertical climb section of the manoeuvre is clearly visible from these plots : over the first 5 seconds there is little cyclic motion and hence little change in attitude, whilst at the same time there is firstly a pulse in collective lever to produce the desired vertical acceleration, followed by an offset in collective setting from the trim position producing the constant vertical velocity climb. The effect of the collective pulse on engine torque and rotorspeed are also apparent with both engines peaking at about 82% of their maximum torque, and the rotorspeed falling by a small amount. After the TDP there is a ramp in forward cyclic stick of 20% to induce a nose down pitch attitude of about 15 degrees in order to achieve the commanded forward acceleration. After this pulse there is a short aft stick pulse to arrest the nose down motion followed by a more sustained but slow forward stick motion to account for the disc flapping backwards as forward speed is increased. The nose down attitude is maintained until about 12 seconds elapsed time at which point a slow aft stick motion begins to raise the nose. Note that the stick forward pulse which initiates the acceleration is much more aggressive than the subsequent stick back motion - this is to reflect the likely piloting strategy of clearing the helideck as quickly as possible after the decision to climb away has been taken. During the acceleration and climb phase the collective is initially increased to produce the desired climb rate, but is subsequently reduced towards the end of the manoeuvre as speed increases, and the desired flight state is reached. With the reduction in collective, the engine torque and power fall whilst the rotorspeed increases slightly. It is also noticeable from Figure 3.3 that there are only very small changes in the lateral cyclic position and roll attitude, whilst there is a gradual change in pedal position as forward speed is increased.

Comparing the discussion above with the piloting comments Appendix 8.1 and 8.2 it is clear that the key features of an initial 2 second pulse in collective and a subsequent pulse in forward cyclic leading to a 15 degree pitch down attitude are closely predicted by the inverse simulation through its defined trajectory. The manoeuvre as defined reaches about 82% of

nominal maximum torque and therefore complies with the AEO requirement in Appendix 8.1(i).

The method is completed by extending the validation process through the inspection of the results using computer animations and graphs by other specialists - in this instance, N. Talbot of the Civil Aviation Authority.

The approach has been used to develop a mathematical model of a landing manoeuvre and this is shown in Appendix 6.

3.2 Conclusions

The stimulus supporting the need for the authentic formulation of manoeuvre models has been stated at the beginning of this chapter. The Joint Aviation Requirements have been analysed in order to place in context the rationale underpinning the development of the manoeuvre formulation method given. The generic manoeuvre formulation approach was demonstrated by its application to a common offshore takeoff manoeuvre. In this instance, the direct comparison of simulated and actual pilot strategies proved to be encouraging and in conjunction with inspection of the results using a purpose-built computer graphics facility, fully vindicates the method.

From a review of Chapter 3, one can identify the key ingredients of the method leading to the formulation of the Towering Takeoff manoeuvre model. They can be summarised as follows:

i) Formulation of a detailed narrative description of pilot strategy of the manoeuvre of interest.

ii) Mathematical modelling of the flight path using polynomial functions time to represent key elements of the pilot strategy.

iii) The application of inverse simulation to obtain theoretical pilot strategy.

iv) Qualitative validation of simulated results by comparison theoretical strategy with that adopted in practice, i.e. the strategy found in i). Application of computer graphics for validation by other specialists.

The generic manoeuvre formulation method has been a crucial technical development in this research programme since it fully integrates all aspects of helicopter offshore operations

into a form suitable for theoretical simulation technique. This is an important feature when the role of the JAR and other operational criteria are considered. Some of these aspects of offshore operations are explored in Chapter 4.

Chapter 4

A New Concept in Rotorcraft Simulation

The study of pilot strategy in response to an engine failure is crucial in any investigation of helicopter offshore operations. In particular, engine failures during takeoff and landing phase of operations can pose a serious threat to vehicle safety, as the low speed nature of these manoeuvres and the proximity of the rig limits pilot strategy. The fundamental importance of engine failures during takeoff and landing manoeuvres is also reflected by the detailed and extensive narrative descriptions of vehicle performance and pilot strategy in response to engine failures found in JAR documents. Indeed, the JAR documentation extends its description of pilot strategy to include specification of pilot reaction time:

"The pilot engine failure recognition time delay before adjustment of the collective pitch control should be a minimum of 1 second unless it can be demonstrated that the pilot will have unmistakable engine failure cues sooner than 1 second."

Clearly, a prerequisite for this study is that the inverse simulation algorithm must be capable of predicting pilot strategy in all flight regimes, including those where an engine failure has occurred. The conventional approach to inverse simulation is to first define the complete manoeuvre in terms of a series of equally spaced time points that form the trajectory of the centre of gravity of the rotorcraft. Since the flight path information is expressed in terms of a time history, the inverse solution progress' in a 'time marching' form evaluating the controls necessary to meet the exigencies of the flight path at each point in the trajectory. When applying this approach to manoeuvres that suffer an engine failure, however, there are two problems, namely:

i) After engine failure, the performance of the helicopter will be impaired by the power and torque limitations and consequently there is no guarantee that the manoeuvre as defined initially, can be still be flown.

ii) Even if the original manoeuvre can still be performed, it is unrealistic to simply continue with inverse simulation exactly from failure point, albeit taking into account the effect of the failed engine. This would assume that the pilot was immediately aware of the engine failure, and was able to compensate for the lost engine infinitely quickly. In effect the time delay due to the pilot's reaction to warning signals etc., has not been included.

To overcome the above problems, a conceptually new rotorcraft simulation algorithm has been developed. The rationale supporting the architecture of the simulation algorithm is explored in the next section.

4.1 The Development of a Novel, Hybrid, Simulation Algorithm Allowing Analysis of Pilot Reaction Time.

In essence the problem to be solved is that, it is no longer possible to completely define the whole manoeuvre without consideration of the changes in vehicle dynamics induced by engine failure. Subsequently, the most convenient approach is to consider the manoeuvre as consisting of various phases, and then apply either the forward or inverse simulation as appropriate. The final scheme adopted is as follows:

i) The complete manoeuvre (a Towering Takeoff for example) is defined over a time interval t=0 to $t=t_m$ as presented in Chapter 3.

ii) A conventional inverse simulation is used up to the point $t = t_{pr} = t_{fail} + t_r$. The implication here is that the engine fails at some time point $t=t_{fail}$ in the manoeuvre, and it takes the pilot a time t_r to react to this failure. The justification for the continuation of inverse simulation over the interval $t=t_{fail}$ to $t=t_{fail} + t_r$ merits brief discussion. It is assumed that during this phase the pilot will not have perceived the engine failure and will therefore continue to fly the manoeuvre as if he had full engine power available. The inverse simulation over this phase therefore calculates the control strategy associated with the engine model simulating a fully operational powerplant.

iii) Before a recovery path can be defined it is necessary to obtain the states and position of the helicopter at the pilot's reaction point. For this information, a conventional time response calculation is employed from $t=t_{fail}$ to $t=t_{pr}$ using the control inputs calculated for the non-engine-failure inverse simulation of this phase, but applied to the helicopter mathematical model with the effect of the engine failure included.

iv) Using the current vehicle earth axis position, velocity and accelerations, the recovery manoeuvre is evaluated from $t=t_{pr}$ to $t=t_R$, where t_R denotes the recovery manoeuvre time. Having obtained a mathematical description of the trajectory in a manner described in the following section, it is possible to return to a conventional inverse simulation and obtain the corresponding control strategy.

The resulting simulation algorithm is termed 'HIFIS' (Helicopter Inverse Forward Inverse Simulation). The operation of this algorithm is illustrated in flowchart form in Figure 4.0 where the separate application of inverse and conventional simulation procedures throughout the complete manoeuvre are evident.

4.2 Extension of the Generic Manoeuvre Formulation Method to Recovery Manoeuvres.

The final phase of the HIFIS program is the inverse simulation of the recovery manoeuvre after the engine failure. As in Chapter 3, the difficulties associated with forming representative mathematical manoeuvre models is derived from the fact that the only suitable information source is provided in terms of the narrative description of pilot strategy.

In adopting this technique for the formulation of recovery manoeuvres profiles, a further technical development is required. Consider the emergency procedures and strategies presented in Appendix 8. These indicate that the recovery manoeuvre employed should either rejoin the aircraft to its original flight path or be a completely new recovery trajectory. Furthermore the recovery action initiated by the pilot must reflect the helicopters current state of safety both in terms of the position which it holds in the pilot's immediate priorities and the rate with which this action is carried out once initiated. For example, a helicopter experiencing a single engine failure just after the critical decision point would result in the pilot immediately initiating a recovery manoeuvre with rapid execution of a pitch down and descent as is shown in Figure 4.1. In contrast, a helicopter suffering an engine failure near the end of a Towering Takeoff manoeuvre would possibly result in the pilot initiating recovery action after checking the immediate cause of the failure - with the recovery manoeuvre undertaken as to cause least disturbance to crew and cargo. The application of matched, low, order polynomial functions of time will not be sufficient to authentically portray these features of pilot strategy.

To create a mathematical description of a recovery manoeuvre, the problem is one of finding a suitable geometric profile to match defined entry and exit conditions. The entry conditions are defined by the final point on the time response calculation over the period from pilot reaction and response time and in effect represents the deviation from the desired trajectory. The exit conditions are defined (by the user) in terms of a desired altitude, flight velocity, climb rate or some combination of these. It is also desirable that the mathematical representation of the flight paths must encapsulate the initial boundary conditions up to and including at least the jerk components, while preventing the generation of unrepresentative points of inflexion. Furthermore it would be useful if a range of recovery flight paths could be generated that satisfy a single recovery manoeuvre boundary condition set, allowing the influence of pilot strategy to be investigated.

The mathematical formulation of a recovery manoeuvre capable of meeting the requirements outlined above are detailed in the following section.

4.2.1 Mathematical Formulation of Generic Recovery Manoeuvre

The requirement for a recovery manoeuvre is for some function h(t) that blends smoothly from the trajectory f(t) resulting from the departure from the desired flight path to some final safe trajectory or condition, (or the original flight path) g(t), see Figure 4.2 The recovery is initiated at the point where the pilot has reacted to the engine failure, and decided upon his strategy for recovery, t_{pr}. It is assumed that the required final point of the recovery manoeuvre is where the original trajectory (or new trajectory) is reached and this occurs at a time t_R.

The recovery manoeuvre is completed at time t_{pr}, at which point either the original trajectory has been regained or a revised trajectory has been joined.

From Figure 4.2, it is clear that,

$$h(t)=g(t)+\phi(t) \qquad (20)$$

where $\phi(t)$ is the function used to undertake the blending process. The entry ($t=t_{pr}$) and exit ($t=t_R$) conditions to the recovery manoeuvre can be written as,

$$h^m(t_{pr}) = g^m(t_{pr}) + \phi^m(t_{pr}) \qquad \text{for m=0 to M}$$

and,

$$h^n(t_R) = g^n(t_R) + \phi^n(t_R) \qquad \text{for n=0 to N}$$

where M and N are the degrees of required derivative continuity at $t=t_{pr}$ and $t=t_R$ respectively. The blending function also satisfies,

$$\phi^m(t_{pr}) = f^m(t_{pr}) - g^m(t_{pr}) \qquad \text{for m=0 to M} \qquad (21a)$$

and,

$$\phi^n(t_R) = 0 \qquad \text{for n=0 to N} \qquad (21b)$$

A suitable function $\phi(t)$ for the blend must now be chosen. In previous inverse simulation work, much use has been made of simple polynomials for flight path definition. The further step of biasing a general polynomial has been taken to allow the variation of speed at which the recovery is undertaken. The general form of the blending function is then,

$$\phi(t) = e^{-\delta t}\, p(t) \qquad (22)$$

where p(t) is a polynomial whose order is chosen to ensure the required derivative continuity at entry and exit is met (the order is then M+N-1), whilst the value δ may be varied to influence the rate at which blending is effectively achieved.

Consider the case where continuity up to the third derivative is required at both the entry and exit of the recovery manoeuvre. This gives the boundary conditions:

i) $t=t_{pr}$ $\quad \phi(t)=\phi(t_{pr})$ $\quad \phi'(t)=\phi'(t_{pr})$ $\quad \phi''(t)=\phi''(t_{pr})$ $\quad \phi'''(t)=\phi'''(t_{pr})$

ii) $t=t_R$ $\quad \phi(t)=0$ $\quad \phi'(t)=0$ $\quad \phi''(t)=0$ $\quad \phi'''(t)=0$

and hence the polynomial, p(t), will take the form:

$$p(t) = a_0 + a_1 t + a_2 t^2 + a_3 t^3 + a_4 t^4 + a_5 t^5 + a_6 t^6 + a_7 t^7$$

Clearly once the values of $p(t_R)$, $p'(t_R)$,....,$p'''(t_R)$ are known it is a simple case of solving eight simultaneous linear algebraic equations to find a_0, ..., a_7. To obtain the values of these boundary conditions, equation (22) must be successively differentiated to give,

$$p(t) = \phi(t)\, e^{\delta t}$$

$$p'(t) = \phi'(t)\, e^{\delta t} + \delta\, \phi(t)\, e^{\delta t}$$

$$p''(t) = \phi''(t)\, e^{\delta t} + 2\delta\phi'(t)\, e^{\delta t} + \delta^2\phi(t)\, e^{\delta t}$$

$$p'''(t) = \phi'''(t)\, e^{\delta t} + 3\delta\phi''(t)\, e^{\delta t} + 3\delta^2\phi'(t)\, e^{\delta t} + \delta^3\phi(t)\, e^{\delta t}$$

This results in the required boundary conditions in terms of $\phi(t)$ and its derivatives, which, at the times $t=t_{pr}$ and $t=t_R$, are given by equations (21a) and (21b). In equation (21a) the values of $f^m(t_{pr})$ are simply the final conditions of the time response calculation performed over the pilot's reaction time.

For the conditions at the final point there are two options. Firstly, if the blend is to return the helicopter back to the original defined trajectory, then it is a case of evaluating $g(t_R)$, $g'(t_R)$, etc. from the known profile, see Figure 4.2. The more likely case is that an alternative flight trajectory will be required simply due to the fact that the original may be unflyable due to the now limited power available. In these circumstances, the new values for $g(t_R)$ and its derivatives need to be determined.

Alternatively, simple acquisition of some predefined flight condition may suffice. For example, recovery from an engine failure after the TDP of a towering takeoff may be considered as the achievement of a steady climb rate at constant heading at some altitude above the sea. Again the values $g(t_R)$, $g'(t_R)$ etc. are readily found.

An example of a recovery manoeuvre rejoining the original flight path is now discussed. Figure 4.3 presents the flight path for a Towering Takeoff manoeuvre. The inverse - forward simulation transition occurs at t=15s with the forward phase being employed for a duration of 5 seconds (a unrealistically long reaction time has been selected as a demonstration). As mentioned previously, the helicopter will 'drift' a small amount from the desired flight path during the forward phase and this is evident from the plot. For the case when it is it necessary to rejoin the original trajectory, an additional blending flight path that provides a smooth transition from the current to the original flight path is required. The four different data sets correspond to the original trajectory and the three values of the recovery lag, δ_z. The benefit of biasing the blending function can be seen as it enables the rate at which the final exit condition is achieved to be controlled.

An example of a recovery manoeuvre for rejoining a new trajectory during a Towering Takeoff is demonstrated in Figure 4.4. The inverse - forward simulation transition occurs at t=5s with the forward phase being employed for a duration of 1 second. The influence of the manoeuvre lags on each of the longitudinal, lateral, altitude and heading time histories is highlighted in Figure 4.5.

The task of obtaining a mathematical description of a recovery trajectory, however, is further complicated for two reasons. Firstly, not only is it important for the mathematical description of the recovery manoeuvre to closely match the actual flight path, but it must also encapsulate the various pilot strategies used when an engine failures occurs during differing phases of the offshore operations considered in this study. Consider the case where a helicopter experiences an engine failure close to the oilrig platform during a landing manoeuvre, the proximity of the rig structure may influence pilot strategy so that heading and altitude become the key flight path parameters crucial to the safety of the helicopter. In the event of an engine failure towards the end of a towering takeoff manoeuvre, however, the influence of helicopter longitudinal velocity could be of prime concern in the piloting strategy. Therefore, the importance of single or multiple flight path parameters in the definition of the recovery trajectory can be accommodated by individually selecting the blending rate parameter, δ, for each of the flight path constraints. This is demonstrated in Figure 4.6, where the longitudinal, lateral, altitude and heading flight path time histories, evaluated using separate values of the blending rate parameter, are shown. The figure clearly shows the importance of individually specifying the blending rate parameter for each of the four flight path constraints of the takeoff and landing manoeuvres. Secondly, the range and scope of helicopter recovery manoeuvres ensures that

if the recovery flight paths are to be realistically portrayed, the blending formulation must be applied individually to each recovery manoeuvre class and this is the topic of the next section.

4.3 Application of Manoeuvring Modelling Method to Continued Takeoff

The manoeuvre modelling method demonstrated in Chapter 3 is now applied to the formulation of a Towering Takeoff accompanied with an engine failure after the takeoff decision point.

Part i) - Formulation of Narrative Description of Pilot Strategy

The pilot strategy for a response to an engine failure during this phase of a Towering Takeoff manoeuvre is given in Appendix 8.3. The key piloting elements of the strategy are included in situ in order to place in context the rationale supporting the selection of corresponding manoeuvre profile.

Part ii) - Mathematical Modelling of Manoeuvre

On recognising the engine failure after the TDP, the adopted pilot strategy is noted as:

".... the helicopter will follow a descending flight path as speed is gained and the pilot will have to lower the collective shortly after the engine ...."

The conditions on completion of the recovery manoeuvre are given as,

".... when 45kts has been established, steady climb is maintained using maximum engine power."

The requirement for the recovery trajectory is to capture these aspects of the pilot strategy. Considering the altitude time history, z(t), the most suitable profile found is shown in Figure 4.7a where it is evident that a blend has been used to transition the rotorcraft from its original trajectory to the final exit manoeuvre. At the end of the manoeuvre, it is assumed the rotorcraft will achieve a flight speed (V_{EXIT}) and rate of climb (v_{EXIT}) at some notional exit point at a height, h_{EXIT}, above the helideck. The altitude time history may then be given by,

$$z(t) = h_z(t) = \phi_z(t) + g_z(t) \qquad t_{pi} < t < t_R$$

where,

$$\phi_z(t) = e^{-\delta_z t}\, p_z(t) \qquad g_z(t) = -h_{EXIT} - \int_t^{t_R} v_{EXIT}\, dt$$

The z component blend gain, δ_z, is chosen to reflect the rate at which the final altitude exit conditions are met and can be used to ensure that the performance requirements outlined in Appendix 8 are satisfied. A seventh order polynomial function of time, $p_z(t)$, is chosen to satisfy the eight boundary conditions given as,

i) $t = t_{pr}$ $\quad p_z(t)=z(t_{pr}) - g_z(t_{pr})$ $\quad p'(t)=\dot{z}(t_{pr})$ $\quad p''(t)=\ddot{z}(t_{pr})$ $\quad p'''(t)=\dddot{z}(t_{pr})$

ii) $t = t_R$ $\quad p_z(t)=0$ $\quad p_z'(t)=0$ $\quad p_z''(t)=0$ $\quad p'''(t)=0$

which can satisfy the fifth order polynomial,

$$p_{\dot{z}}(t) = b_0 + b_1\left(\frac{t^*}{t_R^*}\right) + b_2\left(\frac{t^*}{t_R^*}\right)^2 + b_3\left(\frac{t^*}{t_R^*}\right)^3 + b_4\left(\frac{t^*}{t_R^*}\right)^4 + b_5\left(\frac{t^*}{t_R^*}\right)^5$$

where,

$$t^* = t - t_{pr} \qquad\qquad t_R^* = t_R - t_{pr}$$

The longitudinal manoeuvre profile is governed by the piloting strategy,

".... the pilot action at the TDP is to pitch the nose down, typically to an angle of 15° using a positive forwards cyclic input whether or not an engine failure has occured."

An effective way of incorporating this aspect of the recovery manoeuvre is to specify a longitudinal velocity profile, $\dot{x}(t)$, similar to that illustrated in Figure 4.7b. From this plot it is clear that the combination of a blend and final exit component have been used to define the longitudinal profile. The longitudinal velocity time history during the recovery can be obtained from,

$$\dot{x}(t) = h_{\dot{x}}(t) = \phi_{\dot{x}}(t) + g_{\dot{x}}(t) \qquad\qquad t_{pr} < t < t_R$$

where,

$$\phi_{\dot{x}}(t) = e^{-\delta_{\dot{x}} t}\, p_{\dot{x}}(t) \qquad\qquad g_{\dot{x}}(t) = V_{EXIT}\cos\gamma_{EXIT}$$

and,

$$\gamma_{EXIT} = \sin^{-1}\left(\frac{v_{EXIT}}{V_{EXIT}}\right)$$

The term $\delta_{\dot{x}}$ controls the rate at which the final velocity profile is adopted. The polynomial function of time used in the blend, $p_{\dot{x}}(t)$ is of degree five and satisfies the six boundary conditions,

i) $t = t_{pr}$ $\quad p_{\dot{x}}(t) = \dot{x}(t_{pr}) - V_{EXIT}\cos\gamma_{EXIT}$ $\quad p_{\dot{x}}'(t) = \ddot{x}(t_{pr})$ $\quad p_{\dot{x}}''(t) = \dddot{x}(t_{pr})$

ii) $t = t_R$ $\quad p_{\dot{x}}(t) = 0$ $\quad p_{\dot{x}}'(t) = 0$ $\quad p_{\dot{x}}''(t) = 0$

The formulation of the recovery is completed by defining the lateral and heading manoeuvre profiles and this is most conveniently achieved by specifying the lateral displacement and heading time history denoted by y(t), and $\psi(t)$. Expressions for these are given by,

$$y(t) = h_y(t) = e^{-\delta_y t}\, p_y(t) \qquad t_{pr} < t < t_R$$

$$\psi(t) = h_\psi(t) = e^{-\delta_\psi t}\, p_\psi(t) \qquad t_{pr} < t < t_R$$

Part iii) and iv) - HIFIS Simulation and Validation of Continued Takeoff Manoeuvre

For this case the simulated engine failure occurs 1 second after the TDP (i.e. 6 seconds into the manoeuvre) and the recovery from this initially follows the nose down acceleration of the normal take-off, but is then followed by a much slower climb from below the level of the platform. The demanded exit condition in this case is,

$$h_E = -15\text{m}, \quad V_E = 45 \text{ knots}, \quad v_E = 0.5 \text{ m/s} \ (\cong 100 \text{ ft/min}).$$

and it is evident from Figure 4.8 where the manoeuvre trajectory information is presented, that these conditions are attained.

Note that the given exit height is a displacement form the starting point of the manoeuvre (5m above the deck) and therefore represents a location approximately 10m below the level of the heli-deck. The simulation results are shown in Figure 4.9. The pilot's response occurs during the normal initial pulse of longitudinal cyclic which initiates the acceleration. The first action taken is to apply a second sharp pulse in cyclic to reinforce the nose down pitch attitude (in this case to 8 degrees) to ensure the deck edge is cleared. This input is accompanied by a rapid drop in collective to maintain rotorspeed. The lower collective settings in this case takes the helicopter to a much lower altitude, and combined with smaller longitudinal cyclic inputs produces a much lower rate of climb than in the normal take-off. The effect of the engine governor is clearly visible with the engine torque being reduced when the rotor speed exceed its flight idle value. Two intervals may be observed when the torque of the good engine reaches its

contingency limit. The first begins just after failure, and as a consequence the rotor decelerates as the kinetic energy is absorbed to compensate for the torque deficit needed to initiate the next stage of the manoeuvre. After a further 4 seconds, the strategy of reducing the collective begins to pay dividends and surplus torque is available to accelerate the rotor back to its reference speed - which it reaches 6 seconds later. The demands of the climb-out phase produce the second interval of torque limiting later in the manoeuvre (between 13 and 23 seconds of the elapsed time) and again the plot of the rotor speed shows the initial surrender of kinetic energy to exigencies of the trajectory and its restoration as the manoeuvre severity ameliorates.

Again the results of the simulation may be seen to be generally consistent with the description of section 8.3(ii). As a result of the decrease of collective pitch the rotor speed is generally maintained at its reference value apart from the transitory reductions to 4% below nominal during the periods of torque limiting noted above. The pulse of cyclic to give forward pitch is a little larger in this case to give an accelerated entry into the descent phase.

It is worth noting that the flight path reveals this to be close to the limiting case for this type of manoeuvre. There are two intervals of torque limitation during which the rotorspeed falls significantly and the recovery flight path, in reality, would be close to the surface of the sea.

A range of suitable takeoff and landing recovery manoeuvres have been developed using the preceding method and this is presented for convenience in Appendix 7.

4.4 Conclusions

A discussion of pilot strategy and the analysis of the JAR has revealed the importance of engine failures during the takeoff and landing phases of offshore operations. The technical developments necessary to portray this aspect of helicopter procedures has resulted in a new concept in rotorcraft simulation. It has been demonstrated that the initial pilot reaction is modelled in a natural manner since the changes in the rotorcraft dynamics due to the engine failure are directly accounted for by the application of matched phases of conventional and inverse simulation. The transition from inverse to forward and forward to inverse simulation algorithms is accomplished smoothly and has been shown to produce no adverse effects on the prediction of pilot strategy. The trajectory formulation method presented in Chapter 3 has been extended successfully to manoeuvres that incorporate an engine failure. This has been achieved by the application of a biased polynomial function of time. This technique enables control over the rate at which the new pilot strategy is adopted whilst being flexible sufficiently to permit its application to a wide range of recovery manoeuvres. Comparison of the simulated Continued Takeoff pilot strategy with that used in practice was found to be very encouraging.

There is no precedent for the study of pilot reaction to engine failures using the techniques described above, as not only do they treat the concept of an engine failure in its entirety, but their development is motivated by the philosophy of placing pilot strategy foremost in the investigation. Consequently, the use of these techniques in the case studies presented in the next chapter, will justify a high degree of confidence in the scope and validity of the results.

Chapter 5

Investigation of Rotorcraft Safety Issues In Helicopter Offshore Operations

In the first chapter of this thesis two conditions were identified as necessary before the goal of developing a simulation methodology capable of investigating helicopter offshore operations could be realised. The first condition relates to the development of a validated simulation algorithm that could accurately portray the pilot strategy. How this requirement was satisfied has been demonstrated in Chapters 2, 3 and 4 of this thesis. The second condition concerns the development of an investigation philosophy that utilises key manoeuvre parameters to determine the validity of the pilot strategy. This chapter defines this investigation philosophy and demonstrates its application to the rotorcraft safety issues identified in Chapter 1.

Previous investigations of helicopter takeoff and landing procedures have concentrated on evaluating the maximum rotorcraft mass for a given manoeuvre. Forcing the rotorcraft to operate at these weights effectively prevents investigation of alternative, valid, pilot strategies and clearly this is incompatible for the analysis of the safety issues discussed in Chapter 1. Furthermore, for some offshore manoeuvres, this investigation has shown that evaluating the maximum operational mass of the rotorcraft will result in excessive aircraft operating weights that are not consistent with those found in actual offshore operations. For example, the maximum simulated landing mass for a S61 was found to be 11850kg when the recommended maximum takeoff mass for this aircraft is in fact 7900kg.

By considering the deficiencies mentioned above, a new philosophy has been conceived for this investigation. Firstly pilot strategy is placed foremost in the investigation; instead of determining the success of a manoeuvre solely on vehicle performance, realistic constraints that reflect those restrictions that the pilot would encounter in practice are applied. Secondly, the rotorcraft behaviour is determined for realistic operating weights for all manoeuvres. Finally the aircraft operation and pilot strategy are regulated to ensure compliance with criteria outlined in the Joint Aviation Regulations. By adopting this approach, realistic piloting procedures will be determined for all flight conditions.

This investigation philosophy listed above is now applied in the following sections to takeoff and landing manoeuvres where the conditions,

(i) prevailing wind,

(ii) engine failures with pilot reaction time,

(iii) additional performance for a three engine powerplant in the presence of a single engine failure,

(iv) the presence of discrete gusts,

will be considered.

5.1 Towering Takeoff Manoeuvre

An important parameter in assessing the Towering Takeoff manoeuvre is that of the takeoff distance. In essence, a pilot can exchange takeoff distance with aircraft weight (a reduction in takeoff weight leads to shorter takeoff distances and vice versa) whilst ensuring the rotorcraft has the ability to perform the manoeuvre safely, i.e. within a set of predetermined, bounding mission parameters. It is also important to consider the manoeuvre exposure time. This can be defined as the period of the manoeuvre during which if an engine failure is experienced, due to the limitations of the rotorcraft/pilot strategy, a successful recovery is not possible. Clearly the desire here is to evaluate the maximum aircraft weight that permits zero exposure time since this will ensure vehicle safety in the event of an engine failure.

As will be demonstrated later, another important factor in determining the takeoff distance is that of the prevailing wind. The JAR requirements, however, stipulate only that a helicopter satisfy Category A takeoff and landing criteria up to a maximum wind velocity of 17kts. The question arises whether wind can be used to enhance the rotorcraft takeoff performance or improve the helicopter exposure time.

In this study of takeoff procedures, the aim is to investigate the variation of takeoff distance with helicopter weight, as well as determining the influence of prevailing wind. In addition, a further step is taken by restricting the analysis to those rotorcraft weights that permit zero exposure time since this will provide the most critical analysis of the rotorcraft safety.

5.1.1 Towering Takeoff In Wind

This investigation of the towering takeoff manoeuvre is based on the same aircraft and manoeuvre parameters as employed in Chapter 3. For a rotorcraft equipped with external pitot fixtures only, speed information will expressed relative to the air, however, the use of inverse simulation requires the manoeuvre expressed relative to an Earth fixed axes. To ensure the correct airspeed is achieved, the required exit velocity, V_{EXIT}, of the helicopter in Earth axes can easily be obtained from equation (17). For example, to achieve 70kts exit speed with

respect to the air in the presence of a 20kts head wind, a ground speed of 50kts is required. In this way, increasing head winds will result in shorter takeoff distances, at a given aircraft weight.

To present results, a diagram that portrays the minimum takeoff distance versus wind velocity has been developed. This requires repeated use of the HIFIS simulation algorithm since, for each simulation cycle, the results must be assessed with respect to the manoeuvre mission criteria and the trajectory parameters carefully altered. Figure 5.0 serves to demonstrate this procedure in terms of a flow diagram for an arbitrary manoeuvre. The selection of the manoeuvre criteria highlighted in this plot will be discussed when are required during the course of this chapter.

The task of performing this type of study for a suitable range of wind velocity and heading combinations would increase the computational burden to intolerable levels. Consequently, the ability of the helicopter to perform manoeuvres will only be considered in the case where the wind strikes the rotorcraft head on. Although the author realises that it is sometimes not possible for a takeoff into wind (the physical nature of the oilrig may restrict this), limiting the investigation to head wind cases can be justified. Often, it is the preferred method of departing an oilrig by pilots since it allows the desired safety airspeed to be quickly reached whilst reducing manoeuvre takeoff distance and aircraft exposure time. Indeed, even if the mission goal is in the reciprocal heading to the takeoff direction as evident from the report of Whidbourne (1992), a takeoff directly into wind followed by downwind turn is more desirable than the benefits gained from a 'quicker' downwind takeoff.

Figure 5.1 has been generated using the approach discussed above and highlights the variation of manoeuvre takeoff distance with wind velocity. Two data sets are presented and these correspond to two aircraft masses of 7750 and 8250kg, as indicated on the plot. From the figure it is evident that takeoff distance reduces with wind speed, since the aircraft ground speed over the manoeuvre will be significantly reduced. For wind velocities less than 10kts, the fuselage pitch limit is the dictates the success of the manoeuvre. This can be attributable to the fact that in this region there is sufficient power available to ensure the rotor rpm stays within normal governed settings for both aircraft configurations. In addition it should be noted that for wind speeds less than 10kts, each point on the curve equates to a peak pitch attitude of around -11 degrees. The peak pitch attitude is derived from the datum manoeuvre chosen to be in zero wind and with an aircraft mass of 8250kg. During the intermediate wind speed range ($10 < V_{wind} < 25$ kts.), the demands of the manoeuvre place rotor speed as the governing criteria, hence the minimum rotor angular velocity for this region was selected to be 97%. In this region, the investigation philosophy discriminates quantitatively between the two aircraft configurations since it is evident from the figure that the lighter helicopter can sustain shorter

takeoff distances. The difference in takeoff distances between the two configurations was found to be only around 20m. Beyond 25kts wind speed, the rotorcraft cyclic limits dominate the success of the manoeuvre for both aircraft configurations.

5.1.2 Normal Approach and Landing In Wind

A crucial property of any offshore landing manoeuvre is that the helicopter has a specific position to be attained at the end of the flight path. This important feature has implications on the benefit of a head wind since clearly landing distance can not be reduced in the same sense that takeoff distance was in the previous section. A further complication is that aircraft ground speed must be zero on touch down, although its airspeed in the presence of a head wind will be non zero.

Unlike the towering takeoff, the demands of the landing manoeuvre will mean rotor speed will remain tightly governed to normal operating levels for all reasonable aircraft weights. Careful analysis of the pilot strategy employed in the normal approach and landing manoeuvre in Appendix 8 has revealed the importance of visual cues during the landing with respect to the oilrig platform. As a result peak pitch up attitude of the rotorcraft is vitally important as this will directly relate to the pilot's ability to observe the landing platform. It is realised, however, that cockpit configuration, pilot position etc. will also influence the ability of the aircrew to view the rig, however these factors are considered outwith the scope of this investigation. Clearly if the simulated pilot strategy is to faithfully portray that adopted in practice, this manoeuvre parameter must be incorporated as a governing constraint.

The landing decision point is another important parameter in the landing manoeuvre profile. This notional point in the manoeuvre separates the regions where a 'go around' may be safely executed in the event of an engine failure. If the helicopter suffers an engine failure prior to the LDP, the pilot has the choice of continuing the landing or accelerating the rotorcraft to the baulked landing safety speed and adopting a positive rate of climb. For an engine failure after the LDP, the aircraft must land since it is not assured that the helicopter can avoid the rig structure during the transition to climbing flight. The choice of landing decision point has other important implications. First consider the case of a helicopter initiating a landing from a high LDP with a fast approach speed. The vehicle will require a large pitch up attitude to achieve the necessary deceleration if the helicopter is to approach the rig at a suitable flare height and velocity. Although this type of approach is desirable if an engine failure occurs, the deterioration in view of the landing platform is unacceptable. Now consider the other extreme, that is a low LDP height and rig closure rate, although the view of the rig will be good in the presence of a head wind, the helicopter may encounter severe eddies from the rig structure which may increase pilot workload to intolerable levels. Indeed, during the latter decelerative

phases of the manoeuvre, there is a risk of the helicopter tail boom striking the rig structure. The next paragraphs attempt to quantify the variation of LDP height and other parameters on the vehicles ability to perform a landing.

Presented in Figure 5.2 is the variation of the minimum LDP altitude with wind speed for helicopter weights of 8750 and 9250kg. It is immediately evident from the plot that the demands of the manoeuvre are such that, both helicopter configurations can perform the landing equally well. Consequently, the validity of the manoeuvre is dictated only by the helicopter exceeding the pitch attitude limit specified. The pitch attitude was derived from the maximum value attained during the datum manoeuvre, i.e. that value determined from the reference LDP height (100ft), aircraft weight (8750kg) and without wind. In this instance the limiting pitch attitude was determined to be approximately 10 degrees. As wind speed is increased, the initial approach airspeed is matched by adjusting the ground velocity in the same manner as that employed in the towering takeoff. Thus, lower approach ground speed allows the landing decision point height to be reduced. In practice, for each point on the plot, the landing decision height is reduced until the maximum pitch attitude is re-acquired. In Figure 5.2 each data point denotes the minimum landing decision point height that is possible without exceeding the rotorcraft pitch attitude limit for this manoeuvre. The plot clearly shows that a head wind can have a significant effect on the LDP height.

5.2 Towering Takeoff Procedures Accompanied by an Engine Failure

The physical geometry of the rig structure combined with the priority of ensuring the rotorcraft has the ability to perform a recovery manoeuvre at all times, means that the Towering Takeoff pilot strategy is split into two distinct phases. The ultimate pilot strategy for each phase effectively dictates the nature of the recovery manoeuvres and these strategies are now examined in the following paragraphs.

5.2a Vertical Reject

The height and velocity of the helicopter at TDP are vital in determining the ability of the rotorcraft in performing a successful recovery manoeuvre. A low vertical velocity combined with a low TDP height is desirable if a recovery to the landing platform is to be made, however, in the case of a continued takeoff their is a risk of the rotorcraft striking the rig structure. Another possibility is a high TDP height with a high vertical velocity. Although advantageous in terms of clearing the rig structure in the event of a continued takeoff, this strategy has several draw backs which ultimately limit the height of the TDP. Firstly, effecting a vertical reject manoeuvre below or at the TDP position will increase the chance of reducing rotor speed to dangerous levels beyond which a safe vertical velocity on touch down will not be

possible. A high TDP point will naturally mean a longer recovery manoeuvre over which pilot strategy must be precisely executed if rotor speed is to be conserved. The duration of the recovery manoeuvre is further extended by the fact that it will take a finite period of time for the pilot to arrest the upward vertical motion of the rotorcraft. The tendency of the helicopter to increase altitude after the engine failure is known as 'ballooning' and clearly, faster vertical velocity at the TDP will lead to an greater degrees of 'ballooning'. Finally, a high vertical TDP height will reduce the pilot's view of the landing platform itself and when the rig structure is close, this is an important consideration on vehicle safety.

From the above discussion, the maximum height achieved during the manoeuvre is of significant importance in assessing the success of a manoeuvre particularly when combined with the fact that the rotor speed on touch down must not drop below 80% of flight idle. Consequently, this parameter will be employed in the investigation of vertical reject manoeuvres.

In this investigation, it was found the simulated helicopter could perform the vertical reject manoeuvre for all reasonable vehicle takeoff weights. The peak altitude that could be achieved was found to only decrease a little for large increments in rotorcraft weight.

Figure 5.3 presents the variation of maximum achievable height with respect to the heli-deck as a function of wind speed. In addition, three data sets are shown, relating to TDP heights of 7.5, 10. and 12.5m. For this result the aircraft weight was chosen to be 9250kg. For wind speeds up to 10kts the peak altitude remains relatively constant for a given TDP altitude, since in these wind conditions, the rotor rpm is dominated by the demands of the manoeuvre. At higher wind speeds, the reduction in the power requirements are such that for realistic aircraft weights, the rotor rpm on touch down exceeds the 80% threshold level. As the TDP height increases, the peak balloon altitude increases beyond that implied by the vertical shift in manoeuvre altitude. This is attributable to the fact that for TDP altitudes up to a point, more favourable rotor rpm conservation characteristics are observed during the subsequent vertical descent and this kinetic energy stored in the rotor can be converted into an increase in maximum altitude.

The influence of pilot reaction time on the peak altitude is shown in Figure 5.4. It is evident that a small increase in maximum altitude has been determined. This characteristic is initially surprising, however, the result can be reconciled by recalling the fact that the rotorcraft has increased its altitude by an additional 2.5m before the recovery manoeuvre is executed. However, the absolute increase in altitude of the two second pilot reaction time compared to the one second delay is somewhat less than 2.5m. In this instance, to prevent rotor rpm reducing below the 80% threshold level on touchdown, a quicker execution of the vertical reject must be

employed. In practice, this has been achieved by attaining the maximum rate of descent earlier in the recovery manoeuvre than that exhibited for the quicker pilot reaction time.

5.2b Continued Takeoff

The task of performing a continued takeoff in the proximity of the rig can be considered as the adoption of two piloting tasks that are closely linked yet exhibit fundamentally different properties. The first task of the pilot is to attempt to reduce the power demands made of the remaining operative engine(s) if the rotor rpm is to remain with acceptable levels. Usually a value of 93% is considered appropriate for continued takeoff manoeuvres. As is evident in Appendix 8, the conservation of rotor rpm is achieved by a rapid lowering of the main rotor collective and naturally a descending flight path will follow. In addition to this task, the pilot must also accelerate the rotorcraft into forward flight if the helicopter is to avoid striking the rig structure. Indeed, the JAR documents indicate the helicopter must clear the rig by at least a 15ft radial distance from the heli-deck edge and this criteria is shown in Figure 5.5. It is important to note that the clearance criteria refers to the nearest distance from the rotorcraft to the deck edge and not the centre of gravity as used in the trajectory formulation. As a result, in this research programme, the distance from the tailrotor to the deck edge is assumed to provide a suitable measure of the deck edge clearance. It is perhaps evident from the above discussion that the deck edge clearance distance in conjunction with rotor rpm are the key parameters in determining the success of a manoeuvre.

Presented in Figure 5.6 is the variation of deck edge clearance extrema, both minima and maxima, as a function of wind velocity. The rotorcraft must pass below the level of the heli-deck between the extrema if the manoeuvre is to be successful. These bounding limits are to be expected since they reflect the degree with which the two piloting tasks mentioned above are adopted. The near boundary is governed by the requirement for the helicopter to clear the rig structure. At wind speeds less than 10kts, the figure shows that the near distance increases beyond that of the minimum deck edge clearance dictated in the governing regulations. This feature is attributable to the fact that steep descent recovery strategies require a large vertical acceleration in the Earth fixed z axis direction to avoid the rotorcraft descending into the sea. Consequently, at low wind speeds where the power requirements are high, the rotor kinetic energy is consumed by the demands of the manoeuvre. To prevent the loss of rotor rpm, the peak z deceleration must be decreased and in practice this can be achieved by increasing the distance from the deck edge where the helicopter descends below the level of the heli-deck. As in the near boundary, the far extrema is determined by the requirement that rotor rpm should not decay below 93% of flight idle. The power scheduling of the rotorcraft dominates the profile of the upper boundary, since the pilot priority in this region is biased towards increasing the rotorcraft airspeed as quickly as possible.

The influence of aircraft mass is also shown in Figure 5.6 where the reduction in the deck edge clearance is evident. From the plot, it can immediately be observed that the heavier aircraft cannot perform the continued takeoff until a wind speed has increased beyond 10kts. For wind speeds beyond, 10kts, the minimum rig distance remains unchanged, since in this region the governing criteria is dominated by the need for the rotorcraft to clear the deck edge. It can be seen that the maximum deck edge clearance has greatly reduced on account of the increase in takeoff mass. The sensitivity to aircraft mass is derived from the nature of the pilot strategy in this region; here the emphasis is placed on a recovery manoeuvres that accelerate the rotorcraft away from the rig as quickly as the rotor speed constraint will permit.

The variation of the deck edge clearance with pilot reaction time is shown in Figure 5.7. It should be noted that although the exit conditions for each recovery strategy for a given wind speed are the same, the initial conditions at the start of the recovery manoeuvre will be different due to the change in pilot reaction time. From Figure 5.7, it is evident that the increase of pilot reaction time to two seconds generates a lower boundary that is very similar to that observed for $t_{pr} = 1.0$s. This is due to that fact that the power available from the remaining serviceable engine is sufficient to meet the demands of the recovery manoeuvre. When pilot reaction time is increased further to 2.5 seconds, however, a different characteristic is observed. In this instance the pilot strategy has been executed further into the original manoeuvre and consequently, the rotorcraft position with respect to the rig will be such that a steeper recovery descent will be required if the helicopter is to pass the heli-deck level at its shortest distance. As discussed earlier in this section, steep descents consume rotor kinetic energy and consequently the rig clearance must be increased to prevent this. At higher wind velocities, the collective lever limit is reached during the pullout at the bottom recovery descent and as before, the rig clearance distance must be increased to preserve rotor rpm. The reduction in outer deck edge clearance with increasing pilot reaction is also evident. For low wind speeds, typically a 15m downward shift in the maximum deck clearance distance is shown for the three cases given. It can also be identified that as wind speed increases, the influence of pilot responses on the deck edge clearance deteriorates and consequently the maximum deck edge clearance begins to converge for all three pilot reaction time cases. This characteristic is predominately due to low power requirements of the helicopter associated with the higher wind velocities exhibited during the initial pilot reaction phase. Consequently, the rotor rpm degradation during the pilot intervention time will be less serious compared to the low wind speed cases, and therefore the influence of longer pilot reaction times is reduced. It is interesting to note that for a wind velocity of 5kts, there is only a 11m zone, extending from 20 to 31m from reference position, where a successful continued takeoff can be executed for a pilot reaction time of 2.5s.

5.3 Normal Approach and Landing Procedures Accompanied by An Engine Failure

From section 5.2 of this Chapter, it is evident that the choice of LDP height is a crucial parameter in determining the success of recovery manoeuvre for either a continued or baulked landing in the event of an engine failure. The influence of this parameter is now examined in the following case studies.

5.3a Baulked Landing

For a baulked landing, the variation of the LDP height is largely governed by the need for the rotorcraft to avoid the rig structure by a margin of 35ft as identified in JAR part 29 and this is shown in Figure 5.8. Consequently, the emphasis of the recovery manoeuvre changes from the LDP height to the height lost during the transition to the baulked landing safety speed, V_{BLSS}. It should be recalled that the baulked landing safety speed is attained when the rotorcraft passes at its lowest point in the manoeuvre and is defined as that flight velocity which permits a continuous rate of climb of 100ft/min. In this case study the minimum height lost that the aircraft can achieve will be determined. If it is desired to reduce height loss to a minimum, a rapid acceleration to the BLSS is required, however there is a danger that rotorspeed will decay to unacceptable levels. A gradual recovery to the baulked landing safety speed, although desirable in terms of rotor speed conservation, may leave the rotorcraft in danger of striking the rig platform. Clearly the interdependency of height lost with rotor speed should be incorporated into this investigation. As in the continued takeoff investigation, the minimum rotor rpm was selected from the pilot strategy given in Appendix 8, and was found to be 93% of flight idle.

Investigations have shown that rotorcraft operating mass do not alter the minimum height lost for the vehicle.

Figure 5.9 shows the variation of height lost during the baulked landing as a function of wind velocity. There are two data sets which correspond to pilot reaction times for 1.0 and 2.0 seconds. From the figure it is clear that there exists a optimum height loss for wind speed. Furthermore, the value of wind velocity at which this minima occurs increases with increasing pilot reaction time. Inspection of the y -axis reveals that although an optimum height loss exists, the difference in height loss in the absence of wind is not significant. When commenting on the results presented in Figure 5.9, it is important to consider the proximity of the oilrig. In these results the engine failure occurs at the LDP which chosen to have an altitude of 100ft above the reference position. From the graph it is clear that even without a headwind and a

slow pilot reaction time, the height loss is such that the helicopter will be easily capable of avoiding the landing platform 35ft. margin.

5.3b Continued Landing

During a continued landing, the piloting aim is to preserve rotor speed whilst maintaining an adequate view of the rig throughout the manoeuvre. For a given approach airspeed and descent angle, the correct LDP solution is crucial to the success of the recovery strategy. Too high an LDP height will extend the landing and consequently rotor speed will deteriorate to levels where the final descent to the landing platform cannot be achieved without excessively large rates of descent. A low LDP height will mean a rapid deceleration to ensure the vehicle approaches the rig at a sufficiently low speed and in this case, high fuselage pitch attitudes will be unavoidable.

In Figure 5.10 the variation of LDP height with wind speed for a continued landing is shown. Two cases have been shown and equate to aircraft operating weights of 8250 and 9250kg. It is assumed that the engine failure occurs at the LDP point, whilst pilot reaction time was set to one second. Two constraints have been employed in the generation of this diagram, and these are the maximum fuselage pitch up attitude and the minimum rotor speed. The peak pitch attitude was chosen to be approximately 10 degrees. The minimum rotor speed was obtained from the pilot description of the manoeuvre and found to be 80%. From the figure, it is evident that the boundaries of the pitch and rotor speed limits have left a region in which the landing decision point height may be chosen to ensure a safe recovery to the landing platform. As can be seen from the figure, the maximum LDP height increases with increasing wind velocity. For high prevailing wind speeds, the power requirements of the rotorcraft in this region are significantly reduced and consequently more favourable conditions exist for the conservation of rotor speed. If the minimum rotor rpm is to be achieved on touch down, then the increase rotor kinetic energy can be employed into raising the LDP height. Now consider the influence of the prevailing wind on the lower boundary profile. A similar trend to that exhibited in the case where no engine failure has occurred is observed. This is to be expected since, the rotorcraft is forced to fly along the same trajectory whether an engine failure has occurred or not.

The influence of increased rotorcraft operating mass can be seen from Figure 5.10, where the reduction in the permissible landing decision point region is evident. It should be noted that the rotorcraft can not perform the landing until a wind speed of 5kts is available. As expected, the lower boundary is similar to that where a lighter helicopter mass is employed. As discussed above, this is due to the fact that both aircraft configurations are forced to fly the

same profile. The rotor rpm upper boundary for the heavier configuration has been shifted downwards and this is due the increased torque demands for this aircraft.

Pilot reaction time was found not to be of significance in this investigation. In this instance the low power demands at the LDP ensure that rotor rpm does not decay significantly for reasonable pilot reaction times.

5.4 Analysis of Triple Engine Configuration

Previous sections have identified the importance of rotor rpm and hence the available engine torque on the ability of the helicopter to perform a successful recovery manoeuvre in the event of an engine failure. In an effort to improve rotorcraft safety, the available engine torque for a proposed design can be improved by two means. Firstly, it is possible to boost the contingency torque output from the remaining serviceable engine beyond that stipulated in the Joint Aviation Requirements and this topic has been explored by Trivier et. al. (1992). The maximum torque output from a gas turbine engine is determined largely by the peak allowable temperature of exit turbine (the main rotor gearbox is usually rated at a higher power level than that deliverable from the remaining engine operating at contingency power levels). Operation of the engine at contingency power levels can greatly reduced the fatigue life of the powerplant or even damage it, and as a consequence, a major drawback of this approach is the substantial service requirements of the engine and gearbox after operation at such high power states.

An alternative means of generating extra torque in the event of an engine failure that does not place extreme loads on the remaining engine and transmission system is to provide a triple engine powerplant. This approach has been adopted in the development of the Westland/Agusta EH101 helicopter. In the event of a single engine failure, the three engine configured powerplant can provide around 16% more torque than that of an equivalent power output twin gas turbine powerplant. Although there is an increase in the complexity and weight associated with the three engine configuration, as will be demonstrated shortly, this is offset by the improved safety margins in the event of a engine failure.

The first task in this investigation is the provision of a mathematical model of a three engine powerplant. This has been developed by extending the mathematical model of the twin gas turbine powerplant shown in Chapter 2.3. It is assumed that each engine consumes fuel at third of the rate of an equivalent power single engine powerplant, and consequently the engine governor gain and time constants of the gas turbine mathematical model were modified to suit. To facilitate comparison of the twin and triple engine configuration rotorcraft, the extra weight associated with the three engine powerplant has been neglected in this study.

Initial investigations have revealed that the improved performance of the three engine configuration aircraft makes a direct comparison to the twin engine helicopter difficult. This is because the three engined helicopter has sufficient power available to perform the recovery manoeuvres for all reasonable aircraft weights and conditions with one engine inoperative. This is particularly true for manoeuvres where the power requirements are low as in a baulked or continued landing. Consequently the continued and vertical reject manoeuvres will be examined here after.

For vertical reject manoeuvres, the added performance enable the rotorcraft to sustain a weight increase of 900kg and match the peak balloon heights demonstrated in Figure 5.2. If the same aircraft weight is assumed, and the same recovery strategy employed as in the twin engine configuration, then rotor rpm was found to be 93% on touch down for wind speed less than 10kts.

When continued takeoffs are considered, and the recovery strategy used in Figure 5.4 is replicated for all cases, then an increase in rotor angular velocity from 3.5 to 7% is observed. Alternatively, an increase in helicopter mass of 900kg can be exchanged for the increase in rotor rpm for all wind conditions.

In terms of alternative recovery strategies, at an aircraft mass of 7750kg, the helicopter can perform a continued takeoff, albeit without descending below the level of the heli-deck. Furthermore, if the aircraft operates at a weight of 7630kg, then the helicopter has sufficient power available to complete the original takeoff manoeuvre as intended by the pilot without letting rotor angular velocity drop below 93% of flight idle.

5.5 Analysis of Discrete Gusts During Towering Takeoff and Landing Manoeuvres

Recalling the issues presented in Chapter 2 concerning the validity of the pilot control activity in response to a turbulence stream, this case study will investigate the control response to a discrete gust, the structure of which is adopted from the SDG model of turbulence. Clearly there is a range of gust gradients, H, that could be used as the basis of the gust structure for an investigation of this type. However an important result of the SDG approach follows from the application of the model to the response of a linear system, where it can be shown there exists an optimum or 'tuned' gust length, $\overline{H}$, that causes a corresponding peak response of the system, $\gamma(\overline{H})$, to be observed, (Jones, 1989). Only those gust ramp lengths close to the tuned ramp length will cause a significantly large peak in the helicopter response. The method can be extended to systems that are non-linear or exhibit more than one significant peak response, since in both instances the tuning property is retained. Consequently, it is only necessary to

first identify the critical tuned gust and apply this to the investigation of helicopter offshore manoeuvres.

For this investigation, the analysis of gusts will be considered only during the phases of a manoeuvre where the helicopter is in close proximity to the rig structure. In this environment the issues discussed in Chapter 2.6 concerning the validity of current statistical and spatial properties of the SDG model will be particularly relevant. A further assumption concerns the selection of the peak response function, $\gamma(H)$, of the simulated helicopter in reaction to the gust. Since this thesis is primarily concerned with pilot strategies, it is important to select a parameter that is readily available to a pilot and has important implications on his piloting behaviour. For this investigation, attention will be focused on the normal acceleration of the helicopter, however, there are other parameters that could be employed. For example, Jones (1989), suggested in rough order of importance that vertical acceleration, roll attitude, airspeed or rate of climb were the key parameters that a pilot is likely to respond to during gust/turbulence encounter during takeoff and landing manoeuvres .

The response function of transport helicopter with basic aircraft parameters given as in Table 1, is shown in Figure 5.11. It is evident from this plot that the tuned gust length is approximately 1 second. The corresponding velocity time history of the tuned gust is shown in Figure 5.12.

The pilot strategy and vehicle performance of a helicopter experiencing a tuned down gust 3.0 seconds into a Towering Takeoff manoeuvre is shown in Figure 5.13. A one second pilot reaction time has been assumed, with the pilot recovering to the original trajectory as he perceived at the start of the simulation. Since a down gust has been employed, the rotor inflow angle and therefore the rotor thrust will decrease. Consequently, an increase in main rotor collective will be required for the rotorcraft to continue to meet the demands the manoeuvre and this is evident from Figure 5.13. There is little cyclic or pedal motion required in response to the gust. With respect to the engine parameters, there is an increase in 7% torque output from each engine, whilst the rotor speed remains tightly governed for the duration of the manoeuvre.

Unfortunately, proceeding further poses significant problems if meaningful results are to be obtained. Firstly there are no available regulations with which to demonstrate compliance as has been the basis for previous case studies shown in this Chapter. Secondly, investigations have revealed the response of the rotorcraft to gusts does not in general exceed power criteria or other constraints imposed on the simulation that can be observed during Towering Takeoff and Normal Approach and Landing manoeuvres. As a result analysis of the pilot strategy in response to a gust concerns the overall ride qualities of the helicopter. Bradley et. al. (1994), have shown that the helicopter response to turbulence consists of discrete event with

identifiable structures. The subsequent intrusion into pilot workload requires a sophisticated processing tool that can extract the salient vehicle response amongst a background of low and high frequency signals and a technique of this type was not available during this research programme.

5.6 Conclusions

The application of the HIFIS algorithm to the study of the helicopter safety issues of pilot strategy, rotor configuration and atmospheric effects has been demonstrated in this chapter. The motivation supporting the investigation philosophy has been provided by a new rationale. It has been shown that adopting parameters such as rotorspeed and pitch attitude as well as those found in the JAR for the basis of manoeuvre criteria, the ability of a rotorcraft to perform a manoeuvre can be judged. Furthermore, realistic pilot strategies are ensured. In all instances, the results have been explicable and provide an enlightening contribution to the field of helicopter offshore operations.

In summary, the following points can be made concerning specific case studies,

i) Towering Takeoff: For low wind speeds, the governing criteria was found to be the peak pitch nose down attitude. In the intermediate wind speed range, the rotor rpm becomes a governing factor, whilst at higher wind velocities, the rotorcraft cyclic limits dictate the success of the manoeuvre. The influence of aircraft takeoff mass was found to be small for wind velocities above 10kts.

ii) Normal Approach and Landing: Increasing wind speed permits the landing decision point altitude to be reduced for a given approach airspeed and descent angle. The low power nature of this manoeuvre, means for that reasonable aircraft operational weights, rotor rpm remains tightly governed. Typically, the manoeuvre success is gauged by the peak fuselage pitch attitude and consequently, the minimum LDP height was found to be independent of helicopter mass.

iii) Vertical Reject: For wind speeds up to 10kts, the peak balloon altitude does not vary significantly. At higher wind velocities, the rotor rpm on touch down exceeds the 80% threshold level. Increasing, pilot reaction time does not alter greatly the maximum altitude attained during the vertical reject.

iv) Continued Takeoff: The variation of deck edge clearance possesses extrema, both maxima and minima, which correspond to the biasing placed on the primary tasks embedded in the pilot response to the engine failure. The variation of the extrema for takeoff mass and wind

speed has been demonstrated and shows that small increases in operating mass can significantly degrade the rotorcrafts ability to perform a recovery manoeuvre. The influence of pilot reaction time has been highlighted and it is clear that small increases in pilot reaction time can quickly reduce the ability of the rotorcraft to perform a continued takeoff particularly at low wind speeds.

v) Baulked Landing: The variation of the minimum height loss during a baulked landing manoeuvre has been found to be small for the helicopter configurations considered. The influence of pilot reaction time on the height loss has been considered and even for extended pilot reaction times, the recovery manoeuvre will avoid the rig far beyond the 35ft clearance minima highlighted in the JAR documents.

vi) Continued Landing: The variation of the landing decision point with wind speed exhibits both maxima and minima extrema and this can be attributed to the two manoeuvre criteria applied in this investigation. The upper boundary indicates the ability of the rotorcraft to perform the landing whilst satisfying the rotor rpm constraint on touch down. In this instance, the LDP height can be greatly increased with increasing wind speed. The lower boundary incorporates the pitch attitude limitation and was found to be similar to that experienced during a Normal Approach and Landing. A large increase in landing mass can alter both extrema with the result that the ability of the rotorcraft to perform the landing with this pilot strategy is greatly reduced.

vii) Discrete Gusts: Realistic pilot reaction to discrete gusts has been demonstrated, however, the governing regulations and existing pilot strategy analysis tools are not sufficient to support an investigation of this type.

viii) Triple Engine Configuration: The benefits in the event of an engine failure of a triple engine power plant over an equivalent power output twin engine configuration have been demonstrated. The increased performance of the rotorcraft greatly expands on the pilot strategies available to the pilot and thus the rotorcraft safety.

The application of the HIFIS algorithm using the aforementioned rationale has clearly important implications on the rotorcraft safety issues and these are now discussed in the next, brief, chapter.

Chapter 6

Summary of the Achievements of the Research Program with Respect to Rotorcraft Safety

This brief chapter summarises the achievements of the research presented in this thesis in order to underpin their contribution to rotorcraft safety during offshore operations (The technical achievements of the research are reviewed more critically in Chapter 7).

The importance of pilot strategy on rotorcraft safety was recognised at the outset of this investigation and consequently the realistic portrayal of this aspect of offshore operations has proved to be a persistent theme throughout this investigation. The HIFIS algorithm possesses the ability to determine current or alternative pilot strategies rapidly and safely. This has been demonstrated in Chapter 5, where in effect, a range of pilot strategies have been employed to develop the manoeuvre boundary portraits. Clearly, knowledge of the strategy (or array of strategies) which provide the most viable recovery solution before the start of a manoeuvre would have obvious benefits on rotorcraft safety. Surprisingly, the emphasis on improving rotorcraft safety is not always at the expense of the rotorcraft operating weight (and therefore the operating company). As may be observed in Chapter 5, a useful increase in aircraft takeoff mass can be achieved whilst still ensuring zero exposure time provided there exists a moderate prevailing wind.

The second aspect of rotorcraft safety identified in this thesis is that of helicopter configuration. The further integration of rotorcraft configurations as certification issue has promoted designs such as the Westland/Agusta EH101 and Sikorsky S-92. As outlined in Chapter 1, however, the simulation techniques available to the designer for proving the suitability of new helicopter configuration are still relatively immature when compared to facilities available for fixed wing aircraft. It is in this arena that the HIFIS simulation software can make an important contribution. Indeed, the case study in Chapter 5 concerning the additional performance of a triple engine configuration in the presence of an engine failure could easily be construed as the validation of a formative design concept with respect to the JAR criteria.

The third rotorcraft safety topic addressed in this thesis is that of atmospheric conditions. The influence of wind on the ability of the rotorcraft to perform offshore manoeuvres has been shown to be complex and yet current JAR criteria only suggest a maximum prevailing wind condition for application to helicopter takeoff and landing limits. Here the HIFIS simulation algorithm could be used to expand on these criteria with the

subsequent improvement in rotorcraft safety. As the JAR evolve, the HIFIS software package could provide, further more demanding, wind operational limits for more advanced rotorcraft configurations.

Chapter 7

Conclusions

This brief chapter summarises the achievements of the research described within this thesis in relation to the original aims. The starting point for this investigative programme has been the need for the development of a simulation tool for the investigation of helicopter offshore operations. Despite this, previous investigations have not fully addressed the key features that form an integral part of modern helicopter operations in this environment. This thesis documents the successful development of an innovative simulation tool and its application to the study of rotorcraft safety during helicopter takeoff and landing procedures from offshore platforms.

The application of the Helinv inverse simulation and the HGS helicopter mathematical model were effectively preordained at the start of this research programme. As a result there were several crucial technical developments concerning the application of inverse simulation that were necessary before the investigation could proceed. The first of these concerns the modification to HGS to ensure it did not impose any limitations on the range and validity of the final pilot strategy and vehicle performance determined from the inverse algorithm. These modifications have been demonstrated successfully in Chapter 2.

The development of a technique to formulate representative mathematical models of helicopter offshore manoeuvres has been demonstrated in Chapter 3 of this thesis. The absence of such a method was a major stumbling block in early inverse simulations of offshore manoeuvres. The technique has four steps:

i) Formulation of Narrative of Pilot Strategy
ii) Construction of Mathematical Model of Manoeuvre
iii) Simulation
iv) Qualitative Validation

The last step was facilitated by the application of computer graphics. This allows the presentation of results for other specialists and therefore widens the scope for validation.

The importance of pilot reaction time has been underlined throughout this thesis via discussions of both the Joint Aviation Requirements and the narrative descriptions of pilot strategy found in Appendix 8. As a result, in Chapter 4, a conceptually unique simulation algorithm that employs sequential phases of conventional and inverse simulation techniques to

encapsulate this aspect of pilot strategy has been demonstrated. Comparison of the simulated pilot strategy with the equivalent narrative descriptions was found to be very encouraging for all recovery strategies considered. Where pilot strategy is strictly governed in terms of his piloting options, however, (this is the case when the aircraft returns to the oil rig), then the simulated pilot strategy was found to be particularly close to that adopted in practice. This is to be expected since, when options available to the pilot in terms of recovery strategy are limited and detailed narrative description of the pilot strategy is available, an accurate mathematical description of the manoeuvre evolves naturally. The formulation of a technique for the simulation of pilot reaction time has proven to be the vital step in this research programme. Without this facility, it is not possible to judge the full impact of engine failures on rotorcraft safety during offshore manoeuvres.

The techniques described above have been applied in full to the investigation of the rotorcraft safety topics outlined in Chapter 1. Through the judicious manipulation of the flight path and hence pilot strategy, the studies of takeoff and landing procedures in Chapter 5 have demonstrated successfully that it is possible to identify the limits of a manoeuvre with respect to a series of bounds that reflect the key safety issues available to the pilot in practice. In this way, the HIFIS simulation technique can provide a rapid, versatile and economic system for investigating rotorcraft safety in offshore operations, a facility, the author believes, until now, has not been available. Furthermore, one can be confident that this application is sufficiently representative as to ensure that HIFIS software has wide applicability to other topics in the field offshore operations.

7.1 Future Work

The author suggests several avenues for future research:

i) As discussed in Appendix 8, there are several pilot strategies that can be used to depart and land a helicopter from a raised offshore platform. Although these strategies have been investigated in other studies, it is argued that the innovative tools and analysis techniques presented in this thesis may reveal new important characteristics of these manoeuvres. Clearly, the study of helicopter offshore operations in its entirety must include the analysis of the alternative piloting takeoff and landing procedures, however, for an investigation similar to that discussed here, detailed narrative descriptions of the piloting strategies must be obtained.

ii) As presented in Chapter 2, the validity of the pilot strategy will depend to a large extent on the helicopter mathematical model employed in the inverse algorithm. Since the most helicopter offshore operations are conducted at low speed, the fuselage, tail fin and tail plane aerodynamic forces and moments will be relatively small in comparison to those derived from

the main and tail rotors and consequently any modelling enhancements will concern the main and tail rotor representation. The sophistication of the HGS rotor model, implies that the next step in rotor modelling will require an individual blade representation. Although, it is widely agreed that individual blade models offer higher level of fidelity, they are numerically intensive even for simple trim calculations. When calculating a series of modified trim states as is required during an inverse simulation, the computational effort would be expensive.

iii) In its present form, the helicopter engine gas turbine and governing model is fairly rudimentary and this could be a source of inaccuracies. The adoption of an individual blade helicopter model would justify the update of the engine model on the grounds of consistent levels of sophistication of the rotorcraft modelling elements. In this instance, an appropriate engine model would be that based on the ICV method noted in Chapter 2 with the inclusion of a model of the relevant engine control system. This type of gas turbine representation would be particularly useful during engine failures, where the behaviour of the remaining good engine is crucial to the safety of the rotorcraft.

iv) Any modification to the tail rotor behaviour due to for example, a transmission or blade pitch control failure could seriously endanger the vehicle in the proximity of the oilrig. Alternatively, if the rotorcraft tail rotor struck the rig superstructure then a safe recovery would be unlikely, as demonstrated by the AS332L Super Puma crash reported by Whidbourne (1993). An investigation of this type would require the transmission dynamics to be modelled to account for the decay of the tailrotor effectiveness. As the tail rotor thrust decreases, the rotorcraft fin and fuselage can be used to supplement the yawing moment generated by the tail rotor. It is perhaps evident that under these circumstances, the validity of the look-up tables used to evaluate the aerodynamic forces and moments acting on the fuselage particularly at high angles of incidence and sideslip will be crucial to the success of the study. Finally, the current tail rotor model employed in HGS assumes that the blades are not permitted to flap. As tail rotor speed decreases during a drive failure, however, the interaction of the centripetal and aerodynamic moments acting on the blade may led to an out of plane flapping motion that could exceed the blade structural limits. Clearly, HGS requires this modelling facet needs to be addressed before tail rotor failures can be studied.

References

Anon, 'British Civil Airworthiness Requirements, Part 29', Civil Aviation Authority.

Anon, 'Federal Aviation Regulations, Part 29 - Airworthiness Standards: Transport Category Rotorcraft', U.S. Department of Transportation, Federal Aviation Administration, 1976.

Anon, 'Joint Aviation Requirements, Part 29', Civil Aviation Authority.

Anon,'S-61N Flight Manual', Sikorsky Aircraft, Part 1, Section 2, 1963.

Buckley, E., 'Helicopter Market Trends Ready for Mass Transit', Vertiflite, Vol. 40, No.4, Nov. 1994.

Bradley, R., Sinclair, M., Jones, G., Turner, G., 'Wavelet Analysis of Helicopter Response to Atmospheric Turbulence In Ride Quality Assessment', Twentieth European Rotorcraft Forum, Amsterdam, 1994.

Bradley, R., Thomson, D., 'The Development and Potential of Inverse Simulation for Quantitative Assessment of Helicopter Handling Qualities', Proceedings of the NASA/AHS Conference 'Piloting Vertical Flight Aircraft: Flying Qualities and Human Factors', San Francisco, January 1993.

Bramwell, A. R. S., 'Helicopter Dynamics', Edward Arnold Publishers Ltd., London, 1976.

Cerbe, T., Reichert, G., 'Optimisation of Helicopter Takeoff and Landing', Journal of Aircraft, Vol. 26, No. 9., 1989, pp. 925-931.

Chen, R. T. N., 'A Survey of Nonuniform Inflow Models For Rotorcraft Flight Dynamics and Control Applications', Vertica, Volume 14, No. 2, 1990.

Foley, J., van Dam, A., Feiner, S., Hughes, J., 'Computer Graphics - Principles and Practice', 2nd Edition, Addison Wesley Publishing Ltd., 1992.

Gaonkar, G. H., Peters, D. A., 'Review of Dynamic Inflow Modelling for Rotorcraft Flight Dynamics', Vertica, Volume 12, No. 3, 1988.

Glauert, H., 'A General Theory of The Autogyro', Research Air Ministry, Report No. 1111, November, 1926.

Helicopter Airworthiness Review Panel (HARP),'Review of Helicopter Airworthiness', Civil Aviation Authority, 1984.

Hoblit, F. R.,'Gust Loads on Aircraft : Concepts and Applications', Published by AIAA Education Series, Washington D.C., ISBN 0-930403-45-2.

Jepson, W. D., 'Some Considerations of the Landing and Take-off Characteristics Of Twin Engine Helicopters : Part 1 - Height Velocity Diagrams and Part Power Descents', Technical Branch, Sikorsky Branch, Sikorsky Aircraft Division, United Aircraft Corporation, Stratford, Connecticut, USA.

Jepson, W. D., 'Some Considerations of the Landing and Take-off Characteristics Of Twin Engine Helicopters : Part 2 - Heliport Size Requirements', Technical Branch, Sikorsky Branch, Sikorsky Aircraft Division, United Aircraft Corporation, Stratford, Connecticut, USA.

Jones, J. G., 'Turbulence Models for the Assessment of Handling Qualities During Takeoff and Landings', AGARD Conf., Proc. 106, Ottawa, 1971.

Jones, J. G.,'Statistical Discrete Gust Method for Predicting Aircraft Loads and Dynamic Response', Journal of Aircraft, April 1989, pg 382 - 392.

Knut, L., M., 'New Offshore Helicopter Rig Takeoff and Landing Procedures', Society of Experimental Test Pilots, 33rd Symposium Proceedings, Beverley Hills, California, September, 1989.

Kuczynski, W. A., Cooper, D. E., Twomey, W. J., Howlett, J. J.,' The Influence of Engine/Fuel Control Design On Helicopter Dynamics and Handling Qualities', 35th Annual National Forum of the American Helicopter Society, washington D. C., May, 1979.

Maccallum, N., 'Gas Turbine Transient Performance', Department of Mechanical Engineering, University of Glasgow, 1992.

Padfield, G. D., 'Theoretical Modelling for Helicopter Flight Dynamics: Development and Validation', Proceedings of the 16th ICAS Conference, London, 1988.

Padfield, G. D., 'A Theoretical Model of Helicopter Flight Mechanics For Application to Piloted Simulation', Royal Aircraft Establishment, Technical Report 81048, 1981.

Peters, D. A., Chen, S., 'Momemtum Theory, Dynamic Inflow and the Vortex Ring State', Journal of the American Helicopter Society, July, Vol. 27, No. 3, 1982.

Peters, D. A., HaQuang, N., 'Dynamic Inflow for Practical Applications', Journal of American Helicopter Society, Technical Note, October 1988.

Press, W. H., Teukolsky, S. A., Vettering, W. T., Flannery, B. P., 'Numerical Recipes In Fortran - The Art of Scientific Computing', 2nd Edition, Cambridge University Press, 1992.

Shaydakov, V. I., 'Aerodynamic Calculation for Helicopter Lifting Rotor In Steep Descent (Vortex Ring Method)', News of Higher Educational Institutions, Aviation Technology Series, Russia, Vol. 2, 1967.

Smith, P. M.,' The Influence of System Integrity Requirements On the Development of the Helicopter AFCS', Louis Newmark Ltd., British Aviation Seminar and Exhibition, Bangalore and Delhi, March 1981.

Stevens, B. L., Lewis, F. L., 'Aircraft Control and Simulation', John Wiley & Sons Publishers, 1992.

Stevens, J., Vodegel, H., 'S-76B Certification for Vertical Takeoff and Landing Operations from Confined Areas, National Aerospace Laboratory, Department of Flight Testing and Helicopters, Amsterdam, The Netherlands.

Talbot, N., Private Communication, July, 1993.

Taylor, C. D., Thomson, D. G., Bradley, R., 'Helicopter Takeoff and Landing Procedures In Adverse Conditions Using Inverse Simulation.', Progress Note : Oct. 92 - Sept. 93, Department of Aerospace Engineering, University of Glasgow.

Taylor, C. D., Thomson, D. G., Bradley, R., 'The Mathematical Modelling of Helicopter Offshore Manoeuvres', Internal Report 9217, Department of Aerospace Engineering, University of Glasgow, December 1992.

Thomson, D. G., 'Development of a Generic Helicopter Simulation Model for Application to Inverse Simulation', Department of Aerospace Engineering, University of Glasgow, Internal Report 9216, June 1992.

Thomson, D. G., 'Evaluation of Helicopter Agility Through Inverse Solution of The Equations of Motion', Ph. D. Thesis, Department of Aerospace Engineering, University of Glasgow, May, 1987.

Thomson, D.G., Bradley, R., 'Mathematical Definition of Helicopter Manoeuvres', Department of Aerospace Engineering, University of Glasgow, Internal Report No. 9225, June, 1992.

Thomson, D.G., Bradley, R., 'Prediction of the Dynamic Characteristics of Helicopters In Constrained Flight', The Aeronautical Journal of the Royal Aeronautical Society, December, 1990.

Tomlinson, B., Bradley, R. 'Simulation of Atmospheric Turbulence', 1980.

Tranäpp, N., 'Wind Effects on Helicopter Takeoff and Landing', Fifteenth European Rotorcraft Forum, September 12 -15, 1989, Amsterdam.

Tranäpp, N., Reichert, G., Hepp, H., 'Manoeuvreability Aspects for Helicopter Takeoff and Landing', Eighteenth European Rotorcraft Forum, September 15 -18, 1992, Avignon, France.

Trivier, D., Bosqui, D., '30-Seocond / 2 Minute One Engine Inoperative Certification for the AS332 Super Puma Mk2', Eighteenth European Rotorcraft Forum, Paper 129, September 1992, France.

Vodegel, H., Stevens, J., 'A Computer Program for The Certification of Helicopter Vertical Takeoff and Landing Operations and an Application to the S-76B Helicopter', National Aerospace Laboratory, Department of Flight Testing and Helicopters, Amsterdam, The Netherlands.

Watson, W. A., Philipson, T., Oates, P. J., 'Numerical Analysis - The Mathematics of Computing 2', Edward Arnold Publishers Ltd., 1969.

Whidborne, R. StJ., 'Report on the Accident to AS 332L Super Puma, G- TIGH Near the Cormorant 'A' Platform, East Shetland, On 14 March 1992',Aircraft Accident Report 2/93, Air Accidents Investigation Branch, Department of Transport.

Whidborne, R. StJ., 'Report on the Accident to Sikorsky S61-N, G-BEWL at Brent, East Shetland Basin, On 25 July 1990', Aircraft Accident Report 2/91, Air Accidents Investigation Branch, Department of Transport.

Wolfram, S., 'Mathematica. A System for Doing Mathematics by Computer', 2nd Edition, Addison - Wesley, ISBN 0-201-51502-4, 1991.

Wolkovitch, J.,'Analtyical Prediction of the Vortex - Ring Boundaries for Helicopters in Steep Descents', Journal of the American Helicopter Society, Vol. 17, No. 3, July 1972.

Wood, T., L., Blondino, M., Williams, D., 'M230 Helicopter Performance for Category A Elevated Helipad Operations', Nineteenth European Rotorcraft Forum, Cernobbio, (Como), Italy, September, 1993.

Yoshinori, O., Kawachi, K., 'Optimal Takeoff of a Helicopter for Category A V/STOL Operations', Journal of Aircraft, Vol. 30, No. 2, March -April 1993.

Appendix 1

Helicopter Generic Simulation, HGS

This appendix gives an overview of the helicopter mathematical model, HGS, employed in the inverse simulation package, Helinv.

1.1 Overview of Model

The helicopter mathematical model used in the inverse algorithm is known as Helicopter Generic Simulation (HGS) and was formulated by Thomson (1992).
The model employs the commonly used Euler rigid body equations of motion. These equations assume a body axes set fixed in the fuselage with origin at the vehicle centre of gravity and this is evident from Figure A1.0. The Euler equations of motion with six degrees of freedom are:-

$$\dot{u} = -(wq - vr) + \frac{X}{m} - g\sin\theta$$

$$\dot{v} = -(ur - wp) + \frac{Y}{m} + g\cos\theta\sin\phi$$

$$\dot{w} = -(vp - uq) + \frac{Z}{m} + g\cos\theta\cos\phi$$

$$I_{xx}\dot{p} = (I_{yy} - I_{zz})qr + I_{xz}(\dot{r} + pq) + L$$

$$I_{yy}\dot{q} = (I_{zz} - I_{xx})rp + I_{xz}(r^2 - p^2) + M$$

$$I_{zz}\dot{r} = (I_{xx} - I_{yy})pq + I_{xz}(\dot{p} - qr) + N \qquad \text{..... (A1.1)}$$

where,

X, Y, Z	are the external forces acting on the rotorcraft at the centre of gravity,
L, M, N	are the external moments acting on the helicopter about the body axes,
u, v, w	are the vehicle translational velocities referred to the body axes set,
p, q, r	are the vehicle angular velocities about the body axes,
m	is the total mass of the helicopter,
I_{xx}, I_{yy}, I_{zz}	are the helicopter moments of inertia about the (x_b, y_b, z_b) axes,
I_{xz}	is a product of inertia of the helicopter,
θ, ϕ	are the fuselage pitch and roll attitude angles,
g	is the acceleration due to gravity.

The fuselage attitude rates can be related to the vehicle angular velocities via the kinematic supplement given as:

$$\begin{aligned} \dot{\phi} &= p + q \sin\phi \tan\theta + r \cos\phi \tan\theta \\ \dot{\theta} &= q \cos\phi - r \sin\phi \\ \dot{\psi} &= q \sin\phi \sec\theta + r \cos\phi \sec\theta \end{aligned} \qquad \text{(A1.2)}$$

The transformation from Earth to body axes through the Eulerian angles (ψ, θ, ϕ) is shown in Figure A1.1.

The expressions given for equations (A1.1) and (A1.2) are not unique to helicopter mathematical models and are in fact common to many rigid body simulations. With respect to helicopter simulations, however, a large proportion of the modelling effort is devoted to the formulation of expressions for the external forces and moments denoted by X, Y, Z, L, M and N respectively. In HGS, the total forces and moments are decomposed into their component parts f convenience, with the relevant components being the main rotor (subscript R), tail rotor (TR), fuselage (Fus), tailplane (TP) and fin (Fin). Thus the total forces and moments can be obtained from:-

$$\begin{aligned} X &= X_R + X_{TR} + X_{Fus} + X_{TP} + X_{Fin} \\ Y &= Y_R + Y_{TR} + Y_{Fus} + Y_{TP} + Y_{Fin} \\ Z &= Z_R + Z_{TR} + Z_{Fus} + Z_{TP} + Z_{Fin} \\ L &= L_R + L_{TR} + L_{Fus} + L_{TP} + L_{Fin} \\ M &= M_R + M_{TR} + M_{Fus} + M_{TP} + M_{Fin} \\ N &= N_R + N_{TR} + N_{Fus} + N_{TP} + N_{Fin} \end{aligned}$$

The derivation of the expressions which define the above force and moment components will now be outlined.

1.2 Rotor Model

In general, mathematical models of a helicopter rotor employ the same technique to evaluate the forces and moments acting on a rotor blade, that is both the aerodynamic and inertial forces are determined by integrating the load on a incremental element along the blade span. As the blade velocity varies cyclically as the blade rotates, the loads on each element will be a function not only of radial location but also of azimuthal position, and hence the blade forces and moments will be periodic in nature. The rotor model utilised in HGS assumes a multi-blade representation for the calculation of rotor forces and moments. Adopting this

technique to mathematically model the rotor, the incremental inertial and aerodynamic forces acting on a blade element are analytically integrated along the blade span. Furthermore, it is assumed that only the steady components of the periodic forces and moments generated by the rotor influence the vehicle dynamics. An alternative approach to modelling the rotor is to determine the blade behaviour individually. In this technique, the elemental forces and moments are integrated along the blade span. Individual blade modelling offers a higher fidelity than is possible with a rotor disc representation since the technique readily permits the inclusion of more complex blade geometries and aerodynamic properties.

To enable close loop expressions for the rotor forces and moments, the main rotor blade geometry and configuration is simplified by the following assumptions:

i) the blades are assumed to be rigid with constant chord and aerofoil profile,
ii) the blades are centrally hinged,
iii) the blades have a linear variation in twist incorporated via the twist slope, θ_{tw},
iv) a root cut extends from the blade centre of rotation to some distance, eR, along the span, R.

Likewise, the following assumptions about the aerodynamic properties of the blade have been made:

i) Mach number and unsteady aerodynamic effects are neglected,
ii) blade stall effects (retreating and dynamic) are not modelled,
iii) a constant lift slope curve along the whole span is assumed so that 2-d aerodynamic theory can be applied,
iv) the rotor induced velocity satisfies momentum considerations at the rotor centre, with azimuthal and radial variations superimposed.

1.2.1 Kinematics of a Blade Element

Before the rotor forces and moments can be calculated, the velocity and acceleration of a general blade element must be determined. A series of transformations relating the body axes translational and angular velocities to those of a blade element are required and this is evident from Figure A1.2. The velocity vector of the rotor hub in blade axes, $\mathbf{V_{H_{bl}}}$, can be evaluated from,

$$\mathbf{V_{H_{bl}}} = \underline{\mathbf{T}}_{\mathbf{S_{bl}}}\, \underline{\mathbf{T}}_{\mathbf{H_s}}\, \underline{\mathbf{T}}_{\mathbf{C_h}}\, \mathbf{V_{H_b}}$$

where,

$\underline{\mathbf{T}}_{\mathbf{C_h}}$ is the transformation matrix from body to rotor hub axes,

$\underline{\mathbf{T}}_{\mathbf{H_s}}$ is the transformation matrix between hub and shaft axes,

$\underline{\mathbf{T}}_{\mathbf{S_{bl}}}$ is the transformation matrix from shaft to blade axes.

and,

$$\underline{\mathbf{T}}_{\mathbf{C_h}} = \begin{bmatrix} \cos\gamma_s & 0 & \sin\gamma_s \\ 0 & 1 & 0 \\ -\sin\gamma_s & 0 & \cos\gamma_s \end{bmatrix} \qquad \underline{\mathbf{T}}_{\mathbf{S_{bl}}} = \begin{bmatrix} 1 & 0 & -\beta \\ 0 & 1 & 0 \\ \beta & 0 & 1 \end{bmatrix}$$

$$\underline{\mathbf{T}}_{\mathbf{H_s}} = \begin{bmatrix} -\cos\psi & \sin\psi & 0 \\ -\sin\psi & -\cos\psi & 0 \\ 0 & 0 & 1 \end{bmatrix}$$

where the blade flap angle, β (assumed small such that $\sin\beta \approx \beta$), the blade azimuthal position, ψ, and the rotor shaft tilt angle, γ_s, are shown in Figure A1.2.

The absolute velocity of a point on the rotor blade in blade axes, $\mathbf{V_{P_{bl}}}$, can be given by,

$$\mathbf{V_{P_{bl}}} = \mathbf{V_{H_{bl}}} + (\omega_{bl} \times \mathbf{r_{P/H}}) + \frac{d\mathbf{r_{P/H}}}{dt}$$

When the above expression is expanded, the absolute velocity of a point on the blade in blade axes can be written as,

$$\mathbf{V_{P_{bl}}} = V_{x_{bl}}\,\mathbf{i_{bl}} + V_{y_{bl}}\,\mathbf{j_{bl}} + V_{z_{bl}}\,\mathbf{k_{bl}} \qquad \text{(A1.3)}$$

where ω_{bl} is the angular velocity of the blade in blade axes and $\mathbf{r_{P/H}}$ is the position vector of a general point relative to the rotor hub. The velocity of the rotor hub in body axes, $\mathbf{V_{H_b}}$, can be determined from,

$$\mathbf{V_{H_b}} = \mathbf{V_C} + (\omega_b \times \mathbf{r_{H/C}}) + \frac{d\mathbf{r_{H/C}}}{dt}$$

where,

$\mathbf{V_C}$ is the velocity of the helicopter centre of gravity in body axes,

ω_b is the angular velocity of the helicopter about the body axes,

$\mathbf{r_{H/C}}$ is the position vector of the rotor hub with respect to the centre of gravity in body axes.

Using a similar approach to evaluate the blade accelerations, the acceleration of a point along the rotor span in blade axes, $\mathbf{a_{P_{bl}}}$, can be given by,

$$\mathbf{a_{P_{bl}}} = \mathbf{a_{H_{bl}}} + (\alpha_{bl} \times \mathbf{r_{P/H}}) + \omega_{bl} \times (\omega_{bl} \times \mathbf{r_{P/H}}) + 2\,\omega_{bl} \times \frac{d\mathbf{r_{P/H}}}{dt} + \frac{d^2\mathbf{r_{P/H}}}{dt^2}$$

When the relevant subtitutions have been made, the above expression for the acceleration of a blade element can be expressed in blade axes as,

$$\mathbf{a_{P_{bl}}} = a_{x_{bl}}\,\mathbf{i_{bl}} + a_{y_{bl}}\,\mathbf{j_{bl}} + a_{z_{bl}}\,\mathbf{k_{bl}} \qquad \text{(A1.4)}$$

where α_{bl} is the angular acceleration of the blade axes and $\mathbf{a_{H_{bl}}}$ is the translational acceleration of the hub in blade axes which can be calculated from,

$$\mathbf{a_{H_{bl}}} = \mathbf{T_{S_{bl}}}\,\mathbf{T_{H_S}}\,\mathbf{T_{C_b}}\,\mathbf{a_{H_b}}$$

The term $\mathbf{a_{H_b}}$ is the acceleration of the rotor hub in body axes and is determined from,

$$\mathbf{a_{H_b}} = \mathbf{a_C} + (\alpha_b \times \mathbf{r_{H/C}}) + \omega_b \times (\omega_b \times \mathbf{r_{H/C}}) + 2\,\omega_b \times \frac{d\mathbf{r_{H/C}}}{dt} + \frac{d^2\mathbf{r_{H/C}}}{dt^2}$$

where α_b is the angular acceleration of the body axes evaluated from $\alpha_b = \dfrac{\partial \omega_b}{\partial t}$

1.2.2 Rotor Forces and Moments

The HGS rotor model assumes that there are two forces acting on a blade element and these are attributed to aerodynamic and inertial forces and this is evident from Figure A1.3. The derivation of the rotor forces will be outlined in the following sections.

a) The Rotor Aerodynamic Forces

By considering the normal and tangential airflow over a blade section denoted by U_T and U_P respectively, it is evident from Figure A1.4 that the aerodynamic forces acting on a blade element can be given by,

$$f_{z_{bl}} = -\,l\cos\phi - d\sin\phi \qquad \text{(A1.5)}$$

$$f_{y_{bl}} = d\cos\phi - l\sin\phi \qquad \text{(A1.6)}$$

where l and d denote the lift and drag per unit span respectively and ϕ is the angle of incidence of a blade element.

Several widely used assumptions have been made in HGS in order to derive a suitable multiblade model. Firstly, the tangential velocity is assumed to be very much greater that the normal velocity ($U_T >> U_P$). Assuming the blade angle of attack is small, then ($l \cos\phi >> d \sin\phi$) and invoking the small angle assumption, equations (A1.5) and (A1.6) can be simplified to,

$$f_{z_{bl}} = - l \tag{A1.7}$$

$$f_{y_{bl}} = d - l \phi \tag{A1.8}$$

Using 2 - d aerodynamic theory, the lift and drag force per unit span as function of blade azimuth and radial position can be given by,

$$l(\psi, r_b) = \frac{1}{2} \rho (U_T^2 + U_P^2) c a_o \alpha_{bl} \tag{A1.9}$$

$$d(\psi, r_b) = \frac{1}{2} \rho (U_T^2 + U_P^2) c \delta \tag{A1.10}$$

where,

- a_o is the blade lift curve slope,
- c is the rotor blade chord,
- r_b is the blade element radial position,
- α_{bl} is the blade local angle of attack,
- δ is the blade profile drag coefficient,
- θ is the applied blade pitch angle,
- ρ is the local air density.

Referring to Figure A1.5, the blade angle of attack is the sum of the applied pitch angle, θ, and the inflow angle, ϕ, and can be obtained from,

$$\alpha_{bl} = \theta + \frac{U_P}{U_T}$$

Using this expression in equation (A1.9) and then substituting the resultant expressions for lift and drag in equations (A1.7) and (A1.8), enables the aerodynamic forces in the z and y direction, denoted by $f_{z_{bl}}$ and $f_{y_{bl}}$ respectively, for a blade element of length, dr_b, to be obtained from,

$$f_{z_{bl}} = - \frac{1}{2} \rho c a_o (U_T^2 \theta + U_P U_T) dr_b$$

$$f_{ybl} = \frac{1}{2} \rho c a_0 \left(\frac{\delta}{a_0} U_T^2 - U_P U_T \theta - U_P^2 \right) dr_b$$

The total forces acting on the blade are determined by integrating these elemental forces over the blade span. Recalling that a root cut out of length eR has been assumed, where R is the rotor span and e is the root cut out as a fraction of the total span ($0 < e < 1$), then the nondimensionalised total aerodynamic force coefficients of a single blade can be determined from,

$$C_{zbl} = -\frac{1}{2} s a_0 \int_0^{1-e} \bar{U}_T^2 \theta + \bar{U}_T \bar{U}_P \, d\bar{r}_b \qquad \text{(A1.11)}$$

$$C_{ybl} = \frac{1}{2} s a_0 \int_0^{1-e} \frac{\delta}{a_0} \bar{U}_T^2 - \bar{U}_T \bar{U}_P \theta - \bar{U}_P^2 \, d\bar{r}_b \qquad \text{(A1.12)}$$

where the rotor solidity, s, and the normalised blade radial position, $\bar{r}_b$, are given by,

$$s = \frac{b c}{\pi R} \qquad \bar{r}_b = \frac{r_b - e R}{R}$$

Referring to Figure A1.5 and equation (A1.3), the tangential and normal velocities can be determined from,

$$U_T = -V_{ybl} \qquad U_P = V_{zbl} - v_i$$

where v_i is the rotor induced velocity. The tangential and normal velocities can be expanded to give,

$$U_T = u_H \sin\psi + v_H \cos\psi + r_b \Omega$$

$$U_P = \beta (-u_H \cos\psi + v_H \sin\psi) + w_H - r_b (\dot{\beta} - p_H \sin\psi - q_H \cos\psi) - v_0 -$$

$$+ \frac{r_b}{R} (v_{1s} \sin\psi + v_{1c} \cos\psi)$$

where,

u_H, v_H, w_H	are the rotor hub components of velocity in hub axes,
v_0, v_{1s}, v_{1c}	are the steady and harmonic components of rotor inflow,
Ω	rotor angular velocity,

β is the blade flap angle.

The non-dimensionalised tangential and perpendicular velocities of a blade element can be given as,

$$\bar{U}_T = \mu_x \sin\psi + \mu_y \cos\psi + \bar{r}_b + e \qquad \text{(A1.13)}$$

$$\bar{U}_P = (e\,\alpha_{1c} - \beta\,\mu_x)\cos\psi + (e\,\alpha_{1s} + \beta\,\mu_y)\sin\psi + \mu_z - \lambda_0 - e\beta_0' +$$

$$+ \bar{r}_b\,(-\beta_0' + \alpha_{1c}\cos\psi + \alpha_{1s}\sin\psi) \qquad \text{(A1.14)}$$

where μ_x, μ_y and μ_z are the non-dimensionalised components of the rotor hub velocity.

The induced velocity can be modelled by the expression,

$$\lambda_i = \lambda_0 + \frac{r_b}{R}(\lambda_{1s}\sin\psi + \lambda_{1c}\cos\psi)$$

where λ_0 and (λ_{1s}, λ_{1c}) are the non-dimensionalised uniform inflow component and first harmonic components of main rotor inflow.

Blade flapping is expressed in harmonics of ψ, however only the first harmonics are retained.

$$\beta = \beta_0 + \beta_{1s}\sin\psi + \beta_{1c}\cos\psi + \beta_{2s}\sin 2\psi + ...$$

where β_0 is the blade coning angle, β_{1s} and β_{1c} are the first harmonics of blade flap.

The $'$ terms found in equation (A1.14) are derivatives with respect to ψ, i.e.,

$$\beta_0' = \frac{d\beta_0}{d\psi} \quad \text{etc.}$$

whilst the expressions for α_{1c} and α_{1s} are simply a collection of terms and are given as,

$$\alpha_{1c} = \bar{q}_H - \lambda_{1c} - \beta'_{1c} - \beta_{1s} \qquad \alpha_{1s} = \bar{p}_H - \lambda_{1s} - \beta'_{1s} + \beta_{1c}$$

where $\bar{q}_H$ and $\bar{p}_H$ denote the rotor hub velocities normalised by rotor speed, Ω.

The blade pitch angle is given by the expression,

$$\theta = \theta_0 + \theta_{1s} \sin\psi + \theta_{1c} \cos\psi + \theta_{tw} \frac{r_b}{R}$$

where (θ_0, θ_{1s}, θ_{1c}) are the blade collective, longitudinal and lateral cyclic displacements and θ_{tw} is the blade twist slope.

Having substituted the blade flapping angle, β, into equation (A1.14), it is then possible to evaluate evaluate equations (A1.11) and (A1.12) to obtain the rotor force coefficients. The integration of the these equations with respect to $\bar{r}_b$ is straight forward as they are simple polynomial functions of $\bar{r}_b$, however, the difficulty lies in the manipulation of $\cos\psi$ and $\sin\psi$ and their powers that arise from the substitution of the blade flap and control angle expressions into equations (A1.14) and (A1.11) respectively. These terms have been retained in HGS by using the symbolic manipulation package, Mathematica, (Wolfram, 1991). Furthermore, the powers of $\cos\psi$ and $\sin\psi$ were expressed in terms of multiple angles so that the expressions for the total blade aerodynamic coefficients as a function of its azimuthal travel can be given as,

$$C_{Z_A} = -\frac{1}{2} s\, a_0 \frac{1}{b} (C_{Z_{A_0}} + C_{Z_{A_{1c}}} \cos\psi + C_{Z_{A_{1s}}} \sin\psi + C_{Z_{A_{2c}}} \cos 2\psi + ...)$$

$$C_{Y_A} = -\frac{1}{2} s\, a_0 \frac{1}{b} (C_{Y_{A_0}} + C_{Y_{A_{1c}}} \cos\psi + C_{Y_{A_{1s}}} \sin\psi + C_{Y_{A_{2c}}} \cos 2\psi + ...)$$

where ($C_{Z_{A_0}}$, $C_{Y_{A_0}}$) denote the zeroth components and ($C_{Z_{A_{1c}}}$, $C_{Z_{A_{2c}}}$, ...) respresent the harmonic components of the force coefficients.

It is not appropriate in the context of this appendix to give the expressions for the zeroth and harmonic components of the force coefficients, C_{Z_A} and C_{Y_A}, as they are complex and lengthy, however, they are reproduced in Figure A1.6 (Thomson, 1992).

b) <u>The Rotor Inertial Forces</u>

With respect to Figure A1.3, the elemental inertia forces acting on a blade element of length dr_b can be given as,

$$dX_{I_{bl}} = -m_0 a_{x_{bl}} dr_b \qquad dY_{I_{bl}} = -m_0 a_{y_{bl}} dr_b \qquad dZ_{I_{bl}} = -m_0 a_{z_{bl}} dr_b$$

where,

$a_{x_{bl}}$, $a_{y_{bl}}$, $a_{z_{bl}}$	are the components of blade accelerations in blade axes,
$X_{I_{bl}}$, $Y_{I_{bl}}$, $Z_{I_{bl}}$	are the components of blade inertial forces in blade axes,
m_0	is the blade mass per unit length.

Making the relevant substitutions for the blade accelerations and integrating the resulting expressions gives the blade inertial forces as,

$$X_{I_{bl}} = (a_{H_x} \cos\psi - a_{H_y} \sin\psi + \beta\, a_{H_z})\, m_b + (\omega_x^2 + \omega_z^2)\, M_\beta \qquad \text{(A1.15a)}$$

$$Y_{I_{bl}} = (a_{H_x} \sin\psi + a_{H_y} \cos\psi)\, m_b - (\dot{\omega}_x + \omega_y\, \omega_z)\, M_\beta \qquad \text{(A1.15b)}$$

$$Z_{I_{bl}} = [\beta\, (a_{H_x} \cos\psi - a_{H_y} \sin\psi) - a_{H_z})]\, m_b - (\omega_y\, \omega_z - \dot{\omega}_y)\, M_\beta \qquad \text{(A1.15c)}$$

where the blade mass, m_b, and the blade moment of mass, M_β, are given by,

$$m_b = \int_{eR}^{R} m_0 dr_b \qquad\qquad M_\beta = \int_{eR}^{R} m_0\, r_b\, dr_b$$

and $(\omega_x, \omega_y, \omega_z)$ are the angular velocity components of a blade element in blade axes.

The expansion of equations (A1.15a, .15b, .15c) is complete by including the blade angular velocities and accelerations and flap angle as functions of blade azimuthal position. The resulting equations are then non-dimensionalised (by $\rho\, (\Omega R)^2\, \pi R^2$) and as in the rotor aerodynamic force case, expressed in multiple angle form up to the first harmonic. The blade inertial force coefficients can then be written as,

$$C_{X_I} = C_{X_{I_0}} + C_{X_{I_{1c}}} \cos\psi + C_{X_{I_{1s}}} \sin\psi$$

$$C_{Y_I} = C_{Y_{I_0}} + C_{Y_{I_{1c}}} \cos\psi + C_{Y_{I_{1s}}} \sin\psi$$

$$C_{Z_I} = C_{Z_{I_0}} + C_{Z_{I_{1c}}} \cos\psi + C_{Z_{I_{1s}}} \sin\psi$$

1.2.2 Total Rotor Forces

The total rotor blade forces are obtained by the summation of the inertial and aerodynamic forces. For example, $C_{Y_{bl}} = C_{Y_I} + C_{Y_A}$ etc., giving in component coefficient form,

$$C_{X_{bl}} = C_{X_0} + C_{X_{bl_{1c}}} \cos\psi + C_{X_{bl_{1s}}} \sin\psi$$

$$C_{Y_{bl}} = C_{Y_0} + C_{Y_{bl_{1c}}} \cos\psi + C_{Y_{bl_{1s}}} \sin\psi$$

$$C_{Z_{bl}} = C_{Z_0} + C_{Z_{bl_{1c}}} \cos\psi + C_{Z_{bl_{1s}}} \sin\psi$$

where $C_{X_0} = C_{X_{I_0}}$, $C_{Y_0} = \frac{s}{2}\frac{a_0}{b} C_{Y_{\dot{A}_0}} + C_{Y_{I_0}}$ etc.

The vehicle equations of motion are defined with respect to a body axes set, therefore, the rotor forces are required to be referred to this axes set. This is achieved by first transforming the blade forces from blade to shaft and then from shaft to the hub axes using the transpose the matrices $\underline{\mathbf{T}}_{\mathbf{S_{bl}}}$, $\underline{\mathbf{T}}_{\mathbf{H_S}}$ and $\underline{\mathbf{T}}_{\mathbf{C_h}}$ to give the blade component forces in hub axes as C_{X_h}, C_{Y_h} and C_{Z_h}. During this transformation, it is assumed that only the steady terms contribute to the rotorcraft dynamics and hence the periodic terms that are a function of blade azimuth can be neglected. The final stage is to transform the rotor forces from hub to body axes through the rotor shaft angle, γ_s. The contribution to the external forces of the helicopter due to the main rotor can therefore given by:

$$X_R = \rho\,(\Omega R)^2\,\pi R^2\,[C_{X_h}\cos\gamma_s - C_{Z_h}\sin\gamma_s]$$
$$Y_R = \rho\,(\Omega R)^2\,\pi R^2\,C_{Y_h}$$
$$Z_R = \rho\,(\Omega R)^2\,\pi R^2\,[C_{X_h}\sin\gamma_s + C_{Z_h}\cos\gamma_s]$$

1.2.3 Rotor Moments

Flapping has been included in the HGS model by assuming that the rotor consists of rigid blades which are hinged at the hub and have stiffness in flap. The stiffness of the rotor hub is modelled by a torsional spring of strength K_β. This approach is a simplification of the hinge offset and spring model which can be employed to model fully articulated or hingeless rotor types. The validity of centre of the centre spring equivalent rotor is a topic explored by Padfield (1981).

The total moments acting on a single rotor blade are determined by summing the elemental inertial and aerodynamic moments over the span, and equating them to the restoring moment attributable to the moment at the rotor hub due to blade flap. Motion due to blade flapping can then be written as,

$$\int_{eR}^{R}\left(f_{z_{bl}} - m_0\,a_{z_{bl}}\right) r_b\,dr_b + \beta\,K_\beta = 0 \qquad \text{(A1.16)}$$

The rotor torque is obtained by integrating the elemental torques over the rotor blade span,

$$\int_{eR}^{R}\left(f_{y_{bl}} - m_0\,a_{y_{bl}}\right) r_b\,dr_b = Q \qquad \text{(A1.17)}$$

The integration of equation (A1.17) is undertaken in a manner similar to the integration of the rotor force expressions, that is the aerodynamic and inertial contributions are evaluated separately. Mathematica was used to perform the algebraic manipulations to retain the harmonic torque coefficients during the integration. If the rotor torque is non-dimensionalised (by division by $\rho\,(\Omega\,R)^2\,\pi\,R^3$), then the torque coefficients of a single blade due to acrodynamic and inertial moments can be written as,

$$C_{Q_A} = C_{Q_{A_0}} + C_{Q_{A_{1c}}} \cos\psi + C_{Q_{A_{1s}}} \sin\psi$$

$$C_{Q_I} = C_{Q_{I_0}} + C_{Q_{I_{1c}}} \cos\psi + C_{Q_{I_{1s}}} \sin\psi$$

The total rotor blade torques coefficients can be obtained from,

$$C_Q = C_{Q_0} + C_{Q_{1c}} \cos\psi + C_{Q_{1s}} \sin\psi$$

where,

$$C_{Q_0} = \frac{s\ a_0}{2\ b} C_{Q_{A_0}} + C_{Q_{I_0}} \qquad C_{Q_{1c}} = \frac{s\ a_0}{2\ b} C_{Q_{A_{1c}}} + C_{Q_{I_{1c}}} \quad C_{Q_{1s}} = \frac{s\ a_0}{2\ b} C_{Q_{A_{1s}}} + C_{Q_{I_{1s}}}$$

The rotor moments must be transformed from blade to body axes for use in the vehicle equations of motion. This is achieved by using the transpose of the direction cosine matrices, $\underline{\mathbf{T}}_{\mathbf{S_{bl}}}$, $\underline{\mathbf{T}}_{\mathbf{H_s}}$, and $\underline{\mathbf{T}}_{\mathbf{C_h}}$. If the moments at the rotor hub due to a rotor with b blades are denoted by L_h, M_h and N_h, then the total rotor moments acting at the vehicle centre of gravity can be given as,

$$\begin{aligned} L_R &= L_h \cos\gamma_s - N_h \sin\gamma_s + h_R\ Y_R \\ M_R &= M_h - h_R\ X_R + x_{cg}\ Z_R \\ N_R &= L_h \sin\gamma_s + N_h \cos\gamma_s - x_{cg}\ Y_R \end{aligned}$$

1.2.4 Blade Flapping Equation and Multi - blade Transformation

The flapping motion of blade i can be determined from,

$$\int_{eR}^{R} \left(f_{z_{bl}} - m_0\ a_{z_{bl}} \right) r_b\ dr_b + \beta_i\ K_\beta = 0 \qquad \text{(A1.18)}$$

where the blade acceleration in blade axes is evaluated from equation (A1.4) and can be given as,

$$a_{zbl} = \beta_i\,(-a_{H_x}\cos\psi_i + a_{H_y}\sin\psi_i) + a_{H_z} +$$
$$+r_b\,[-\ddot{\beta}_i - \Omega^2\,\beta_i + (\dot{q}_H + 2\,\Omega\,p_H)\cos\psi_i + (\dot{p}_H - 2\,\Omega\,p_H)\sin\psi_i]$$

Substituting this expression into equation (A1.18) and non-dimensionalising the resultant expression by Ω^2, then the flapping equation can be written as,

$$\beta_i'' + \left[\lambda_\beta^2 + \frac{M_b R}{I_\beta}\left(\eta_x\cos\psi_i - \eta_y\sin\psi_i\right)\right]\beta_i = 4n_\beta\int_0^{1-e}\left(\overline{U}_T^2\theta + \overline{U}_T\overline{U}_P\right)(\bar{r}+e)d\bar{r}_b$$

$$+\frac{M_\beta\,R}{I_\beta}\eta_z + 2\left[\left(\frac{q_H'}{2} + \bar{p}_H\right)\cos\psi_i + \left(\frac{p_H'}{2} - \bar{p}_H\right)\sin\psi_i\right] \qquad \text{(A1.19)}$$

where normalised flap frequency, λ_β, the blade flapping moment of inertia, I_β, and the blade inertia number, n_β, are given by,

$$\lambda_\beta^2 = \frac{K_\beta}{I_\beta\,\Omega^2} + 1 \qquad I_\beta = \int_{eR}^{R} m_0 r_b^2 dr_b \qquad n_\beta = \frac{\rho c a_0 R^4}{8I_\beta}$$

Other terms evident from equation (A1.19) are given as,

$$\beta_i'' = \frac{d^2\beta_i}{d\psi^2} \qquad q_H' = \frac{\dot{q}_H}{\Omega^2} \qquad p_H' = \frac{\dot{p}_H}{\Omega^2}$$

The expansion of equation (A1.19) is completed by substituting the normalised component velocities given by equations (A1.13) and (A1.14). The resulting equation can be used to describe flapping motion of an individual blade, however, the flapping model implemented in HGS requires the flapping motion be described in multi-blade co-ordinates.

In HGS, equation (A1.19) is solved by applying the multi-blade transformation which effectively transforms the individual blade angles, β_i (i=1 to n), into the multi-blade co-ordinates given as the coning angle, β_0, the longitudinal and lateral flapping angle, β_{1s} and β_{1c}, and the differential coning angle, β_d. By applying the multi-blade transformation for a four blade rotor, the individual blade angles, $\beta_I = (\beta_1\ \beta_2\ \beta_3\ \beta_4)^T$, can be determined as follows,

$$\beta_I = \underline{L}_\beta\,\beta_M$$

where,

$$\underline{L}_\beta = \begin{bmatrix} 1 & -1 & \cos\psi & \sin\psi \\ 1 & 1 & \sin\psi & -\cos\psi \\ 1 & -1 & -\cos\psi & -\sin\psi \\ 1 & 1 & \sin\psi & \cos\psi \end{bmatrix}$$

$$\beta_M = (\beta_0\ \beta_d\ \beta_{1s}\ \beta_{1c})^T$$

Incorporating the multi-blade transformation into the flapping equation and expressing the resulting periodic equation in non periodic form, allows the flapping equation to be written as,

$$\beta''_M + \mathbf{C}_{M_0}\,\beta'_M + \mathbf{D}_{M_0}\,\beta_M = \mathbf{h}_{M_0} \qquad \text{(A1.20)}$$

The expressions found in the $\mathbf{C}_{M_0}$, $\mathbf{D}_{M_0}$ and $\mathbf{h}_{M_0}$ matrices are lengthy in nature and the reader is referred to Thomson (1992) for a complete formulation.

Equation (A1.20) can be solved for the multi-blade angles, however the solution is often simplified by assuming quasi-steady blade flapping. This assumption implies that the blade flapping dynamics are decoupled from the fuselage dynamics and therefore have little effect on the forces and moments applied by the rotor to the fuselage. The quasi-steady blade flapping motion becomes,

$$\beta_M = \mathbf{D}^{-1}_{M_0}\mathbf{h}_{M_0}$$

which can be readily solved for the vector β_M due to its algebraic nature.

1.3 The Tail Rotor Model

The modelling of the tail rotor is essentially the same as the main rotor, the exception being the assumption that the tail rotor hub is rigid so that no blade flapping occurs. The rotor blades are assumed to have constant chord, root cut out and linearly varying blade twist. The rotor inflow representation is of the same form, however, the inertial forces and moments of the rotor are assumed small and therefore ignored.

1.3.1 Tail Rotor Total Forces and Moments

The rotor forces and moments are evaluated in a manner similar to the main rotor. Neglecting inertial forces, the normalised force and torque coefficients for the whole rotor can be determined from,

$$C_{Z_{TR_{trbl}}} = -\frac{1}{2} s_{TR}\, a_{0_{TR}} \int_0^{1-e_{TR}} \bar{U}_{T_{TR}}^2 \theta_{TR} + \bar{U}_{T_{TR}}\, \bar{U}_{P_{TR}}\, d\bar{r}_{b_{TR}}$$

$$C_{Y_{TR_{trbl}}} = \frac{1}{2} s_{TR}\, a_{0_{TR}} \int_0^{1-e_{TR}} \frac{\delta_{TR}}{a_{0_{TR}}} \bar{U}_{T_{TR}}^2 - \bar{U}_{T_{TR}}\, \bar{U}_{P_{TR}} \theta_{TR} - \bar{U}_{P_{TR}}^2\, d\bar{r}_{b_{TR}}$$

$$C_{Q_{TR_{trbl}}} = \frac{1}{2} s_{TR}\, a_{0_{TR}} \int_0^{1-e_{TR}} \left[\frac{\delta_{TR}}{a_{0_{TR}}} \bar{U}_{T_{TR}}^2 - \bar{U}_{T_{TR}}\, \bar{U}_{P_{TR}} \theta_{TR} - \bar{U}_{P_{TR}}^2 \right] \bar{r}_{b_{TR}}\, d\bar{r}_{b_{TR}}$$

where s_{TR} is the solidity of the tail rotor, δ_{TR} is the drag coefficient of a tail rotor blade and $a_{0_{TR}}$ the lift curve slope of the tail rotor blade profile. These expressions were evaluated using Mathematica and neglecting terms in $2\psi_{TR}$ and higher gives the periodic forces and moments coefficients as,

$$C_{Z_{TR_{trbl}}} = -\frac{1}{2} s_{TR}\, a_{0_{TR}} \left(C_{Z_{0_{TR}}} + C_{Z_{1c_{TR}}} \cos\psi_{TR} + C_{Z_{1s_{TR}}} \sin\psi_{TR}\right)$$

$$C_{Y_{TR_{trbl}}} = -\frac{1}{2} s_{TR}\, a_{0_{TR}} \left(C_{Y_{0_{TR}}} + C_{Y_{1c_{TR}}} \cos\psi_{TR} + C_{Y_{1s_{TR}}} \sin\psi_{TR}\right)$$

$$C_{Q_{TR_{trbl}}} = -\frac{1}{2} s_{TR}\, a_{0_{TR}} \left(C_{Q_{0_{TR}}} + C_{Q_{1c_{TR}}} \cos\psi_{TR} + C_{Q_{1s_{TR}}} \sin\psi_{TR}\right)$$

Neglecting periodic terms and denormalising, the moment components due to the offset of the tail rotor hub forces can be added to the tail rotor moments to give the force and moment contribution of the tail rotor in body axes as,

$$X_{TR} = \rho (\Omega_{TR} R_{TR})^2 \pi R_{TR}^2 C_{X_{TR_{trh}}} \qquad Y_{TR} = -\rho (\Omega_{TR} R_{TR})^2 \pi R_{TR}^2 C_{Z_{TR_{trh}}} \qquad Z_{TR} = \rho (\Omega_{TR} R_{TR})^2 \pi R_{TR}^2 C_{Y_{TR_{trh}}}$$

$$L_{TR} = h_{TR}\, Y_{TR}$$

$$M_{TR} = -\rho (\Omega_{TR} R_{TR})^2 \pi R^3_{TR} C_{Q_{TR_{trh}}} + (x_{cg} + l_{tr})\, Z_{TR} - h_{TR}\, X_{TR}$$

$$N_{TR} = -(x_{cg} + l_{tr})\, Y_{TR}$$

where $C_{X_{TR_{trh}}}$, $C_{Y_{TR_{trh}}}$, $C_{Z_{TR_{trh}}}$ and $C_{Q_{TR_{trh}}}$ are the tail rotor force and moment coefficients in tail rotor hub axes. The terms x_{cg} and l_{tr} are the distances of the centre of gravity and tail rotor hub from the fuselage reference point respectively and are shown in Figure A1.7.

1.4 The Fuselage Forces and Moments

Derived from wind tunnel tests, the fuselage force and moment coefficients are denoted by $C_{X_{Fus}}$, $C_{Y_{Fus}}$, $C_{Z_{Fus}}$, $C_{L_{Fus}}$, $C_{M_{Fus}}$ and $C_{N_{Fus}}$. These coefficients were determined as functions of the fuselage angle of incidence, α_{Fus}, and side slip, β_{Fus}. The fuselage angle of incidence and side slip can be given by,

$$\alpha_{Fus} = \tan^{-1}\left(\frac{w}{u}\right) \qquad \beta_{Fus} = \sin^{-1}\left(\frac{v}{V_f}\right)$$

where the flight velocity is given by $V_f = \sqrt{u^2 + v^2 + w^2}$.

The force and moment coefficient information was included in the mathematical model of the helicopter via a series of look-up tables for convenience.
As the forces and moments were measured from a reference point directly below the rotor hub, a distance x_{cg} from the centre of gravity, the force and moments can be given by,

$$\begin{aligned}
X_{Fus} &= \rho\,(\Omega R)^2\,\pi R^2\,C_{X_{Fus}} \\
Y_{Fus} &= \rho\,(\Omega R)^2\,\pi R^2\,C_{Y_{Fus}} \\
Z_{Fus} &= \rho\,(\Omega R)^2\,\pi R^2\,C_{Z_{Fus}} \\
L_{Fus} &= 0 \\
M_{Fus} &= \rho\,(\Omega R)^2\,\pi R^3\,C_{M_{Fus}} + x_{cg}\,Z_{Fus} \\
N_{Fus} &= \rho\,(\Omega R)^2\,\pi R^3\,C_{N_{Fus}} - x_{cg}\,Y_{Fus}
\end{aligned}$$

1.5 Fin and Tailplane Forces and Moments

The fin and tailplane forces coefficients, $C_{Y_{Fin}}$ and $C_{Z_{TP}}$, are also obtained from from look-up tables which are functions of the fin side slip angle, β_{Fin}, and tailplane angle of incidence, α_{TP}. The fin local angle of side slip can be calculated from,

$$\beta_{Fin} = \beta_T + \beta_{local}$$

where β_T denotes the fixed angle of incidence of the fin relative to the fuselage centreline. The incidence due to the relative airflow passing over the airfoil, β_{local}, can be evaluated from,

$$\beta_{local} = \sin^{-1}\left(\frac{v + ph_{Fin} - r\left(x_{cg} + l_{Fin}\right)}{\sqrt{\left(u - qh_{Fin}\right)^2 + \left(v + ph_{Fin} - r\left(x_{cg} + l_{Fin}\right)\right)^2 + \left(w + q\left(x_{cg} + l_{Fin}\right)\right)^2}} \right)$$

The tailplane angle of incidence is given by,

$$\alpha_{TP} = \alpha_T + \alpha_{local}$$

where α_T denotes the fixed angle of incidence of the tailplane and α_{local} represent the angle of attack of the tailplane due to the relative airflow and can be calculated from,

$$\alpha_{local} = \tan^{-1}\left(\frac{w + q\left(x_{cg} + l_{Fin}\right)}{u - qh_{TP}} \right)$$

Hence, the contribution of the tailplane of area S_{TP}, and fin of surface area S_{Fin}, to the exteranl forces and moments can be obtained from,

$X_{TP} = 0$	$X_{Fin} = 0$
$Y_{TP} = 0$	$Y_{Fin} = \rho\ (\Omega\ R)^2\ S_{Fin}\ C_{Y_{Fin}}$
$Z_{TP} = \rho\ (\Omega\ R)^2\ S_{TP}\ C_{Z_{TP}}$	$Z_{Fin} = 0$
$L_{TP} = 0$	$L_{Fin} = Y_{Fin}\ h_{Fin}$
$M_{TP} = Z_{TP}\ (x_{cg} + l_{TP})$	$M_{Fin} = 0$
$N_{TP} = 0$	$N_{Fin} = Y_{Fin}\ (x_{cg} + l_{Fin})$

where,

l_{Fin} is the distance from the fuselage datum point to the centre of pressure of the fin,

h_{Fin} is the height of the fin above the fuselage reference point,

l_{TP} is distance of the tailplane behind the fuselage reference point,

h_{TP} is the height of the tailplane above the fuselage reference position.

1.6 Glauert Inflow Model

The current rotor inflow model used in HGS employs the established method of representing the induced rotor inflow as the sum of a uniform and first order inflow harmonics with radial variation. The resulting model has the form,

$$v_i = v_0 + \frac{r_b}{R}\left(v_{1s} \sin\psi + v_{1c} \cos\psi \right) \qquad \text{(A1.21)}$$

where v_i is the induced velocity at the rotor, v_0 uniform inflow component, and v_{1s}, v_{1c} are the harmonic components of rotor inflow. The terms r_b and R denote the radial position from the centre of the rotor and the blade span respectively. The rotor azimuthal position is given by, ψ. Glauert appreciated that the rotor would behave very much like an equivalent finite wing of span equal to the rotor diameter, giving an upwash at the leading edge of the rotor and an increase in induced velocity at the trailing edge and consequently the term v_{1c} was included to model this effect (Bramwell, 1976). Equation (A1.21) can be nondimensionalised by division by (Ω R) to give,

$$\lambda_i = \lambda_0 + \frac{r_b}{R}\left(\lambda_{1s} \sin\psi + \lambda_{1c} \cos\psi\right)$$

where,

$$\lambda_0 = \frac{v_0}{\Omega R} \qquad \lambda_{1s} = \frac{v_{1s}}{\Omega R} \qquad \lambda_{1c} = \frac{v_{1c}}{\Omega R}$$

The nondimensionalised uniform inflow component, λ_0, can be determined from momentum considerations and can be calculated from,

$$\lambda_0 = \frac{C_T}{2\sqrt{\mu^2 + (\mu_z - \lambda_0)^2}} \qquad \text{(A1.22)}$$

where,

C_T is the rotor thrust coefficient,

μ is the inplane velocity vector of the rotor hub,

μ_z is the velocity of the rotor hub perpendicular to the rotor hub plane.

The evaluation of the longitudinal inflow component λ_{1c} is aided by the inclusion of an additional rotor hub - wind axes set. This axes set is aligned so that its x-axis is collinear with the resultant inplane velocity of vector of the rotor hub. As is shown in Figure A1.8, the orientation of this axes set is obtained by a rotation about the rotor hub z axis through the rotor side slip angle, ψ_w. Therefore, the harmonic induced flow components can be obtained from,

$$\begin{bmatrix} \lambda_{1c} \\ \lambda_{1s} \end{bmatrix} = \begin{bmatrix} \cos\psi_w & -\sin\psi_w \\ \sin\psi_w & \cos\psi_w \end{bmatrix} \begin{bmatrix} \lambda_{1cw} \\ \lambda_{1sw} \end{bmatrix}$$

The rotor side slip angle ψ_W is given by,

$$\psi_W = \tan^{-1}\left(\frac{\mu_y}{\mu_x}\right)$$

where μ_x and μ_y are the nondimensionalised components of rotor hub velocity.

A theoretical value of the longitudinal induced velocity, λ_{1cw}, is stated by Bramwell (1976). It was obtained by considering that when the rotor moves forward through the air, it leaves behind a vortex wake in the form of an elliptical cylinder generated by a series of vortex rings parallel to rotor disc. From this analysis the slope of the ratio λ_i/λ_0 at the rotor centre was found to be $\tan(\chi/2)$, where χ is the wake angle shown in Figure A1.9. Thus the longitudinal inflow components in the wind axes can be obtained from,

$$\lambda_{1cw} = \lambda_0 \tan\left(\frac{\chi}{2}\right) \qquad \chi < \frac{\pi}{2}$$

$$\lambda_{1cw} = \lambda_0 \cot\left(\frac{\chi}{2}\right) \qquad \chi > \frac{\pi}{2}$$

By making the transformation from hub to wind axes, the lateral component of induced velocity is zero,

$$\lambda_{1sw} = 0$$

A description of the use of the uniform and harmonic inflow components in the HGS model is outlined section (A1.22) of this appendix.

1.7 Mathematical Formulation of a Single Engine Power Plant

The original single engine model incorporated into HGS was formulated by Padfield (1981) and relates the engine torque, Q_E, to the rotor speed, Ω, by the following,

$$\dot{\Omega} = (Q_E - Q_R - G_{TR}\, Q_{TR}) / I_{TR} + \dot{r} \qquad \text{(A1.23)}$$

where Q_R and Q_{TR} are the main and tail rotor torque's respectively, G_{TR} the tail rotor gear ratio, I_{TR} is the sum of the main rotor, tail rotor, and transmission polar moments of inertia. The coupling between engine and fuselage is achieved in the above expression through the inclusion of the angular yaw rate, $\dot{r}$.

The engine torque is automatically controlled by a governing system that relates changes in rotor speed, $\Delta\Omega$, to changes in fuel flow, Δw_f. This part of the governing system is specified in terms of a simple first order lag with gain K_{e1} and time constant τ_{e1}. Its transfer function is given by,

$$\frac{\Delta w_f}{\Delta\Omega} = \frac{K_{e1}}{1+\tau_{e1}\, s} \qquad \text{(A1.24)}$$

The increment in fuel flow change and rotor speed are given by,

$$\Delta w_f = w_f - w_{f_{IDLE}}$$

and,

$$\Delta\Omega = \Omega - \Omega_{IDLE}$$

where $w_{f_{IDLE}}$ and Ω_{IDLE} are the fuel flow and main rotor speed at flight idle. The second part of the governing system relates the changes in fuel flow to changes in engine torque, ΔQ_E and has the form,

$$\frac{\Delta Q_E}{\Delta w_f} = K_{e2}\left(\frac{1+\tau_{e2}\, s}{1+\tau_{e3}\, s}\right) \qquad \text{(A1.25)}$$

where,

K_{e2} is the gain associated with the engine response to fuel flow,
ΔQ_E the change in rotor torque from flight idle ($\Delta Q_E = Q_E - Q_{E_{IDLE}}$),
$Q_{E_{IDLE}}$ is the rotor torque at flight idle and assumed to have the value $Q_{E_{IDLE}}=0$,
τ_{e2} and τ_{e3} are time constants which are functions of engine torque and are given by the linear functions,

$$\tau_{e2} = \tau_{e20} + \tau_{e21}\left(\frac{Q_E}{Q_{E_{MAX}}}\right)$$

$$\tau_{e3} = \tau_{e30} + \tau_{e31}\left(\frac{Q_E}{Q_{E_{MAX}}}\right)$$

where $Q_{E_{MAX}}$ is the maximum allowable engine torque output.

Combining equations (A1.24) and (A1.25) gives the equations of motion of a power plant and for a single engine system can be shown to be of the form,

$$\ddot{Q}_E = \frac{1}{(\tau_{c1}\,\tau_{c3})}\left(-(\tau_{e1} + \tau_{e3})\,\dot{Q}_E - Q_E + K_3\,(\Omega - \Omega_{IDLE} + \tau_{e2}\,\dot{\Omega})\right)$$

....(A1.26)

where,

$$K_3 = K_{e_1} K_{c_2}$$

Appendix 2

The Inverse Simulation Algorithm, Helinv

This Appendix aims to present a detailed discussion of the algorithm employed in the inverse simulation package, Helinv. Prior to detailing the architecture of the inverse simulation algorithm, it is useful to give to a statement of the general inverse problem.

2.1 Statement of Inverse Problem

The task of simulating an arbitrary dynamic system's response to a given set of inputs is well known and can be formally described by the initial value problem,

$$\dot{\mathbf{x}} = \mathbf{f}(\mathbf{x},\mathbf{u}) \qquad \mathbf{x}(0) = \mathbf{x_0} \tag{A2.1}$$

$$\mathbf{y} = \mathbf{g}(\mathbf{x}) \tag{A2.2}$$

where $\mathbf{x}$ is the system state vector and $\mathbf{u}$ is the control vector. Equation (A2.1) represents the response of the mathematical model over a period of time, t, to a given predetermined series of controls, $\mathbf{u}$ and initial conditions, $\mathbf{x_0}$. Equation (A2.2) enables the output of system, $\mathbf{y}$, to be observed from the from the state vector, $\mathbf{x}$.

In the inverse method, the simulation of the system is carried out in a reciprocal manner, that is the control vector, $\mathbf{u}$, is calculated to ensure the system's response matches that imposed by a predetermined output vector, $\mathbf{y}$.

2.2 Inverse Simulation Algorithm, Helinv

The inverse simulation algorithm is best appreciated by consideration of the mechanisms with which the helicopter is controlled in reality. As tool to aid the description of the behaviour of the helicopter, it is useful to assume that the four helicopter controls can be decoupled, then the influence of the helicopter controls can then be explained as follows. The main rotor collective largely contributes to the dominant component of main rotor thrust of the helicopter and this acts in a direction co-linear with the z axis and subsequently determines the vertical motion of the helicopter. The longitudinal cyclic influences the fore and aft inclination of the rotor disc and hence the orientation of the rotor thrust vector, and consequently, the longitudinal cyclic controls the fore and aft motion of the rotorcraft. Similarly, lateral cyclic displacements control the roll orientation of the rotor disc and therefore determine the lateral

motion of the helicopter. To balance the engine torque necessary to drive the main rotor, a tail rotor produces an opposing moment due to its offset from the centre of gravity. The pedal displacements determine the tail rotor thrust and this leads to a yawing moment about the vehicle body axis which influences the directional motion of the helicopter.

It is perhaps apparent, from the above discussion, that in the context of helicopter inverse simulation, the most convenient way to define the output of the system, $\mathbf{y}$, is by specification of the trajectory of the vehicle centre of gravity in terms of its longitudinal, lateral and vertical position with respect to an Earth fixed axes denoted by, x_e, y_e and z_e. Using this rationale, however, the inverse algorithm has six equations with which to solve for the four unknown controls and three Euler attitude angles. In order to obtain a unique solution, it is clear a further constraint must be applied to the vehicle. Considering the control of the helicopter, the selection of the heading, ψ, is an appropriate parameter as it most easily controlled by the tail rotor collective.

The complexity of the helicopter mathematical model implied by $\mathbf{f}$ in equation (A2.1) precludes an inverse algorithm based on an analytical solution. This is evident from the expressions used to evaluate the forces and moments acting on the rotorcraft derived in Appendix 1, which can be seen to be complex nonlinear algebraic functions of many vehicle states and configurational parameters. Consequently, an iterative solution scheme must be adopted. A Newton - Raphson scheme has been employed to solve the equations of motion, as this method permits the helicopter controls to be quickly and accurately established at each time point in the trajectory.

In the Newton - Raphson algorithm discussed by Press et. al. (1992), a system of N equations can be expressed as,

$$F_k(q_1, q_2, ..., q_N) = 0 \qquad k = 1, 2, ..., N.$$

and if $\mathbf{q}_j$ denotes an estimate of the vector of unknowns, and $\mathbf{F}_j$ denotes the entire vector of the functions, F_k, then a better estimate, $\mathbf{q}_{j+1}$, can be obtained from,

$$\mathbf{q}_{j+1} = \mathbf{q}_j + \mathbf{J}^{-1}\,\mathbf{F}_j$$

where $\mathbf{J}$ denotes the Jacobian matrix.

In the mathematical model of the helicopter shown in Appendix 1, an engine model has been included. This extra degree of freedom is incorporated via the rotor speed, Ω, so that the

unknowns are increased from six to seven and hence the Helinv inverse algorithm solves for $\mathbf{q} = (\theta, \phi, \Omega, \theta_0, \theta_{1s}, \theta_{1c}, \theta_{0tr})$.

In the Helinv inverse algorithm the equations of motions are rearranged to give,

$$F_1(\theta, \phi, \Omega, \theta_0, \theta_{1s}, \theta_{1c}, \theta_{0tr}) = -m(\dot{u} + w\,q - v\,r) + X - m\,g\sin\theta = 0$$

$$\vdots \qquad\qquad \vdots$$

$$F_6(\theta, \phi, \Omega, \theta_0, \theta_{1s}, \theta_{1c}, \theta_{0tr}) = -\dot{r}\,I_{zz} + (I_{xx} - I_{yy})\,p\,q + I_{xz}(\dot{p} - q\,r) + N = 0$$

$$F_7(\theta, \phi, \Omega, \theta_0, \theta_{1s}, \theta_{1c}, \theta_{0tr}) = \ddot{Q}_E\,\tau_{e1}\tau_{e2} + (\tau_{e1} + \tau_{c3})\,\dot{Q}_E + Q_E - K_3(\Omega - \Omega_{idle} + \tau_{e2}\,\dot{\Omega}) = 0$$

The inverse algorithm solves the equations of motion by first providing an initial guess of the vector of unknowns, **q**. The basis of the algorithm is the calculation of the rates of the unknown attitudes $\dot{\theta}$ and $\dot{\phi}$ by numerical differentiation. This allows the unsteady terms in the equations of motion to be calculated thereby converting the helicopter equations of motion to a set of nonlinear algebraic expressions. The Newton - Raphson scheme can then be used to provide a better estimate of the unknown vector, **q**. As the output vector, **y**, expresses the flight path in the form of a time history, the inverse algorithm is cast in a 'time marching' form and solves the vehicle equations of motion at each point in the trajectory.

The complex nature of the expressions that form the body velocities, vehicle forces and moments etc., means that the calculation sequence of the inverse algorithm must be undertaken in a specific order. The next sections aim to highlight this sequence whilst providing a detailed discussion of the inverse algorithm itself.

2.2.1 Flight Path

The first task of the inverse simulation is to define the flight path over a series of n equally spaced time intervals so that at,

$$t = 0, \qquad i=1$$

and at,

$$t = t_m, \qquad i=n+1$$

where the index i denotes the i^{th} time point, t represents time and t_m the total manoeuvre time.

For time point i, the three Earth-axes positions can be given as,

$$x_{c_i} = x_c(t_i) \qquad y_{c_i} = y_c(t_i) \qquad z_{e_i} = z_e(t_i)$$

and these can be differentiated with respect to time as the flight path is usually a simple polynomial to give the Earth-axes translational velocities and accelerations given by,

$$\dot{x}_{c_i} = \dot{x}_c(t_i) \qquad \dot{y}_{e_i} = \dot{y}_c(t_i) \qquad \dot{z}_{e_i} = \dot{z}_c(t_i)$$

$$\ddot{x}_{e_i} = \ddot{x}_e(t_i) \qquad \ddot{y}_{e_i} = \ddot{y}_c(t_i) \qquad \ddot{z}_{e_i} = \ddot{z}_e(t_i)$$

In helicopter inverse simulation, it should be recognised that there are many methods which can be adopted to specify the helicopter trajectory and these are utilised by Thomson and Bradley (1992) and Taylor, Thomson and Bradley (1993). The formulation given above has been adopted in the context of this appendix for clarity.

2.2.2 Additional Constraints

Neglecting temporarily the rotorspeed equation, the inverse solution algorithm can be described as the solution of the six rigid body equations of motion for seven unknowns (θ_0, θ_{1s}, θ_{1c}, θ_{0tr}) and (θ, ϕ, ψ). If a unique solution is to be found then clearly additional constraint must be specified. This can be achieved by either specifying a heading or side slip constraint.

a) Heading Constraint

If a heading constraint is applied, then the heading angle is specified directly as a function of time,

$$\psi_i = \psi(t_i)$$

from which the yaw rate and acceleration can be easily determined by differentiating the function.

b) Sideslip Constraint

When it is more convenient to constrain sideslip, e.g. in turning flight where heading is changing constantly, the side slip angle is expressed as $\beta_i = \beta(t_i)$. The sideslip velocity and acceleration can then be determined from,

$$v = V \sin\beta_i$$

$$\dot{v} = \dot{V} \sin\beta_i + \dot{\beta}_i V \cos\beta_i$$

where V denotes the flight path velocity and $\dot{\beta}_i$ the side slip acceleration.

The side slip velocity can be determined from the transformation of the Earth based velocity components ($\dot{x}_e$, $\dot{y}_e$, $\dot{z}_e$) to the aircraft body axes. The side slip velocity can be determined from,

$$v = m_1 \dot{x}_e + m_2 \dot{y}_e + m_3 \dot{z}_e \qquad \text{(A2.3)}$$

where ,

$$m_1 = \sin\phi \sin\theta \cos\psi - \cos\phi \sin\psi$$
$$m_2 = \sin\phi \sin\theta \sin\psi + \cos\phi \cos\psi$$
$$m_3 = \sin\phi \cos\theta$$

Equation (A2.3) can be rearranged to give,

$$a \cos\psi + b \sin\psi + c = 0 \qquad \text{(A2.4)}$$

where ,

$$a = \dot{x}_e \sin\phi \sin\theta + \dot{y}_e \cos\phi$$
$$b = -\dot{x}_e \cos\phi + \dot{y}_e \sin\phi \sin\theta$$
$$c = \dot{z}_e \sin\phi \cos\theta - v$$

If values of θ and ϕ are available, then equation (A2.4) can be solved numerically for ψ using a Newton - Raphson method (Press et. al., 1992).

2.2.3 Evaluation of Body Attitude Angles and Rates

An initial guess at the vehicle pitch and roll attitude angle are made at the start of each iteration, j, of the Newton - Raphson method. Considering the pitch attitude, θ, the initial estimate is given by,

$$\theta_{i,j} = \begin{cases} \theta_e & \text{for } j = 1,\ i = 1 \\ \theta_{i-1} & \text{for } j = 1 \\ \theta_{i,j-1} & \text{for } j > 1 \end{cases}$$

thus for the first iteration at each time point, i, in the trajectory, it is evident that the previous value of value, i-1, is used as an initial estimate. Furthermore, for the first iteration at time t = 0, the estimate of pitch attitude assumes a predetermined value, θ_e, available at the start of the simulation. The roll attitude, ϕ, and the rotor speed, Ω, are treated in a similar manner.

Using numerical differentiation it is possible to evaluate the first and second derivatives with respect to time of the pitch attitude angle. The first and second derivatives of pitch attitude with respect to time, $\dot{\theta}_{i,j}$ and $\ddot{\theta}_{i,j}$ can be determined from,

$$\dot{\theta}_{i,j} = \frac{\theta_{i,j} - \theta_{i-1}}{t_i - t_{i-1}}$$

$$\ddot{\theta}_{i,j} = \frac{\overline{\theta}_{i,j} - 2\,\overline{\theta}_{i-1} - \overline{\theta}_{i-2}}{(t_i - t_{i-1})^2}$$

The roll attitude and rotor velocity derivatives with respect to time are evaluated similarly.

2.2.4 Evaluation of Body Translational Velocities and Accelerations

The vehicle body axes translational velocities are evaluated by a series of transformations of the Earth fixed velocities ($\dot{x}_c$, $\dot{y}_c$, $\dot{z}_e$) via the Euler attitude angles (θ, ϕ, ψ). This transformation is the transpose of that implied by equation (A2.2) where the output, **y**, is related to the system state vector, **x**, through the function **g**. Therefore the vehicle translational velocities for the j^{th} iteration of time point i can then be found from,

$$\begin{bmatrix} u_{i,j} \\ v_{i,j} \\ w_{i,j} \end{bmatrix} = \begin{bmatrix} l_1 & l_2 & l_3 \\ m_1 & m_2 & m_3 \\ n_1 & n_2 & n_3 \end{bmatrix} \begin{bmatrix} \dot{x}_{e_i} \\ \dot{y}_{e_i} \\ \dot{z}_{e_i} \end{bmatrix}$$

where (l_1, l_2, ..., n_3) are the direction cosines of the form,

$$l_1 = \cos\theta_{i,j} \sin\psi_i \qquad \text{etc.}$$

The rotorcraft body axes accelerations can be found by differentiating equation (A2.7) give,

$$\begin{bmatrix} \dot{u}_{i,j} \\ \dot{v}_{i,j} \\ \dot{w}_{i,j} \end{bmatrix} = \begin{bmatrix} l_1 & l_2 & l_3 \\ m_1 & m_2 & m_3 \\ n_1 & n_2 & n_3 \end{bmatrix} \begin{bmatrix} \ddot{x}_{e_i} \\ \ddot{y}_{e_i} \\ \ddot{z}_{e_i} \end{bmatrix} + \begin{bmatrix} \dot{l}_1 & \dot{l}_2 & \dot{l}_3 \\ \dot{m}_1 & \dot{m}_2 & \dot{m}_3 \\ \dot{n}_1 & \dot{n}_2 & \dot{n}_3 \end{bmatrix} \begin{bmatrix} \dot{x}_{e_i} \\ \dot{y}_{e_i} \\ \dot{z}_{e_i} \end{bmatrix}$$

where ($\dot{l}_1$, $\dot{l}_2$, ..., $\dot{n}_3$) are the derivatives with respect to time of the direction cosines where,

$$\dot{l}_1 = -\dot{\theta}_{i,j} \sin\theta_{i,j} \sin\psi_i + \dot{\psi}_i \cos\theta_{i,j} \cos\psi_i \qquad \text{etc.}$$

2.2.5 Evaluation of Body Rotational Velocities and Accelerations

The vehicle rotational angular velocities about the body fixed axes set for the i^{th} time point and j^{th} iteration of the Newton - Raphson scheme can be determined by rearranging equation (A1.2) to give,

$$\begin{aligned} p_{i,j} &= \dot{\phi}_{i,j} - \dot{\psi}_i \sin\theta_{i,j} \\ q_{i,j} &= \dot{\theta}_{i,j} \cos\phi_{i,j} + \dot{\psi}_i \cos\theta_{i,j} \sin\phi_{i,j} \\ r_{i,j} &= \dot{\psi}_i \cos\theta_{i,j} \cos\phi_{i,j} - \dot{\theta}_{i,j} \sin\phi_{i,j} \end{aligned}$$

which can be differentiated to give the corresponding angular accelerations as,

$$\begin{aligned} \dot{p}_{i,j} &= \ddot{\phi}_{i,j} - \ddot{\psi}_i \sin\theta_{i,j} - \dot{\psi}_i \dot{\theta}_{i,j} \sin\theta_{i,j} \\ \dot{q}_{i,j} &= \ddot{\theta}_{i,j} \cos\phi_{i,j} - \dot{\theta}_{i,j} \dot{\phi}_{i,j} \sin\phi_{i,j} + \ddot{\psi}_i \cos\theta_{i,j} \sin\phi_{i,j} + \\ &\quad + \dot{\psi}_i (-\dot{\theta}_{i,j} \sin\theta_{i,j} \sin\phi_{i,j} + \dot{\phi}_{i,j} \cos\theta_{i,j} \cos\phi_{i,j}) \\ \dot{r}_{i,j} &= \ddot{\psi}_i \cos\theta_{i,j} \cos\phi_{i,j} - \ddot{\theta}_{i,j} \sin\phi_{i,j} - \dot{\theta}_{i,j} \dot{\phi}_{i,j} \cos\phi_{i,j} + \\ &\quad + \dot{\psi}_i (-\dot{\theta}_{i,j} \sin\theta_{i,j} \cos\phi_{i,j} - \dot{\phi}_{i,j} \cos\theta_{i,j} \sin\phi_{i,j}) \end{aligned}$$

2.2.6 Determination of Forces and Moments

With estimates of all the states now available, it is possible to evaluate the external forces and moments as detailed in Appendix 1.

Once the net contribution of individual forces and moments generated by the constituent parts of the helicopter is determined, all the information is present with which the functions F_1, F_2, ..., F_7 can be calculated.

2.2.7 Update of Current Estimate of Controls, Attitude Angles and Rotor Speed

The Newton - Raphson scheme employed in this inverse algorithm has the structure,

$$\begin{bmatrix} \theta_{j,j+1} \\ \vdots \\ \vdots \\ \theta_{0tr_{i,j+1}} \end{bmatrix} = \begin{bmatrix} \theta_{i,j} \\ \vdots \\ \vdots \\ \theta_{0tr_{i,j}} \end{bmatrix} - \begin{bmatrix} \left(\frac{\partial F_1}{\partial \theta}\right)_{i,j} & \cdots & \left(\frac{\partial F_1}{\partial \theta_{0tr}}\right)_{i,j} \\ \vdots & & \vdots \\ \vdots & & \vdots \\ \left(\frac{\partial F_7}{\partial \theta}\right)_{i,j} & \cdots & \left(\frac{\partial F_7}{\partial \theta_{0tr}}\right)_{i,j} \end{bmatrix}^{-1} \begin{bmatrix} F_1(\theta,\phi,\Omega,\theta_0,\theta_{1s},\theta_{1c},\theta_{0tr})_{i,j} \\ \vdots \\ \vdots \\ F_7(\theta,\phi,\Omega,\theta_0,\theta_{1s},\theta_{1c},\theta_{0tr})_{i,j} \end{bmatrix}$$

.....(A2.5)

The entries of the Jacobian can be determined from a numerical differentiation scheme based on central differences. For example, the upper left entry of the Jacobian, can be evaluated from,

$$\left(\frac{\partial F_1}{\partial \theta}\right)_{i,j} = \frac{F_1\left(\theta+\delta\theta,\phi,.....,\theta_{0_{tr}}\right)_{i,j} - F_1\left(\theta-\delta\theta,\phi,.....,\theta_{0_{tr}}\right)_{i,j}}{2\delta\theta}$$

for a small displacement in θ denoted by $\delta\theta$. The other entries of the Jacobian can be determined in a similar fashion. It should be noted that by employing this method to calculate the Jacobian, fourteen positive and negative perturbations of the functions are required.

Once the Jacobian has been evaluated, it is inverted using a standard matrix inversion routine. Following this, a better estimate of the seven unknowns can be determined from equation (A2.5). Steps 2.2.2 to 2.2.7 are repeated until the unknowns have converged to the desired levels.

Once the unknown control, attitude and rotor speed parameters are determined for the the i^{th} time point, the solution algorithm steps forward one point and the unknowns re-evaluated via sequence 2.2.2 to 2.2.7. This process is repeated until the the unknown controls etc. are determined for the whole manoeuvre.

Appendix 3

Dynamic Inflow Model of Peters and Haquang

The dynamic inflow model of Peters and HaQuang has the form,

$$\underline{\mathbf{M}}\begin{bmatrix}\dot{\lambda}_0\\ \dot{\lambda}_{1sw}\\ \dot{\lambda}_{1cw}\end{bmatrix}+\underline{\mathbf{L}}_{\mathbf{nl}}^{-1}\begin{bmatrix}\lambda_0\\ \lambda_{1sw}\\ \lambda_{1cw}\end{bmatrix}=\begin{bmatrix}C_{Tw}\\ -C_{Lw}\\ -C_{Mw}\end{bmatrix}_{aerodynamic} \qquad \text{(A3.1)}$$

where $\underline{\mathbf{M}}$ is the apparent mass matrix and is defined as:

$$\underline{\mathbf{M}}=\begin{bmatrix}\frac{128}{75} & 0 & 0\\ 0 & -\frac{16}{45\pi} & 0\\ 0 & 0 & -\frac{16}{45\pi}\end{bmatrix}$$

Here $\underline{\mathbf{L}}_{\mathbf{nl}}$ is the nonlinear inflow gain matrix in the wind - hub axes set and relates the uniform, lateral and longitudinal inflow components to the thrust, rolling and pitching moment coefficients. The matrix is non-diagonal, thus highlighting the cross coupling that occurs between the inflow states in this theory. The non-linear inflow gain matrix is defined as:

$$\underline{\mathbf{L}}_{\mathbf{nl}} = \underline{\mathbf{L}}^{-1}\,\underline{\mathbf{V}}$$

and $\underline{\mathbf{L}}$ is referred to the wind - hub axes set and is defined as:

$$\underline{\mathbf{L}}=\begin{bmatrix}\frac{1}{2} & 0 & \frac{15\pi}{64}\left(\frac{1-\sin\alpha}{1+\sin\alpha}\right)^{\frac{1}{2}}\\ 0 & \frac{-4}{1+\sin\alpha} & 0\\ \frac{15\pi}{64}\left(\frac{1-\sin\alpha}{1+\sin\alpha}\right)^{\frac{1}{2}} & 0 & \frac{-4\sin\alpha}{1+\sin\alpha}\end{bmatrix}$$

The wake angle, α, is defined similarly to that utilised in the Glauert model and is defined as,

$$\alpha=\tan^{-1}\left[\frac{|\mu_z-\lambda_m|}{\mu}\right]$$

The mass flow parameter matrix $\underline{\mathbf{V}}$ is given by,

$$\underline{\mathbf{V}} = \begin{bmatrix} V_T & 0 & 0 \\ 0 & V_M & 0 \\ 0 & 0 & V_M \end{bmatrix}$$

where V_T is the total resultant flow through the rotor disc,

$$V_T = \sqrt{\mu^2 + (\mu_z - \lambda_m)^2}$$

where λ_m denotes the normal induced velocity due to rotor thrust. The mass flow parameter V_M, is the weighted velocity component (Gaonkar and Peters, 1988) and is given by,

$$V_M = \frac{d(V_T.\lambda_m)}{d\lambda_m} = \frac{\mu^2 + (\mu_z - 2\lambda_m)(\mu_z - \lambda_m)}{V_T}$$

It is necessary to express the rotor forces and moments in hub axes and therefore,

$$\begin{bmatrix} C_{Tw} \\ -C_{Lw} \\ -C_{Mw} \end{bmatrix} = \underline{\mathbf{T}}_{hub_w} \begin{bmatrix} C_T \\ -C_L \\ -C_M \end{bmatrix}$$

$$\begin{bmatrix} \lambda_0 \\ \lambda_{1sw} \\ \lambda_{1cw} \end{bmatrix} = \underline{\mathbf{T}}_{hub_w} \begin{bmatrix} \lambda_0 \\ \lambda_{1s} \\ \lambda_{1c} \end{bmatrix}$$

where the rotation matrix, $\underline{\mathbf{T}}_{hub_w}$ denotes the transformation from hub to wind axes is given by,

$$\underline{\mathbf{T}}_{hub_w} = \begin{bmatrix} 1 & 0 & 0 \\ 0 & \cos\psi_w & \sin\psi_w \\ 0 & -\sin\psi_w & \cos\psi_w \end{bmatrix}$$

Therefore, in hub axes, equation (A3.1) becomes,

$$\underline{\mathbf{M}}\begin{bmatrix}\dot{\lambda}_0\\ \dot{\lambda}_{1s}\\ \dot{\lambda}_{1c}\end{bmatrix}+\underline{\tilde{\mathbf{L}}}_{\mathbf{nl}}^{-1}\begin{bmatrix}\lambda_0\\ \lambda_{1s}\\ \lambda_{1c}\end{bmatrix}=\begin{bmatrix}C_T\\ -C_L\\ -C_M\end{bmatrix}_{\text{aerodynamic}} \qquad \text{(A3.2)}$$

where,

$$\underline{\tilde{\mathbf{L}}}_{\mathbf{nl}}^{-1}=\underline{\mathbf{V}}\,\underline{\mathbf{T}}_{\text{hub}_w}^{\Gamma}\,\underline{\mathbf{L}}^{-1}\underline{\mathbf{T}}_{\text{hub}_w}$$

The normal induced flow, λ_m, due to the rotor thrust can be determined from,

$$\lambda_m=\frac{1}{2}\begin{bmatrix}1\\0\\0\end{bmatrix}^T\underline{\mathbf{T}}_{\text{hub}_w}^{T}\,\underline{\mathbf{L}}^{-1}\underline{\mathbf{T}}_{\text{hub}_w}\begin{bmatrix}\lambda_0\\ \lambda_{1s}\\ \lambda_{1c}\end{bmatrix}$$

Appendix 4

Mathematical Model of an Artificial Stability and Flight Control System

The mathematical model of the artificial stability and flight control system given by Padfield (1981) is now presented. Each of the collective, longitudinal and lateral cyclic control channels will be discussed in turn.

i) Collective Channel

The pilot contribution to collective pitch, θ_{0_p}, is given by,

$$\theta_{0_p} = g_{co} + g_{c1}\,\eta_c$$

where g_{co}, g_{c1} are gearing constants and η_c is the collective lever position ($0 \leq \eta_c \leq 1$). The gearing constants are derived from the blade upper and lower collective pitch limits. The autostab contribution to collective swashplate angle, θ_{0_a}, is obtained from a normal accelerometer so that,

$$\theta_{0_a} = k_g \Delta n$$

where,

$$\Delta n = 1 + \frac{a_z}{g}$$

and,

k_g is the accelerometer feedback gain ,
a_z is the normal body axis acceleration as measuresed by an accelerometer,
g is the acceleration due to gravity.

The net displacements from the pilot and autostab are passed through a hydraulic actuator modelled as a first order lag, so that its transfer function has the form,

$$\frac{\theta_0}{\theta_{0_p} + \theta_{0_a}} = \frac{1}{1+\tau_{c4}\,s}$$

where,

τ_{c4} is the actuator time constant,

θ_o is the combined collective displacement after actuation

It should be noted that the representation of a hydraulic actuator via a first order lag implies that the effect of compressibility and leakage of the hydraulic fluid and inertia of the actuator moving components has been neglected. Furthermore, no nonlinear saturation functions have been included and consequently the actuator mechanism will achieve any commanded position that is requested of it.

ii) Longitudinal Cyclic Channel

In the flight control system, the pilot contribution to longitudinal cyclic displacement prior to mixing, $\theta_{1s_p}{}^*$, is derived from contributions of the longitudinal cyclic and collective lever positions. The latter is included to alleviate the coupling incurred from longitudinal stick and collective lever inputs that occur with changes in airspeed. Thus the longitudinal cyclic contribution from the pilot can be given by,

$$\theta_{1s_p}{}^* = g_{1s0} + g_{1s1}\,\eta_{1s} + (g_{sc0} + g_{sc1}\,\eta_{1s})\,\eta_c$$

where,

g_{1s0}, g_{1s1} are gearing constants associated with the longitudinal cyclic,
g_{sc0}, g_{sc1} are gearing constants associated with the collective contribution,
η_{1s} is the pilot longitudinal cyclic stick position ($0 \le \eta_{1s} \le 1$).

The autostabiliser contribution to longitudinal cyclic, $\theta_{1s_a}{}^*$, is obtained from the proportional and derivative action feedback of the pitch attitude, θ, and pitch rate, q. The proportional and derivative feedback terms are included to control the long and short term longitudinal response of the helicopter respectively. An additional feed forward term based on pilot stick and current cyclic trim position with respect to some datum is also included. This feature of the longitudinal channel permits improved vehicle response to a given longitudinal cyclic input. Another equally important characteristic of this type of control law is discussed by Smith (1981) where it is observed that for a given trimmed actuator position, the inclusion of the stick position signal reduces the change in series actuator offset resulting from changes in airspeed. This is important if the actuator is to remain within its authority and hardovers with significant offsets are to be avoided. The longitudinal autostabiliser contribution can be obtained from,

$$\theta_{1s_a}{}^* = k_\theta\,\theta + k_q\,q + k_{1s}\,(\eta_{1s} - \eta_{1so})$$

where,

k_θ is a proportional action feedback gain,

k_q is a derivative action feedback gain,

k_{1c} is the feed forward gain,

η_{1so} is the reference (trim) longitudinal stick position, $(0 \leq \eta_{1s0} \leq 1)$.

As in the collective case, the combined autostabiliser and pilot contributions to longitudinal cyclic are passed through a hydraulic actuator which in this mathematical model is represented as a first order lag. The transfer function is then given by,

$$\frac{\theta_{1s}^*}{\theta_{1s_p}^* + \theta_{1s_a}^*} = \frac{1}{1+\tau_{c_1} s}$$

where τ_{c_1} is the time constant associated with the longitudinal actuator.

One of the coupling effects exhibited by a helicopter can be attributed to the rotor phase lag and its influence on vehicle behaviour has also been addressed. To help ameliorate this effect, the longitudinal and lateral cyclic displacements are mixed or 'phased' after actuation. In practice, this phasing is achieved by the geometric arrangement of the pitch link attachments from the swashplate to the blade cuffs. Consider the case where the lateral and longitudinal actuation servo's are located at $\psi = 0$ and 90 degrees. If the reduction in phase angle is around 15^o say, then for a fore and aft tilt of the rotor disc, the maximum actuator displacement occurs when the rotor blade is at an azimuthal location of 105 degrees. The actuator arrangement is modelled by the following simple expressions,

$$\theta_{1s} = \theta_{1s}^* \cos \psi_f + \theta_{1c}^* \sin \psi_f$$

$$\theta_{1c} = \theta_{1c}^* \cos \psi_f - \theta_{1s}^* \sin \psi_f$$

where,

θ_{1s}, θ_{1c} are the longitudinal and lateral cyclic displacements at the swashplate after mixing ,

θ_{1s}^*, θ_{1c}^* are the longitudinal and lateral cyclic stick displacements prior to mixing,

ψ_f is the cyclic mixing angle .

iii) Lateral Cyclic Channel

The lateral cyclic displacement at the swashplate due to pilot inputs, θ_{1c}^*, is a function of cyclic stick movements only and is given by,

$$\theta_{1c}^* = g_{1c0} + g_{1c1}\,\eta_{1c}$$

where,

g_{1c0}, g_{1c1} are stick gearing constants,
η_{1c} is the pilot lateral cyclic stick displacement ($0 \le \eta_{1c} \le 1$).

The autostabiliser contribution to the lateral cyclic channel is derived from the proportional and derivative action feedback of roll attitude, ϕ, and roll rate, p, respectively. An additional feed forward term based on lateral stick position with respect to some datum value is also included and serves the same purpose as the feed forward in the longitudinal channel. Thus the lateral cyclic contribution from the autostab, $\theta_{1c_a}^*$, and is obtained from,

$$\theta_{1c_a}^* = k_\phi\,\phi + k_p\,p + k_{1c}\,(\eta_{1c} - \eta_{1co})$$

where,

k_ϕ is a proportional action feedback gain,
k_p is a derivative action feedback gain,
k_{1c} is the feed forward gain,
η_{1so} is the reference pilot stick position, ($0 \le \eta_{1c0} \le 1$).

The transfer function of the combined pilot and autostab contributions is given as,

$$\frac{\theta_{1c}^*}{\theta_{1c_p}^* + \theta_{1c_a}^*} = \frac{1}{1+\tau_{c2}\,s}$$

where τ_{c2} the time constant of the actuator.

iv) Yaw Channel

The pilot contribution to tail rotor blade pitch angle is made up from signals from both the collective lever and pedal positions. A linear relationship is used to combine the collective and pedal inputs into an equivalent term known as cable length, η_{ct}. The cable length is expressed in the following manner,

$$\eta_{ct} = g_{ct0}\,(1 - \eta_p) + (1 - 2\,g_{ct0})\,\eta_c$$

where,

g_{cto} is the gearing constant used in the combination of collective lever and pedal displacements,

η_p is the pilot pedal displacement, $(0 \leq \eta_p \leq 1)$.

The pilot contribution to tail rotor collective, θ_{ot_p}, can then be given by,

$$\theta_{ot_p} = g_{to} + g_{t1}\,\eta_{ct}$$

where g_{to} and g_{t1} are gearing constants.

The kinematic coupling between collective and pedal channels through the effective cable length reduces pilot workload associated with changes in collective lever position. A drawback of this system, however, is that when performing a landing in the autorotation regime with a collective pitch 'burst', the helicopter may yaw and the pilot may find that he has insufficient opposing pedal travel. The aircraft will then land with some yaw rate and if this is of sufficient magnitude, can lead to the rotorcraft overturning.

The autostabiliser contribution to the yaw channel, θ_{ot_a}, is obtained from proportional and derivative action feed back of the heading, ψ, and yaw rate, r. A 'heading - hold' facility is also included. The autostab contribution can be written as,

$$\theta_{ot_a} = k_\psi\,(\psi - \psi_H) + k_r\,r$$

where,

k_ψ, k_r is the proportional and derivative action feed back respectively,

ψ_H is the heading hold term that is adjustable by the pilot.

The transfer function of the combined pilot and autostab contributions to the tail rotor collective displacement is given as,

$$\frac{\theta_{ot}}{\theta_{ot_p} + \theta_{ot_a}} = \frac{1}{1 + \tau_{c3}\,s}$$

where τ_{c3} the time constant of the actuator.

Appendix 6

Mathematical Model of the Normal Approach and Landing Manoeuvre

This appendix documents the application of the manoeuvre formulation and validation technique outlined in Chapter 3 to the Normal Approach and landing.

Step i) - Formulation of Narrative Description of Pilot Strategy

A detailed description of the pilot strategy for a Towering Takeoff manoeuvre is given in Appendix A8.2.

Step ii) - Mathematical Modelling of Manoeuvre

A portrait of the Normal Approach and Landing flight profile is shown in Figure A6.0 from which it is evident that there are three key phases of this manoeuvre. The mathematical modelling of these distinct phases of the flight profile can be conveniently overcome by representing the complete manoeuvre as the combination of individual trajectories and this rationale is evident from the formulation of the flight paths given in the next section. A conventional Earth fixed axis set is presupposed. Vertically offset from the initial helicopter position, the z-axis points downward, the x-axis is in the direction of flight and is level with the heli-deck and the y-axis completes the right-handed triad. The velocity and acceleration time histories used as input for the inverse simulation are related to this axes set.

Examination of pilot comments and the regulatory documents for the Normal Approach and Landing reveals that flight velocity and approach angle are the intrinsic parameters associated with the manoeuvre. The task of modelling the flight path is based on the knowledge of these parameters, however, it is also necessary to specify the velocity, V_{LDP}, the descent rate v_{LDP}, and the height, h_{LDP}, at the landing decision point (LDP). Furthermore the maximum descent angle, γ_{MAX}, and the flare height, h_{FLR} at the flare point must be given. Also it will become apparent that it is necessary to specify the peak deceleration and the time taken to achieve this during the primary deceleration phase. This parameter is performance related and will depend on the power deficit of the helicopter, however, conditional upon sufficient power available, the proximity of the rig will strongly influence the magnitude of the deceleration.

For these considerations, a mathematical model of a Normal Approach and Landing manoeuvre is now given.

Steady Descent Phase ($0 < t < t_{LDP}$)

During this phase the pilot strategy is given by,

"During the stabilised approach the flight path speed will be typically in the region of 30 - 40 kts, with a descent rate of 300ft/min."

from which it is evident that the key piloting parameters are the approach flight speed, V_{LDP}, and rate of descent, v_{LDP}. The flight path velocity and descent rate time histories can be given by,

$$V(t) = V_{LDP}$$

$$v(t) = V_{LDP} \sin \gamma_{LDP}$$

where γ_{LDP} is the LDP descent angle. The landing decision point height is assured by integration of the descent rate profile:

$$h_1 - \int_0^{t_{LDP}} v(t)dt = h_{LDP}$$

where h_1 denotes the initial manoeuvre height.

Primary Deceleration Phase ($t_{LDP} < t \leq t_{FLR}$)

It is crucial for this phase of the manoeuvre to capture the principle features of the pilot strategy and this is given as,

"At the LDP, the combined use of collective and longitudinal cyclic is used to decelerate the aircraft and increase the descent angle to 10 -15 deg. Typically for this, the aircraft nose is pitched up to a constant value...."

The most appropriate way of portraying this aspect of the manoeuvre is to specify a longitudinal acceleration time history, $\ddot{x}(t)$, that includes a constant deceleration phase. Clearly a transient deceleration must also be incorporated to transition the helicopter from its trimmed flight mode at the LDP to some maximum constant deceleration, $\ddot{x}_{min}$, at time t_1. The time t_1 is

selected to suit the nature of the manoeuvre, while a smoothly connected, piecewise cubic polynomial in time was chosen to achieve the transition, Figure A6.1a. The longitudinal acceleration can then be expressed as,

$$t_{LDP} < t \le t_1 \qquad \ddot{x}(t) = \ddot{x}_{min}\left[-2\left(\frac{t - t_{LDP}}{t_1 - t_{LDP}}\right)^3 + 3\left(\frac{t - t_{LDP}}{t_1 - t_{LDP}}\right)^2\right]$$

$$t_1 < t \le t_{FLR} \qquad \ddot{x}(t) = \ddot{x}_{min}$$

As in the Towering Takeoff manoeuvre, it it evident that cubic polynomials were chosen as they provided adequate continuity whilst being simple to implement.

In addition to specifying the acceleration time history, the nature of the piloting strategy indicates that descent angle should also be defined. It is assumed in this model of the Approach and Landing manoeuvre that descent angle increases from γ_{LDP} to some maximum value γ_{MAX} over the period t_{LDP} to t_1. The descent angle, γ_{MAX}, is maintained until the flare point is reached. As in the expressions for $\ddot{x}(t)$, a cubic polynomial function of time was used to achieve the transition in descent angle. The functions required for variation in descent angle can be given as,

$$t_{LDP} < t \le t_1 \qquad \gamma(t) = (\gamma_{MAX} - \gamma_{LDP})\left[-2\left(\frac{t - t_{LDP}}{t_1 - t_{LDP}}\right)^3 + 3\left(\frac{t - t_{LDP}}{t_1 - t_{LDP}}\right)^2\right] + \gamma_{LDP}$$

$$t_1 < t \le t_{FLR} \qquad \gamma(t) = \gamma_{MAX}$$

and shown in Figure A6.1b.

In this formulation of the Normal Approach and Landing manoeuvre, the maximum descent angle is specified. Recalling that the longitudinal velocity profile, $\dot{x}(t)$, can be obtained from,

$$\dot{x}(t) = \int^t \ddot{x}(t)dt$$

then the peak deceleration value, $\ddot{x}_{min}$, can be chosen to ensure that the flare height is achieved from,

$$h_1 - \int_0^{t_{FLR}} \dot{x}(t)\tan\gamma(t)dt = h_{FLR}$$

Final Flare Phase ($t_{FLR} < t \leq t_m$)

As the helicopter enters the final flare phase, the requirement is for the vehicle to simultaneously decelerate until the ground velocity becomes zero while reducing altitude until the helicopter lands on the helideck. The pilot strategy is given as,

"At the flare point the vehicle is typically 25ft above the landing surface.... Longitudinal cyclic stick displacements are used to progressively reduce any remaining positive nose up attitude while gradually reducing flight speed. Collective is used to descend the vehicle towards the heli-deck."

The flare is conveniently modelled by using a cubic polynomial of time to represent the longitudinal acceleration time history, $\ddot{x}(t)$. The deceleration is varied from its maximum value, $\ddot{x}_{min}$, to zero over the period t_{FLR} to t_m. The function required for this is given as,

$$\ddot{x}(t) = -\ddot{x}_{min}\left[-2\left(\frac{t - t_{FLR}}{t_m - t_{FLR}}\right)^3 + 3\left(\frac{t - t_{FLR}}{t_m - t_{FLR}}\right)^2\right] + \ddot{x}_{min} \qquad t_{FLR} < t \leq t_m$$

and is shown in Figure A6.1c. The duration of the final flare phase is chosen to reflect the proximity of the oilrig platform and is a parameter of the mathematical model.

Considering the altitude strategy,

"Collective is used to descend the vehicle towards the heli-deck."

a suitable expression fifth order polynomial function in time, z(t), has been found from the boundary conditions at the flare point and at the end of the manoeuvre. These are given as,

a) $t=t_{FLR}$ $\quad z = -h_{FLR}$ $\quad \dot{z} = \dot{z}_{FLR}$ $\quad \ddot{z} = \ddot{z}_{FLR}$

b) $t=t_m$ $\quad z = 0$ $\quad \dot{z} = -v_E$ $\quad \ddot{z} = 0$

The altitude profile is shown in Figure A6.1d.

The Normal Approach and Landing is a pure longitudinal manoeuvre and thus the final constraint is simply given by,

$$\dot{y}(t) = 0$$

The definition of the Normal Approach and Landing is completed by specifying the additional constraint that the heading should be maintained constant throughout.

Step iii) and iv) - Inverse Simulation and Validation of Towering Takeoff Manoeuvre

The mathematical representation of the Approach and Landing manoeuvre requires only a few basic parameters with which the flight path, velocity and acceleration time histories can be evaluated. These are :

$$V_{LDP} = 35\text{kts},\ h_{LDP} = 30.5\text{m (100ft.)},\ v_{LDP} = 1.5\text{m/s (300ft/min)}$$
$$\ddot{x}_{MIN} = 1.0\text{m/s}^2,\ t_1 - t_{FLR} = 2.5\text{s},\ \gamma_{MAX} = 7^o$$
$$h_{FLR} = 25\text{ft.},\ V_{FLR} = 9\text{kts},\ t_m - t_{FLR} = 9\text{s},$$
$$t_m = 29\text{s},\ v_{TM} = 1.5\text{m/s (300ft/min)}.$$

These values are representative of those values found during Normal Approach and Landing manoeuvres to offshore platforms.

The first 4 seconds of the manoeuvre correspond to the initial approach, a phase where constant flight speed and rate of descent are adopted and this strategy is evident from Figure A6.2. When the landing decision point (LDP) is reached, the primary deceleration phase is entered and spans the period t = 4 - 15s. At the LDP, the descent angle is gradually increased to a value 7° over a period of 2.5s and combined with the high initial approach speed, leads to an initial increase in descent rate to a peak value of 2m/s. From the acceleration time history a rapid increase in deceleration to 1.0m/s^2 is achieved 2.5 seconds after the LDP. Furthermore this value of deceleration is sustained for 12s until the flare point is reached 20 seconds into the manoeuvre. The constant deceleration results in velocity decreasing linearly over the primary deceleration phase and this is clear from the velocity time history. At the flare point 25ft. above the helideck and 30ft. from the landing point, a flight speed of 9kts. is attained. For the remaining 9 seconds left until the end of the manoeuvre, flight speed is gradually reduced until the final flight velocity of 2kts obtained on touchdown. The rapid increase in descent rate with gradual reduction in flight velocity results in a rapid increase in descent angle to 90° at the end of the manoeuvre as seen in the descent angle time history.

Once the trajectory information has been calculated, it can then be used as input to the inverse simulation to obtain the corresponding vehicle control displacements necessary for the helicopter to follow the flight path. A helicopter configuration relating to a medium weight transport aircraft as commonly found in offshore operations has been adopted for this study. The controls and flight states generated for such an aircraft flying a Normal Approach and Landing manoeuvre are now discussed.

The inverse simulation results of a Normal Approach and Landing manoeuvre is depicted in Figure A6.3. The steady descent section is clearly visible from the plots and has a duration of 4 seconds. The cyclic stick is close to centre and the body attitudes reflects this - fuselage roll angle is small while the vehicle is pitched 2° up affording good pilot vision of the landing platform. The main rotor collective is at a low setting due to the limited demands of the flight profile and consequently the engine torque output is less than 40%. The pedal displacement is sufficient to maintain heading. At the landing decision point, the accelerative demands of the flight path results in the main rotor collective being lowered and longitudinal cyclic moved aft by 8%. An additional forward pulse of longitudinal cyclic arrests the rotor discs aft motion and results in the vehicle achieving a 8° nose up attitude. As the vehicle decelerates, main rotor collective progressively increases to reduce the descent rate. Furthermore, as the forward motion of the helicopter reduces, there is a tendency of the rotor disc to pitch forward and therefore a slow progressive aft motion of the longitudinal cyclic is necessary to maintain the deceleration. During this period the vehicle nose follows the longitudinal cyclic motion and gently pitches upward to a maximum value of approximately 9.5° after 20 seconds. At the flare point the collective is set to 30% and a small input in forward cyclic initiates a nose down pitching motion that gently and smoothly reduces the helicopter pitch attitude over the remaining 9 seconds of the manoeuvre. This attitude change is of much longer duration than that employed during the initial deceleration phase as this reflects the pilot awareness of the rig structure. As ground speed falls to below 1kt. the helicopter enters the final vertical descent phase 14ft. above the ground. Vertical velocity is increased slowly until a final rate of descent of 300ft/min is achieved to complete the manoeuvre. It is also evident from Figure A6.3 that there is little roll and lateral cyclic motion throughout the manoeuvre and that pedal displacement gradually reduce over the flight.

Appendix 7

Mathematical Models of Recovery Manoeuvres

The formulation of the Vertical Reject, Baulked Landing and Continued Landing recovery manoeuvres are now presented.

7.1 Engine Failure Prior To Takeoff Decision Point (Vertical Reject)

Step i) - Formulation of Narrative Description of Pilot Strategy

A detailed description of the pilot strategy for a Vertical Reject manoeuvre is given in Appendix A8.1.

Step ii) - Mathematical Modelling of Manoeuvre

The key elements of the pilot strategy are:

"The pilot will make a rapid downward collective lever input on recognising the engine failure."

"Once the flight path has been reversed ... The rate of descent will depend on the power deficit an would typically be 800ft/min"

An appropriate way to incorporate the above aspects of the vertical reject pilot strategy wa found to be to specify the vertical velocity time history in a manner similar to that shown in Figur A7.0. In this representation of the manoeuvre, it is assumed that the reduction of main rotor collective will reverse the upward vertical motion of the rotorcraft until the vehicle has achieved a peak, vertical descent velocity, v_{MAX}. This phase of the manoeuvre is completed when the helicopter approaches the flare height, h_{FLR} after a time, t_{FLR}. The cyclic and pedals controls are used to maintain the rotorcraft's position over the helideck throughout this phase of the manoeuvr

The reversal of the upward vertical motion is captured by a blending function. This is an important feature of the model as it permits control over the rate with which collective is lowered i response to the engine failure. The descent rate over this period is obtained from,

$$\dot{z}(t) = h_{\dot{z}}(t) = \phi_{\dot{z}}(t) + g_{\dot{z}}(t) \qquad t_{pr} < t < t_{FLR}$$

The expressions $\phi_{\dot{z}}(t)$ and $g_{\dot{z}}(t)$ denote the blend and final trajectory function respectively and are given by,

$$\phi_{\dot{z}}(t) = e^{-\delta_{\dot{z}}\, t}\, p_{\dot{z}}(t) \qquad\qquad g_{\dot{z}}(t) = v_{MAX}$$

The manoeuvre gain $\delta_{\dot{z}}$ is chosen (by the user) to reflect the demands of the manoeuvre an permits control over the rate at which the final maximum descent velocity is reached. The polynomial, $p_{\dot{z}}(t)$, is required to show continuity up to the third derivative at entry and exit of the vertical reject manoeuvre and hence there are six boundary conditions given as,

i) $t = t_{pr}$ $\quad p_{\dot{z}}(t)=\dot{z}(t_{pr}) - v_{MAX}$ $\quad p_{\dot{z}}'(t)=\ddot{z}(t_{pr})$ $\quad p_{\dot{z}}''(t)=\dddot{z}(t_{pr})$

ii) $t = t_R$ $\quad p_{\dot{z}}(t)=0$ $\quad p_{\dot{z}}'(t)=0$ $\quad p_{\dot{z}}''(t)=0$

which can satisfy the fifth order polynomial,

$$p_{\dot{z}}(t) = b_0 + b_1\left(\frac{t^*}{t_R^*}\right) + b_2\left(\frac{t^*}{t_R^*}\right)^2 + b_3\left(\frac{t^*}{t_R^*}\right)^3 + b_4\left(\frac{t^*}{t_R^*}\right)^4 + b_5\left(\frac{t^*}{t_R^*}\right)^5$$

where,

$$t^* = t - t_{FLR} \qquad\qquad t_R^* = t_R - t_{FLR}$$

The final flare phase of the vertical reject manoeuvre is governed by the pilot strategy:

"The helicopter is allowed to descent vertically ... until reaching a height of approximately 15ft. above the heli-deck at which point a large collective-up input is made."

A smoothly connected fifth order polynomial function of time has been used to model this strategy and is given as,

$$\dot{z}(t) = (v_{TD} - v_{MAX})\left[6\left(\frac{t - t_{FLR}}{t_R - t_{FLR}}\right)^5 - 15\left(\frac{t - t_{FLR}}{t_R - t_{FLR}}\right)^4 + 10\left(\frac{t - t_{FLR}}{t_R - t_{FLR}}\right)^3\right] + v_{MAX} \qquad t_{FLR} < t < t_R$$

where the descent velocity on touch down, v_{TD}, is achieved after a time t_R.

The altitude time history throughout the vertical reject manoeuvre may be evaluated from,

$$\int_{t_{pr}}^{t} \dot{z}(t)\,dt = z(t) \qquad t_{pr} < t < t_R$$

It is assumed in this model of the vertical reject, the helicopter returns to the heli-deck with vertical motion only and no translational position offset. In addition, at the end of the manoeuvre the rotorcraft attains its original heading as employed at the start of the takeoff. Thus, the definitic of vertical reject manoeuvre is completed by specifying the longitudinal, lateral and heading time histories as,

$$x(t) = h_x(t) = e^{-\delta_x t}\, p_x(t)$$

$$y(t) = h_y(t) = e^{-\delta_y t}\, p_y(t) \qquad t_{pr} < t < t_R$$

$$\psi(t) = h_\psi(t) = e^{-\delta_\psi t}\, p_\psi(t)$$

The terms δ_x, δ_y and δ_ψ denote the blend gains chosen (by the user) to control the rate at which the final flight path is achieved. For each of the seventh order polynomial functions of time, $p_x(t)$, $p_y(t)$ and $p_\psi(t)$, eight boundary conditions are selected to ensure the blend exhibits continuity up to and including the jerk components.

Step iii) and iv) - Inverse Simulation and Validation of Vertical Reject Manoeuvre

In the following example, the engine failure occurs 1 second before the TDP (i.e. 4 seconds into the manoeuvre) and recovery is by means of a rejected take-off, landing back on the heli-deck. This gives the following exit conditions

$$h_E = -5\text{m}, \quad v_E = 1.5 \text{ m/s} \ (\equiv 300 \text{ ft/min}).$$

Note that the manoeuvre is initiated from a height of 5m above the helideck (15ft, approx.) and hence the final altitude of -5m places the helicopter back on the platform deck. The trajectory time histories for this manoeuvre is shown in Figure A7.1.

The results from this simulation are given in Figure A7.2. The pilot's reaction (at 5 seconds) to the engine failure in this case is to reduce collective to conserve rotorspeed and arrest the upward motion. The upwards travel of the helicopter is completed at about 7.5 seconds. There is then a gradual decrease causing the rate of descent of 800ft/min to be

acheived as required. As the deck is approached, a rapid increase of 25% in main rotor collective can be observed to cushion the landing on touchdown. After the failure of the engine the torque of the remaining engine rises to its contingency maximum and remains there until the manoeuvre is completed.

There is good agreement with the piloting description of Appendix A8.1. The decrease of collective results in Nr being maintained within 6% of its reference value until it is dissipated in the final increase of collective applied in order to minimise the impact on touch down. The maximum rate of descent is approximately 800ft/min, as required.

7.2 Engine Failure Prior To Landing Decision Point (Baulked Landing)

Step i) - Formulation of Narrative Description of Pilot Strategy

A detailed description of the pilot strategy for a Baulked Landing manoeuvre is given in Appendix A8.2.

Step ii) - Mathematical Modelling of Manoeuvre

The adopted pilot strategy for the baulked landing comprises accelerative and climbing constituents. The altitude pilot strategy is noted as:

"The baulked landing safety speed is maintained during the subsequent fly away to complete the manoeuvre with a positive rate of climb of approximately 300ft/min."

An effective means of incorporating this strategy is to specify a vertical velocity profile su as that shown in Figure A7.3a. The most fundamental parameters associated with this phase are tl rate of climb, v_E and altitude, h_E, at the exit altitude and consequently knowledge of these parameters forms the basis of the manoeuvre.

A blend function has been used in the formulation of this profile as it permits control over the rate at which the final steady climb rate is attained. The vertical velocity profile is given as,

$$\dot{z}(t) = h_{\dot{z}}(t) = \phi_{\dot{z}}(t) + g_{\dot{z}}(t) \qquad t_{pr} < t < t_R$$

where,

$$\phi_{\dot{z}}(t) = e^{-\delta_{\dot{z}} t}\, p_{\dot{z}}(t) \qquad g_{\dot{z}}(t) = -v_E$$

The polynomial, $p_{\dot{z}}(t)$, is required to show continuity up to the third derivative at entry and exit of the baulked landing manoeuvre and hence there are six boundary conditions given as,

i) $t = t_{pr}$ $\quad p_{\dot{z}}(t)=\dot{z}(t_{pr}) + v_E$ $\quad p_{\dot{z}}'(t)=\ddot{z}(t_{pr})$ $\quad p_{\dot{z}}''(t)=\dddot{z}(t_{pr})$

ii) $t = t_R$ $\quad p_{\dot{z}}(t)=0$ $\quad p_{\dot{z}}'(t)=0$ $\quad p_{\dot{z}}''(t)=0$

The altitude time history throughout the baulked landing manoeuvre may be evaluated from

$$\int_{t_{pr}}^{t} \dot{z}(t)\, dt = z(t) \qquad t_{pr} < t < t_R$$

The manoeuvre is completed when the vertical velocity satisfies the conditions,

$$-(1+\varepsilon)\, v_E < \dot{z}(t_R) < -(1-\varepsilon)\, v_E$$

where ε is a small, positive, number available from the start of the simulation.

Consideration of the baulked landing pilot strategy detailed in Appendix A8.2, reveals that an important parameter during this manoeuvre is the time at which rotorcraft reaches its minimum height above the reference position. This manoeuvre time can be determined when the following inequality condition is satisfied,

$$-\varepsilon\, \dot{z}(t) < \dot{z}(t_{MIN}) < \varepsilon\, \dot{z}(t)$$

The next stage in the definition of the baulked landing manoeuvre is the selection of the form of the flight path velocity time history. The pilot strategy for this aspect of the manoeuvre is given as:

"Longitudinal cyclic will be used to accelerate the helicopter into a descending forward flight mode. Typically a pitch down nose attitude of 10deg will be used to rapidly achieve the baulked landing safety speed of around 41 - 45kts."

In this representation, it is assumed that longitudinal cyclic stick displacements are employed to accelerate the rotorcraft to the baulked landing safety speed, V_{BLSS}. As this speed is reached, the vehicle will attain its lowest height above the reference altitude and the pilot will transition the rotorcraft into climbing flight. During the climb portion of the recovery manoeuvre, the baulked flight landing speed is maintained until the notional exit point is reached. A piecewise

smooth polynomial function of time was used to obtain the profile shown in Figure A7.3b for the flight path acceleration. Its construction is given below as,

$$t_{pr} < t \leq t_1 \qquad \dot{V}(t) = d_0 + \left(\frac{t - t_{pr}}{t_1 - t_{pr}}\right)\left[d_1 + d_2 \left(\frac{t - t_{pr}}{t_1 - t_{pr}}\right) + d_3 \left(\frac{t - t_{pr}}{t_1 - t_{pr}}\right)^2 \right]$$

$$t_1 < t \leq t_2 \qquad \dot{V}(t) = \dot{V}_{MAX}$$

$$t_2 < t \leq t_{MIN} \qquad \dot{V}(t) = \left[1 - 3 \left(\frac{t - t_2}{t_{MIN} - t_2}\right)^2 + 2 \left(\frac{t - t_2}{t_{MIN} - t_2}\right)^3 \right] \dot{V}_{MAX}$$

$$t_{MIN} < t \leq t_R \qquad \dot{V}(t) = 0$$

Cubic polynomials were chosen to represent the transient phases on the grounds that they permit a suitable degree of continuity to be incorporated whilst being relatively simple to implement. The values of the maximum acceleration, $\dot{V}_{MAX}$, must be provided by the user. The time, t_{MIN}, is available (from the altitude time history), however, the intermediate times of the transient accelerations, t_1 and t_2, must also be supplied.
In this model of the baulked landing, it has been assumed that the duration of the transition accelerations are related by the parameter, α, such that,

$$t_{MIN} - t_2 = \alpha\,(t_1 - t_{pr})$$

The value of α is selected to suit the characteristics of the manoeuvre.

The times t_1 and t_2 can be determined by imposing the exit condition that at $t = t_{MIN}$ the baulked landing safety speed has been reached. This can be achieved by integration of the acceleration profile:

$$V_{BLSS} - V(t_{pr}) = \int_{t_{pr}}^{t_{MIN}} \dot{V}(t)\,dt$$

The velocity throughout the manoeuvre may be determined from,

$$V(t) = \int^{t} \dot{V}(t)\,dt$$

The remainder of the flight path definition is specified by defining the lateral displacement and heading time histories in a manner similar to that employed during the case where and engine

failure occurs after the TDP during a Towering Takeoff manoeuvre. The longitudinal velocity tim history may then determined from,

$$\dot{x}(t) = \sqrt{V(t)^2 - \dot{y}(t)^2 - \dot{z}(t)^2}$$

The longitudinal positional and acceleration information denoted by x(t) and $\ddot{x}(t)$ respectively can be obtained by evaluating the appropriate derivatives and integrals.

Step iii) and iv) - Inverse Simulation and Validation of Baulked Landing Manoeuvre

For this case, the engine failure occurs one second before the LDP, that is 3 seconds into the manoeuvre. Pilot response time is taken to be 1 second and the recovery is by means of a baulked landing manoeuvre that transitions the helicopter from the approach trajectory to some climb - out flight path in a smooth and safe manner. The baulked landing safety speed is specified to be 45kts. and the manoeuvre is completed when the aircraft achieves a positive, steady rate of climb of 300ft/min. The trajectory information is shown in Figure A7.4.

It is evident from the simulation results shown in Figure A7.5, the response to the engine failure at 4 seconds involves a series of rapid longitudinal cyclic stick inputs that characterise the helicopters acceleration from approach to baulked landing safety speeds. The recovery trajectory is entered via a forward pulse of longitudinal cyclic of approximately 10% which results in a 6º pitch attitude change after 1.5 seconds. A small aft motion of the cyclic after the initial pulse prevents excessive forward tilt of the rotor disc, while the subsequent secondary forward longitudinal cyclic stick pulse at 6.5 seconds assures constant flight path acceleration. After the peak nose down attitude has been achieved, longitudinal stick is relaxed and the aircraft immediately pitches upward over a period of 1.5 seconds to a final pitch up attitude of approximately 2º. In conjunction with the cyclic stick displacements used in response to the engine failure, the pilot increases main rotor collective sharply by almost 7% to prevent excessive height loss and meet the acceleration requirements of the trajectory. Once the vehicle has reached its maximum pitch down attitude, collective is increased further by 4% and thus ensuring the descent motion of helicopter is arrested 8 seconds after the engine failure is recognised. The maximum height loss is 10m, while the helicopter overflies the rig at an altitude of 21m and flight velocity of 45kts with a positive climb rate of 50ft/min. After the single engine failure, the remaining good engine reaches a transient peak torque output of 98%. As the baulked landing safety speed is achieved, the torque output decreases to 87% for the remainder of the manoeuvre. During the complete manoeuvre rotor speed is tightly constrained to its reference value.

The results of the simulation generally compare well with the description of the manoeuvre given in Appendix A8.2. Furthermore the baulked landing safety speed is achieved as the minimum altitude in the trajectory is reached. The single remaining engine provides sufficient torque to keep rotor speed within specified operating limits. Finally, the approach manoeuvre and subsequent recovery strategy, quite clearly comply with the JAR requirements of a baulked landing in the event of a single engine failure up to and including the landing decision point.

7.3 Engine Failure After Landing Decision Point

Step i) - Formulation of Narrative Description of Pilot Strategy

A detailed description of the pilot strategy for a Continued Landing manoeuvre is given in Appendix A8.2.

Step ii) - Mathematical Modelling of Manoeuvre

On recognising an engine failure after the LDP, the pilot is committed to continuing the landing manoeuvre and this is evident from the narrative of his strategy:

"....the resulting strategy is similar to that found during the normal approach and landing...."

As the salient features of this manoeuvre are included in the longitudinal and vertical parameters it is pertinent to consider the application of the blend formulation to these first. The blend of the longitudinal and vertical position information denoted by, x(t) and z(t) is given by the following expressions,

$$x(t) = h_x(t) = \phi_x(t) + g_x(t) \qquad t_{pr} < t < t_R$$

$$z(t) = h_z(t) = \phi_z(t) + g_z(t) \qquad t_{pr} < t < t_R$$

where,

$$\phi_x(t) = e^{-\delta_x t}\, p_x(t) \qquad \phi_z(t) = e^{-\delta_z t}\, p_z(t)$$

The functions $g_x(t)$ and $g_z(t)$ are in fact the longitudinal and vertical position time histories of the normal approach and landing manoeuvre as defined in Appendix A6.1 of this thesis. The parameters, δ_x and δ_z are available at the start of the simulation and are selected to ensure a smooth transition back to the original flight path. The seventh order polynomial functions, $p_x(t)$ and $p_z(t)$ were chosen to satisfy eight boundary conditions.

The blend of the lateral and heading parameters is achieved via the following expressions,

$$y(t) = h_y(t) = \phi_y(t) + g_y(t) \qquad t_{pr} < t < t_R$$

$$\psi(t) = h_\psi(t) = \phi_\psi(t) + g_\psi(t) \qquad t_{pr} < t < t_R$$

where,

$$\phi_y(t) = e^{-\delta_y t}\, p_y(t) \qquad \phi_\psi(t) = e^{-\delta_\psi t}\, p_\psi(t)$$

The polynomials functions of time $p_y(t)$ and $p_\psi(t)$ are of eighth order. The terms δ_y and δ are user defined to ensure the original flight path is attained. The functions, $g_y(t)$ and $g_\psi(t)$ are both zero due to the nature of the original Normal Approach and Landing manoeuvre.

Step iii) and iv) - Inverse Simulation and Validation of Continued Landing Manoeuvre

In this example of an engine failure after the LDP, the failure is assumed to occur 3 seconds into the manoeuvre with the pilot response time specified again as one second. The recovery trajectory takes the form of a smooth transition back to the original flight path until the landing manoeuvre is completed and this demonstrated in the flight path information shown in Figure A7.6.

The inverse simulation results are shown in Figure A7.7 where it is evident that the response to the engine failure is limited with only some relaxation of the right pedal being used to counteract any adverse nose - left - yaw tendency of the aircraft. The pitch and roll attitude response of the helicopter is very similar to that found in case where no engine failure occurs. The engine failure can be clearly be seen from the engine torque time histories. The remaining good engine responds by increasing its torque output by 35% while the rotor speed remains tightly governed. Clearly the torque excess of the remaining engine is sufficient to meet the exigencies of the manoeuvre. As the manoeuvre progresses beyond the pilot response time, cyclic, collective and pedal displacements exhibit the same piloting strategies as those found in the case where no engine failure occurs. From the torque plot, however, the decreasing descent rate and flight speed puts increasing demands on the powerplant and thus the remaining engine torque output steadily increases beyond its normal operating limit to a maximum value of 105% approximately 19 seconds after the engine failure. At the same time as engine torque output reaches it limiting value, main rotor speed starts to decay, however, the drop in rotorspeed is not significant.

The simulation results compare well those discussed in section Appendix A8.2. The collective lever stays within its specified limits while the final rotor speed is very similar to that found during a vertical reject manoeuvre.

Appendix 8

Piloting Strategies Employed in Helicopter Offshore Operations

8.1 Piloting Strategies Associated With Takeoff Manoeuvres

There are several key strategies with which the helicopter can depart an offshore raised platform and some of these are now discussed. The first technique is known as the Backup Technique and has been detailed by Wood et. al. (1993). The strategy is configured to allow the pilot to maximise visual contact with the far right corner of the landing platform even through the initial stages of the transition to the takeoff safety speed. The manoeuvre is shown in Figure A8.0 and starts with the rotorcraft climbing to an altitude of 40 - 60ft above the heli-deck, at which point it is necessary to transition the helicopter to a rearwards climbing flight mode for the pilot to maintain an adequate view of the heli-deck. As the aircraft climbs through an altitude of 200ft above the landing platform, the rearward motion is reversed and the rotorcraft accelerates forward to the best rate of climb airspeed. Although this strategy enables particularly favourable forward visual cues of the heli-deck for the pilot (important if the rotorcraft has to return to the landing platform in the event of an engine failure), the aft motion of the helicopter is undesirable, since rearward visibility of the surrounding rig structure is severely limited to the aircrew by the physical restrictions of the vehicle cockpit. Indeed under adverse weather conditions, on a unfamiliar heli-deck, the adoption of this takeoff strategy could be considered inadvisable.

Another important takeoff technique is known as the 'Static Offset Takeoff Technique'. Investigated by Lande (1989) and Wood (1993), this technique effectively uses a lateral offset of the helicopter to ensure the pilot can maintain an adequate view of the landing platform and this strategy is shown in Figure A8.1. The manoeuvre begins with the helicopter performing a lateral climbing transition to an altitude of 35ft. above the heli-deck, whilst lateral position is judged sufficient when the tip of the rotor is coincident with the edge of the heli-deck. Once the helicopter has achieved a stabilised hover at this point, the vehicle accelerates into forward climbing flight to complete the takeoff. Although this manoeuvre enables the rotorcraft to clear the deck more efficiently than the backup technique mentioned above, the rotorcraft parasite fuselage drag is increased. In addition, if an engine failure is experienced prior to the helicopter establishing a hover, the vehicle must return to the landing platform. In this instance, the problem of the landing the helicopter is aggravated by the need to arrest the rotorcraft's lateral motion sufficiently to prevent it overturning on reaching the landing platform or overshooting the heli-deck entirely.

For this investigation of helicopter offshore operations, it is the Towering Takeoff or Dynamical Vertical Takeoff technique that has been employed as the principle takeoff strategy. Simulator studies (Lande, 1989) have shown that the Towering Takeoff is superior in all respects to the Backup Technique and Static Offset Takeoff in terms of rotorcraft performance and ease with which the strategy can be implemented by the aircrew. Using Talbot (1993) and the S-61N flight manual (1963) as a guide, a detailed narrative description of the pilot strategy supplied employed during the Towering Takeoff is now given.

8.1.1 Piloting Aspects of Flying the Towering Take-off Manoeuvre

The Towering Take-off is commonly used during multi-engine helicopter offshore operations as an efficient means of departing from elevated heli-decks, giving the best possibility to survive an engine failure during the take-off manoeuvre. An engine failure during this low speed phase of flight will quickly result in unacceptable loss of rotor RPM (Nr) unless prompt pilot action is taken to lower the collective and therefore reduce the power required to that available from the remaining good engine of a twin engine helicopter. This reduction of collective pitch results in a loss of height so the pilot has to ensure that the aircraft will either land back on the heli-deck below, or ensure sufficient forward motion that the flight path will clear the deck edge by a safe margin. This latter case can only be achieved when sufficient height has been gained and therefore there is a critical height above the heli-deck, known as the Take-off Decision Point (TDP), before which the take-off must be rejected and a landing carried out onto the heli-deck, and after which the take-off can be continued, albeit descending past and below the deck edge into forward flight.

The optimum technique for any given situation and type of helicopter is dependent on various factors :

i) All-Engine Operating Power. There must be sufficient All-Engines Operating (AEO) power available to allow a vertical climb in the ambient conditions at the actual helicopter weight.

ii) Single Engine Power. There must be sufficient One Engine Inoperative (OEI) power to allow an adequately low rate of descent at touchdown for the Rejected Take-Off (RTO) case, and to allow deck edge clearance and subsequent climb away for the Continued Take-Off (CTO).

iii) Wind Speed. The wind speed over the heli-deck will affect the power required and any head wind component may allow increased weights or require modifications to the piloting strategy.

iv) View and Heli-deck Size. The view from the helicopter will be a non-performance related factor that will limit the maximum height for the TDP as the pilot requires to maintain a view of the heli-deck at all times up to the TDP or the maximum height reached during the reversal of direction necessary during an RTO. It follows that for a given helicopter, the smaller the heli-deck, the lower the maximum TDP.

v) Handling Qualities. Severe cross couplings between axes will influence the precision and ease with which the required manoeuvres can be carried out. A significant factor will be the ease with which the relevant power limit (engine or transmission) can be set. This will involve engine response characteristics and indeed the clarity and characteristics of the cockpit instruments the pilot will use.

8.1.2 The Piloting Strategy for a Towering Take-off

Without giving detailed consideration to all the factors noted in section 8.1.1, a general strategy that would be valid for many situations operating from a normal size heli-deck (22.2m diameter) is described below:

i) Initial Hover. The helicopter would start from a position sitting on the centre of the heli-deck with the cyclic control and yaw pedals close to central, and the collective lever fully down. To establish the initial hover, collective pitch is applied progressively whilst cyclic and pedal inputs are made to counteract any cross coupling between axes as the helicopter lifts off and to maintain the position over the centre of the heli-deck. The initial hover height will be 15 ft and the amount of collective applied will depend on the thrust required to achieve that height.

ii) Vertical Climb. From the initial hover, collective pitch is applied quickly, within approximately 2 seconds, until an engine or transmission limit is reached or the rate of climb is approximately 500 ft per minute. Cyclic and pedal inputs are made as required to maintain position over the centre of the heli-deck.

iii) Take-off Decision Point. A likely TDP would be 50 ft as indicated by Radio Altimeter. At the TDP, the pilot would make a positive forward cyclic input to achieve a nose down, accelerative attitude. A usual nose down attitude would be 15 degrees in order to accelerate the helicopter towards the initial climbing speed.

iv) Acceleration and Climb. After achieving the required nose down attitude at TDP, as speed increases, the pilot allows the nose to rise progressively until the helicopter ceases to accelerate as it reaches the initial climbing speed of 70 knots. The nose will

rise due to flap-back caused by the effects of increasing airspeed through the rotor, to pilot longitudinal cyclic inputs, or to a combination of both depending on the characteristics of the particular helicopter. During the acceleration, lateral cyclic and pedal inputs are made to achieve wings level balanced flight. The collective may require adjustment to keep within engine and transmission limits and to establish a desirable initial rate of climb of 1000 feet per minute.

8.1.3 Piloting Strategy for Recovery from Engine Failure During a Towering Takeoff

Having discussed both the piloting aspects and the inverse simulation of the normal towering take-off procedure, the piloting approach in the event of an engine failure is now described before the techniques associated with the inverse simulation of this situation are outlined.

i) Failure Before TDP

The objective on recognising an engine failure before TDP is to reverse the upwards vertical motion promptly, conserve and maintain Nr during a vertical descent and carryout a smooth touchdown on the heli-deck using all the power available from the remaining engine and stored energy in the rotor. Taking these in turn :

a) Flight Path Reversal. The pilot will make a rapid downwards collective lever input on recognising the engine failure. The size of the input will depend on the rate of climb at the point of recognition. In general, rate of climb will increase as the vertical climb portion of the towering take-off progresses, so it follows that the larger inputs are required close to the TDP. Cyclic control and yaw pedal inputs are made to compensate for cross couplings to ensure that the helicopter remains over the heli-deck.

b) Conserving Nr and Vertical Descent. Once the flight path has been reversed, it will be necessary to conserve adequate Nr and therefore stored energy to cushion the touchdown. To achieve this, the collective is set such that the remaining engine is producing maximum power, usually by reducing Nr by 1% - 2% below the normal governed setting. With this power set, the descent is monitored and cyclic control and yaw pedal inputs are made as necessary to maintain the vertical descent. The rate of descent will depend on the power deficit and would typically be 800 feet per minute.

c) Touchdown. The helicopter is allowed to descend vertically as described above until reaching a height of approximately 15 ft above the heli-deck at which point a large collective-up input is made. The purpose of this is to use rotor kinetic energy to

produce additional thrust for a short period of time in order to achieve a smooth touchdown. The point at which the collective input is made depends on the rate of descent and rotor inertia and will vary between helicopter types. After touchdown, the collective is lowered fully.

ii) Failure Just After TDP

The key objectives with an engine failure just after TDP are to ensure rotorspeed remains within acceptable limits and to translate from the hover into forward flight. If the performance scheduling is correct, increasing speed reduces the power required to the point where the helicopter will be able to climb using the power available from the remaining engine. Increasing speed also causes a forward translation that is used to ensure that the helicopter misses the edge of the heli-deck. The pilot action at TDP is to pitch the nose down, typically to an angle of 15 - 20 degrees, using a positive forward cyclic input whether or not an engine has failed. If an engine has failed, such that the failure is recognised as or after the forward cyclic input is made, the correct course of action is to continue with the take-off rather than try to land back on the heli-deck. In this case, the helicopter will follow a descending flight path as speed is gained, and the pilot will have to lower the collective shortly after the engine failure to prevent the rotor speed falling below the acceptable minimum. Some loss of rotor speed is probably desirable as when airspeed is low most rotors are more efficient at lower rotor speed. As airspeed increases, the nose will tend to rise and in any case will be positively raised at, typically, 35 knots to reduce height loss and establish airspeed at that required for the single engine climb, typically 45 knots. The sequence of events can be summarised as :

a) Engine failure is recognised as forward cyclic is made at TDP,
b) nose is pitched down to 15 degrees,
c) collective is lowered to keep Nr within limits,
d) nose will rise as speed increases and at 35 knots longitudinal cyclic inputs are made to establish speed at 45 knots,
e) when 45 knots has been established, a steady climb is maintained using maximum engine power.

During this manoeuvre, which involves predominantly longitudinal cyclic and collective pitch inputs, appropriate lateral cyclic and yaw pedal inputs will be made to maintain wings level balanced flight.

iii) Failure Well After TDP

An engine failure well after TDP will have similar objectives to the case above but clearly the closer the helicopter is to the desired climbing speed of 45 knots, the less will be the need for the pilot to increase airspeed by pitching the nose down and the less will be the height loss. The collective lever will, however, have to be lowered to prevent Nr dropping below the acceptable limits.

8.2 Piloting Strategies Associated With Landing Manoeuvres

There are several strategies that a pilot can use to land a helicopter which adhere to Category A landing regulations, the first of which is known as the Static Offset Landing manoeuvre. This strategy employs a similar rationale to that employed in the equivalent takeoff manoeuvre discussed in section 8.1 of this appendix. The manoeuvre consists of a gradual deceleration and reduction in altitude towards the landing platform. As the relative velocity of the rotorcraft with respect to the rig reduces to zero, the helicopter should be positioned one rotor radius from the deck edge while at an altitude of 35ft above the landing platform as is evident from Figure A8.2. Once the pilot establishes a hover at this point, the helicopter traverses and descends to land on the heli-deck. Although this strategy ensures good visibility of the landing platform at all times for the aircrew, the final stages of the manoeuvre incorporates a significant low speed component which is undesirable in the event of an engine failure.

Another important landing strategy is that known as the Dynamic Landing, or alternatively for this investigation, Normal Approach and Landing manoeuvre. This strategy is designed to maintain rotorcraft airspeed for most of the manoeuvre whilst ensuring the pilot has an adequate view of the oilrig landing platform at all times. Drawing from the information detailed by Talbot (1993), a narrative description of the pilot strategy employed during the Normal Approach and Landing is now presented.

8.2.1 Piloting Aspects of Normal Approach and Landing Manoeuvres

The Normal Approach and Landing is a manoeuvre commonly employed by pilots in helicopter offshore operations as it is a means of landing a helicopter on an elevated heli-deck while ensuring that at all times the vehicle is capable of surviving a single engine failure. The manoeuvre is defined to allow variations in pilot technique, skill and alertness and is equally applicable to differing vehicle configurations (centre of gravity and mass etc.). Furthermore the flight path and pilot techniques required are suitable for use in adverse weather, night

operations, and conditions of single engine failure. Finally the Approach and Landing manoeuvre is valid at the approved WAT (Weight, Altitude, Temperature) condition.

If an engine failure occurs at any point prior to and including the landing decision point (LDP), the pilot may elect to land or to 'go around' by executing a baulked landing. For an engine failure prior to the LDP, this notional point in the manoeuvre must be specified in such a way as to permit acceleration to the baulked landing safety speed, V_{BLSS} at an altitude of no less that 35ft. above the heli-deck. After passing the LDP, the helicopter no longer has sufficient energy to assure transition to the baulked landing condition without striking the landing surface, and the pilot must continue the landing. Therefore the LDP represents the commit point for the landing manoeuvre in much the same way as the takeoff decision point (TDP) does in the Towering Takeoff. It is therefore appropriate to specify the LDP in terms of speed, altitude and a descent angle. For Cat. A profiles the LDP is typically 100 -150ft above the landing surface.

A simple, repeatable and effective pilot strategy is borne from the Category A requirements and these strategies are now discussed.

8.2.2 A Possible Piloting Strategy for a Normal Approach and Landing

a) Initial Descent : The helicopter starts the manoeuvre in a steady trimmed descending flight mode. During the stabilised approach the flight path speed will be typically in the region of 30 - 40 kts, with a descent rate of 300ft/min and this corresponds to a descent angle of approximately 5deg. The vehicle will have a small pitch - nose - up attitude thus ensuring adequate pilot view of the heli-deck. This steady trimmed flight state is maintained until the landing decision point is reached.

b) Landing Decision Point: When the vehicle approaches the LDP, a modified flight profile is adopted. At the LDP, the combined use of collective and longitudinal cyclic is used to decelerate the aircraft and increase the descent angle to 7 -12 deg. Typically for this, the aircraft nose is pitched up to a constant value via the long. cyclic and the collective is lowered. The decrease in collective will depend on the initial flight speed and ultimate descent angle. The magnitude of the pitch nose up is determined by the proximity of the rig, initial flight speed and peak descent angle. Lateral cyclic is used to maintain wings level, while pedal displacements are issued to keep the heading constant. Note that a 'crabbing' approach can be employed during this phase to produced enhanced visibility through side view panels.

c) Flare Point : At the flare point the vehicle is typically 25ft above the landing surface. Flight speed is very low and below that measurable from external pitot fixtures. For this reason visual cues from the rig a very important during this phase. Longitudinal cyclic stick displacements are used to progressively reduce any remaining positive nose up attitude while gradually reducing flight speed. Collective is used to descend the vehicle towards the heli-deck. Lateral cyclic and pedal displacements are used to maintain wings level and heading as appropriate.

8.2.3 A Possible Piloting Strategy for a Normal Approach and Landing With an Engine Failure

i) Failure before LDP

On recognising an engine failure, the pilot priorities are to prevent excessive rotor speed decay using remaining engine power, rapidly transition the vehicle to forward flight attaining the baulked landing safety speed and avoid collision with the rig structure by descending to no more than 35ft above the landing surface. Considering these piloting goals the following strategy develops:

a) The pilot will lower main rotor collective ensuring the rotor speed stays within acceptable limits. Typically rotor speed should not be allowed to drop below 93.5%. Longitudinal cyclic will be used to accelerate the helicopter into a descending forward flight mode. Typically a pitch down nose attitude of 15-20deg will be used to rapidly achieve the baulked landing safety speed of around 41 - 45kts. Lateral cyclic and pedal controls are used to maintain wings level and heading respectively

b) If the performance scheduling is correct, then as V_{BLSS} is approached, the remaining good engine should provide sufficient power to prevent excessive loss in altitude. At this point main rotor collective can be increased to reduce descent rate. Furthermore, as flight speed increases, the nose will pitch up due to rotor flap back and positive longitudinal cyclic inputs by the pilot and the helicopter will enter a climbing mode. The baulked landing safety speed is maintain during the subsequent fly away to complete the manoeuvre with a positive rate of climb of approximately 300ft/min.

ii) Failure After LDP

For an engine failure after the LDP, pilot strategy is severely limited by low the energy capabilities of the helicopter and the proximity of the rig structure. Consequently, the resulting strategy is similar to that found during the normal approach and landing except for a more rapid

rate of descent being employed during the final touch down phase. The descent has the characteristics of a vertical reject manoeuvre during a towering takeoff as an increased descent rate is adopted (around 800ft/min) and with rotor speed on landing not dropping below 80%.

Appendix 9

Helicopter Offshore Graphical Simulation, Hogs

This appendix gives an overview of the helicopter offshore graphical simulation package, Hogs.

9.1 Overview of Hogs Software

Developed on a Silicon Graphics Iris Indigo work station, the Hogs software permits real-time, three dimensional animation, of a simulated helicopter performing takeoff and landing manoeuvres in the presence and absence of engine failures. Written in the C programming language, the software makes extensive use of the graphics libraries provided within the Silicon Graphics work station. The animated rotorcraft is similar to that employed in current helicopter offshore operations with rotating, transparent, virtual main and tail rotor that have been provided to enhance visual cues. The simulated helicopter 'flies' in a environment consistent with that found with helicopter operations which includes; oilrig platforms, tug boats and background scenery. The Hogs package requires the trajectory and Euler attitude angle time histories as input and these can be supplied by either the Helinv or HIFIS simulation algorithms.

9.2 Overview of Computer Graphic Techniques Employed In Hogs

As in flight mechanics modelling, it is convenient in computer graphics to set up Earth fixed and body fixed origins and frames of reference. This approach greatly simplifies the task of rendering the synthesised helicopter, as it allows the rotorcraft geometry to be expressed independently of the vehicle location in the computer graphic orthogonal Earth axes set. It is conventional in computer graphics for the Earth origin to be located arbitrarily with the y axis point vertically upwards, and the x and z axis oriented to form a right handed axes set. The position of the helicopter is taken to be the location of the centre of gravity of the rotorcraft in the Earth axes and this is evident from Figure A9.0.

The objective of the Hogs package is to provide real-time, dynamic graphics of a prescribed helicopter performing an offshore related manoeuvre. While realistic, computer animated imagery of the synthesised helicopter is desirable, real-time animation of the helicopter manoeuvre is a priority. Consequently, due to the limited computer power available, the aforementioned requirement has been achieved by making several assumptions related to the operation of the simulation graphics:

(i) The scenery is free to move in translation only.

(ii) The helicopter is free to rotate about its centre of gravity only.

These two assumptions about the operation of the simulation graphics effectively separates the animation of the scenery and helicopter into two independent tasks and this simplifies the drawing algorithms used to calculate the primitive geometries.

Further assumptions must be placed on the drawing of the animation primitives themselves and these are:

(i) Simple (less than four vertices), flat, polygons of single colour shading have been employed in the formulation of the of animated primitives except when considering the helicopter where Gouraud or intensity (see Foley, van Dam et. al.) shading has been employed.

(ii) Front facing polygons (those that are visible) are determined by a counter clockwise numbering sequence. Or alternatively, in viewing co-ordinates, the vector dot product of panel normal and the vector from the observer to any point on the panel results in a positive value.

(iii) The omission of depth calculations (z -buffering).

The first assumption greatly simplifies the task of synthesising solid, three dimensional surfaces which form the basis of the simulation algorithm. The Hogs software, employs a flat polygon meshing technique to model a three dimensional curved surface as demonstrated in Figure A9.1. Individual panels can be readily formed, since the three dimensional co-ordinate information of each vertex is known at the start of the simulation. This meshing technique can be easily extended to the synthesis of a complete surface such as the example helicopter shown in Figure A9.2.

The colouring of the polygon surfaces in all cases except for the rotorcraft has been achieved using a single faceted or flat shading technique. In essence, the light intensity at the polygon surface is sampled once at the its centre and this value is held constant across the polygon to reconstruct the polygon's shade. This type of shading is only appropriate if the polygon represents the actual surface being modelled and is not an approximation to a curved surface. An alternative form of shading, known as Gouraud or intensity shading, has been used in the rendering of the helicopter as its surface geometry includes complex three

dimensional curves. This type of shading uses linear interpolation of the vertex intensities across each edge of the polygon and then along each scan line of the polygon, see Figure A9.3. Using this technique, the light intensity is distributed across the polygon face, faithfully reproducing the highlights that occur in practice when an object is illuminated.

The unit normal of each vertex must also be determined as this information is employed in the simulation lighting and panel rendering calculation. An estimate of this 'true' normal may be obtained from the unit normals of the surrounding panels. The normal of a panel is determined from the cross product of two adjacent edge vectors. For example, the normal, $\underline{\mathbf{n}}_{p1}$, of panel 1, shown in Figure A9.1 is given by,

$$\underline{\mathbf{n}}_{p1} = \frac{\left(\underline{\mathbf{V}}_{j+1} - \underline{\mathbf{V}}_j\right) x \left(\underline{\mathbf{V}}_{j-1} - \underline{\mathbf{V}}_j\right)}{\left|\left(\underline{\mathbf{V}}_{j+1} - \underline{\mathbf{V}}_j\right) x \left(\underline{\mathbf{V}}_{j-1} - \underline{\mathbf{V}}_j\right)\right|}$$

where $\underline{\mathbf{V}}_{j-1}$, $\underline{\mathbf{V}}_j$ and $\underline{\mathbf{V}}_{j+1}$ are the position vectors in body axes of the j-1, j and j+1 vertices.

The true unit normal of vertex, j, can be estimated from the average of the n adjacent panel unit normals, viz:

$$\underline{\mathbf{n}}_j = \frac{\sum_{k=1}^{n} \underline{\mathbf{n}}_{pk} \delta_k}{\left|\sum_{k=1}^{n} \underline{\mathbf{n}}_{pk} \delta_k\right|}$$

The term δ_k is used to weight a normal vector when a discontinuity in the surface being modelled exists.

In addition, the task of determining the visibility of a polygon must be also addressed. Consider an arbitrary closed polyhedral surface. Assume that all the surface panels are defined such that their surface normals point out of the polyhedron. Those polygons facing away from the observer lie on a part of the polyhedron whose visibility is completely obscured by other closer polygons. In addition, if the resulting picture is to be correctly portrayed, the invisible back facing polygons must be removed from the calculation. The second assumption mentioned above can be used to resolve this. Using the counter clockwise rule for polygons it is possible to determine whether a polygon is to be drawn or omitted since backward facing polygons will have a negative dot product value and this is evident from Figure A9.4.

The third assumption has particularly important implications as the z-buffering calculation permits the distance of each primitive from the observer in the viewing environment to be determined and hence which surfaces are closer and thus visible to the observer. In the absence of this information the objects must be drawn in a 'list priority' order ensuring that a correct picture results if the objects are rendered in that sequence. For example, if no object overlaps another along the z axis, then the objects need only be sorted in increasing z, and rendered in that order. Consequently, further objects are obscured by closer ones as pixels from the closer objects overwrite those of the more distant ones. If an object overlaps in the z direction, it is still possible to determine a correct order as is evident from Figure 9.5a. If objects cyclically over lap, or penetrate each other, as in Figure 9.5b and 9.5c, there is no correct order and in this instance these instances it is necessary to split the objects to make a linear order possible. The computational burden of splitting objects in order to determine the correct list priority is significant and consequently has been omitted to retain realtime operation of the software.

9.2.1 The HOGS Drawing Algorithm

The task of the software algorithm is to generate and draw a picture frame every 1/30th of second. This refresh rate will ensure a suitably smooth motions of the simulation environment whilst keeping computational effort to desirable levels. The use of dynamic graphics in comprehending large amounts of information is especially effective when there is some means of controlling the simulation motion dynamics. With motion dynamics, objects can be moved or tumbled with respect to a stationary point. The objects can also remain stationary and the viewer can move around them, pan to select a portion of the view, and zoom in or out for more or less detail and it is this type of motion dynamics that has been incorporated into the Hogs algorithm. This motion feature is demonstrated in Figure A9.6, where the observer may view the helicopter from an arbitrary position on the surrounding imaginary sphere.

The final simulation architecture as employed in the Hogs software is as follows:

(i) Initialisation of geometrical information for landscape and helicopter primitives. Specify light position and red, green and blue colour content.

(ii) Define viewing volume, observer viewing positions and prepare memory for animation. Specify colour information of all polygons.

(iii) Read in flight path and Euler attitude information.

(iv) Check for input for motion dynamic changes (mouse driven), and rotate viewing positions accordingly.

(v) Use input data to translate landscape axes set and draw scenery into back buffer (rear half of allocated memory).

(vi) Use input data to rotate helicopter body fixed axes set. Determine location of main and tail rotor in view volume axes and draw outward portions. Draw helicopter. Draw inward (viewed) main and tailrotor primitives.

(vii) Compute simulation time and 'operation time', and adjust simulation step as necessary.

(viii) Swap memories buffers (rear portion of memory copied to front and rear portion cleared) and draw information to screen.

The graphical animation progress via the sequence (iv) to (viii) drawing the picture frames each 1/30th of a second.

As an annex to this thesis, a video tape has been made of the Hogs graphics package in use.

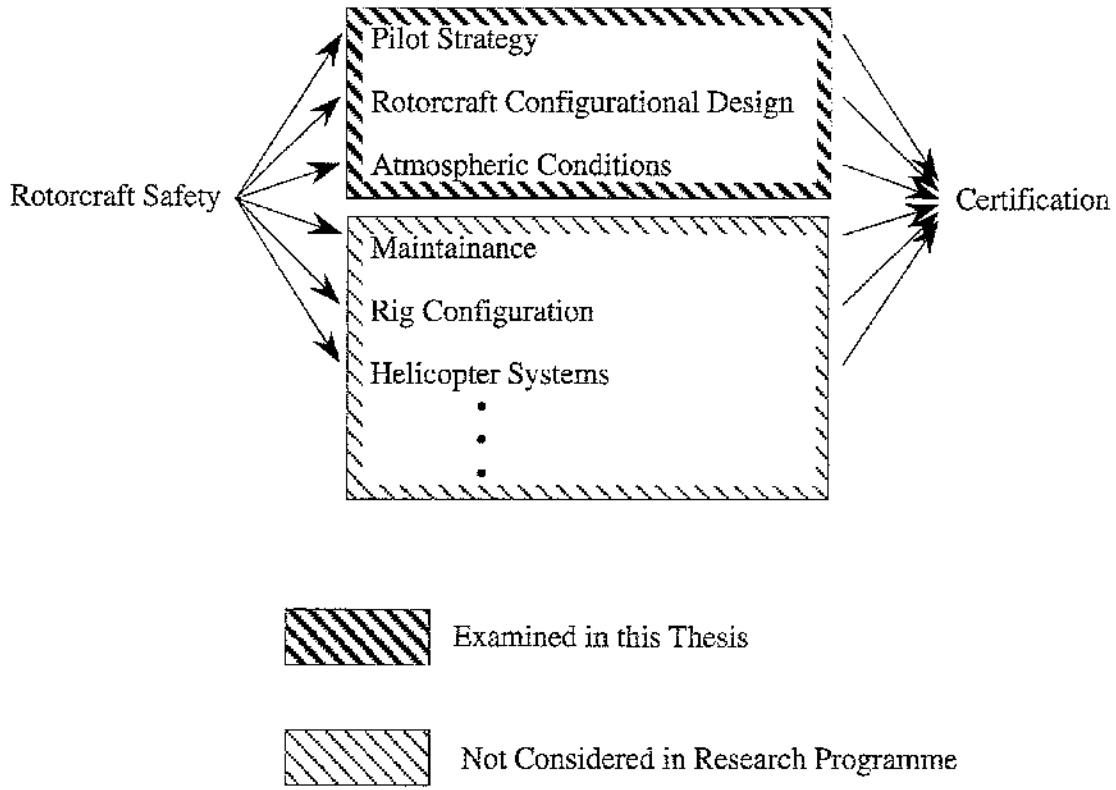

Figure 1 : The Contribution of Rotorcraft Operational Issues Towards Safety

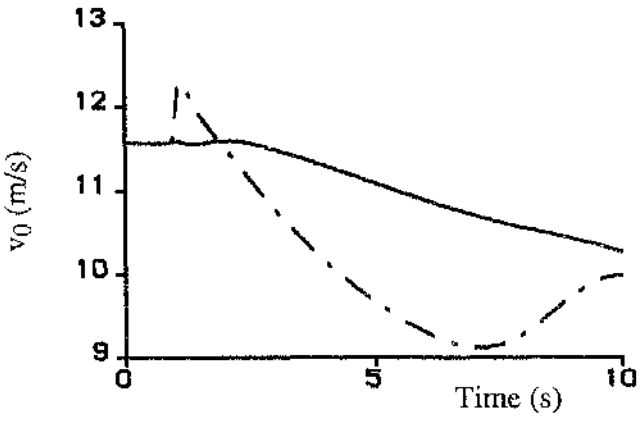

Figure 2.0a : Uniform Induced Flow

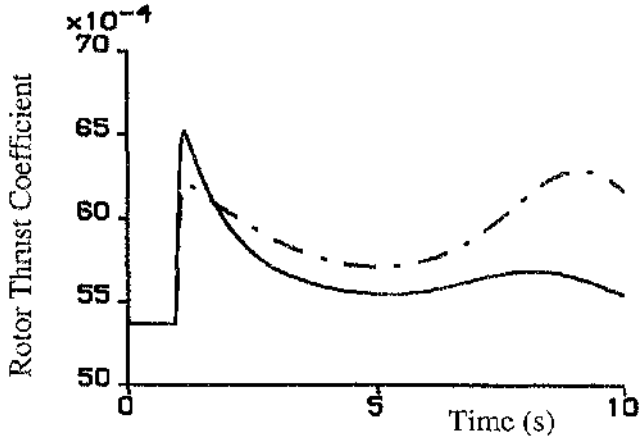

Figure 2.0b : Rotor Thrust Coefficient

Dynamic Inflow

Glauert Inflow

Figure 2.0 : 5% Step Input From Trim of Main Rotor Collective

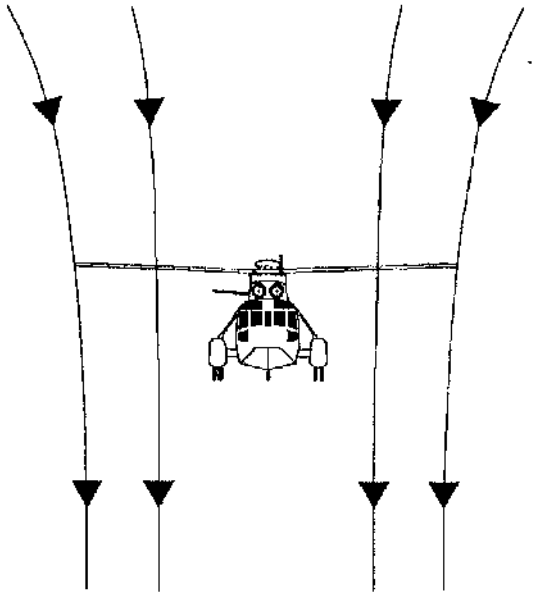

Figure 2.1a : Helicopter State

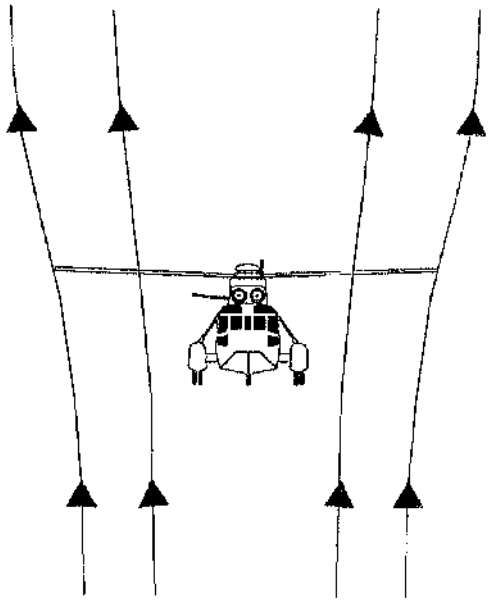

Figure 2.1b : Windmill State

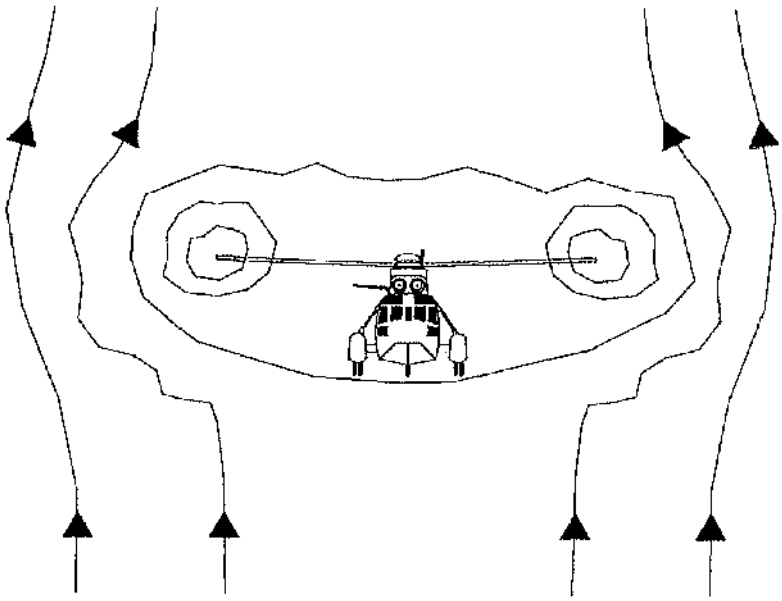

Figure 2.1c : Vortex Ring State

Figure 2.1 : Three Flow States of a Helicopter Rotor

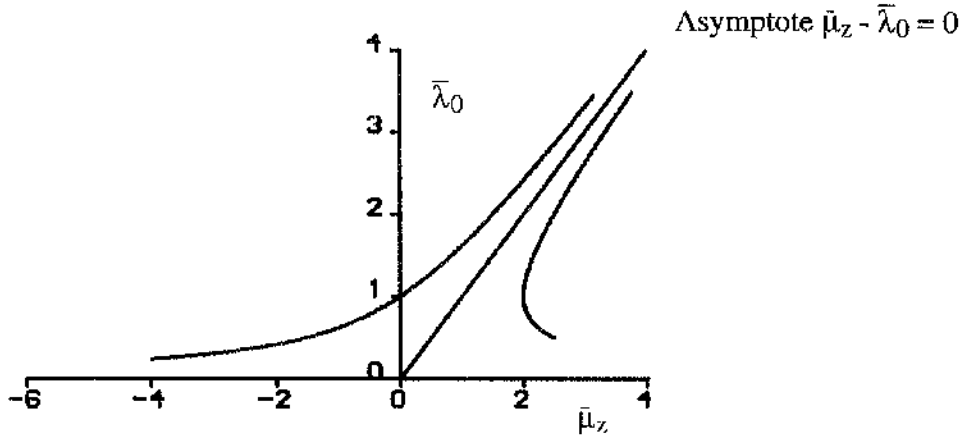

Figure 2.2 : Asymptotic Behaviour of Glauert Inflow Model

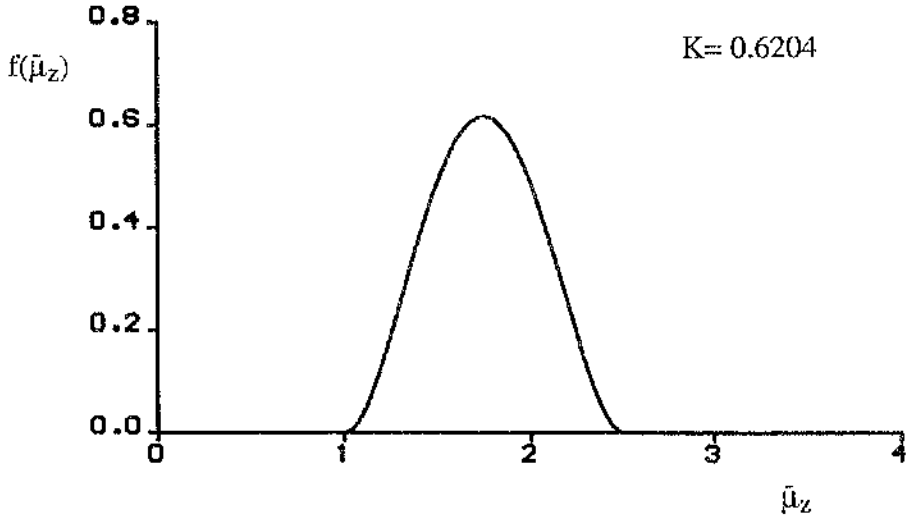

Figure 2.3 : Residual Velocity Function

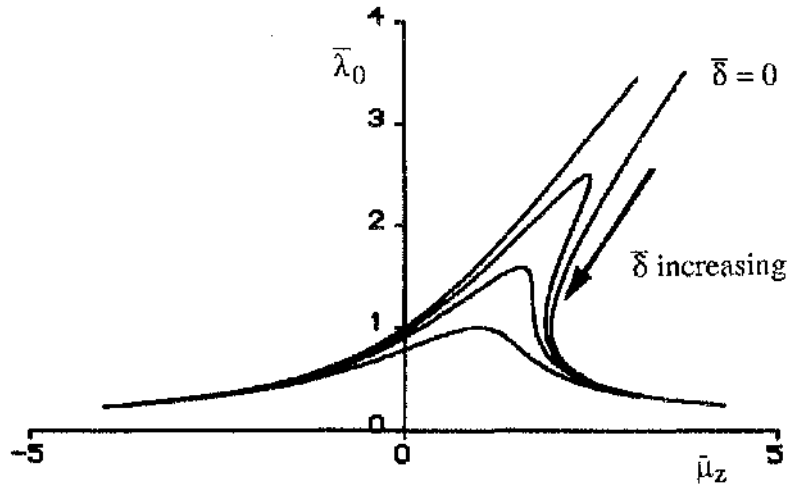

Figure 2.4 : Variation of Residual with Inflow

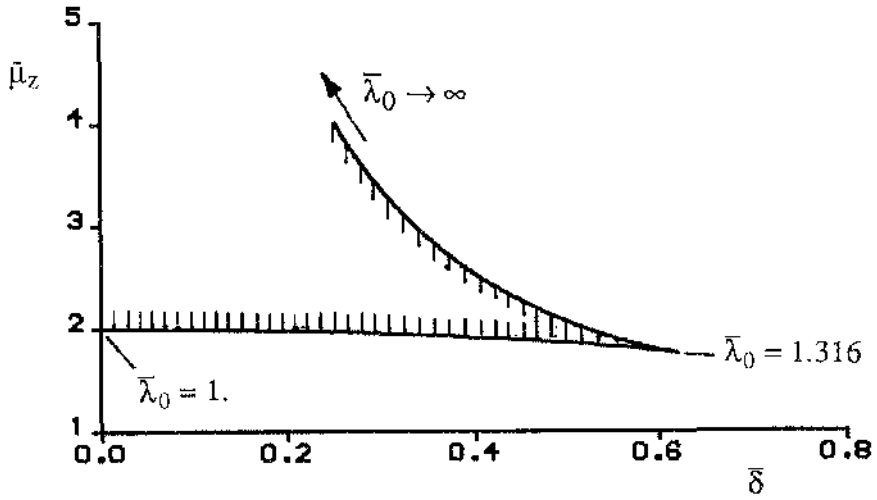

Figure 2.5 : The Variation of Multiple Roots to the Glauert Inflow Model

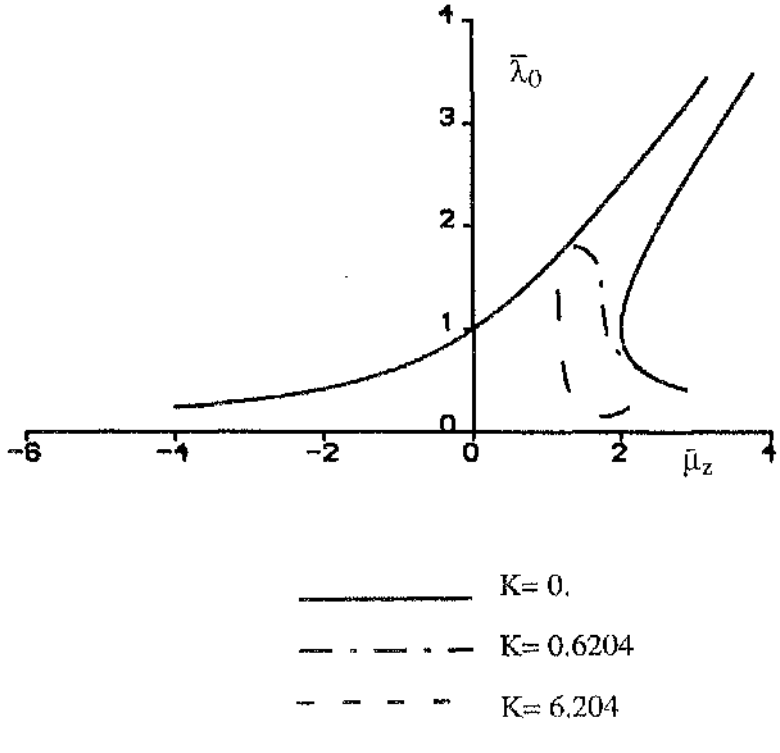

Figure 2.6 : Behaviour of Glauert Inflow Model With Residual Function

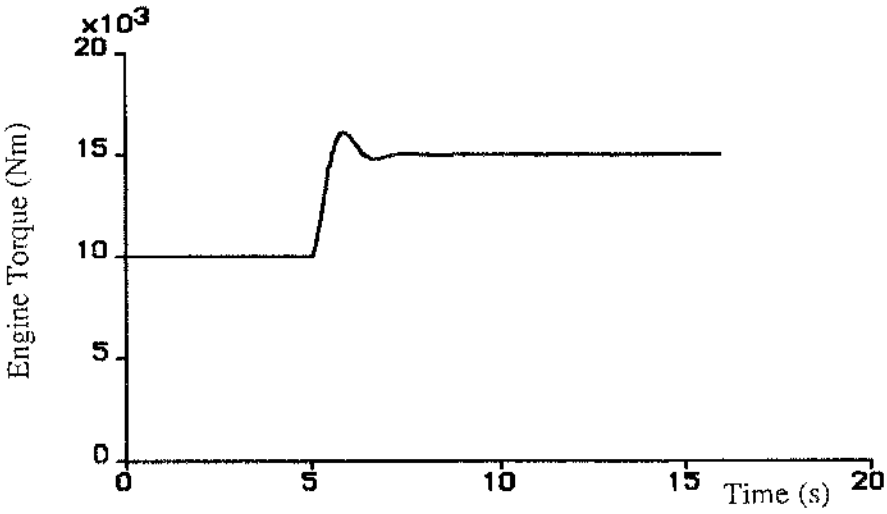

Figure 2.7 : Step Input In to Torque Demand to Non-limited Engine

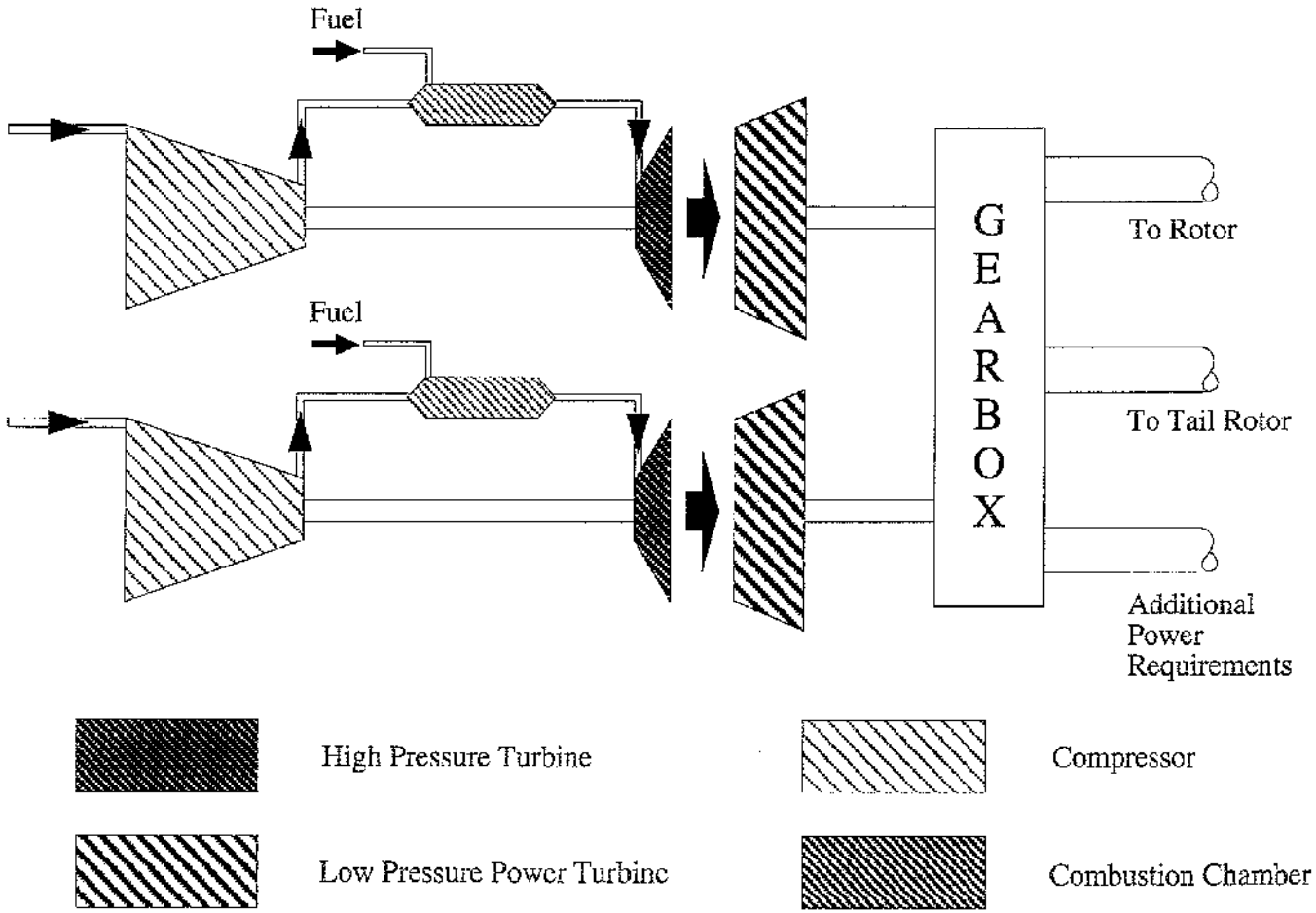

Figure 2.8 : Schematic Diagram of Twin Engine Helicopter Powerplant

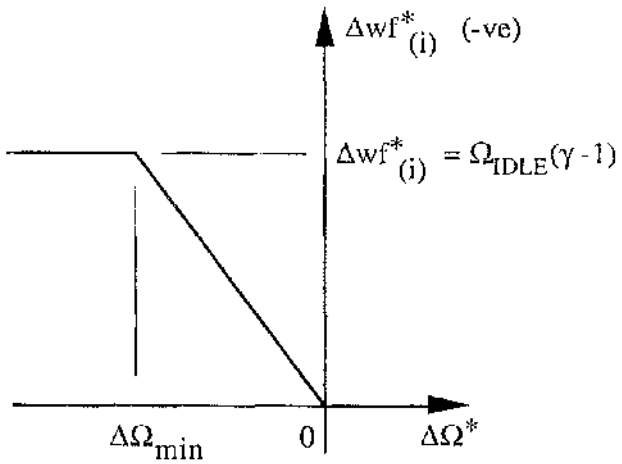

Figure 2.9 : Fuel Flow Schedule

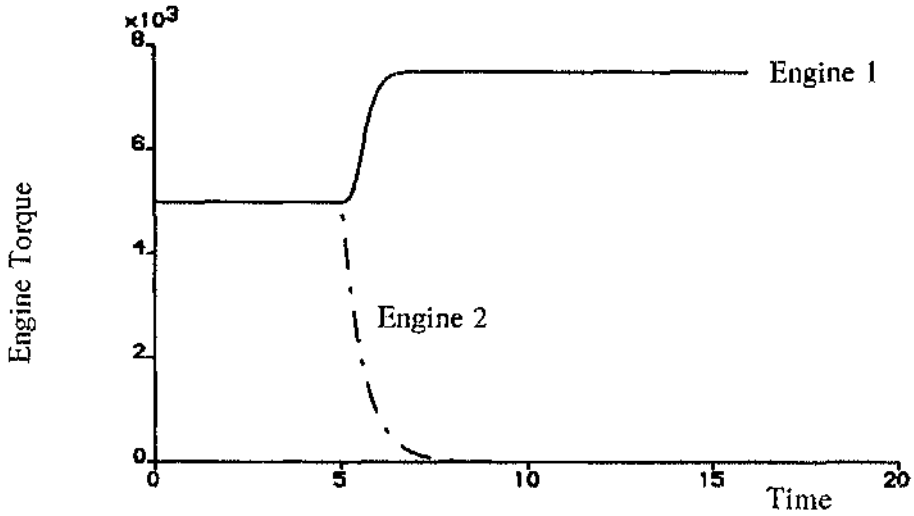

Figure 2.10 : Torque Limited Engine Response to Engine Failure

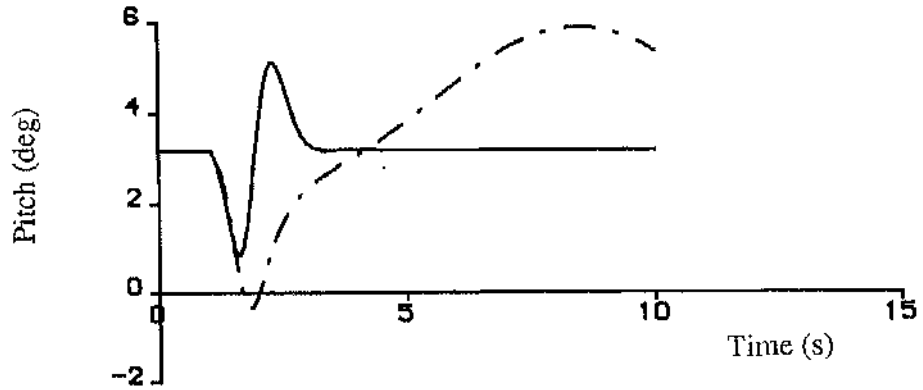

Figure 2.11a : Pitch Response

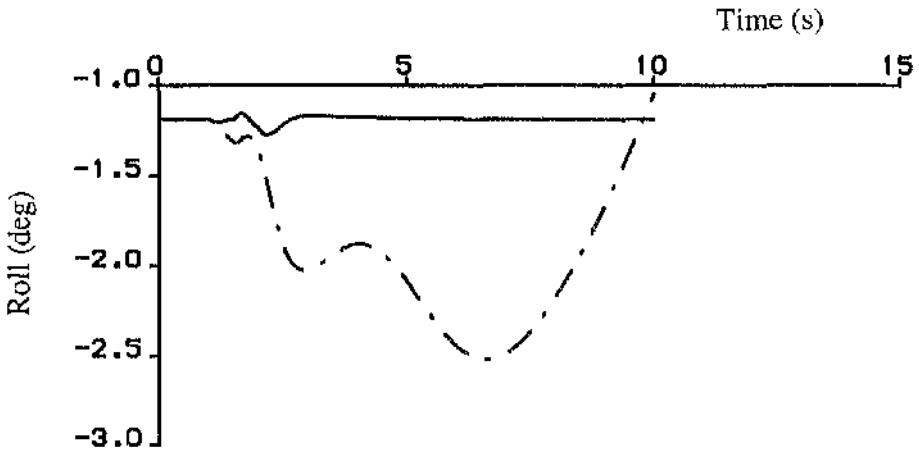

Figure 2.11b : Roll Response

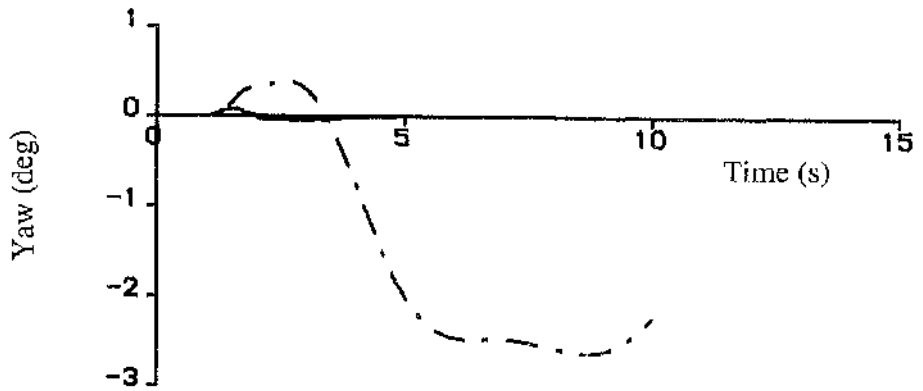

Figure 2.11c : Yaw Response

With AFCS

Without AFCS

Figure 2.11 : Response of Rotorcraft To Longitudinal Stick Doublet With and Without SAS

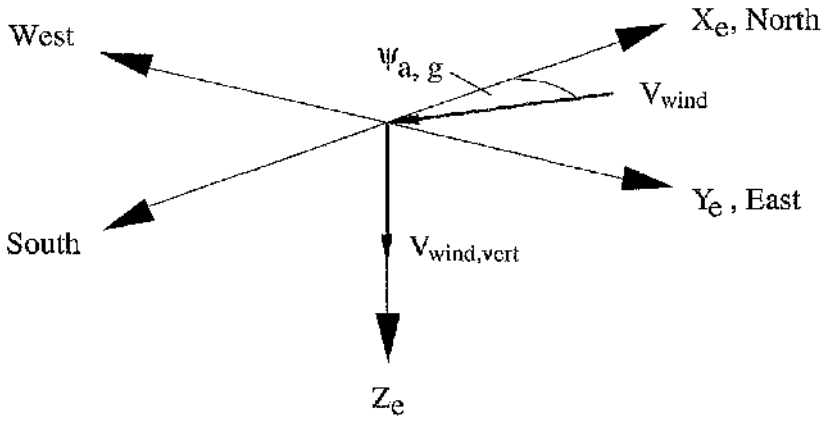

Figure 2.12 : Definition of Wind Velocity In Earth Axes

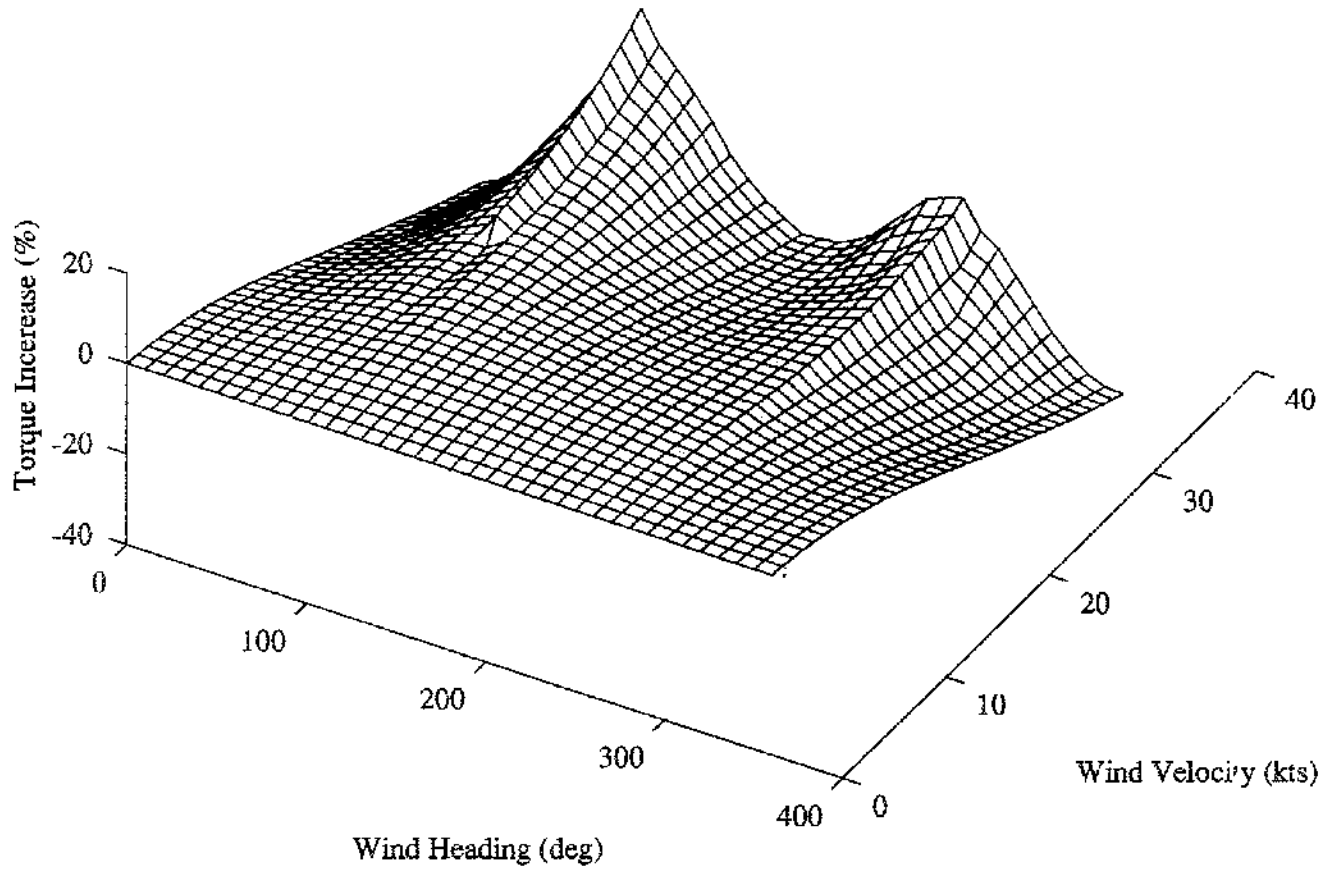

Figure 2.13 : Variation of Engine Torque with Wind Speed and Heading

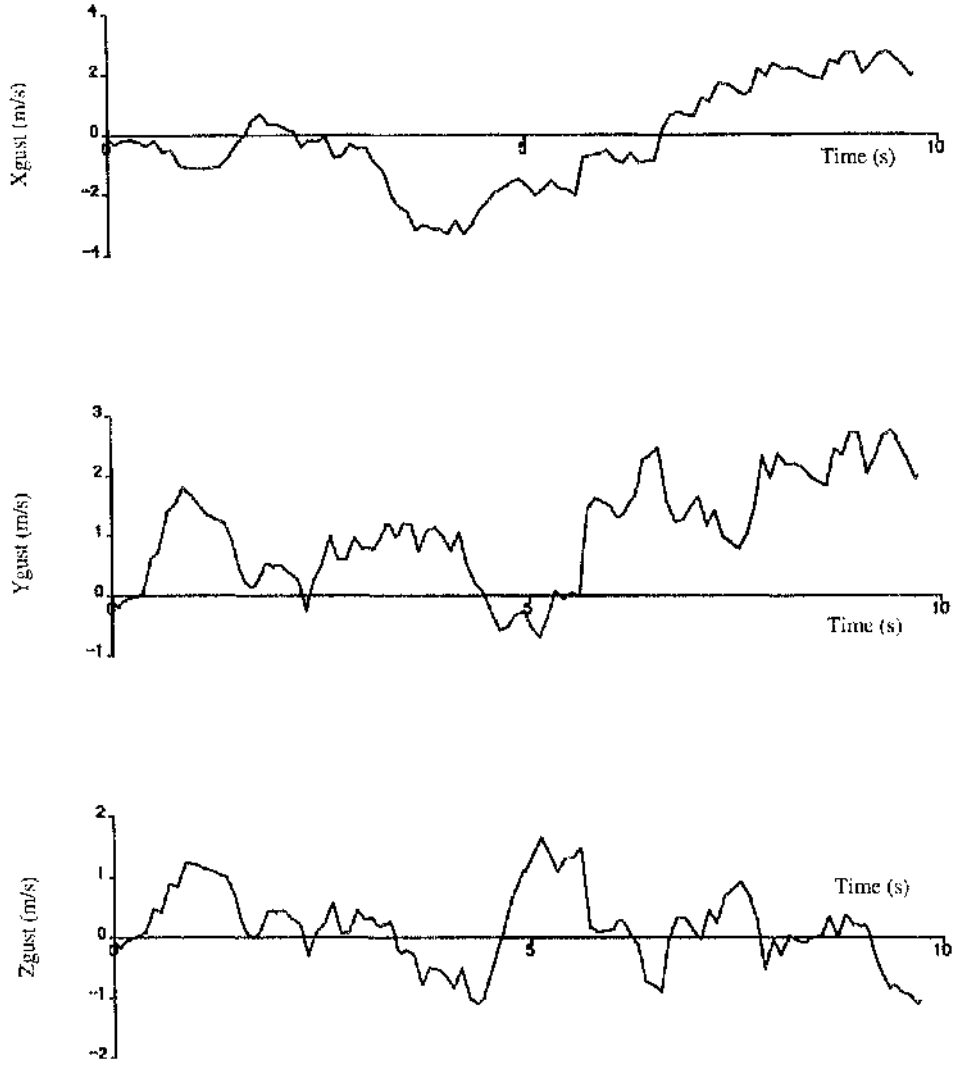

Figure 2.14 : SDG Turbulence Stream (F = 0.8, $\sigma = 0.9$)

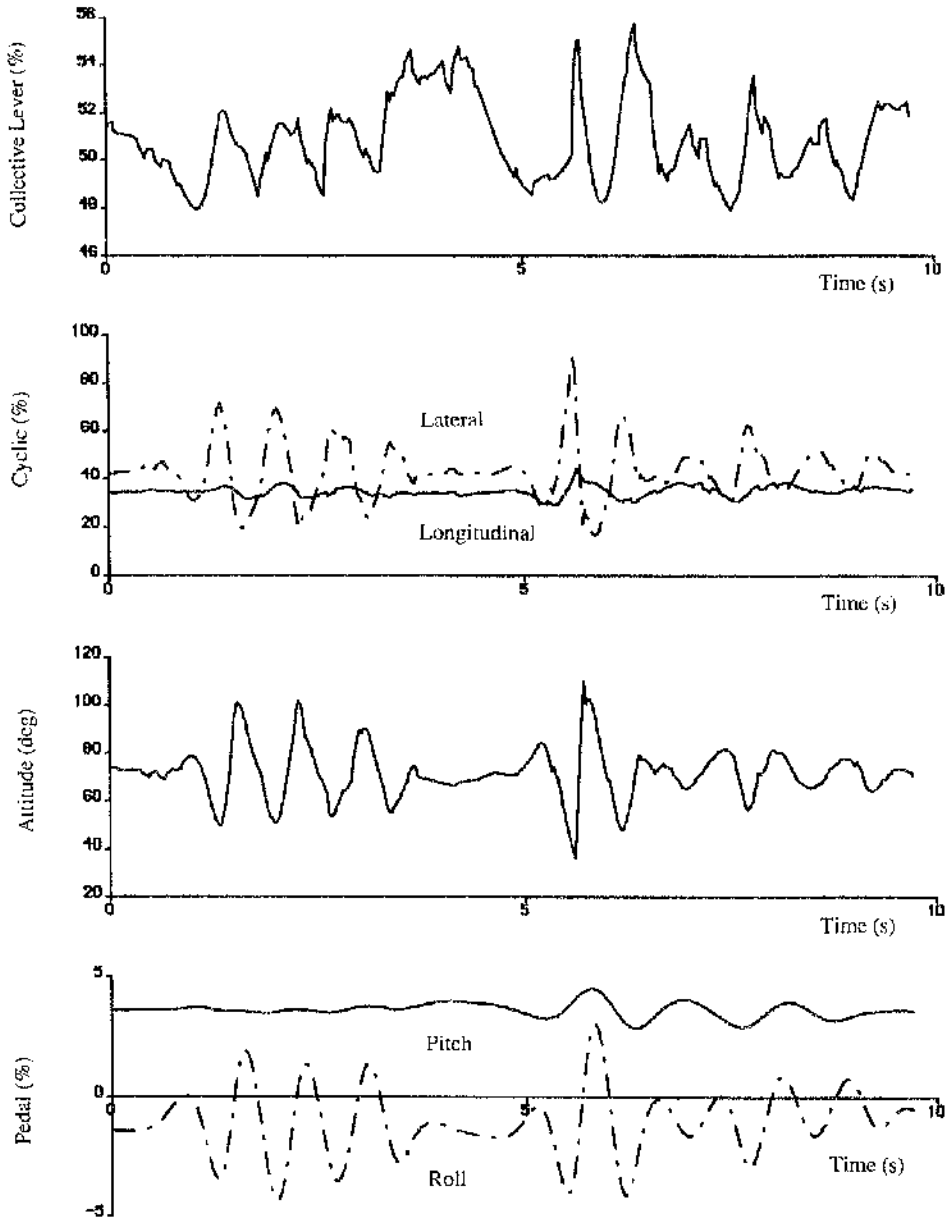

Figure 2.15 : Inverse Simulation of Helicopter Response to Turbulent Stream

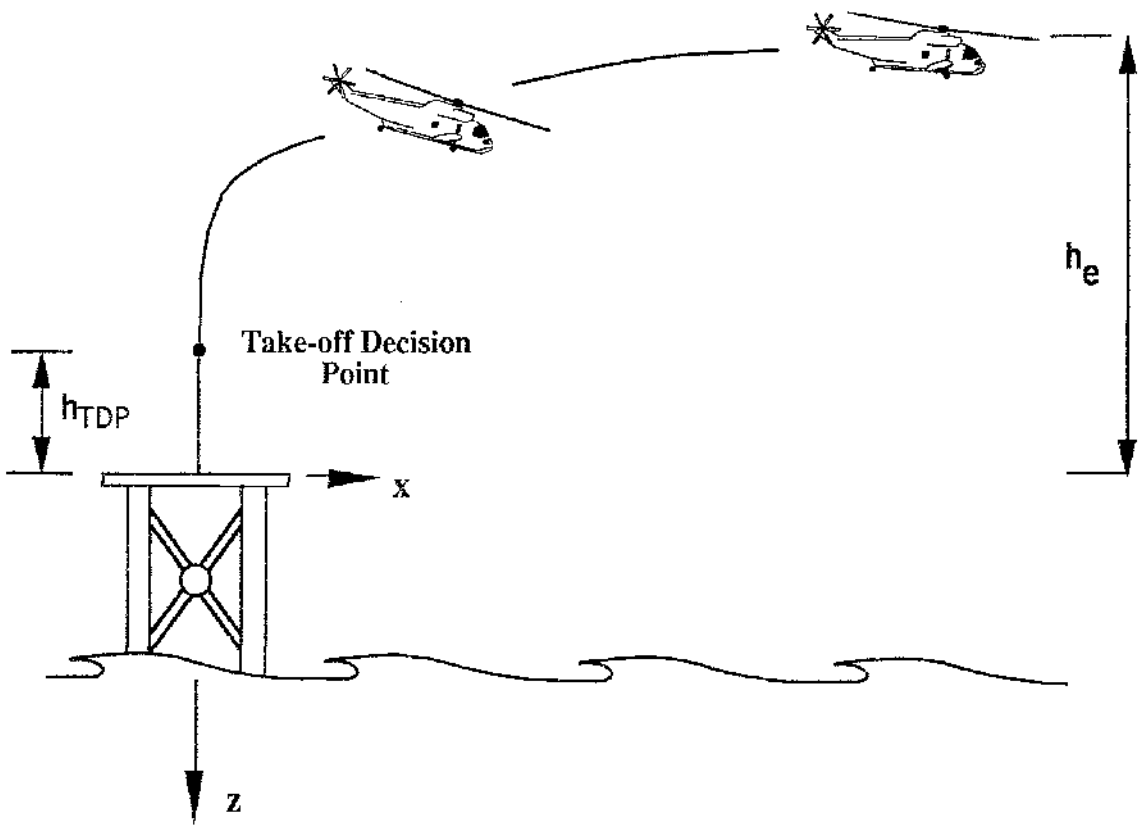

Figure 3.0 : Towering Takeoff Manoeuvre

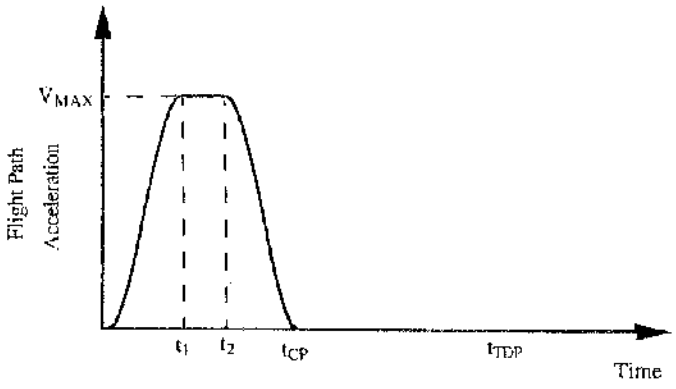

Figure 3.1a : Flight Path Acceleration

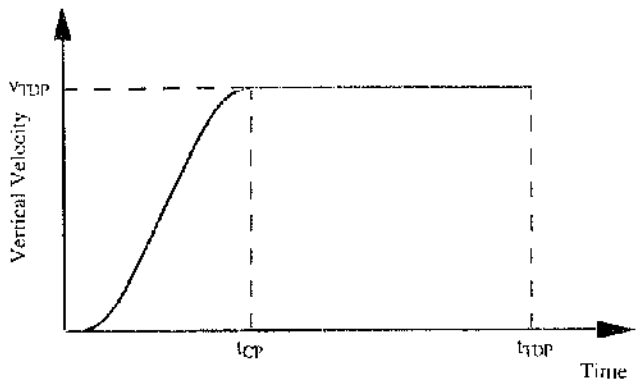

Figure 3.1b : Vertical Velocity

Figure 3.1 : Trajectory Information Employed During Towering Takeoff

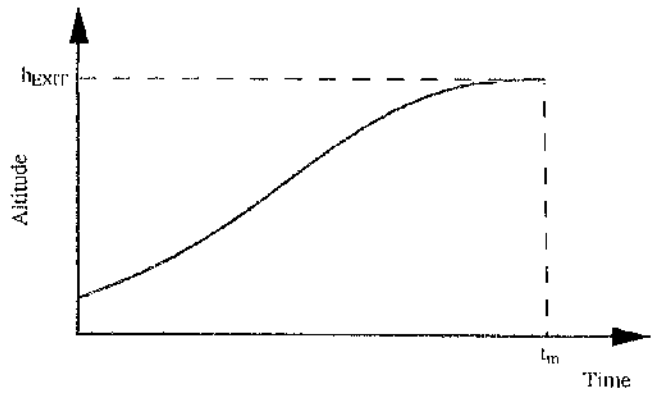

Figure 3.1c : Altitude

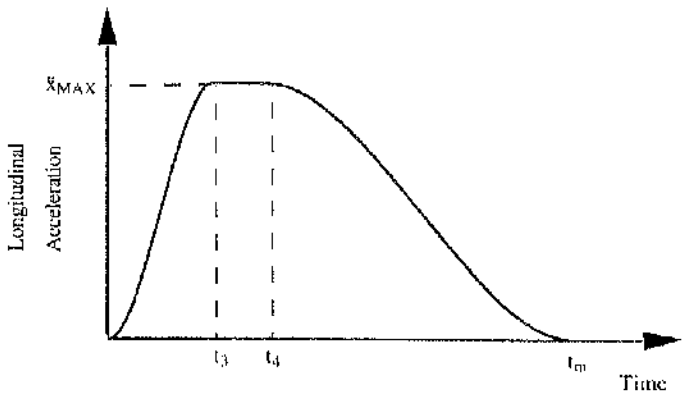

Figure 3.1d : Longitudinal Acceleration

Figure 3.1 : Trajectory Information Employed During Towering Takeoff (Continued)

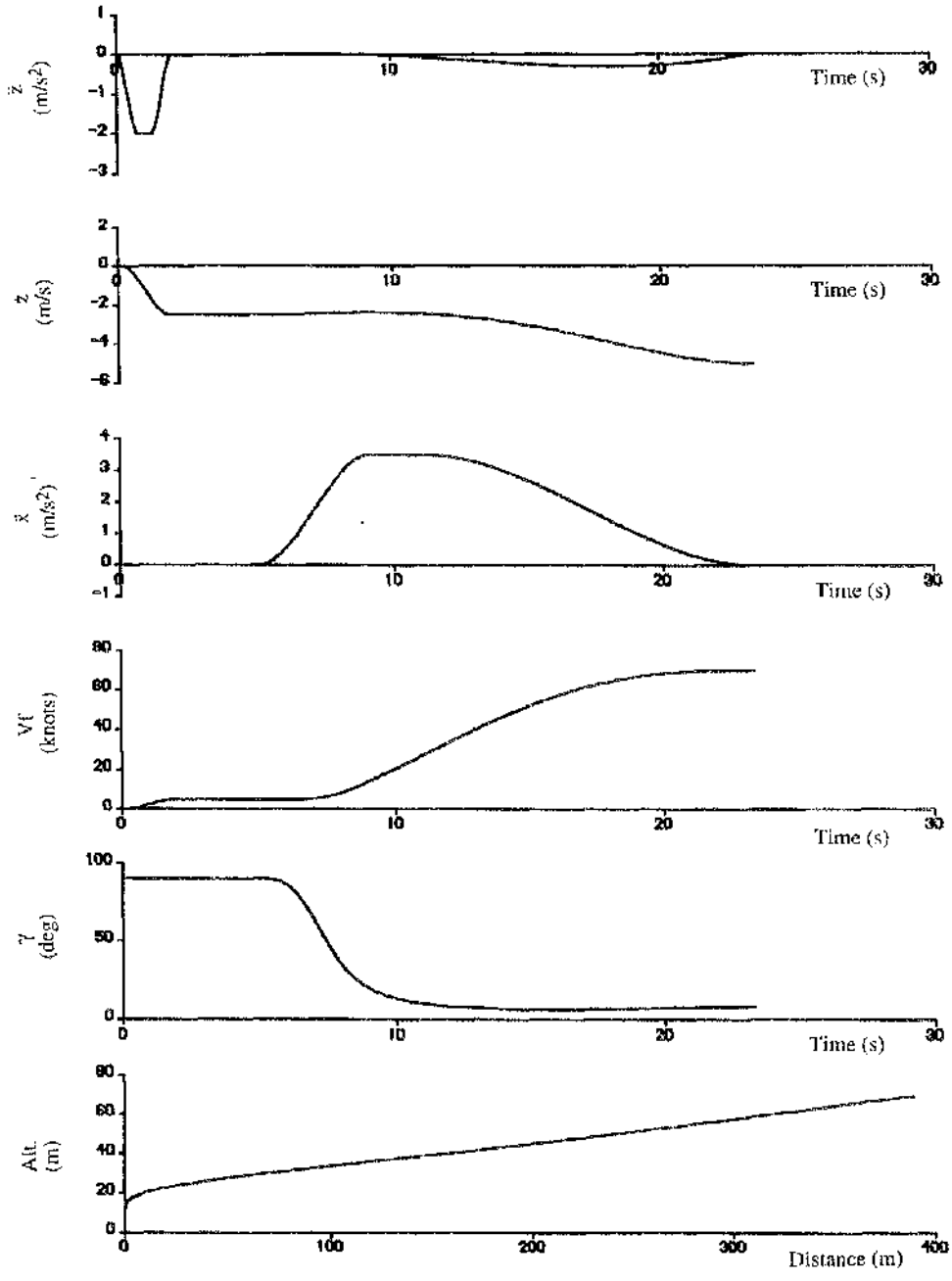

Figure 3.2 : Flight Path Information Calculated For Towering Takeoff

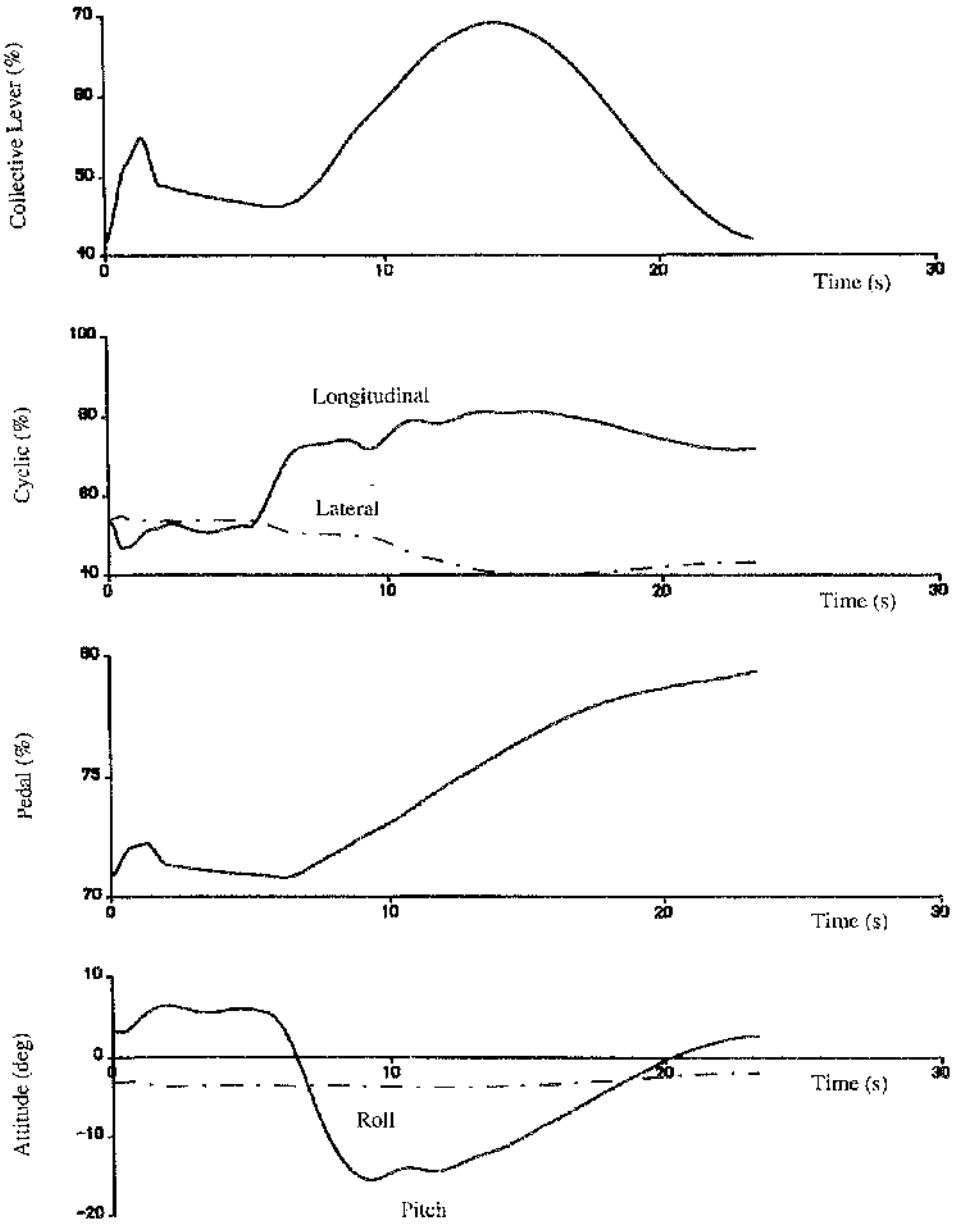

Figure 3.3 : Inverse Simulation of Towering Takeoff

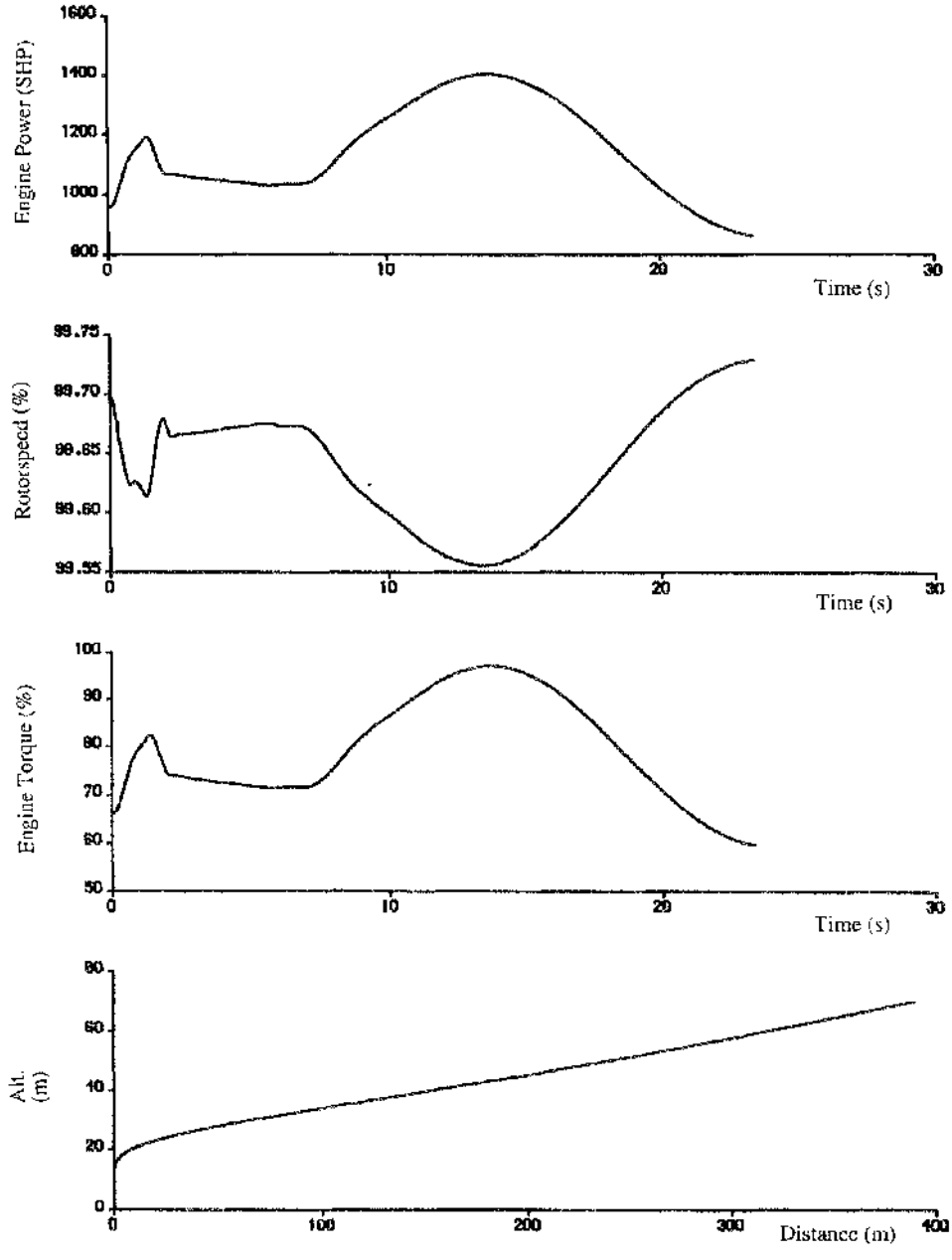

Figure 3.3 : Inverse Simulation of Towering Takeoff (Continued)

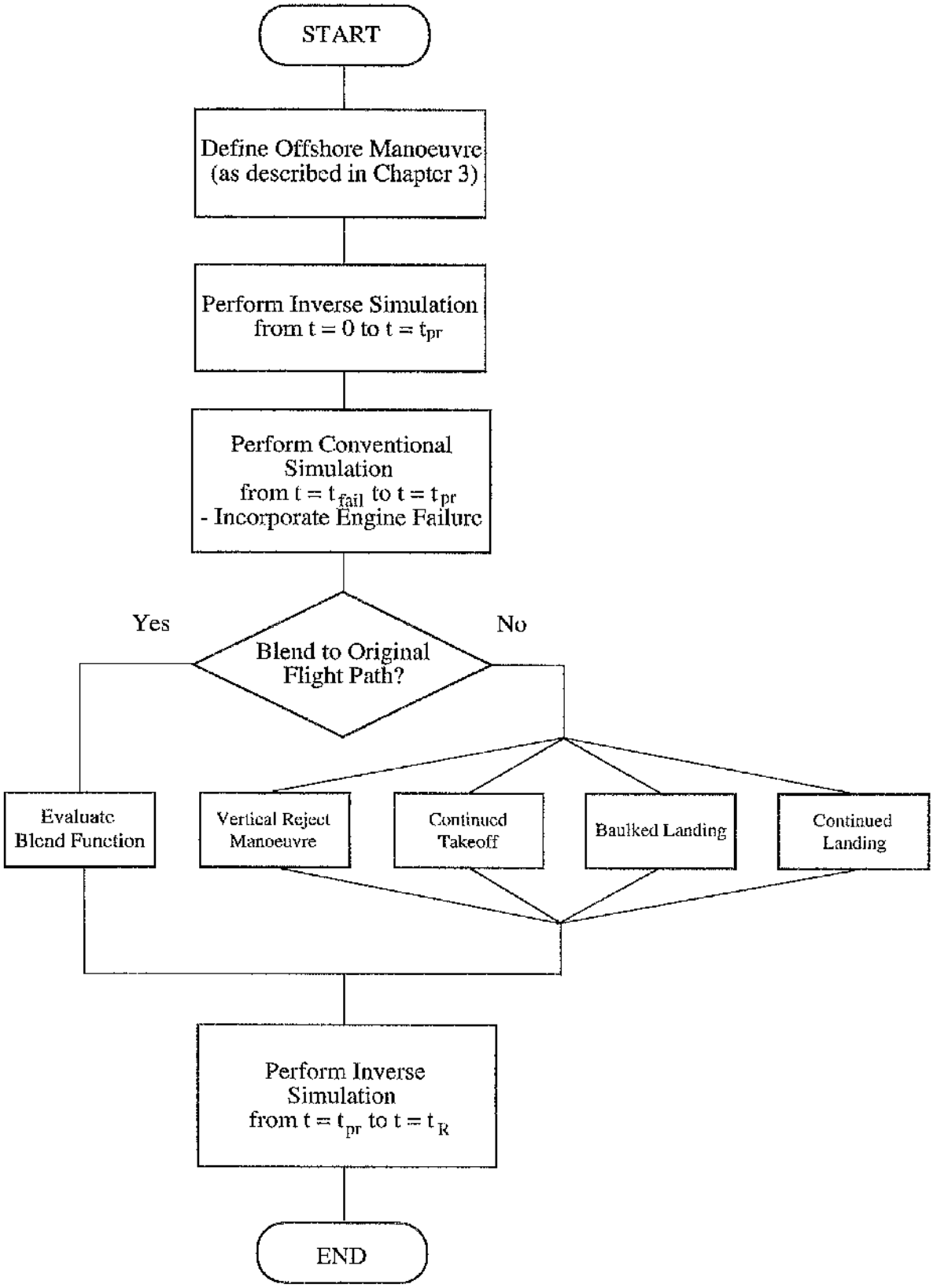

Figure 4.0 : Flow Diagram of HIFIS Algorithm

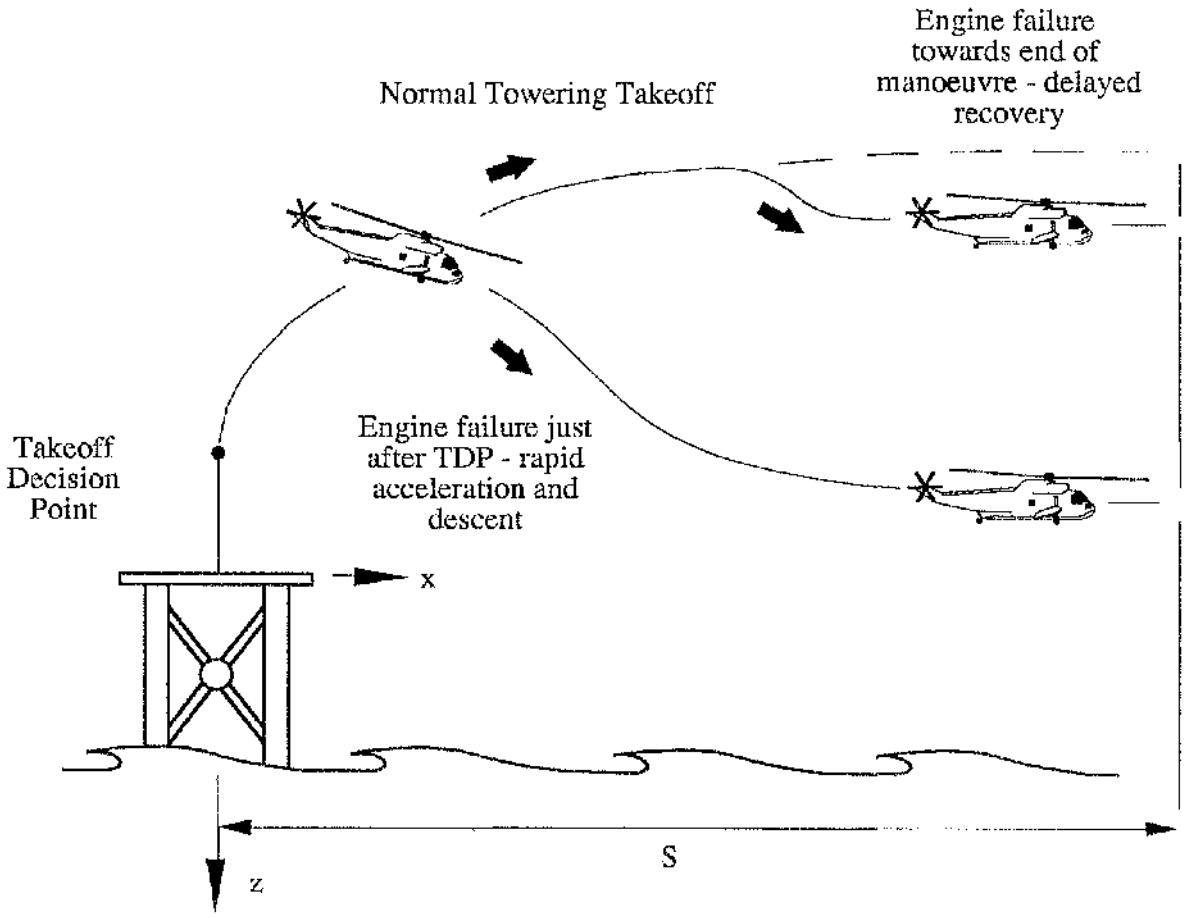

Figure 4.1 : Variation of Recovery Manoeuvre With Engine Failure Time

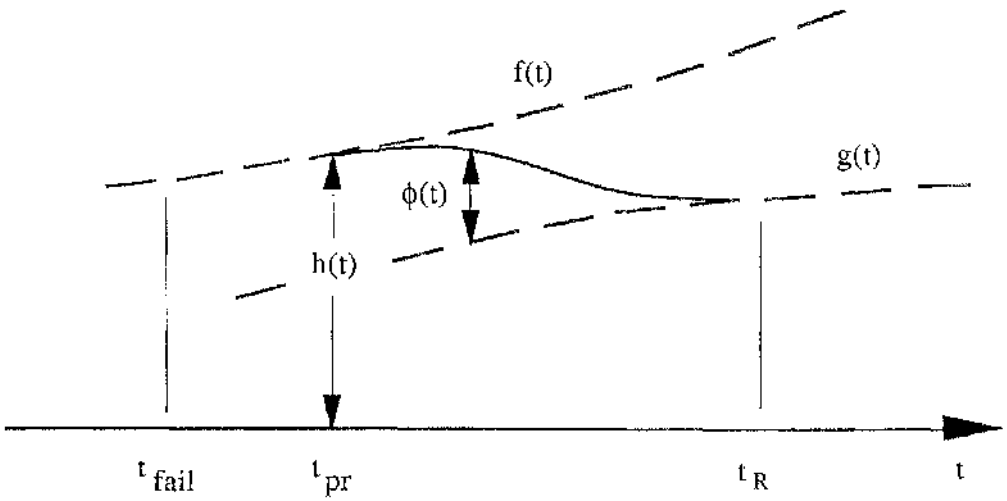

Figure 4.2 : Blending Flight Path Definition

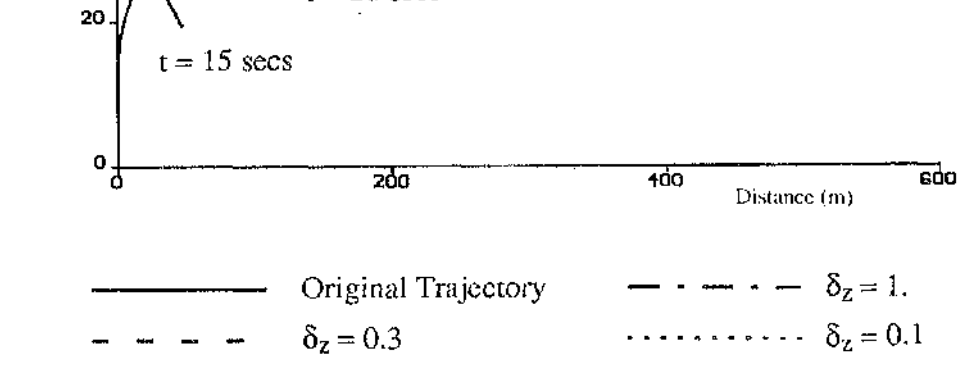

Figure 4.3 : Rejoin to Original Manoeuvre for Towering Takeoff

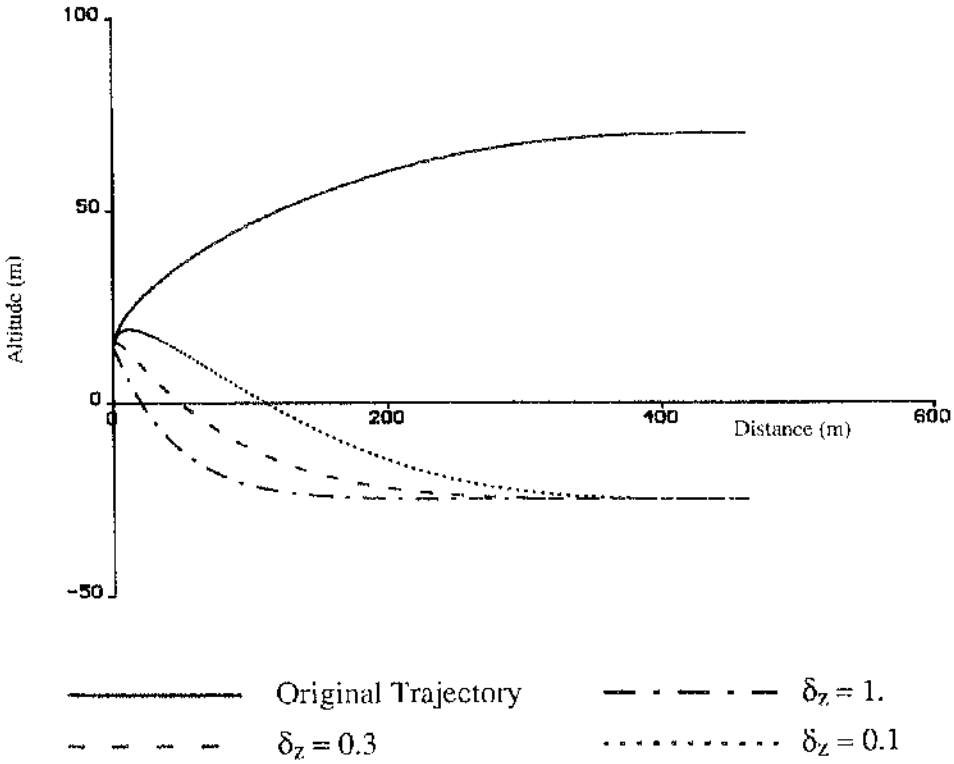

Figure 4.4 : Rejoin to New Trajectory for Towering Takeoff

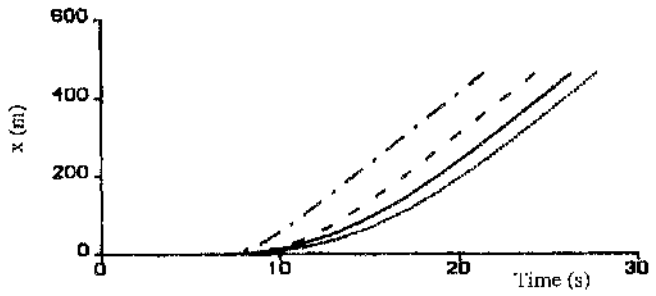

Figure 4.5a : Longitudinal Time History

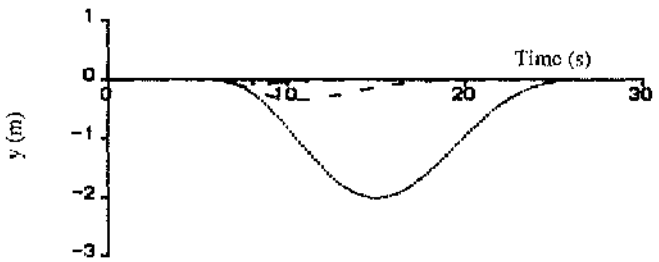

Figure 4.5b : Lateral Time History

——— Original Trajectory — · — · — $\delta_x, \delta_y, \delta_z, \delta_\psi = 1$

– – – – $\delta_x, \delta_y, \delta_z, \delta_\psi = 0.3$ · · · · · · · · · · $\delta_x, \delta_y, \delta_z, \delta_\psi = 0.1$

Figure 4.5 : Trajectory Components for Rejoin to Recovery Manoeuvre for Towering Takeoff

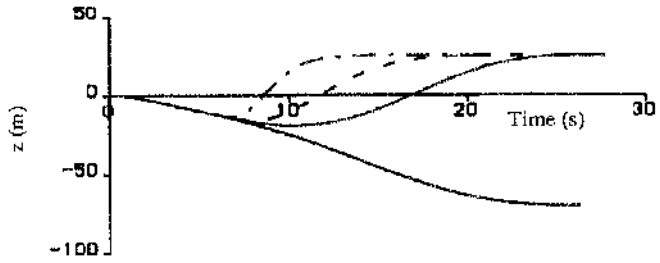

Figure 4.5c : Vertical Time History

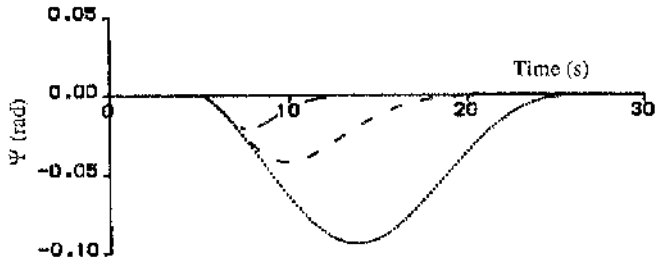

Figure 4.5d : Heading Time History

——————— Original Trajectory — · — · — $\delta_x, \delta_y, \delta_z, \delta_\psi = 1$

– – – – $\delta_x, \delta_y, \delta_z, \delta_\psi = 0.3$ · · · · · · · · · · $\delta_x, \delta_y, \delta_z, \delta_\psi = 0.1$

Figure 4.5 : Trajectory Components for Rejoin to Recovery Manoeuvre for Towering Takeoff (Continued)

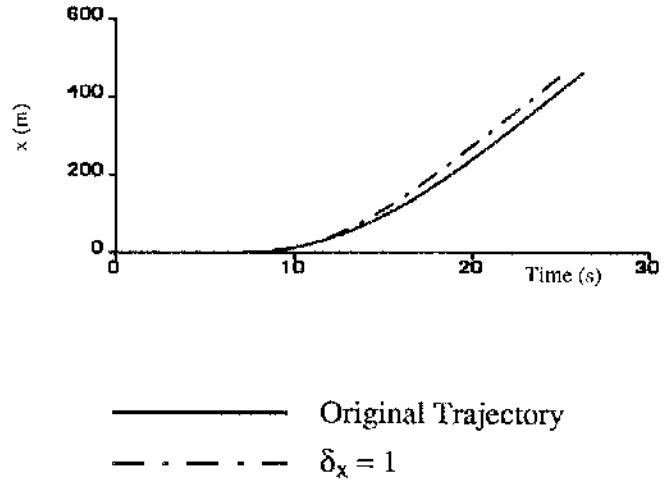

Figure 4.6a : Longitudinal Time History

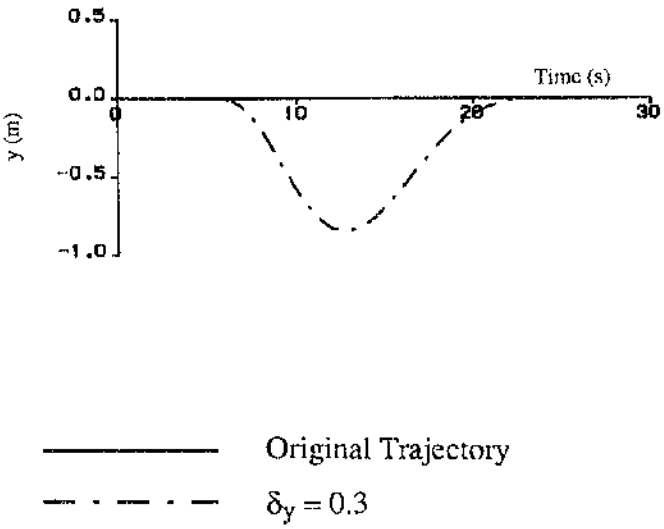

Figure 4.6b : Lateral Time History

Figure 4.6 : Tailoring of Individual Trajectory Components for New Flight Path

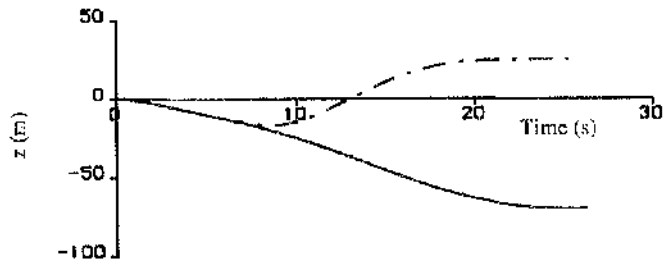

Original Trajectory

$\delta_z = 0.1$

Figure 4.6c : Vertical Time History

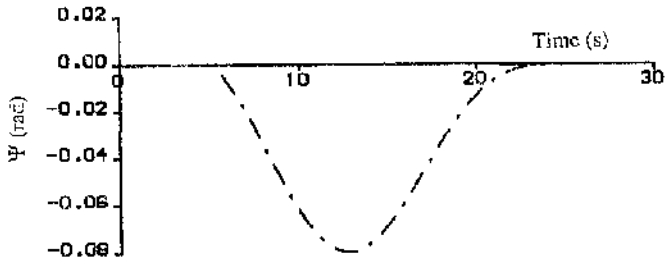

Original Trajectory

$\delta_\psi = 0.01$

Figure 4.6d : Heading Time History

Figure 4.6 : Tailoring of Individual Trajectory Components for New Flight Path (Continued)

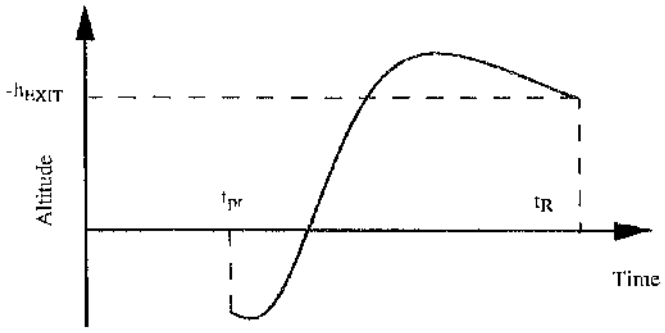

Figure 4.7a : Altitude

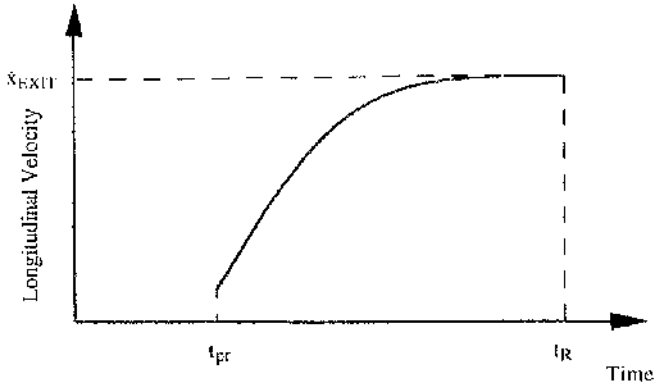

Figure 4.7b : Longitudinal Acceleration

Figure 4.7 : Trajectory Information Employed During Continued Takeoff

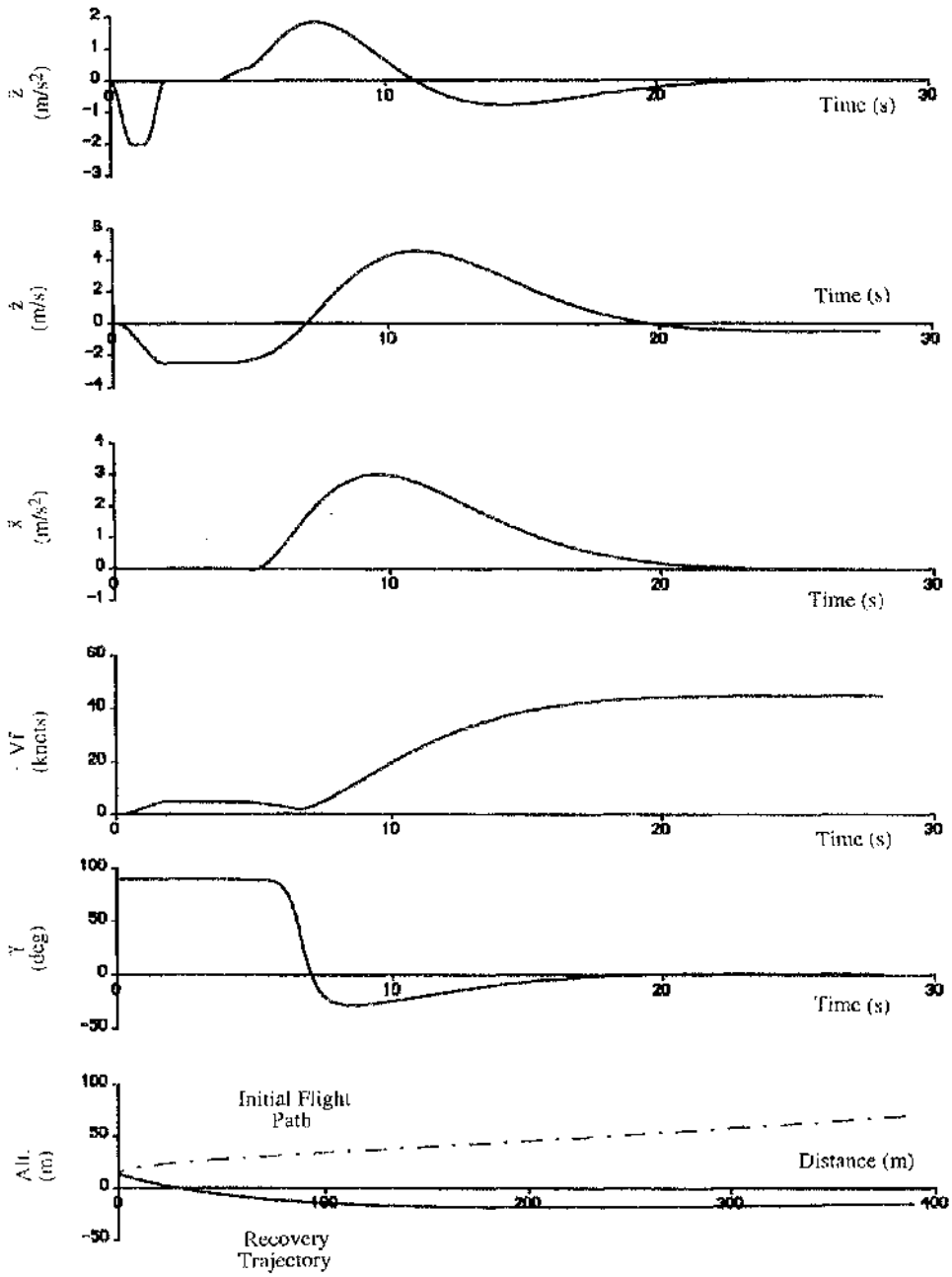

Figure 4.8 : Flight Path Information for Engine Failure After TDP During Towering Takeoff

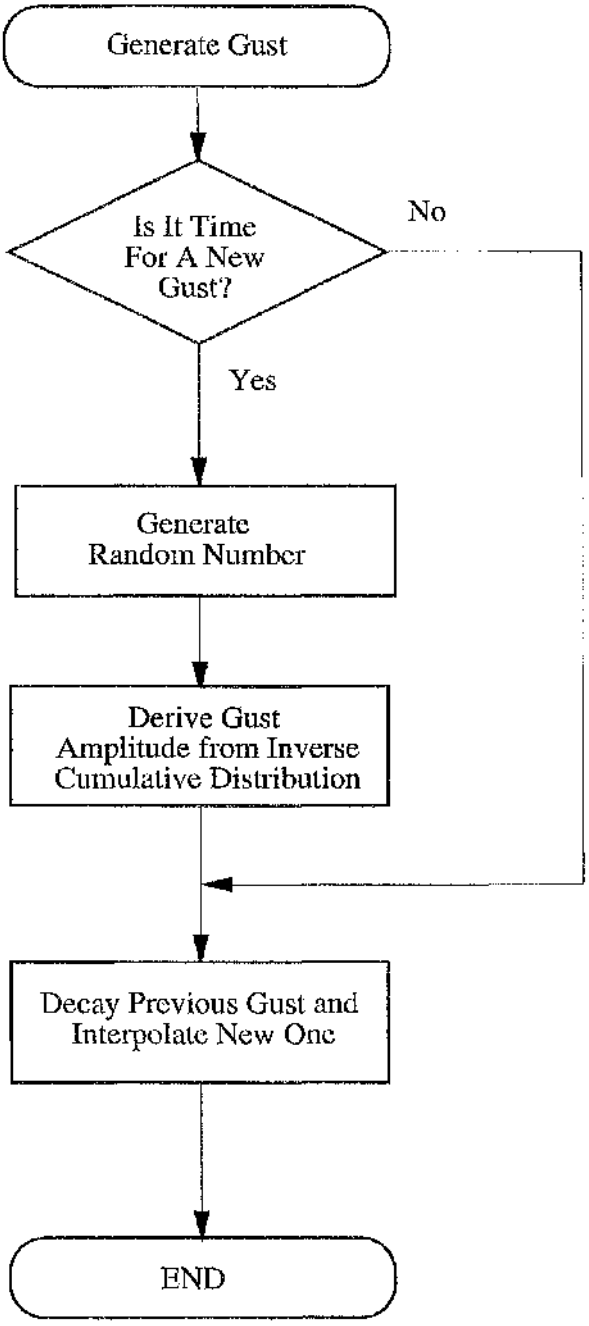

Figure A5.4 - Generation of Single Gust

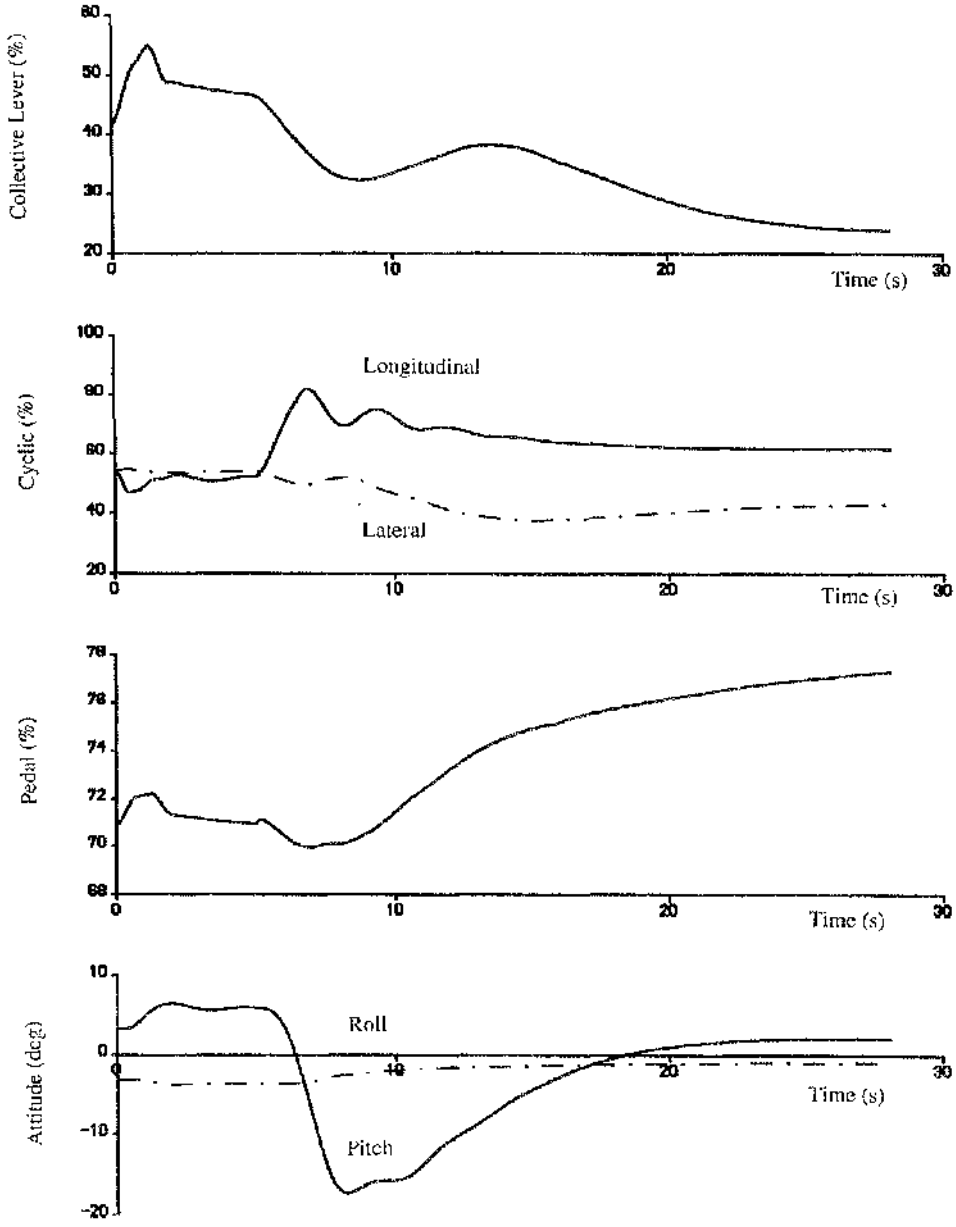

Figure 4.9 : Inverse Simulation of Engine Failure After TDP During Towering Takeoff

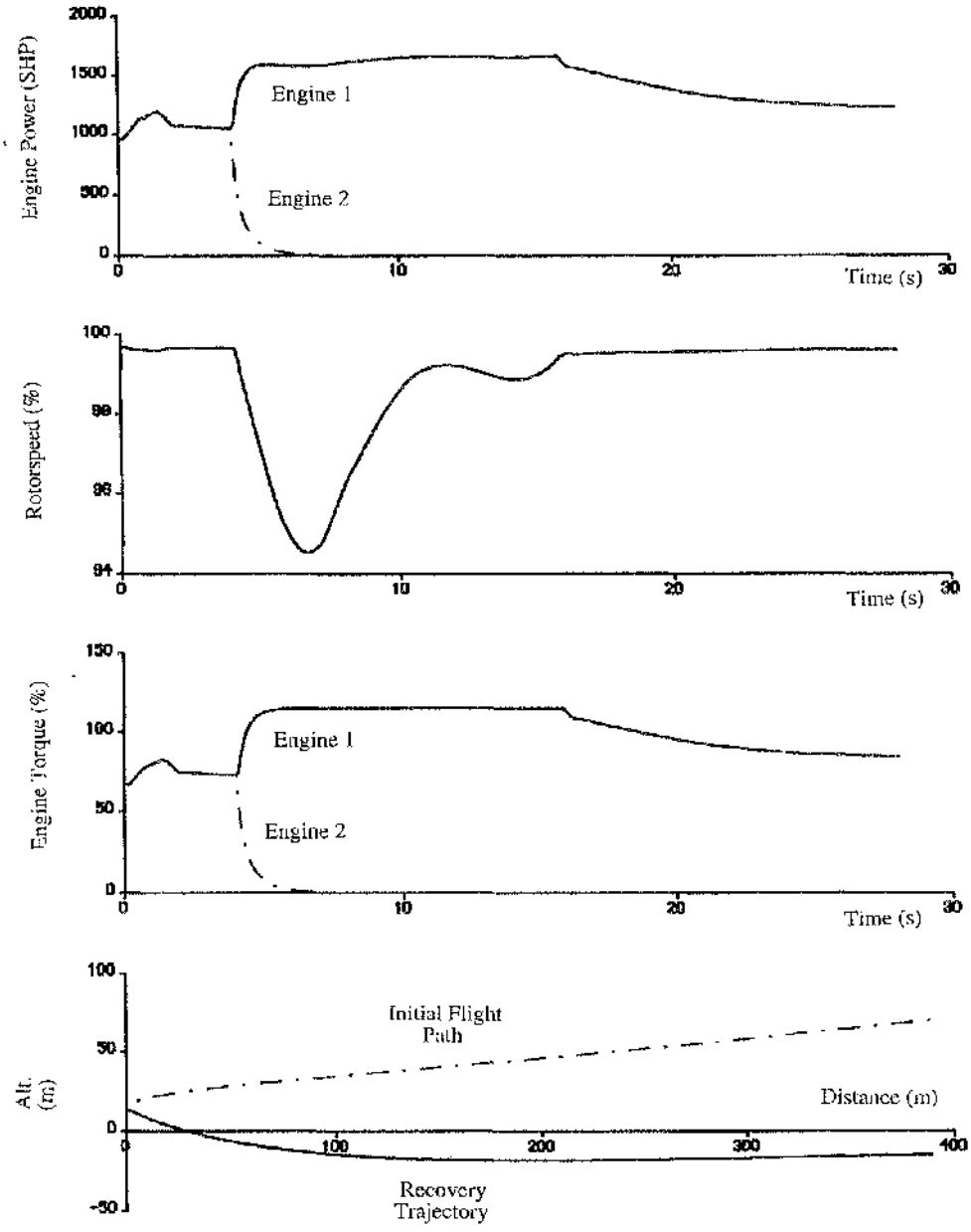

Figure 4.9 : Inverse Simulation of Engine Failure After TDP During Towering Takeoff (Continued)

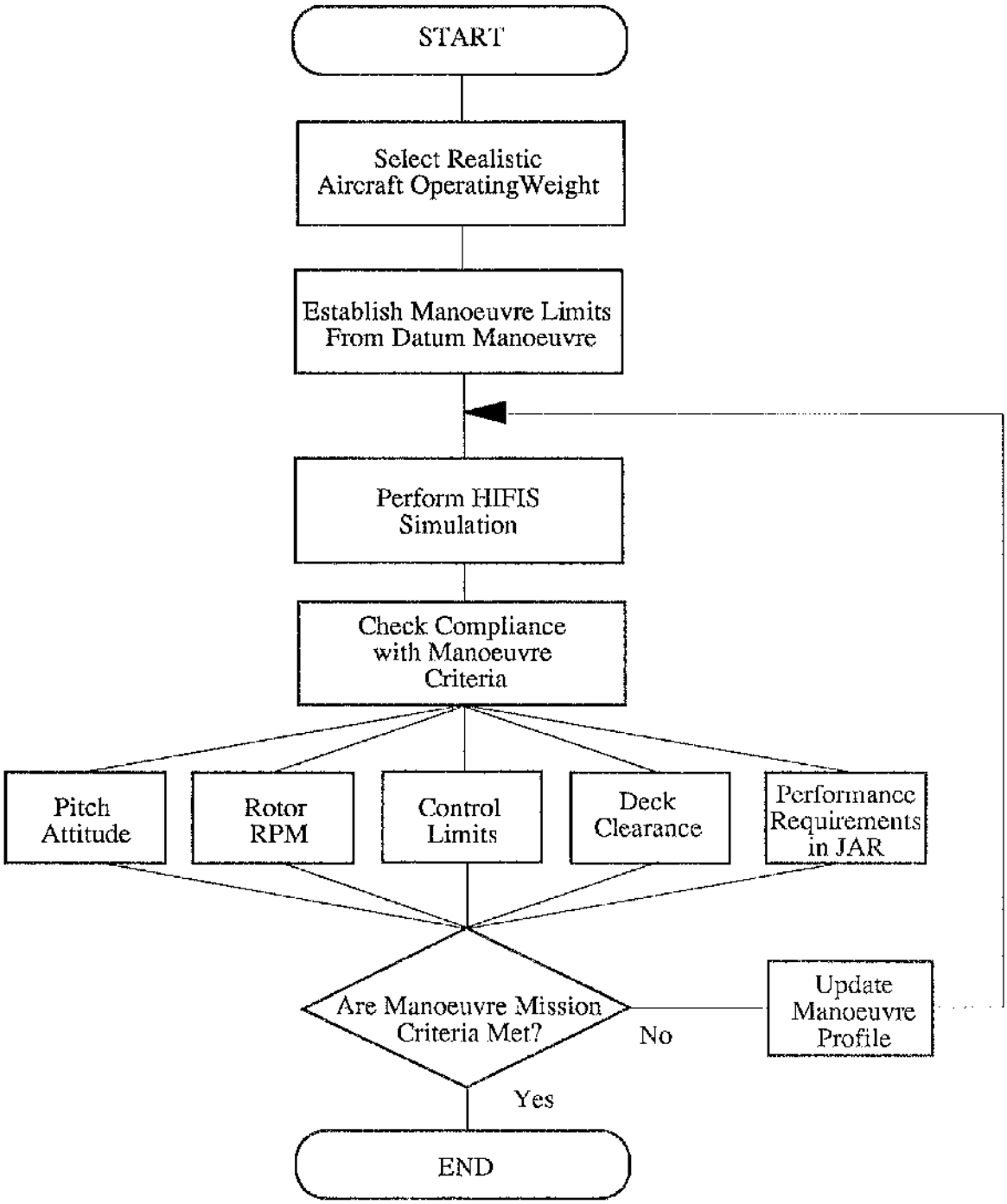

Figure 5.0 : Flow Diagram of Offshore Investigation Philosophy

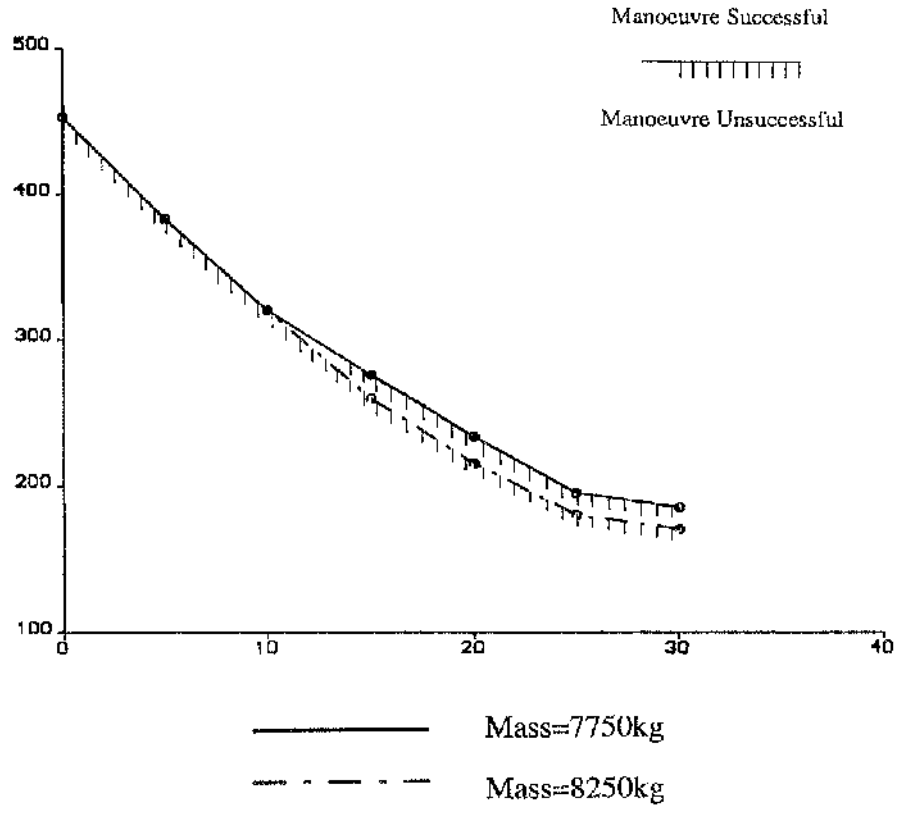

Figure 5.1 : Variation of MinimumTakeoff Distance with Wind Speed

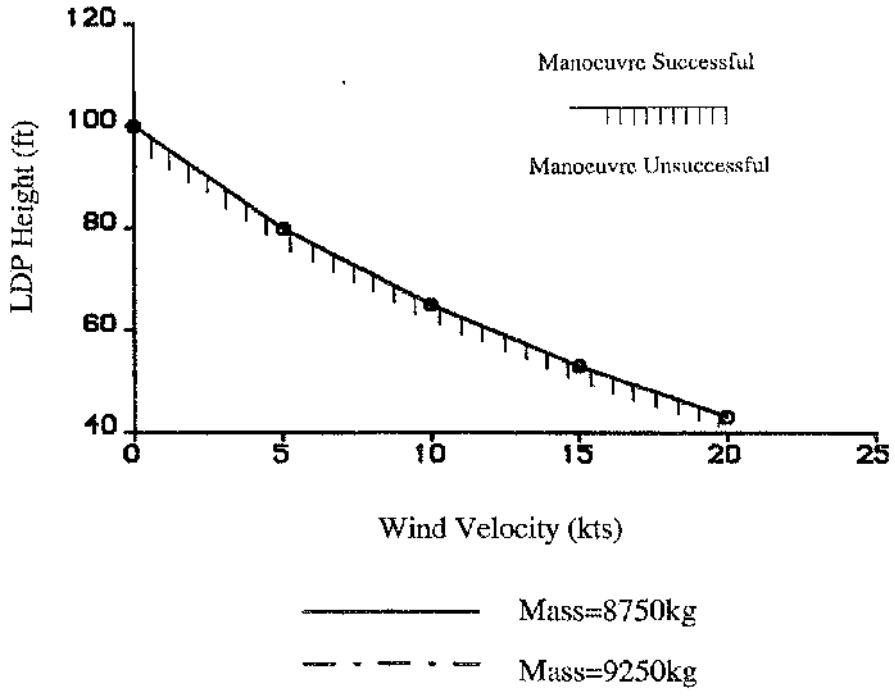

Figure 5.2 : Variation of Minimum LDP Height with Wind Speed

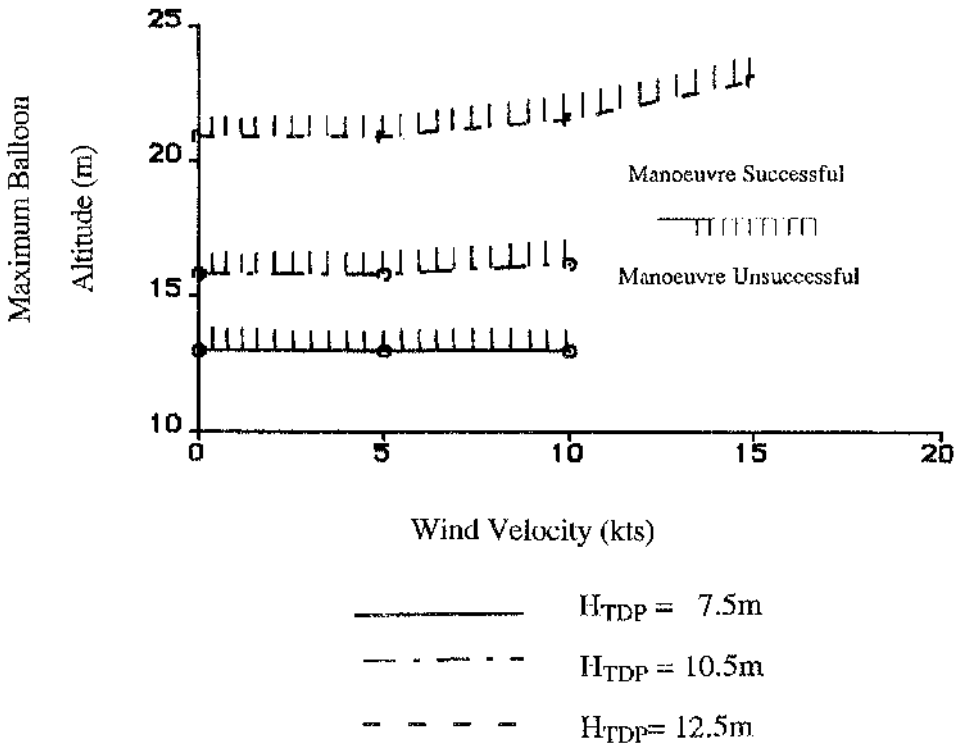

Figure 5.3 : Variation of Maximum Balloon Altitude with Wind Speed

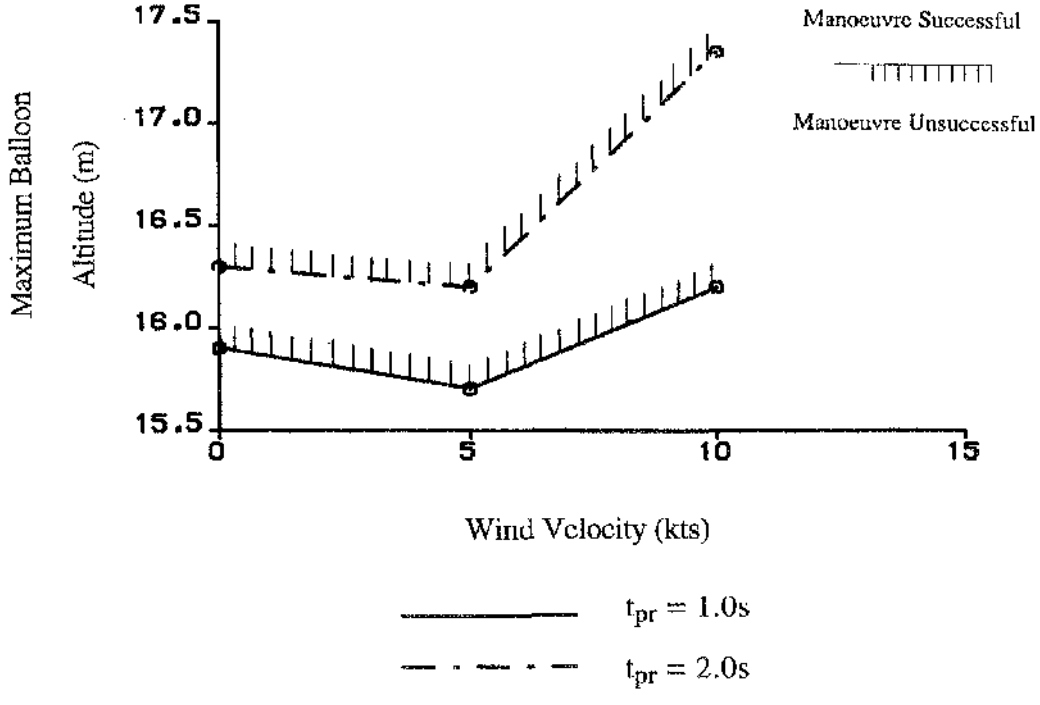

Figure 5.4 : Variation of Maximum Balloon Altitude with Wind Speed

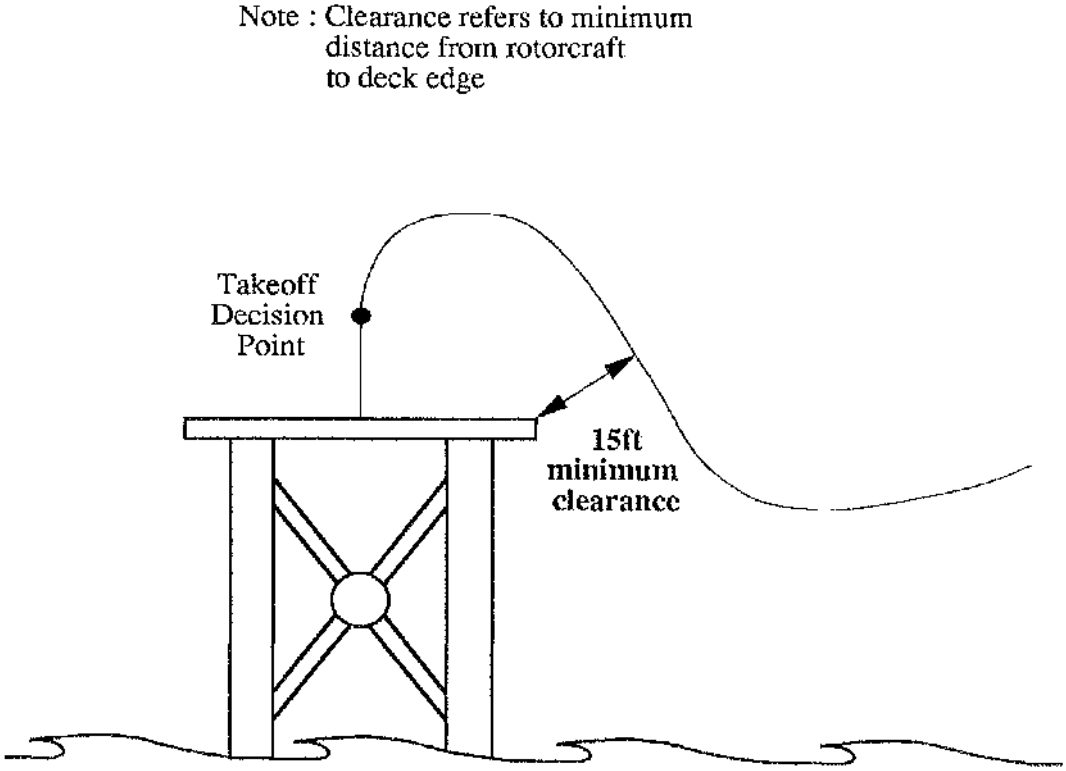

Figure 5.5 : Portrait of Deck Edge Clearance Criteria (Adapted from JAR 29.59)

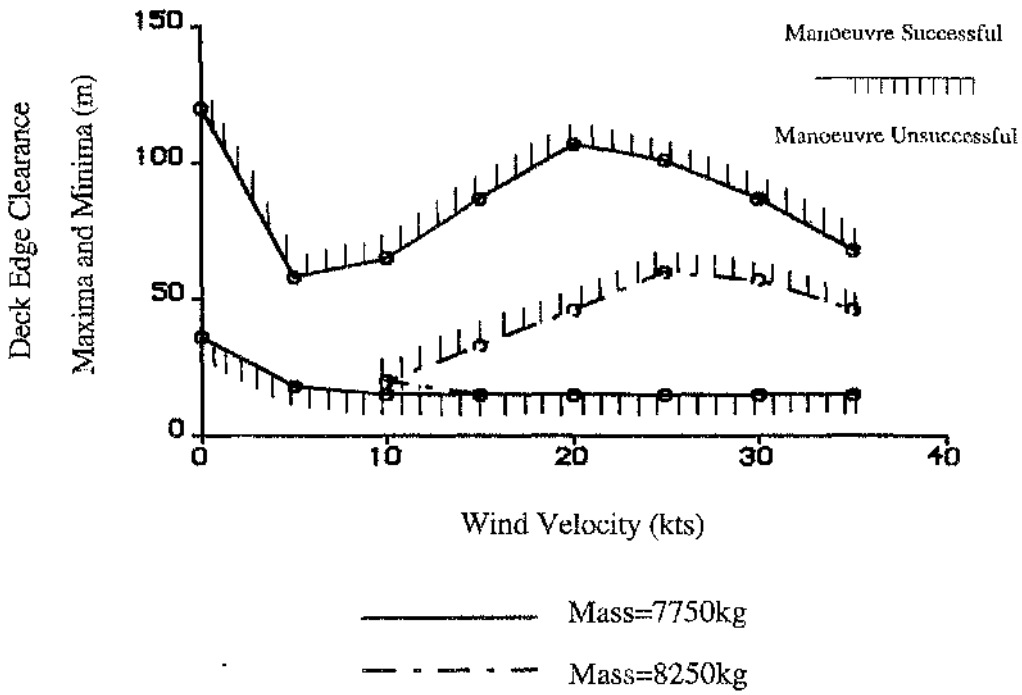

Figure 5.6 : Variation of Deck Edge Extrema with Wind Speed

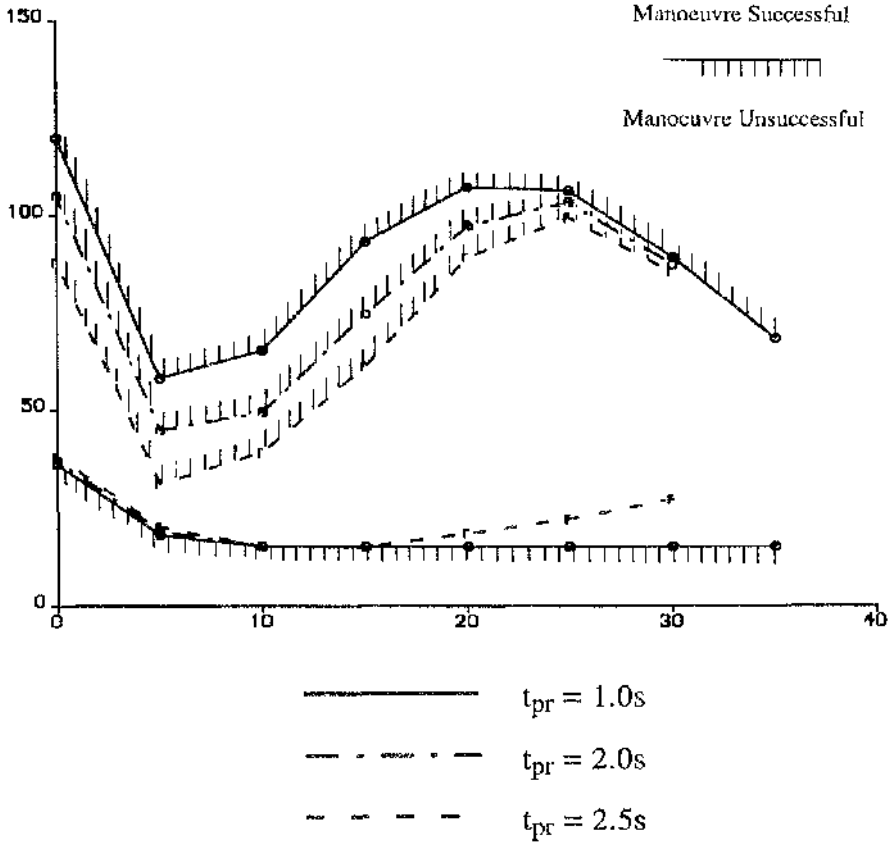

Figure 5.7 : Variation of Deck Edge Extrema with Wind Speed

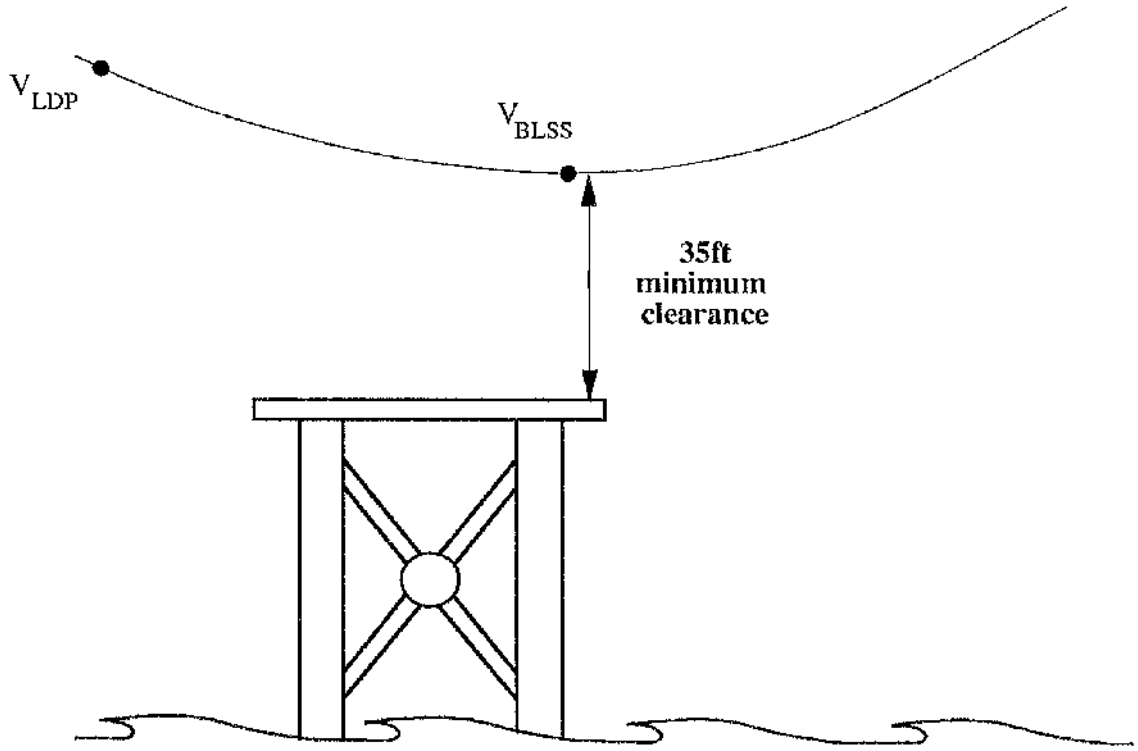

Figure 5.8 : Portrait of Deck Clearance Criteria For Baulked Landing (Adapted from JAR 29.75)

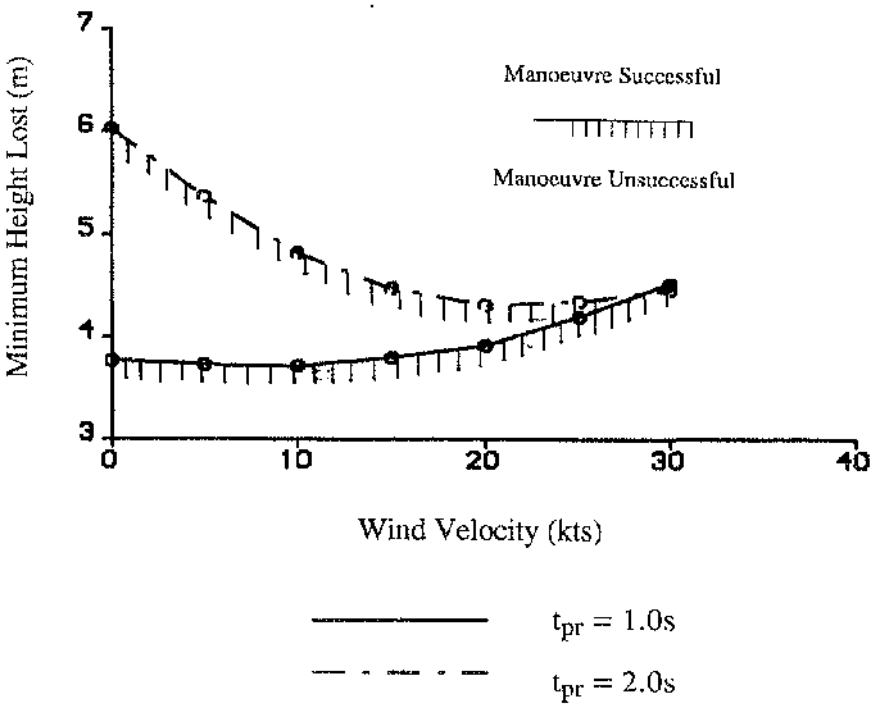

Figure 5.9 : Variation of Minimum Height Loss with Wind Speed

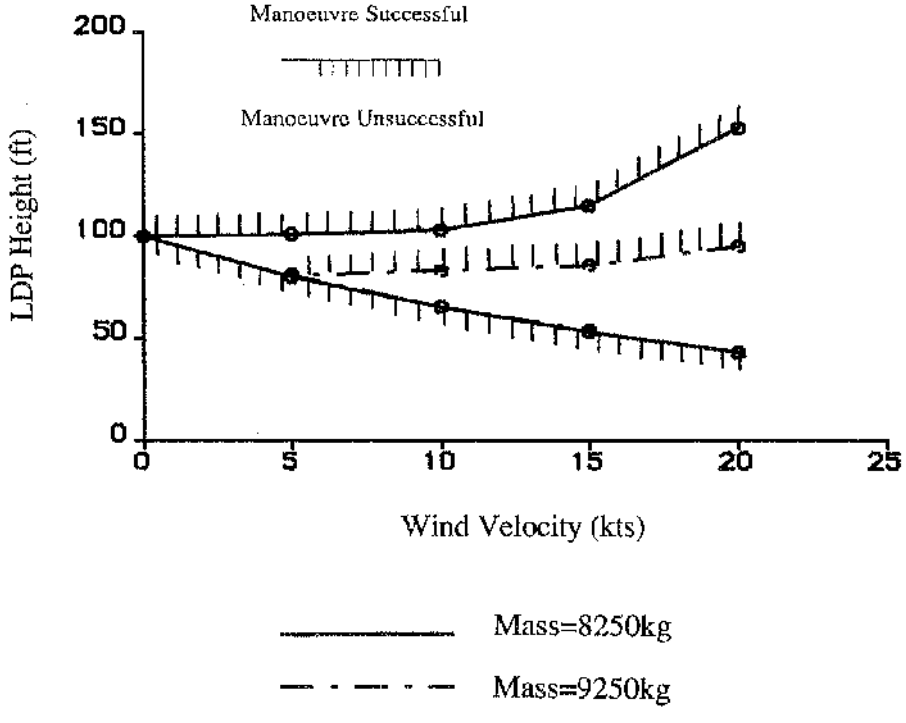

Figure 5.10 : Variation of LDP Height with Wind Speed

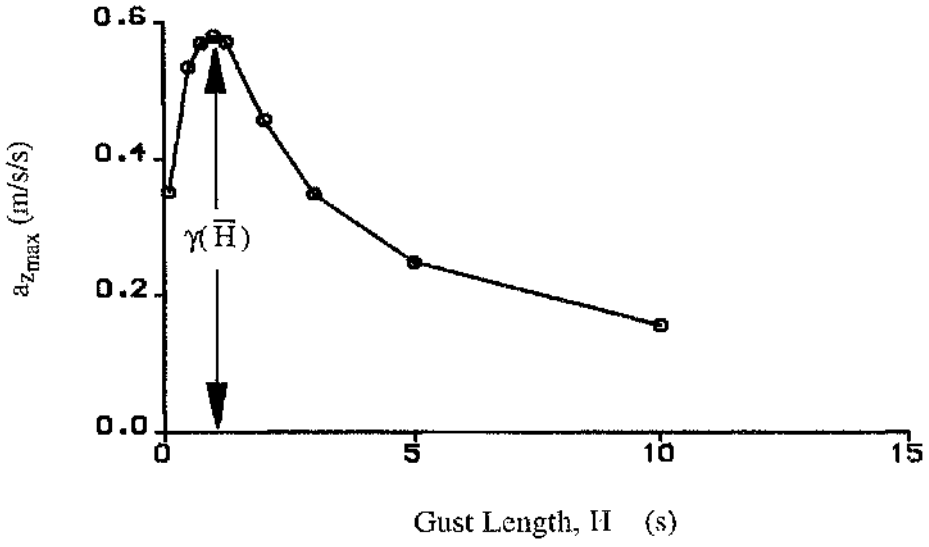

Figure 5.11 : Discrete Gust Response Function

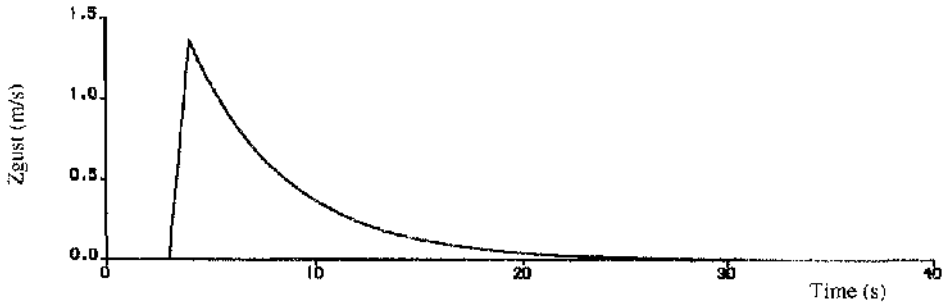

Figure 5.12 : Tuned Discrete Gust

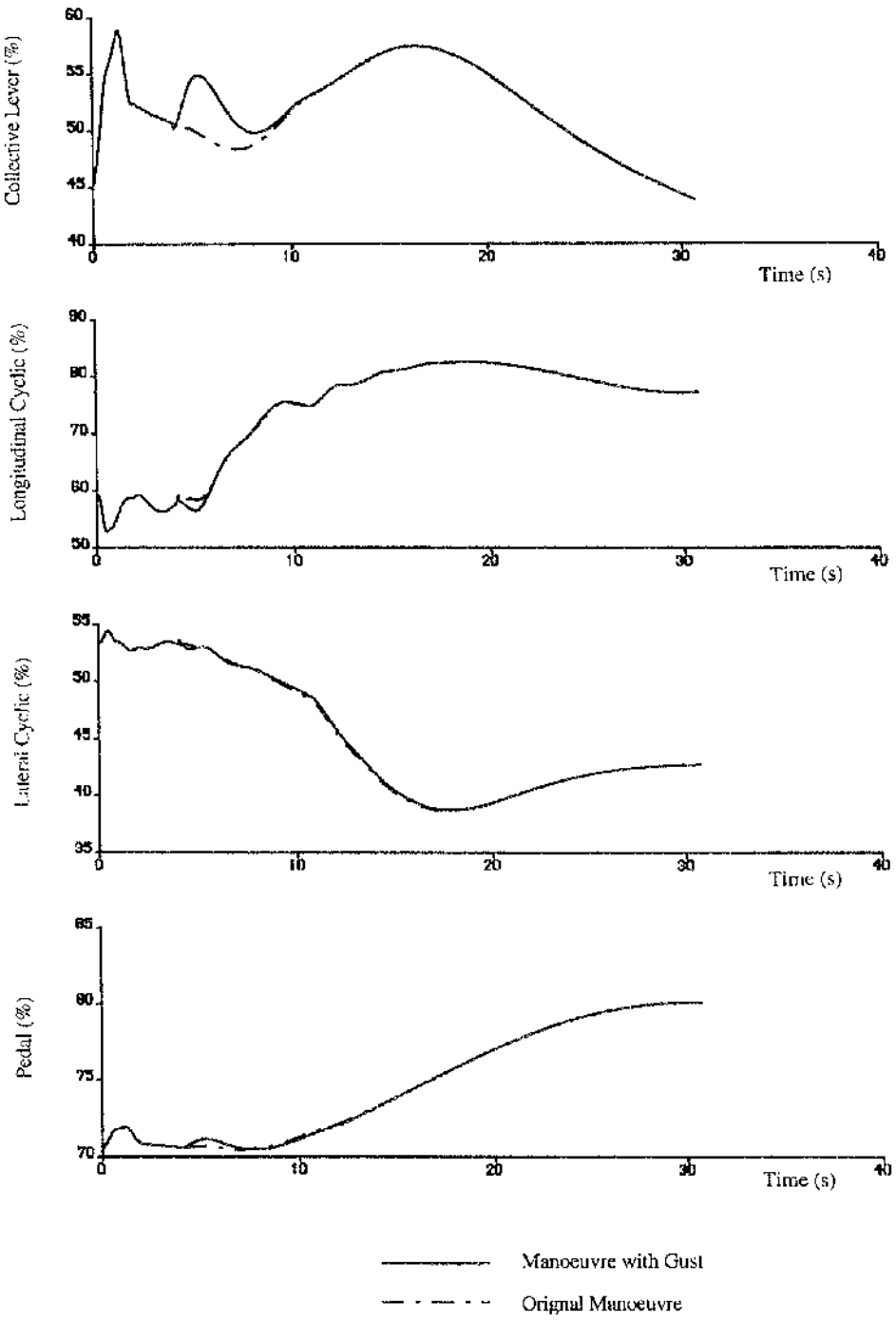

Figure 5.13 : Helicopter Response to Discrete Gust

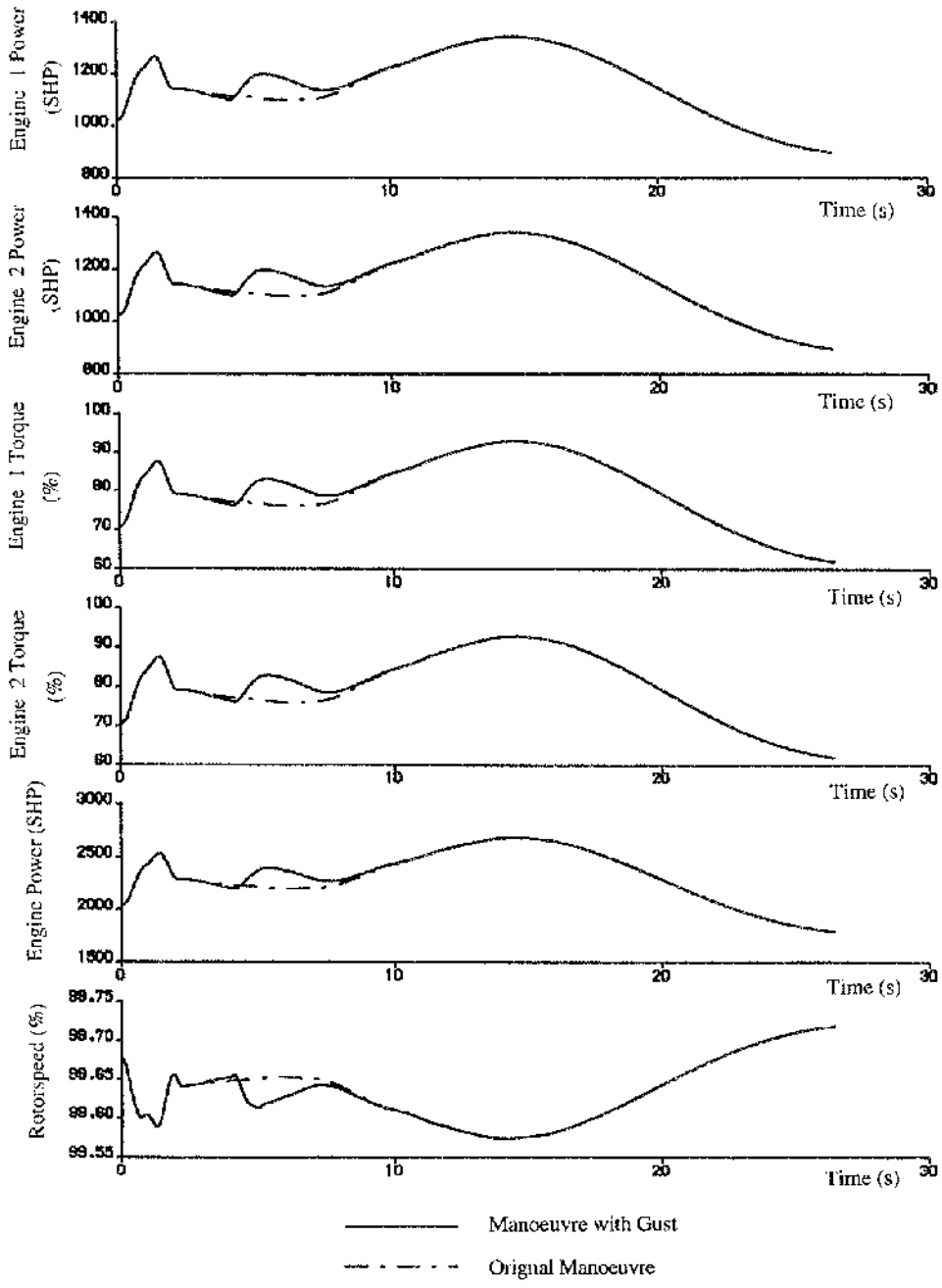

Figure 5.13 : Helicopter Response to Discrete Gust (Continued)

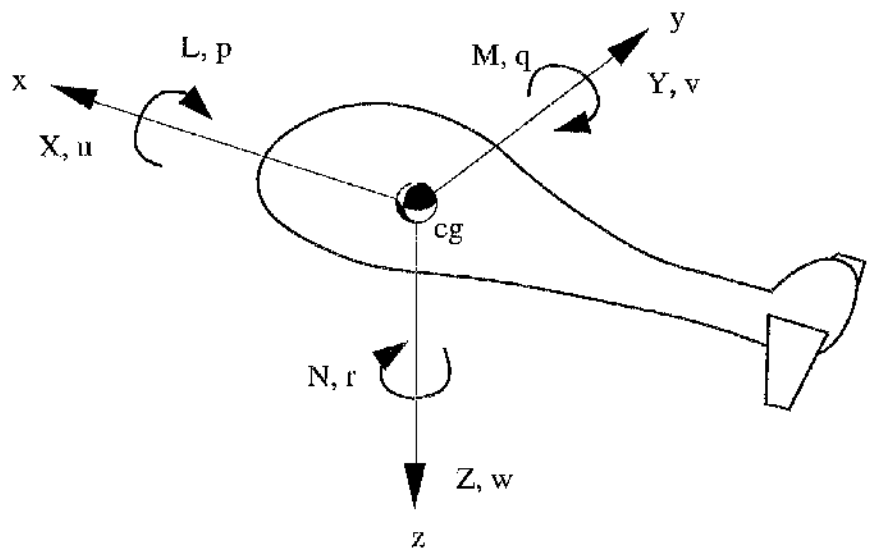

Figure A1.0 : Body Fixed Axes Set

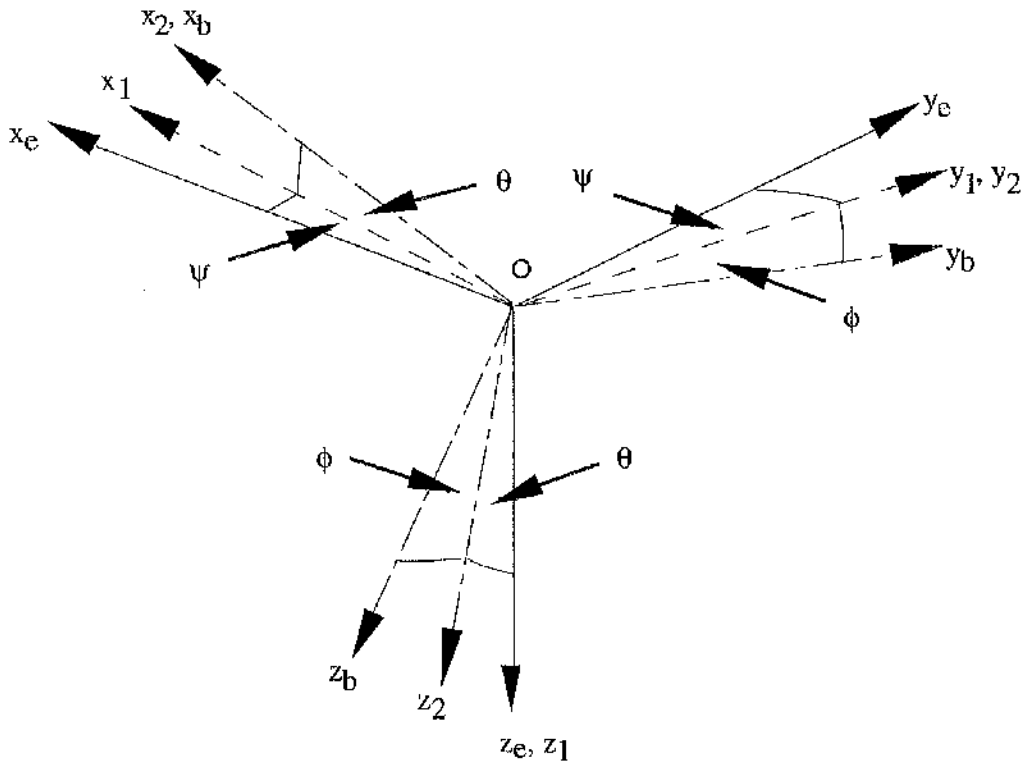

Figure A1.1 : Euler Angle Transformation

b body axes set

h hub axes set (fixed in hub)

s shaft axes (rotates with shaft)

bl blade axes (fixed in blade, origin in root)

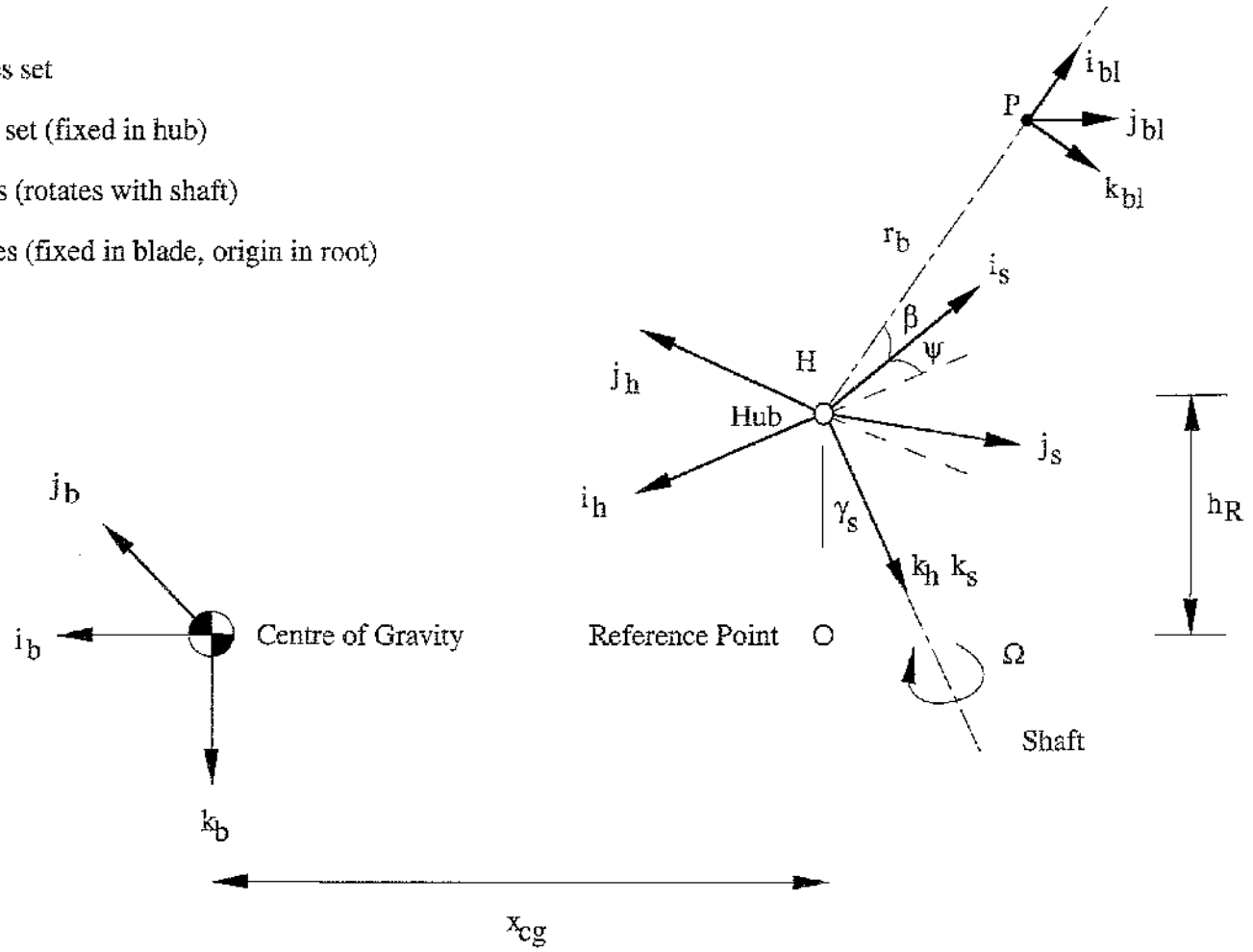

Figure A1.2 : Axes Set For Main Rotor Blade Kinematics

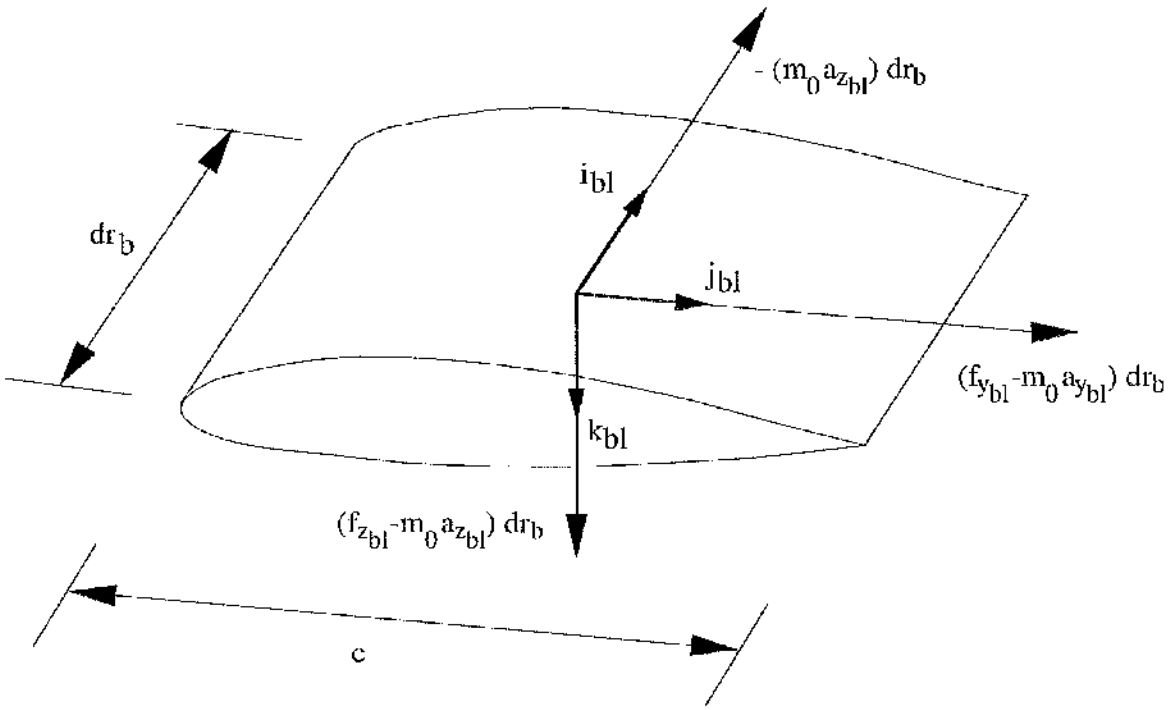

Figure A1.3 : Forces on A Blade Element

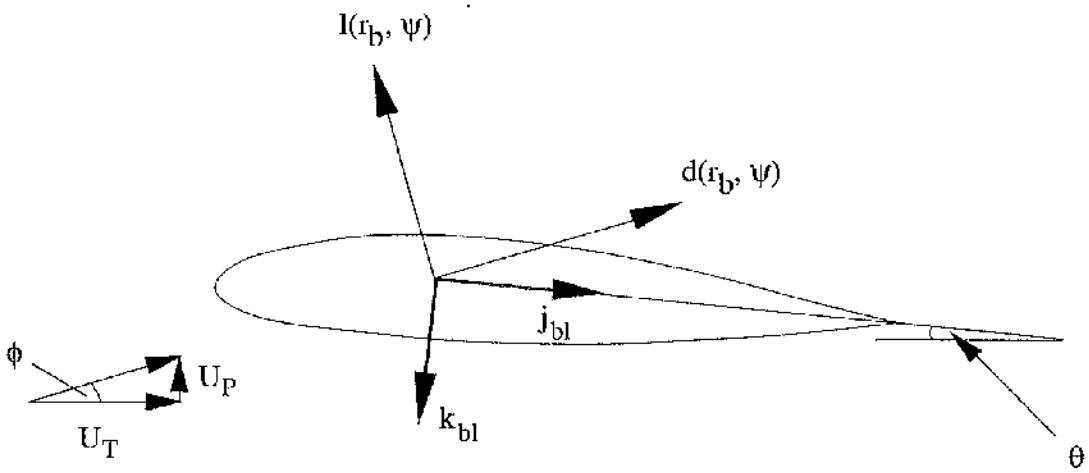

Figure A1.4 : Lift and Drag On a Blade Element

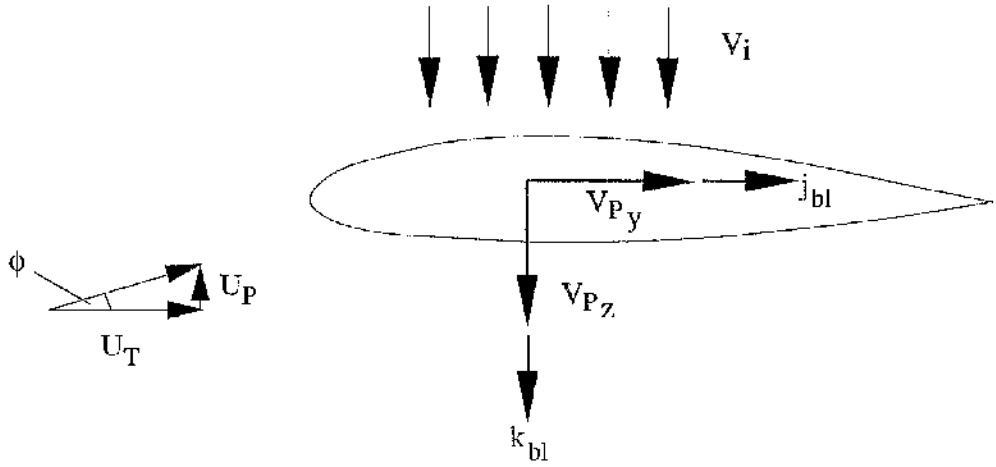

Figure A1.5 : Blade Element Velocities

$$C_{Y_{A_{1s}}} = \theta_{1_c}\{ -\tfrac{1}{8}(1-e^2)[(\alpha_{1c}-\beta_{1_s})\mu_x + (\alpha_{1s}+\beta_{1_c})\mu_y] + \tfrac{1}{4}(1-e)\beta_0(\mu_x^2-\mu_y^2)\} +$$
$$\theta_{1_s}\{\tfrac{1}{3}\beta_0'(1-e^3) - \tfrac{1}{2}(1-e^2)(\mu_z-\lambda_0) - \tfrac{1}{8}(1-e^2)[(3\alpha_{1s}-\beta_{1_c})\mu_x + (\alpha_{1c}+3\beta_{1_s})\mu_y] -$$
$$\tfrac{1}{2}(1-e)\beta_0\mu_x\mu_y\} +$$
$$\theta_0\{-\tfrac{1}{3}(1-e^3)\alpha_{1s} + \tfrac{1}{2}(1-e^2)(\beta_0'\mu_x - \beta_0\mu_y) - \mu_x(1-e)(\mu_z-\lambda_0) + \tfrac{1}{4}(1-e)\beta_{1c}(\mu_x^2 -$$
$$\mu_y^2) - \tfrac{1}{2}(1-e)\beta_{1_s}\mu_x\mu_y\} +$$
$$\theta_{tw}\{-\alpha_{1s}(\tfrac{1}{4} - \tfrac{1}{3}e) + \tfrac{1}{3}(1-\tfrac{3}{2}e+\tfrac{1}{2}e^3)(\beta_0'\mu_x - \beta_0\mu_y) - \tfrac{1}{2}\mu_x(\mu_z-\lambda_0)(1+2e-e^2) +$$
$$\tfrac{1}{8}\beta_{1c}(\mu_x^2 - \mu_y^2)(1-e)^2 - \tfrac{1}{4}\beta_{1s}\mu_x\mu_y(1-e)^2\} +$$
$$\alpha_{1s}[\tfrac{2}{3}(1-e^3)\beta_0' - (\mu_z-\lambda_0)(1-e^2) - \tfrac{3}{4}\beta_{1_s}\mu_y(1-e^2) + \tfrac{1}{4}\beta_{1_c}\mu_x(1-e^2)] +$$
$$\tfrac{1}{4}\alpha_{1_c}(1-e^2)(\beta_{1_s}\mu_x - \beta_{1_c}\mu_y) + \beta_0\mu_y[\beta_0'(1-e^2) - 2(1-e)(\mu_z-\lambda_0) - \tfrac{3}{2}\beta_{1_s}\mu_y(1-e) +$$
$$\beta_{1_c}\mu_x(1-e)] - \tfrac{1}{2}\beta_0\beta_{1x}\mu_x^2(1-e) + \frac{\delta}{a_0}(1-e^2)\mu_x$$

$$C_{Y_{A_{1c}}} = \theta_{1_c}\{\tfrac{1}{3}\beta_0'(1-e^3) - \tfrac{1}{2}(1-e^2)(\mu_z-\lambda_0) - \tfrac{1}{8}(1-e^2)[(\alpha_{1s}-3\beta_{1_c})\mu_x + (3\alpha_{1c}+\beta_{1_s})\mu_y] +$$
$$\tfrac{1}{2}(1-e)\beta_0\mu_x\mu_y\} +$$
$$\theta_{1_s}\{-\tfrac{1}{8}(1-e^2)[(\alpha_{1c}-\beta_{1_s})\mu_x + (\alpha_{1s}+\beta_{1_c})\mu_y] + \tfrac{1}{4}(1-e)\beta_0(\mu_x^2-\mu_y^2)\} +$$
$$\theta_0\{-\tfrac{1}{3}(1-e^3)\alpha_{1c} + \tfrac{1}{2}(1-e^2)(\beta_0'\mu_y + \beta_0\mu_x) - \mu_y(1-e)(\mu_z-\lambda_0) +$$
$$\tfrac{1}{4}(1-e)\beta_{1s}(\mu_x^2-\mu_y^2) + \tfrac{1}{2}(1-e)\beta_{1_c}\mu_x\mu_y\} +$$
$$\theta_{tw}\{-\alpha_{1c}(\tfrac{1}{4} - \tfrac{1}{3}e) + \tfrac{1}{3}(1-\tfrac{3}{2}e+\tfrac{1}{2}e^3)(\beta_0'\mu_y + \beta_0\mu_x) - \tfrac{1}{2}\mu_y(\mu_z-\lambda_0)(1-e)^2 +$$
$$\tfrac{1}{8}\beta_{1s}(\mu_x^2 - \mu_y^2)(1-e)^2 + \tfrac{1}{4}\beta_{1c}\mu_x\mu_y(1-e)^2\} +$$
$$\alpha_{1c}[\tfrac{2}{3}(1-e^3)\beta_0' - (\mu_z-\lambda_0)(1-e^2) + \tfrac{3}{4}\beta_{1_c}\mu_x(1-e^2) - \tfrac{1}{4}\beta_{1_s}\mu_y(1-e^2)] +$$
$$\tfrac{1}{4}\alpha_{1_s}(1-e^2)(\beta_{1_s}\mu_x - \beta_{1_c}\mu_y) + \beta_0\mu_x[-\beta_0^{*}(1-e^2) + 2(1-e)(\mu_z-\lambda_0) - \tfrac{3}{2}\beta_{1_c}\mu_x(1-e) +$$
$$\beta_{1_s}\mu_y(1-e)] - \tfrac{1}{2}\beta_0\beta_{1c}\mu_y^2(1-e) + \frac{\delta}{a_0}(1-e^2)\mu_y$$

Figure A1.6 : Expressions for Zeroth and Harmonic Components of the Force Coefficients C_{YA}, C_{ZA}, (Continued).

$$C_{Z_{A_0}} = -\frac{1}{3}\beta_0'(1-e^3) + \frac{1}{2}(1-e^2)(\mu_z - \lambda_0) + \frac{1}{4}(1-e^2)[\mu_x(\alpha_{1_s} - \beta_{1_c}) + \mu_y(\alpha_{1_c} + \beta_{1_s})] + \frac{1}{2}(1-e^2)(\theta_{1_c}\mu_y + \theta_{1_s}\mu_x) + [\frac{1}{3}(1-e^3) + \frac{1}{2}(1-e)\mu^2]\theta_0 + [\frac{1}{4}\{1+\mu^2(1-e)^2\} - \frac{1}{3}e]\theta_{tw}$$

$$C_{Z_{A_{1c}}} = \frac{1}{3}\alpha_{1c}(1-e^3) + \mu_y(1-e)(\mu_z - \lambda_0) - \frac{1}{2}(1-e^2)(\beta_0'\mu_y + \beta_0\mu_x) - \frac{1}{4}(1-e)\beta_{1_s}(\mu_x^2 - \mu_y^2) + \frac{1}{2}(1-e)(\theta_{1_s} - \beta_{1_c})\mu_x\mu_y + [\frac{1}{3}(1-e^3) + (1-e)(\frac{1}{4}\mu^2 + \frac{1}{2}\mu_y^2)]\theta_{1_c} + \mu_y(1-e^2)\theta_0 + \mu_y(\frac{2}{3} - e + \frac{1}{3}e^3)\theta_{tw}$$

$$C_{Z_{A_{1s}}} = \frac{1}{3}\alpha_{1s}(1-e^3) + \mu_x(1-e)(\mu_z - \lambda_0) - \frac{1}{2}(1-e^2)(\beta_0'\mu_x - \beta_0\mu_y) - \frac{1}{4}(1-e)\beta_{1_c}(\mu_x^2 - \mu_y^2) + \frac{1}{2}(1-e)(\theta_{1_c} + \beta_{1_s})\mu_x\mu_y + [\frac{1}{3}(1-e^3) + (1-e)(\frac{1}{4}\mu^2 + \frac{1}{2}\mu_x^2)]\theta_{1_s} + \mu_x(1-e^2)\theta_0 + \mu_x(\frac{2}{3} - e + \frac{1}{3}e^3)\theta_{tw}$$

Figure A1.6 : Expressions for Zeroth and Harmonic Components of the Force Coefficients C_{YA}, C_{ZA}, (Reproduced Courtesy of Thomson (1992))

b body axes set

trh tail rotor hub axes set (fixed in hub)

trbl tail rotor blade axes set (fixed in blade, origin at root, rotates with blade)

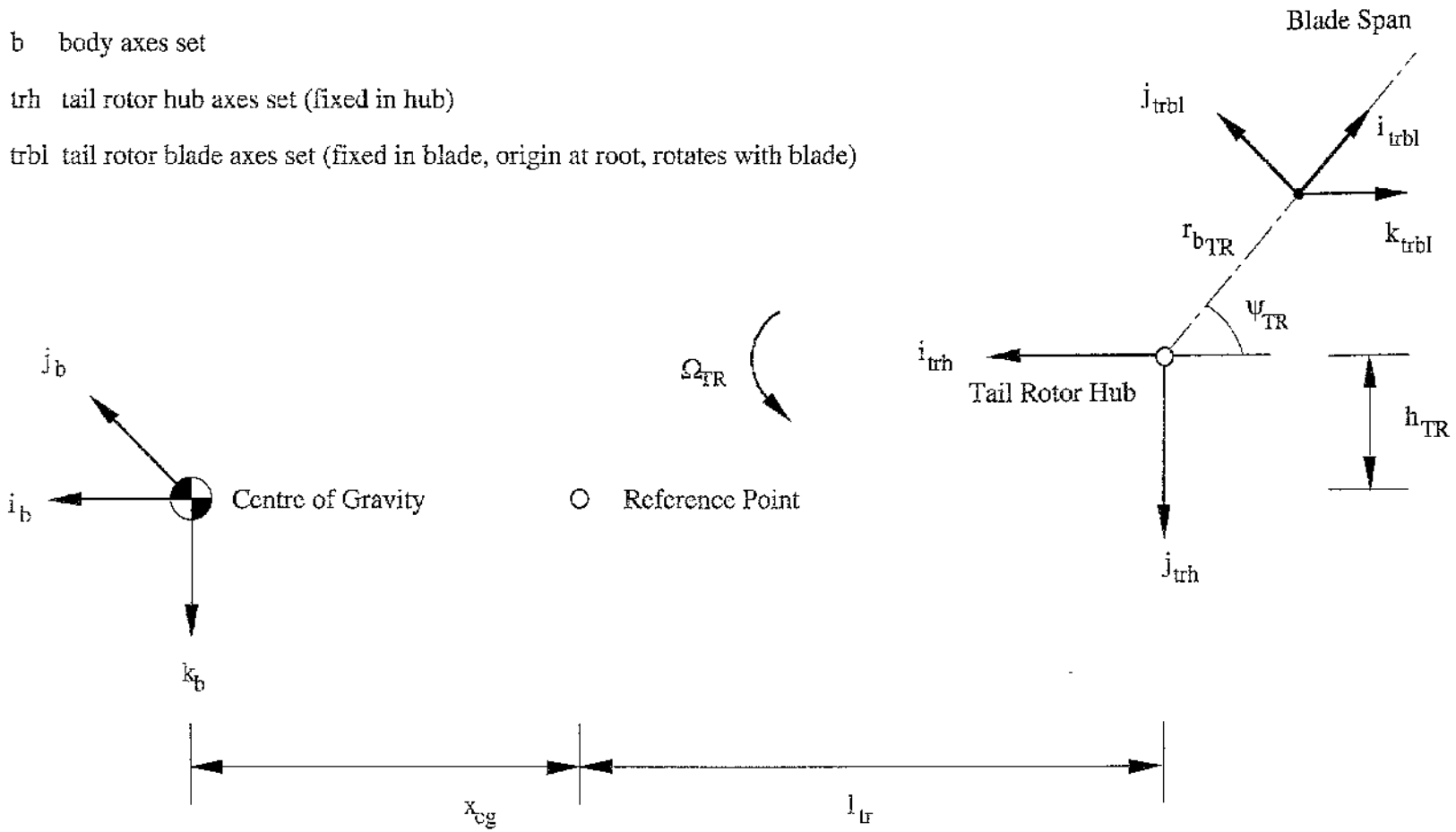

Figure A1.7 : Axes Set For Tail Rotor Blade Kinematics

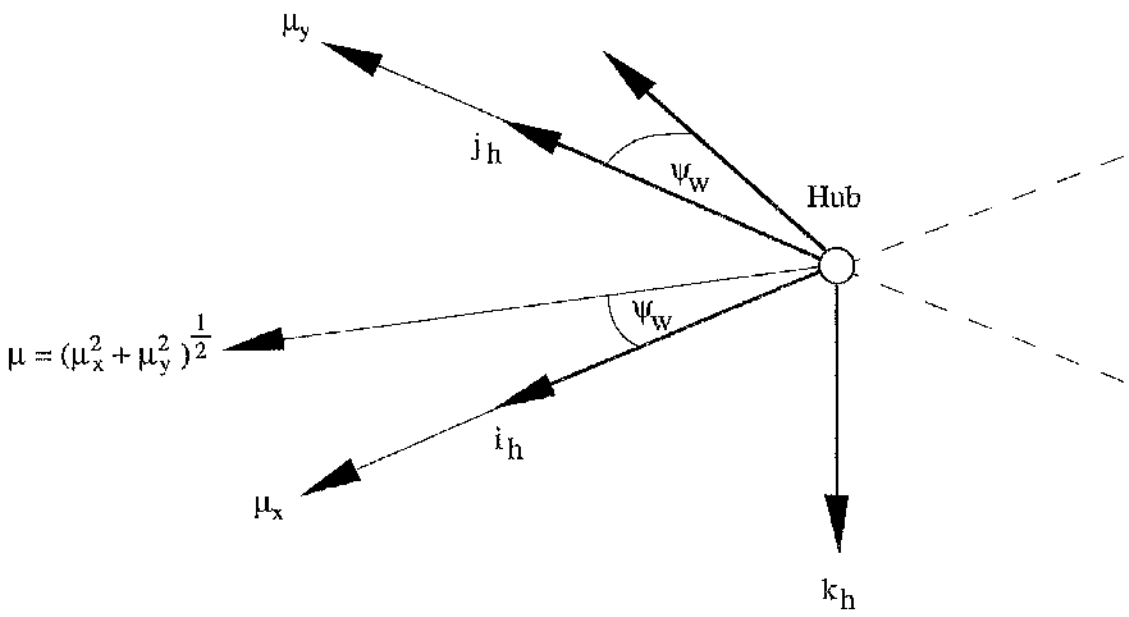

Figure A1.8 : Rotor Side Slip Angle

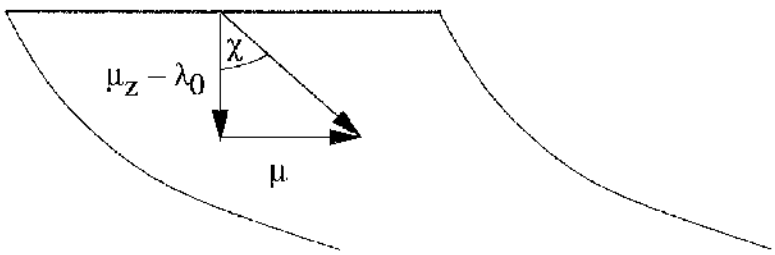

Figure A1.9 : Rotor Wake Angle

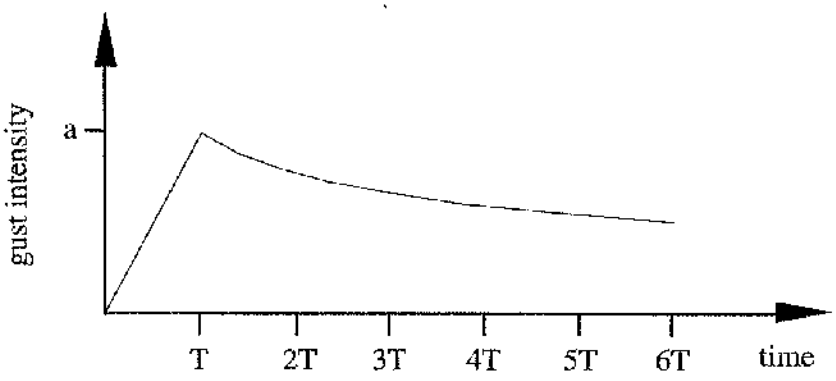

Figure A5.0a - Ramp Gust

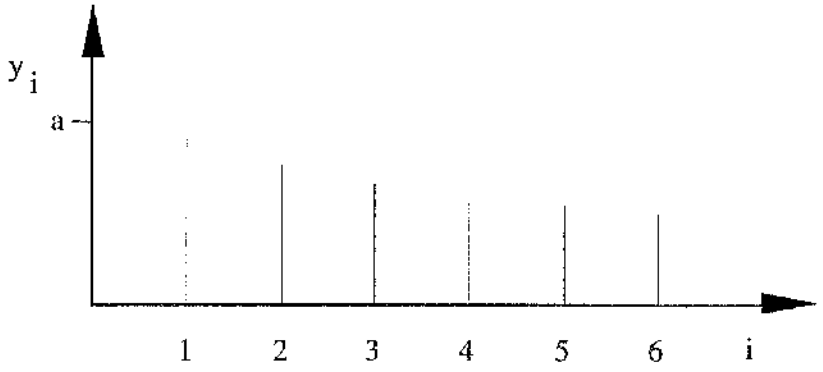

Figure A5.0b - The Sequence y_i

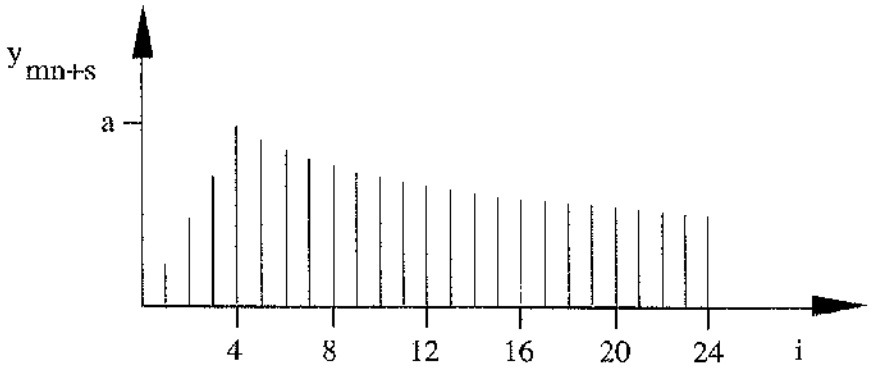

Figure A5.0c - The Sequence y_i, (m = 4)

Figure A5.0 - Formulation of Gust

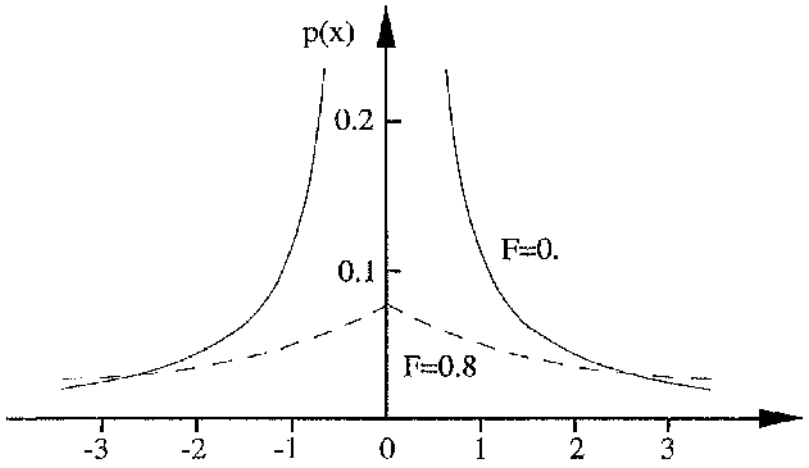

Figure A5.1 - Probability Density Distribution

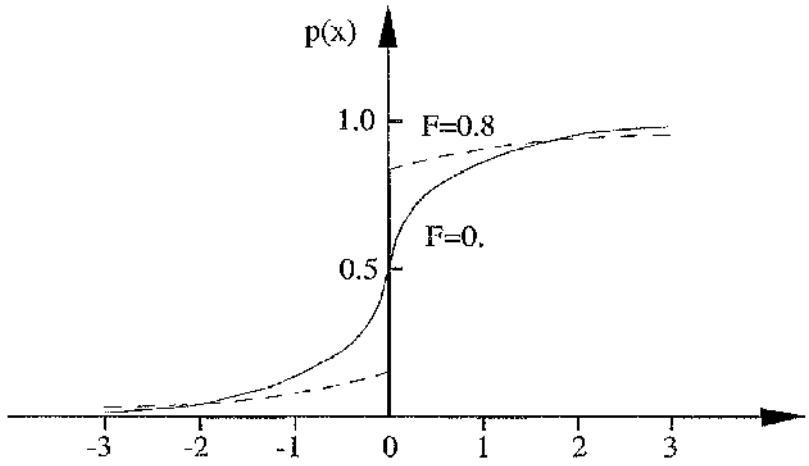

Figure A5.2 - The Cumulative Distribution

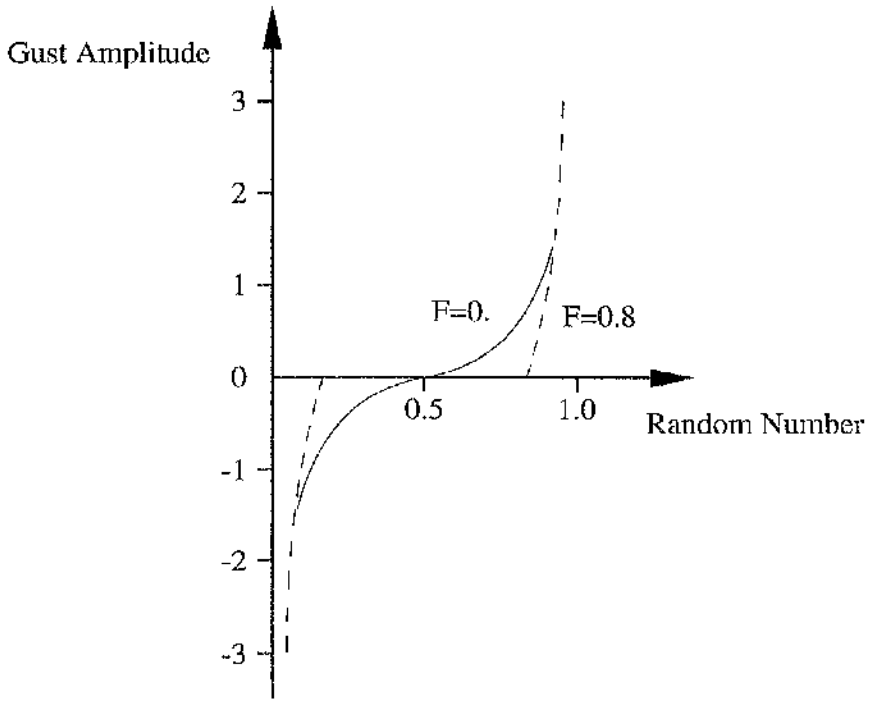

Figure A5.3 - Gust Amplitude Distribution (Inverse Cumulative Distribution)

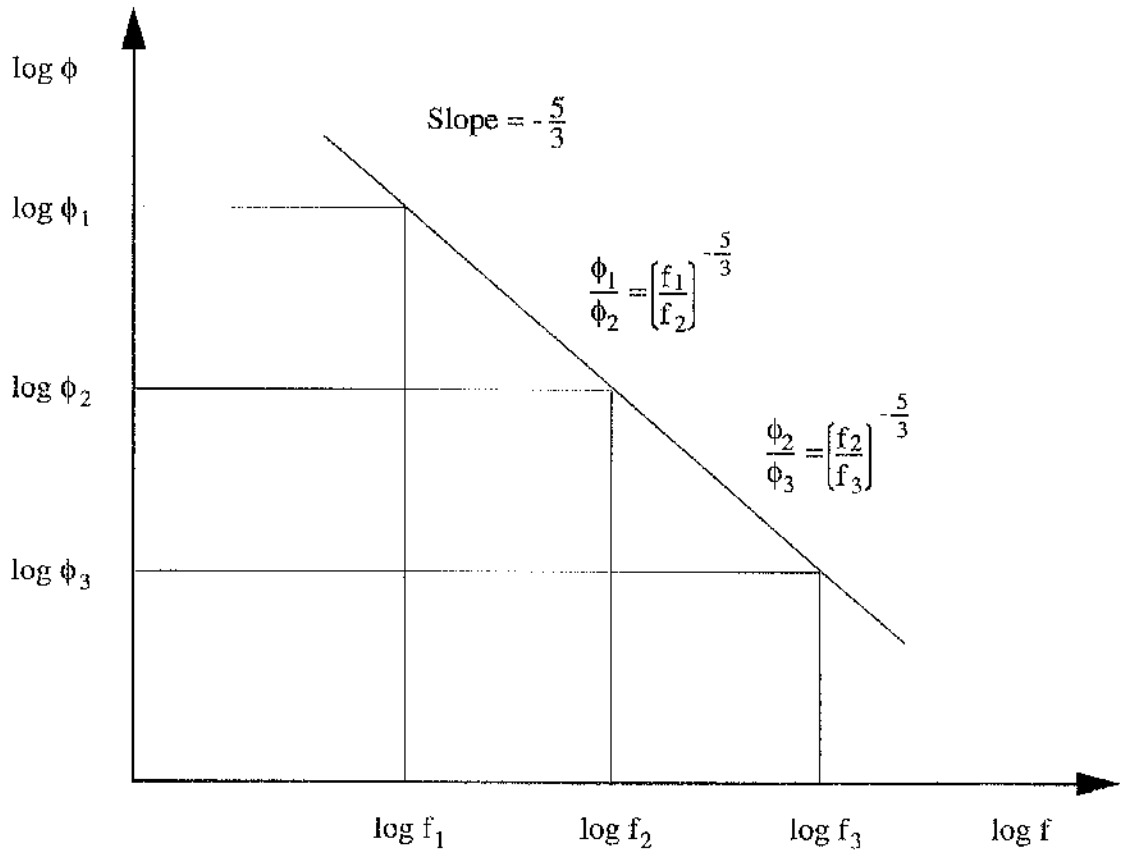

Figure A5.5 - Combination of Three Channels

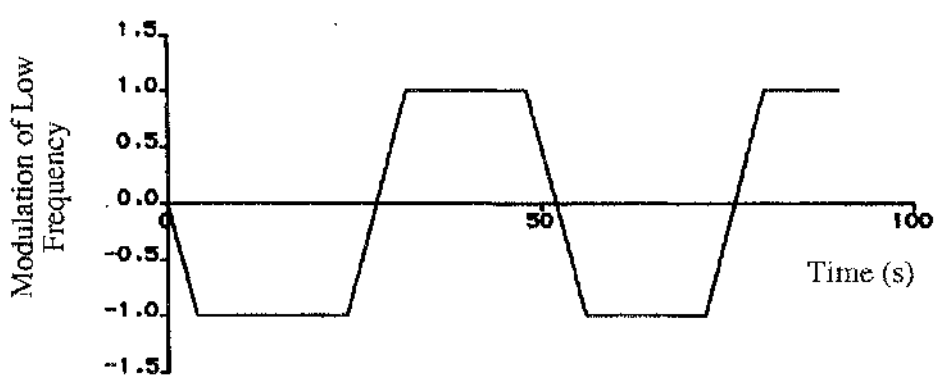

Figure A5.6a : Low Frequency Stream

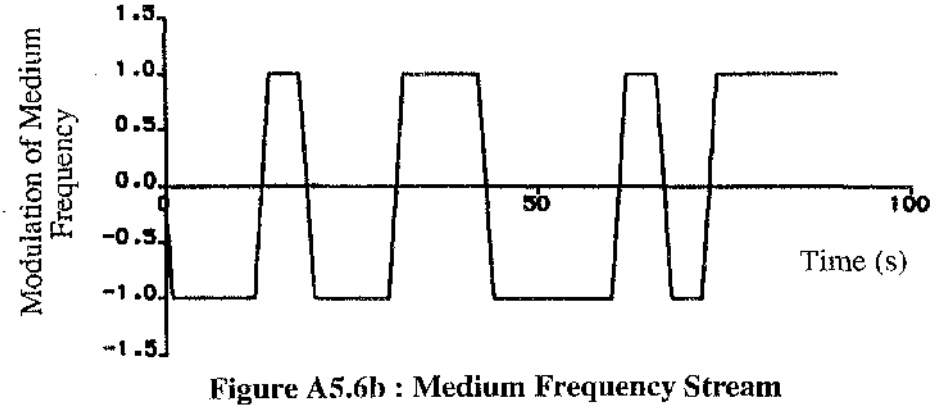

Figure A5.6b : Medium Frequency Stream

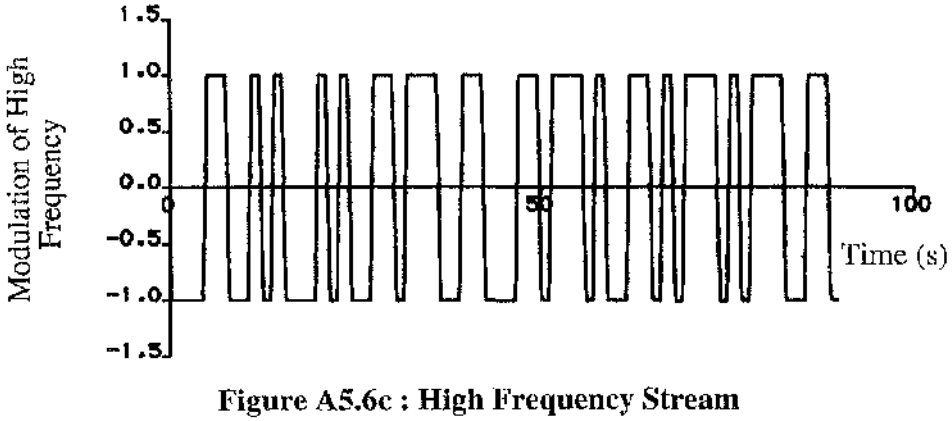

Figure A5.6c : High Frequency Stream

Figure A5.6 : Decorrelation Functions Employed In Generation of Turbulent Stream

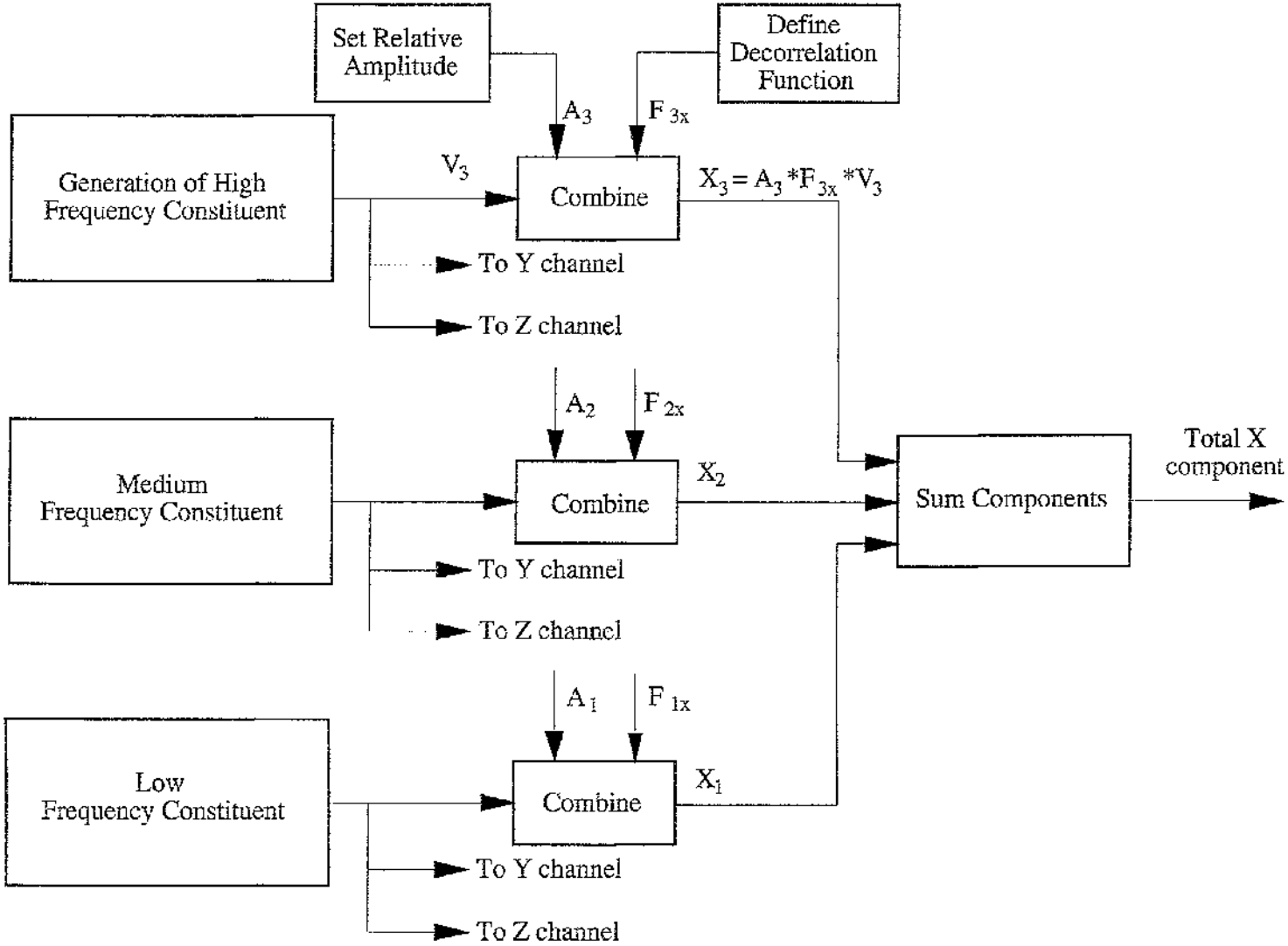

Figure A5.7 - Overall Formulation of Gust

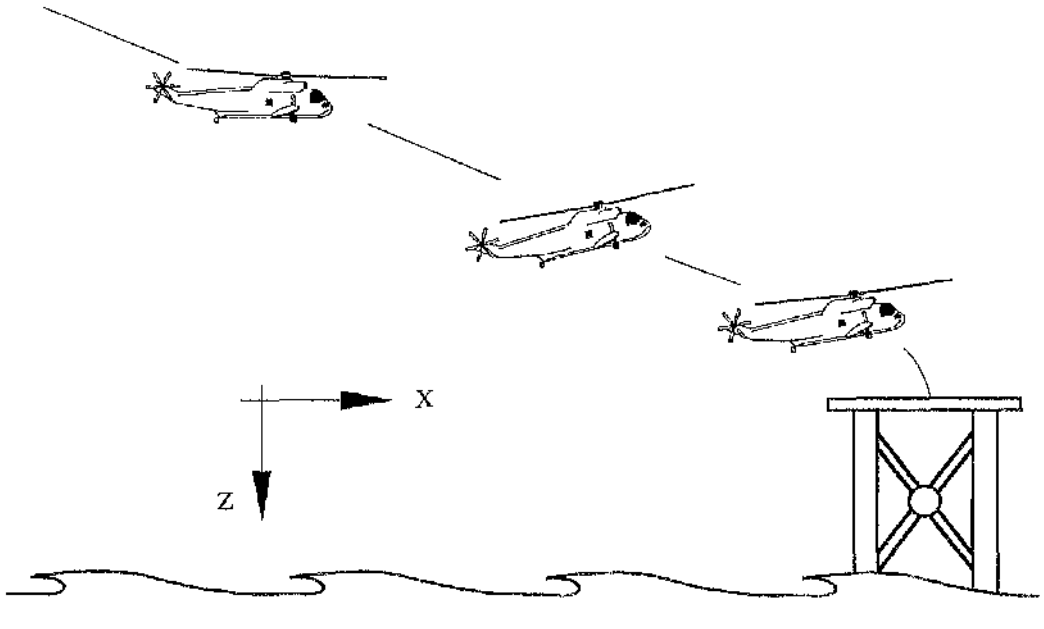

Figure A6.0 : Normal Approach and Landing

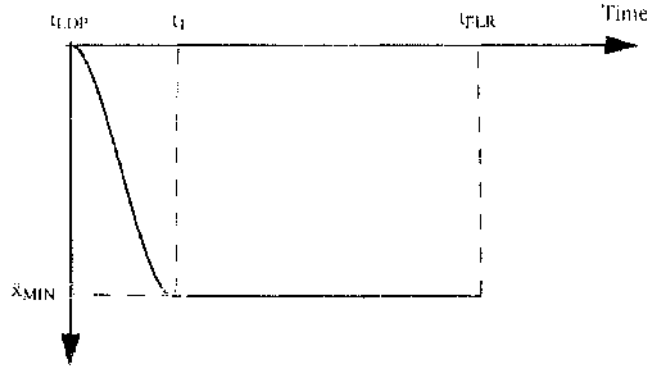

Figure A6.1a : Longitudinal Acceleration

Figure A6.1b : Descent Angle

Figure A6.1 : Trajectory Information Employed During Normal Approach and Landing

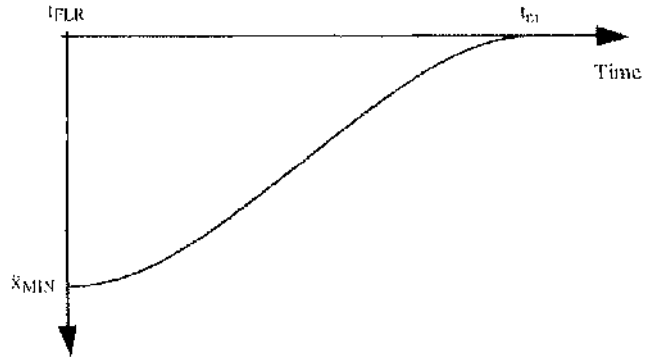

Figure A6.1c : Foward Acceleration

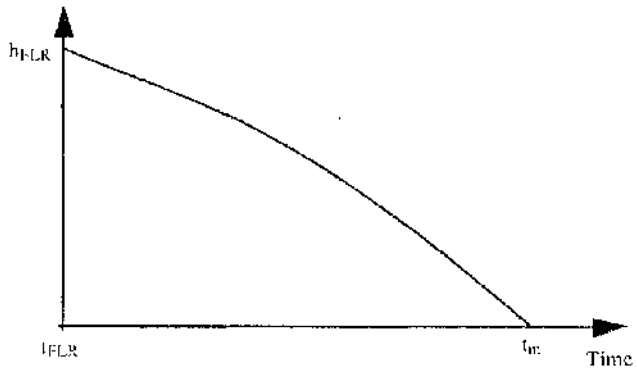

Figure A6.1d : Altitude

Figure A6.1 : Trajectory Information Employed During Normal Approach and Landing (Continued)

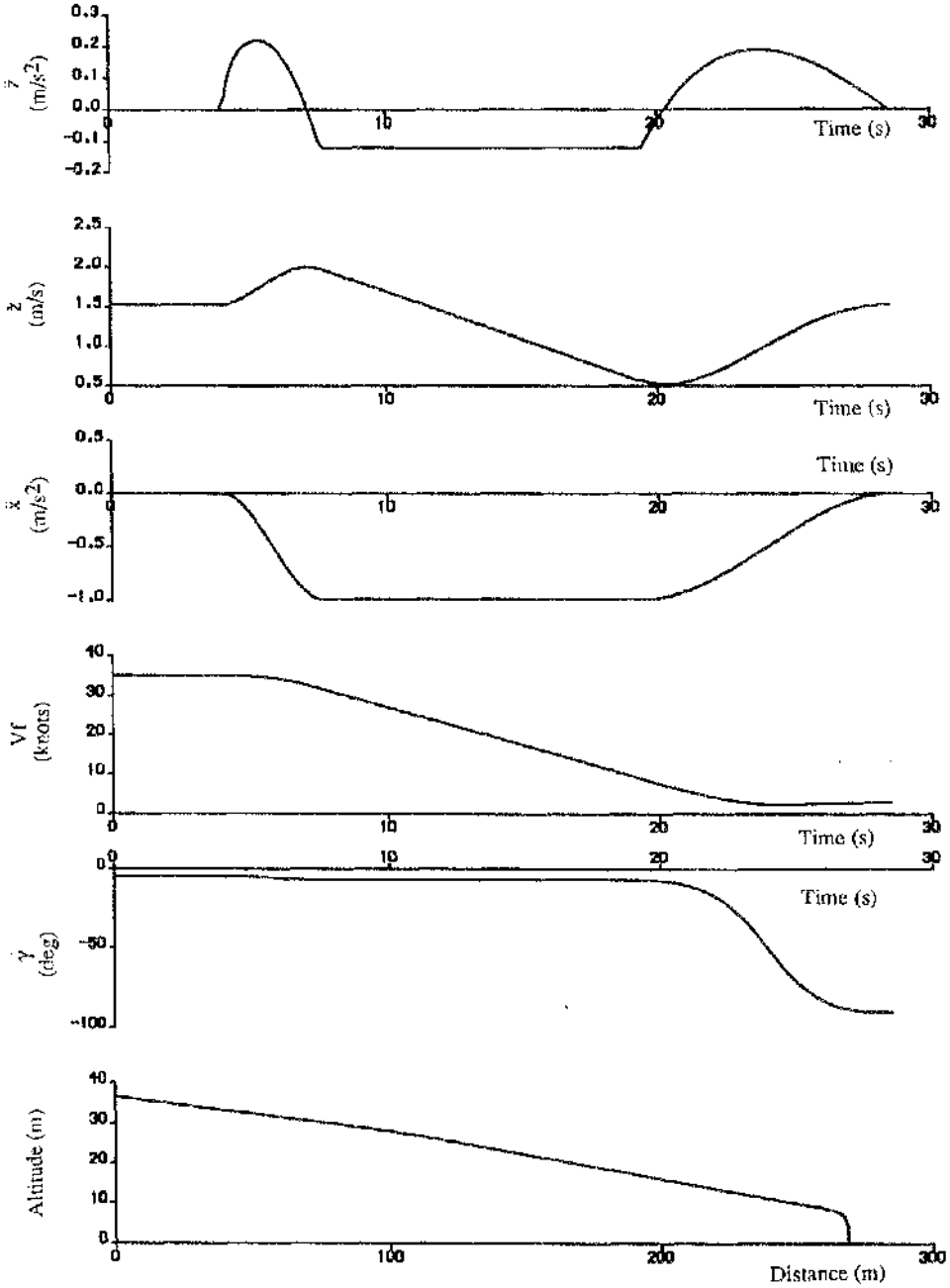

Figure A6.2 : Flight Path Information Calculated For Normal Approach and Landing

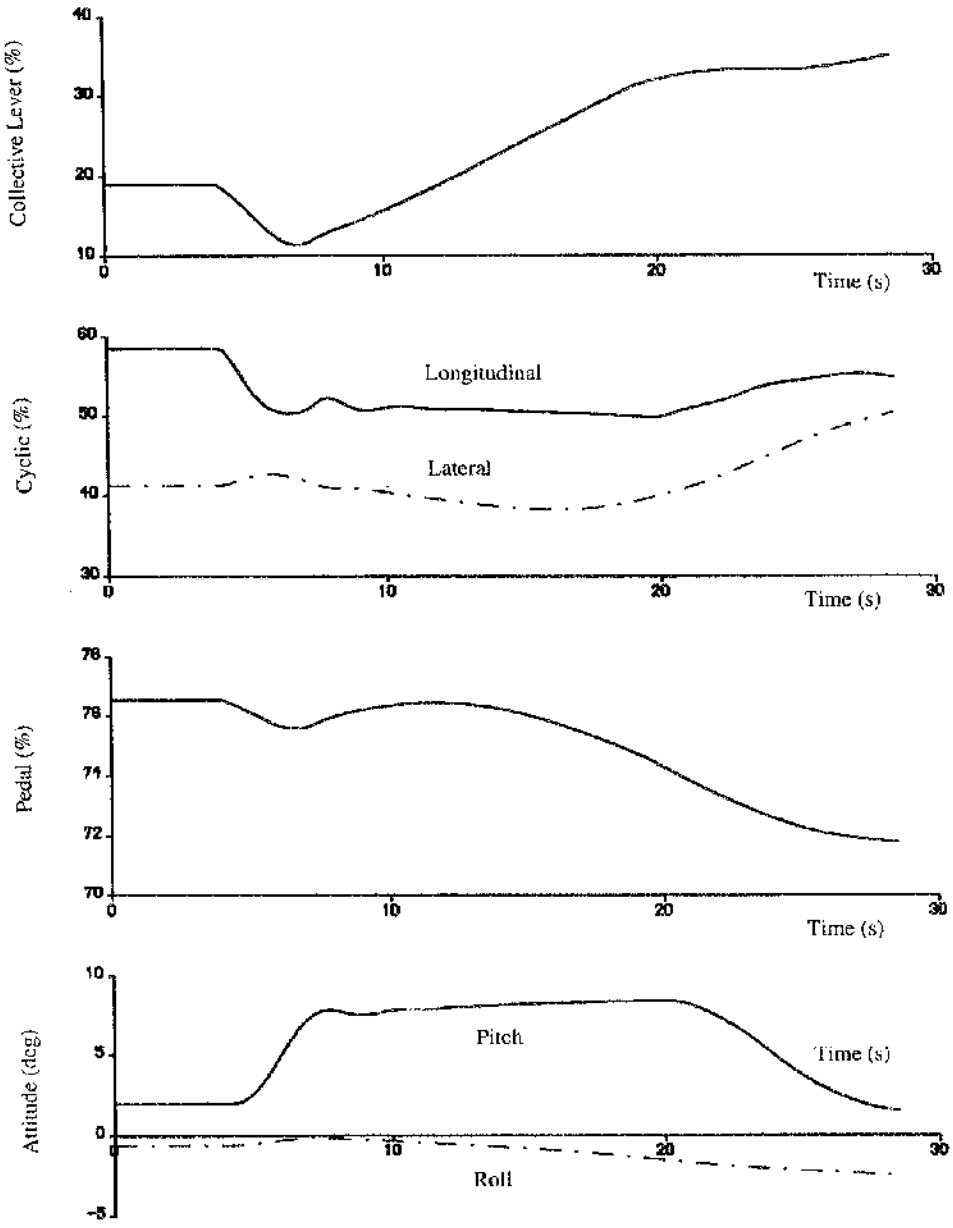

Figure A6.3 : Inverse Simulation of Normal Approach and Landing

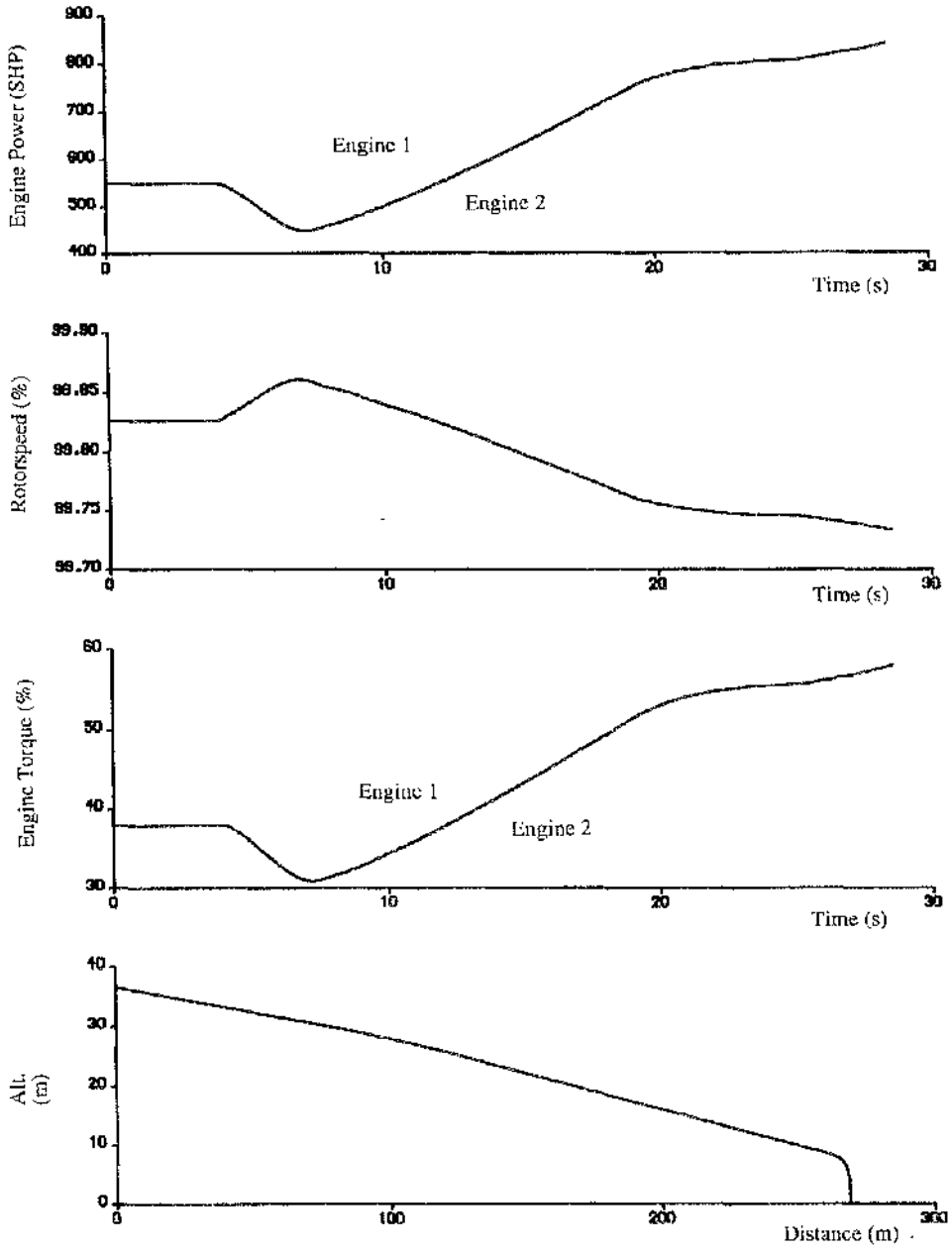

Figure A6.3 : Inverse Simulation of Normal Approach and Landing (Continued)

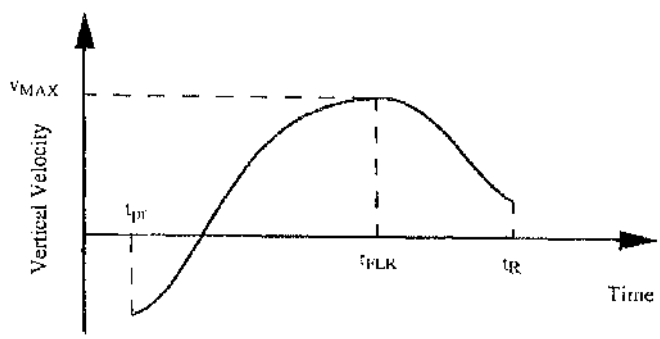

Figure A7.0 : Vertical Velocity Information for Vertical Reject Manoeuvre

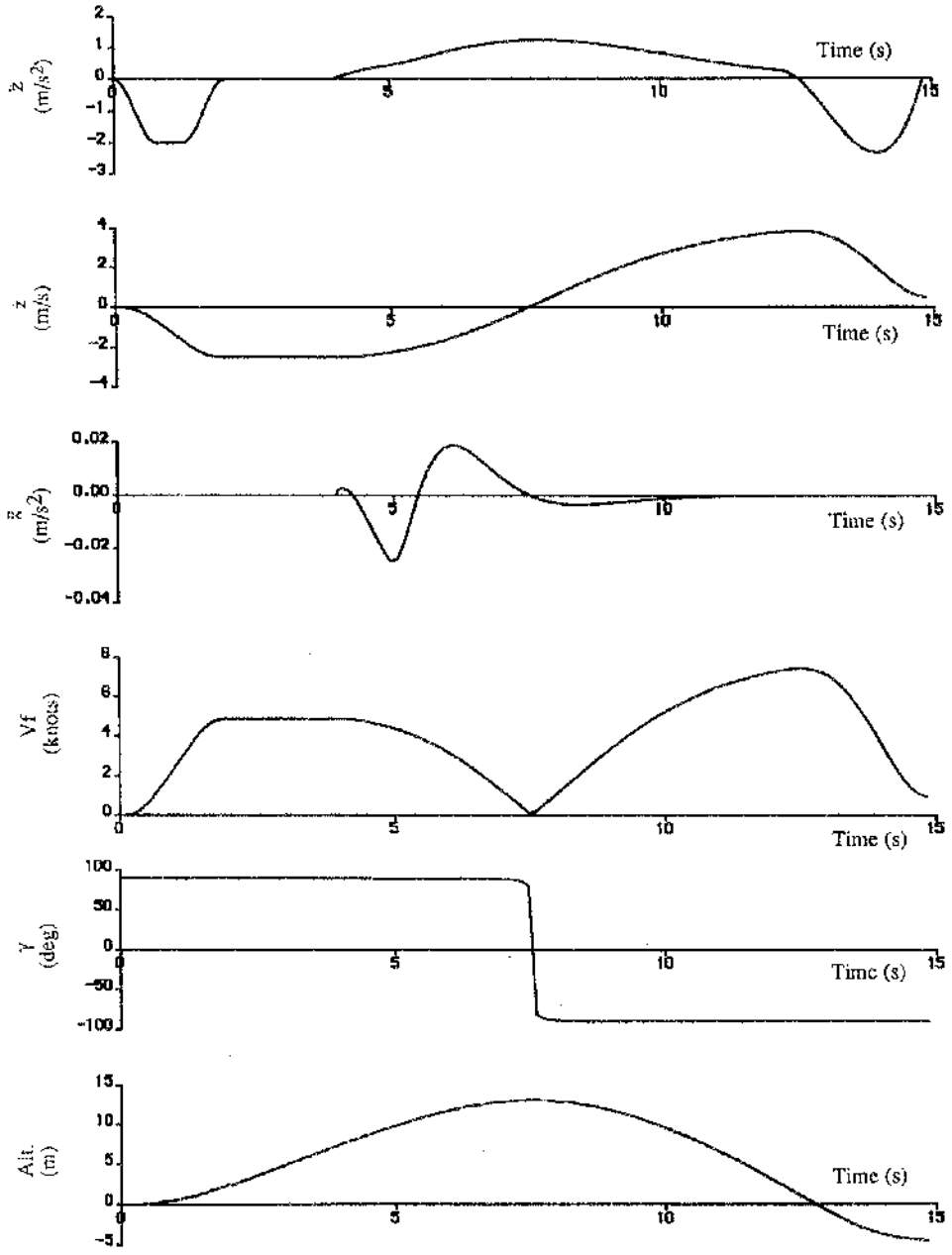

Figure A7.1 : Flight Path Information for Engine Failure Prior To TDP During Towering Takeoff

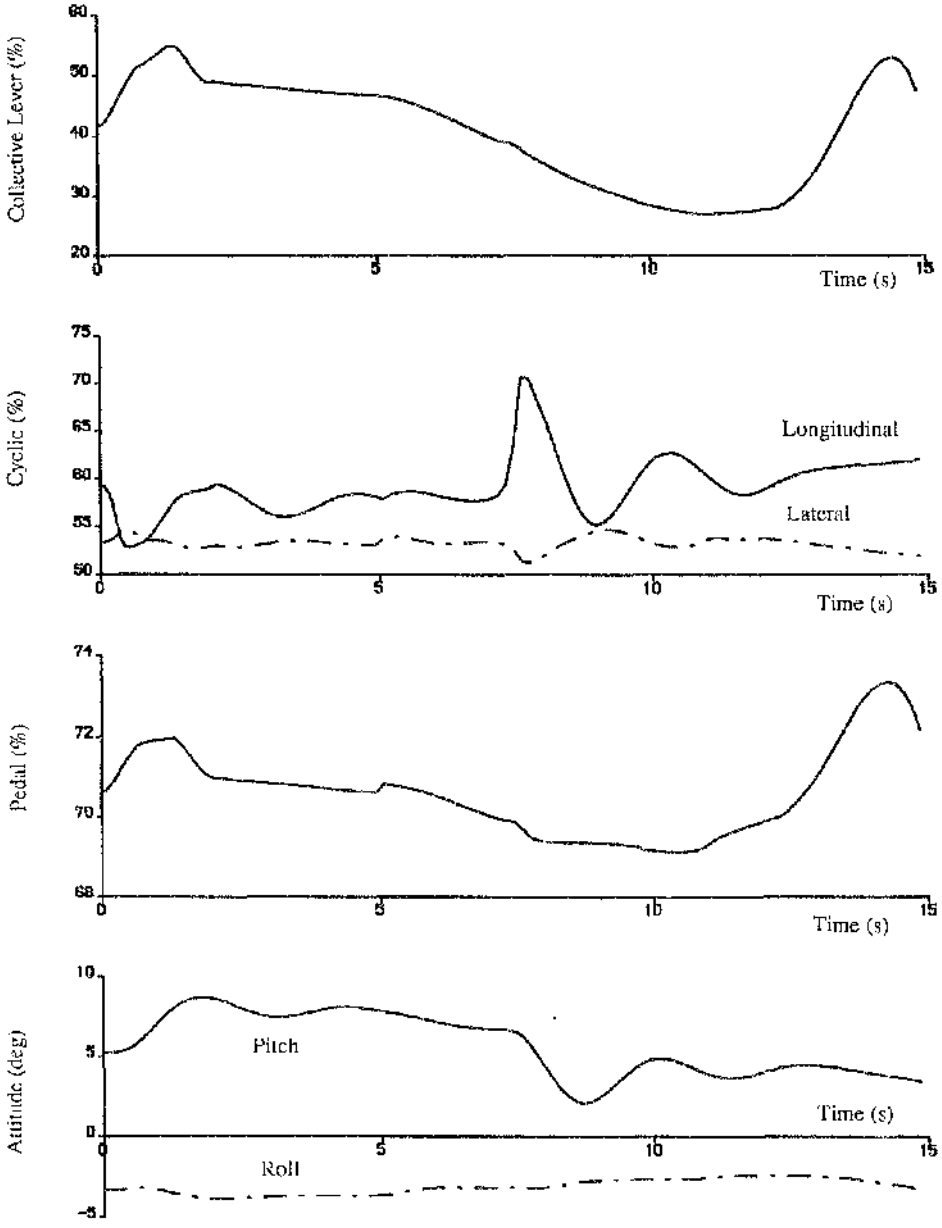

Figure A7.2 : Inverse Simulation of Engine Failure Prior to TDP During Towering Takeoff

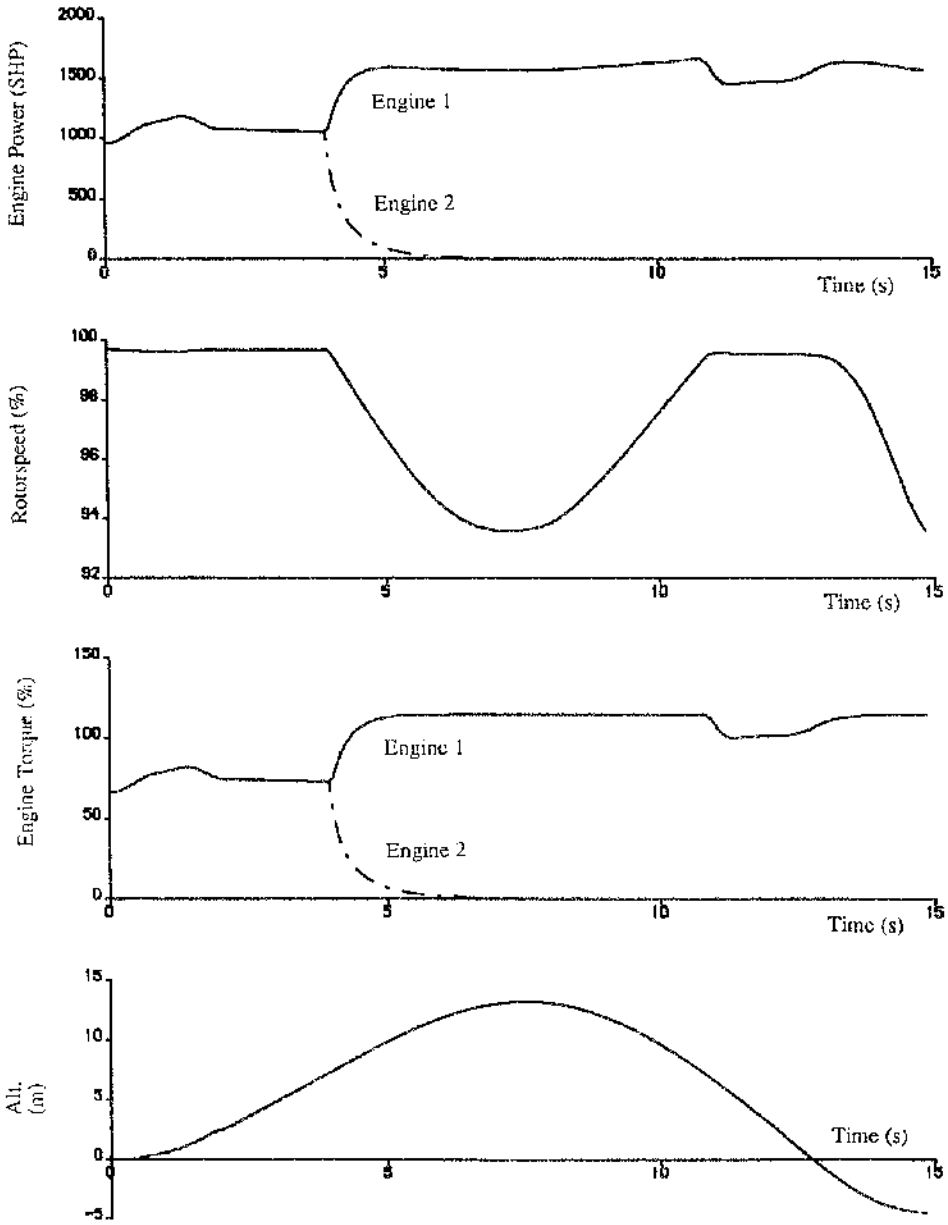

Figure A7.2 : Inverse Simulation of Engine Failure Prior to TDP During Towering Takeoff (Continued)

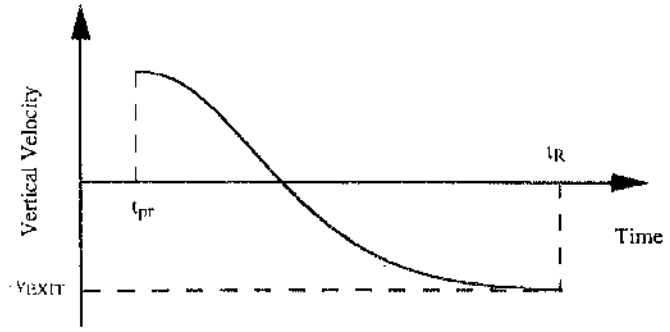

Figure A7.3a : Vertical Velocity

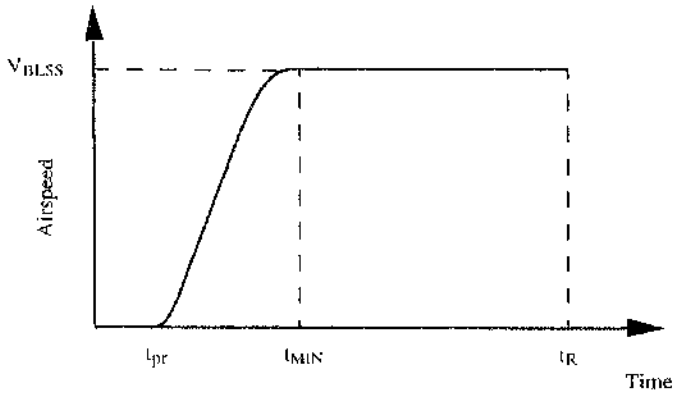

Figure A7.3b : Airspeed

Figure A7.3 : Trajectory Information For Engine Failure Prior to LDP

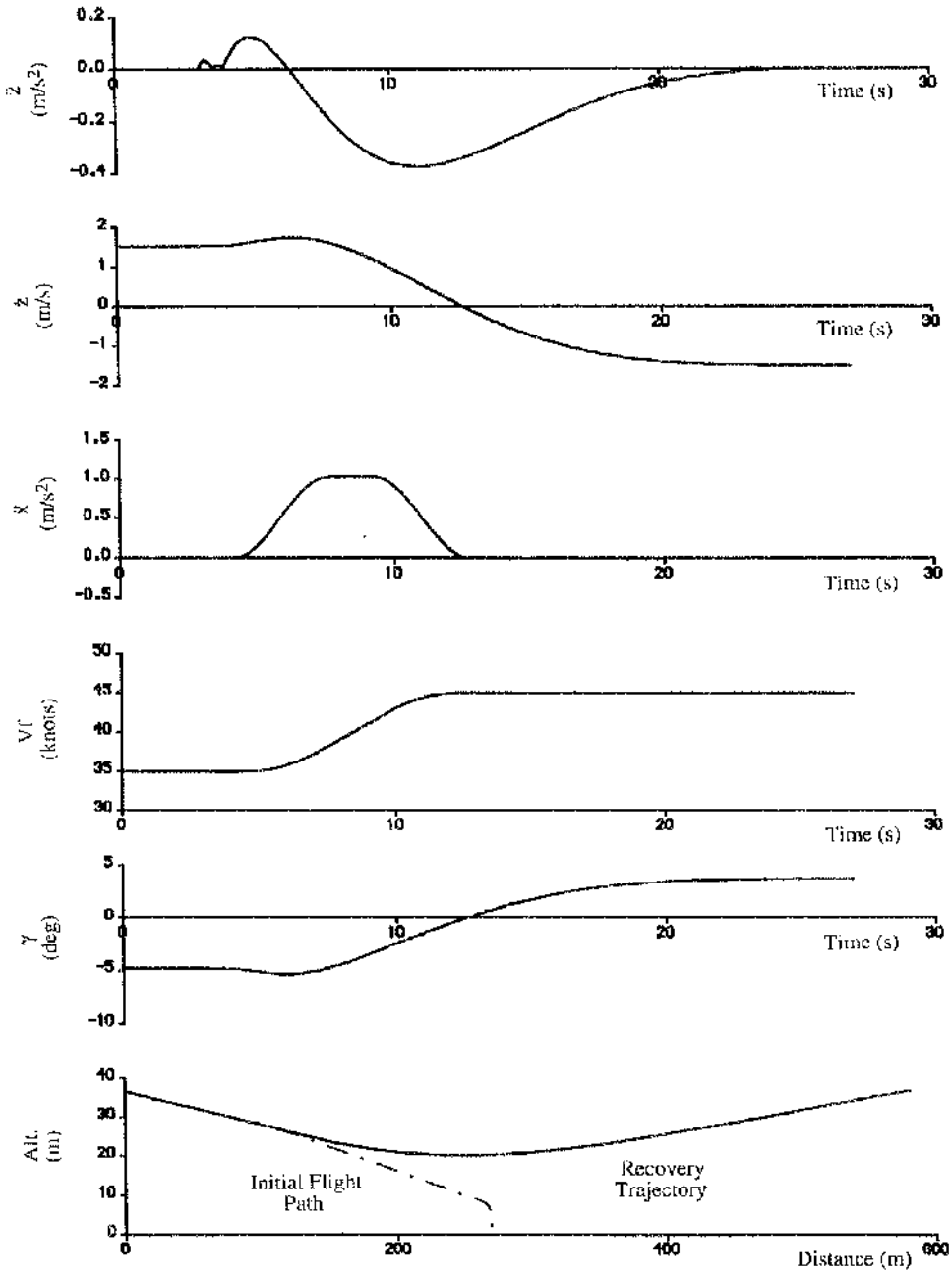

Figure A7.4: Flight Path Information for Engine Failure Prior To LDP During Normal Approach and Landing

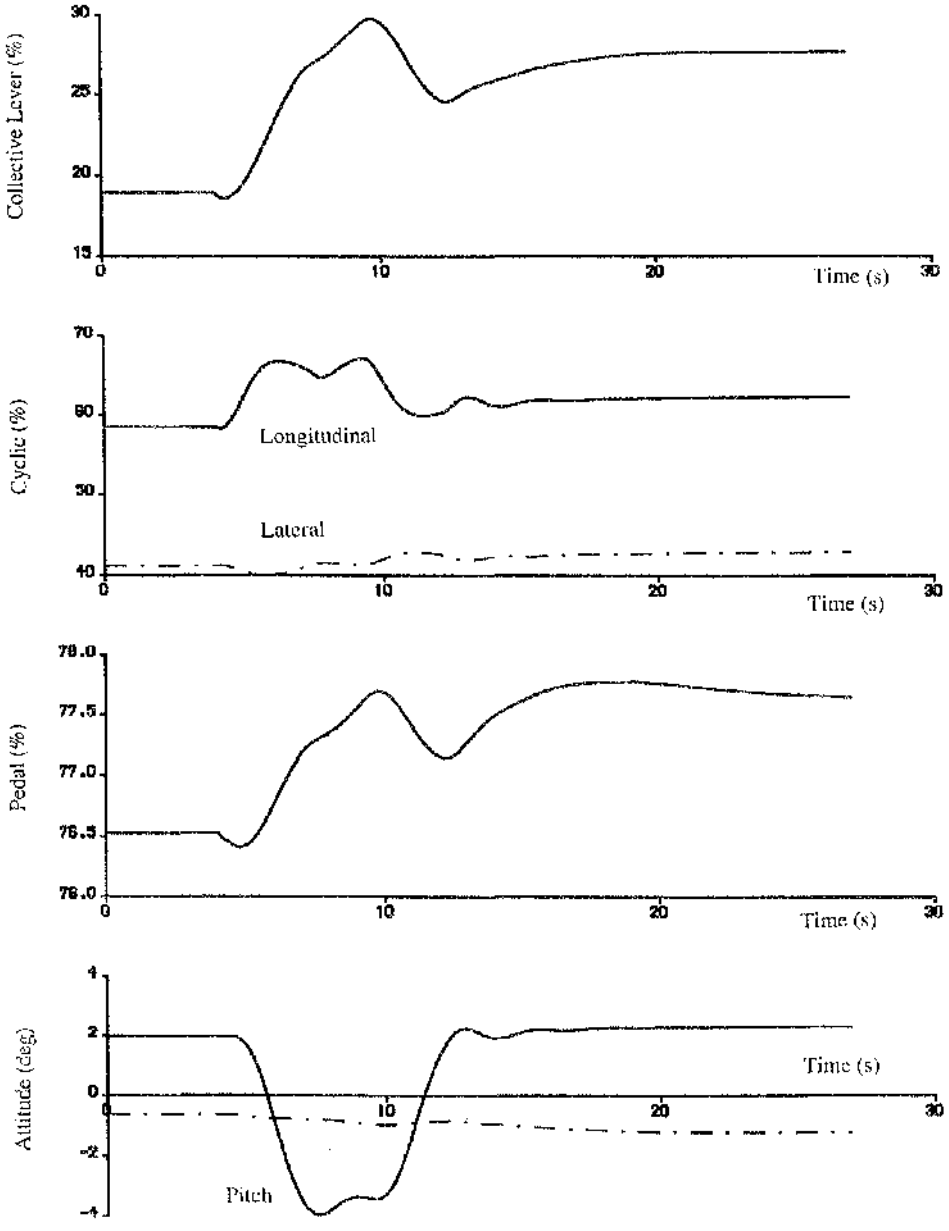

Figure A7.5 : Inverse Simulation of Engine Failure Prior to LDP During Normal Approach and Landing

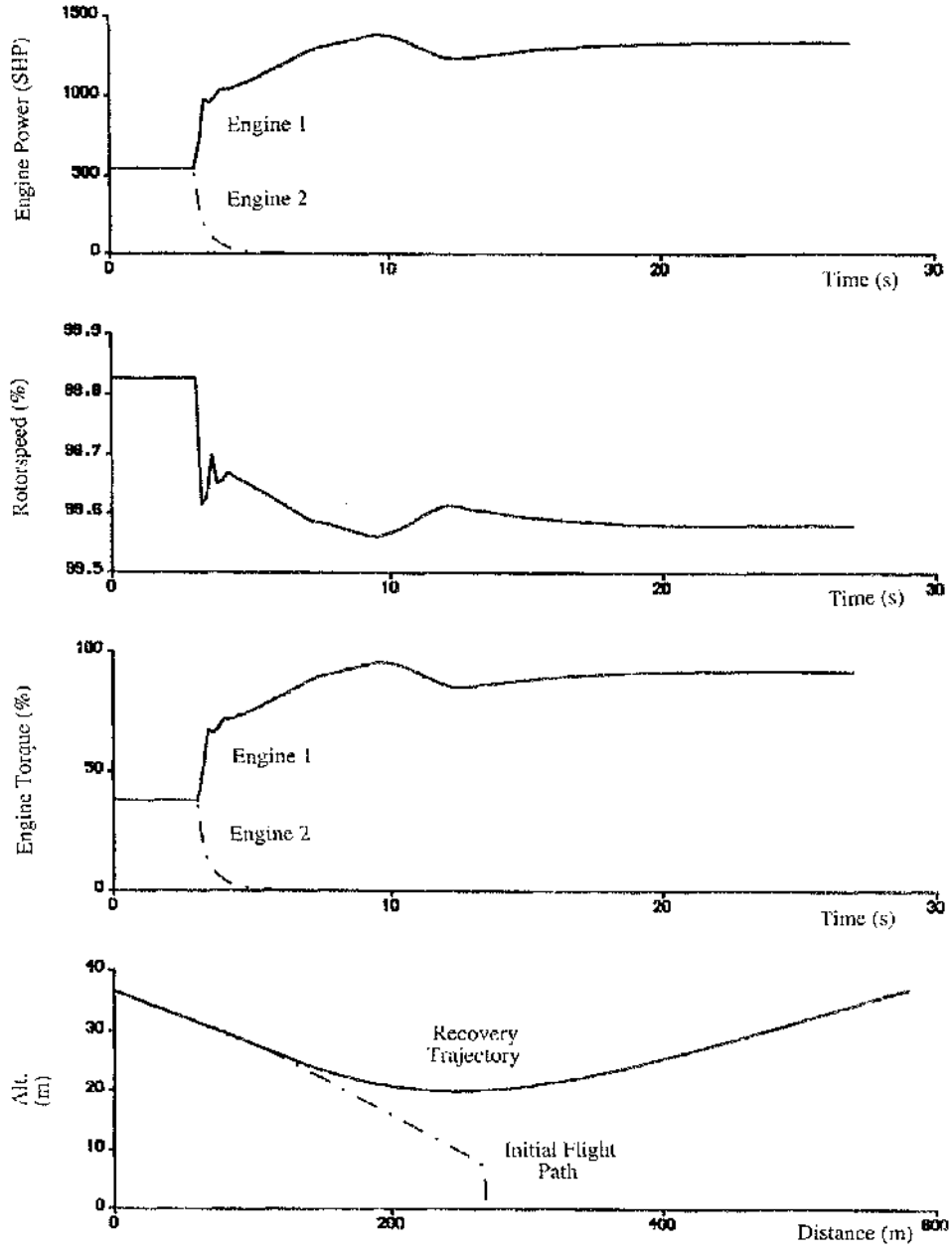

Figure A7.5 : Inverse Simulation of Engine Failure Prior to LDP During Normal Approach and Landing (Continued)

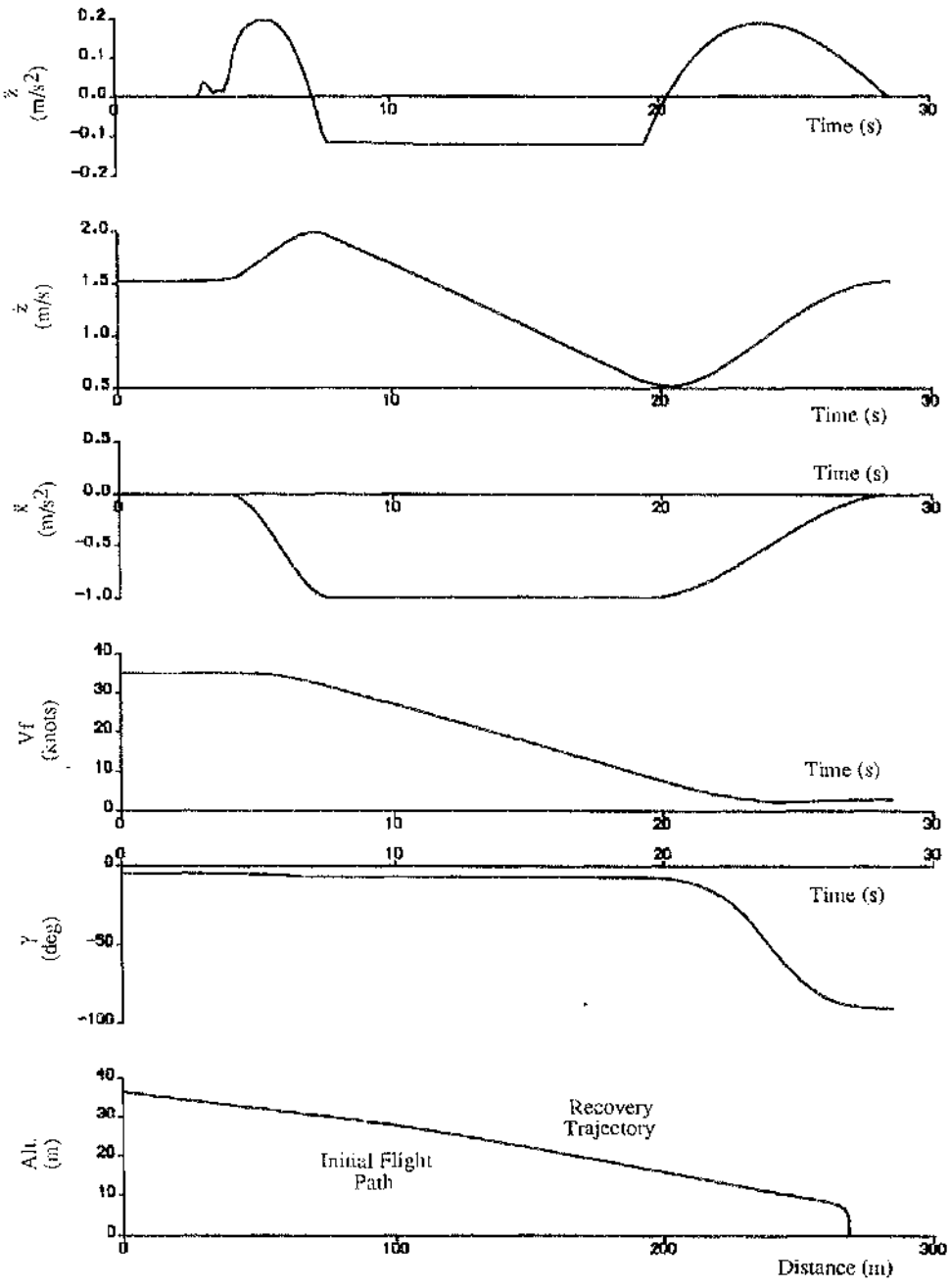

Figure A7.6 : Flight Path Information for Engine Failure After LDP During Normal Approach And Landing

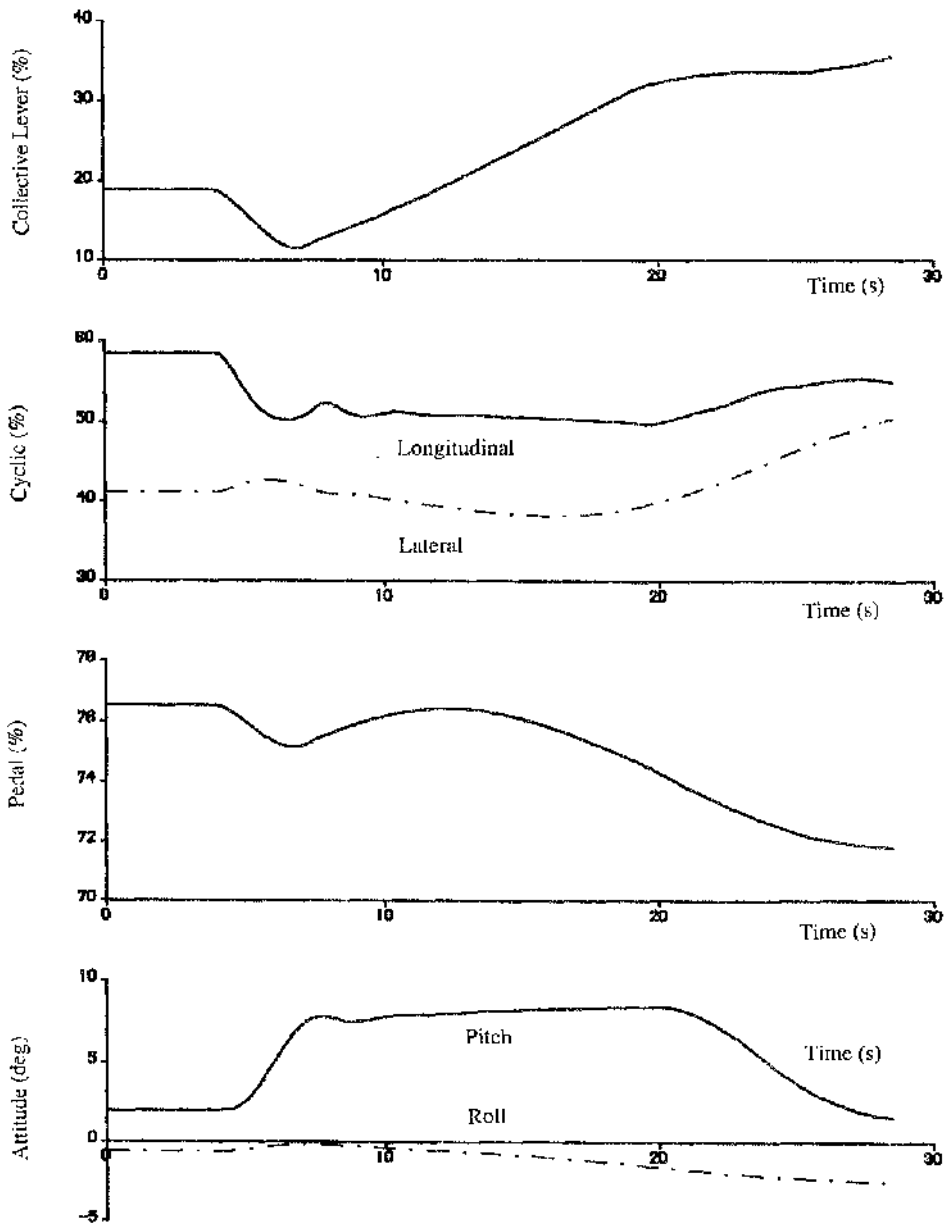

Figure A7.7 : Inverse Simulation of Engine Failure After LDP During Normal Approach and Landing

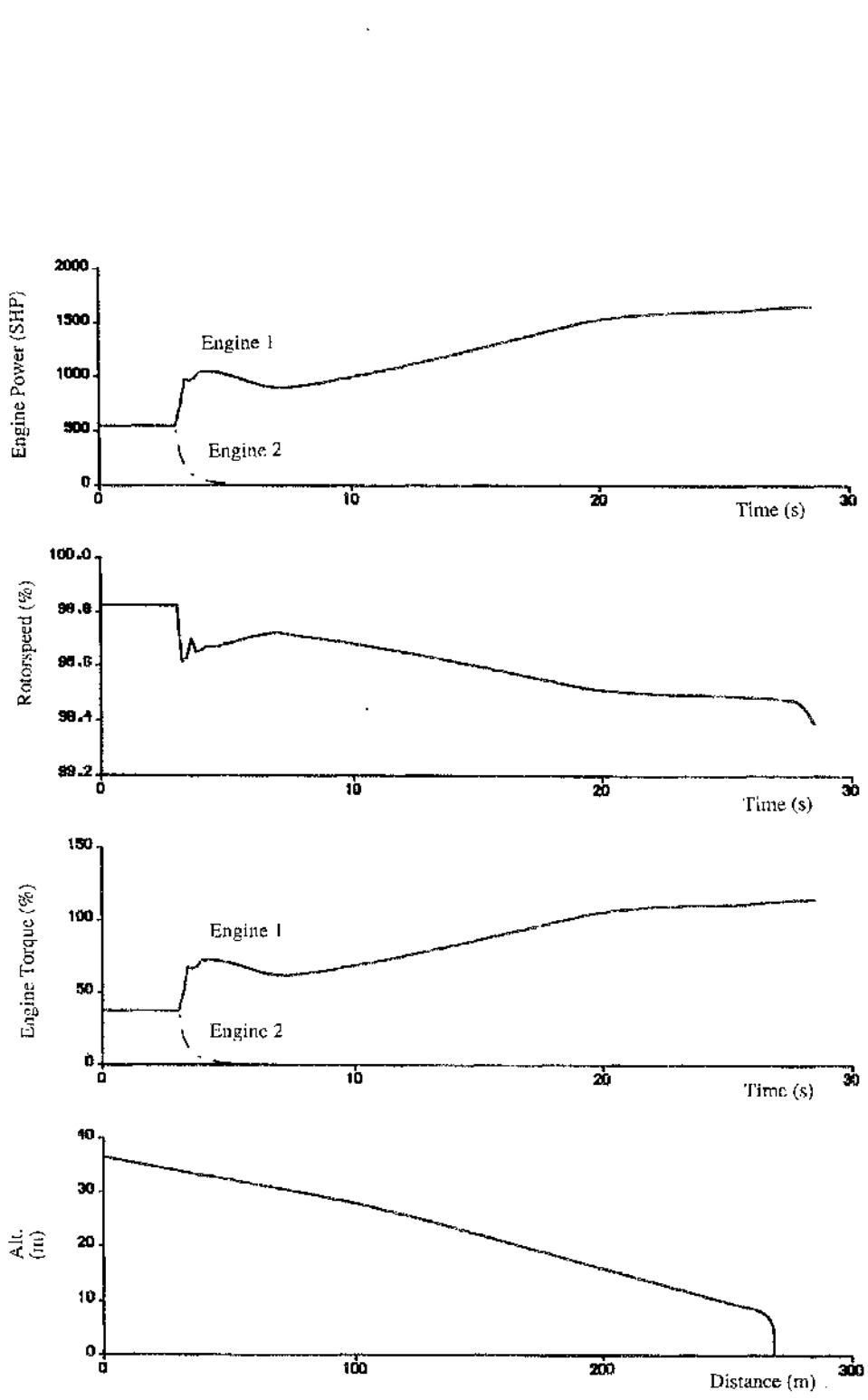

Figure A7.7 : Inverse Simulation of Engine Failure After LDP During Normal Approach and Landing (Continued)

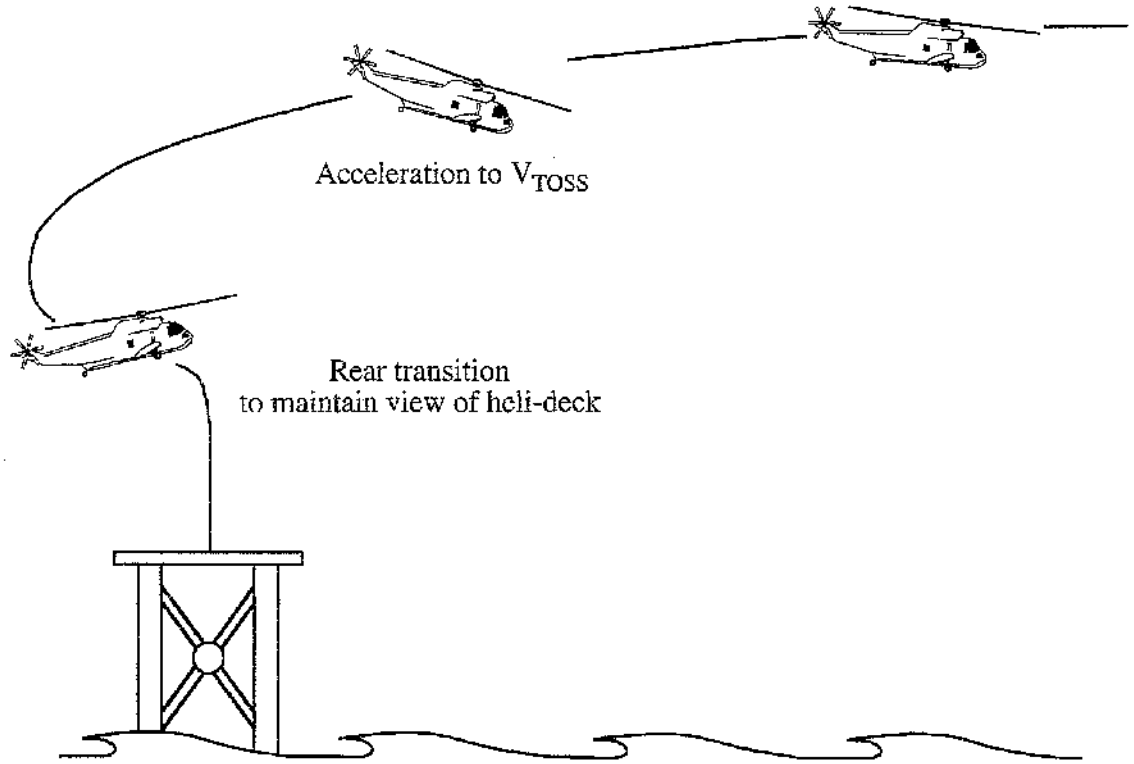

Figure A8.0 : Vertical Backup Takeoff Technique

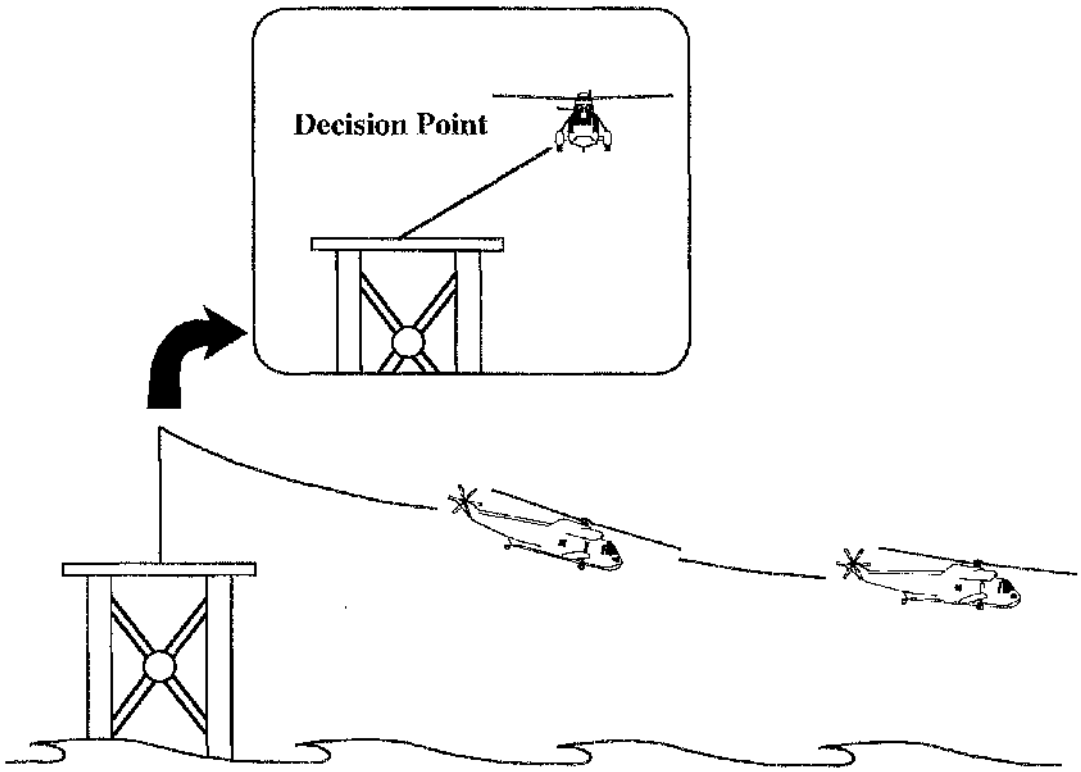

Figure A8.1 : Static Offset Takeoff Technique

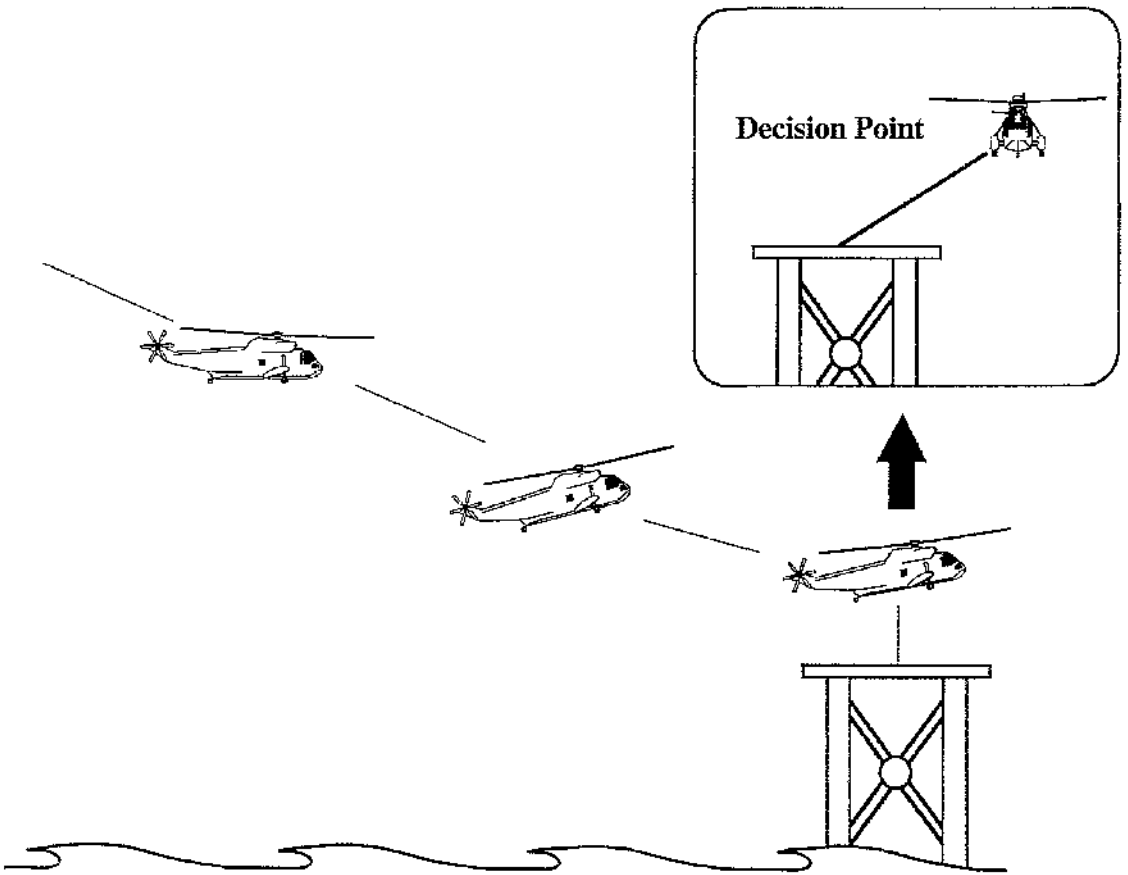

Figure A8.2 : Static Offset Landing Manoeuvre

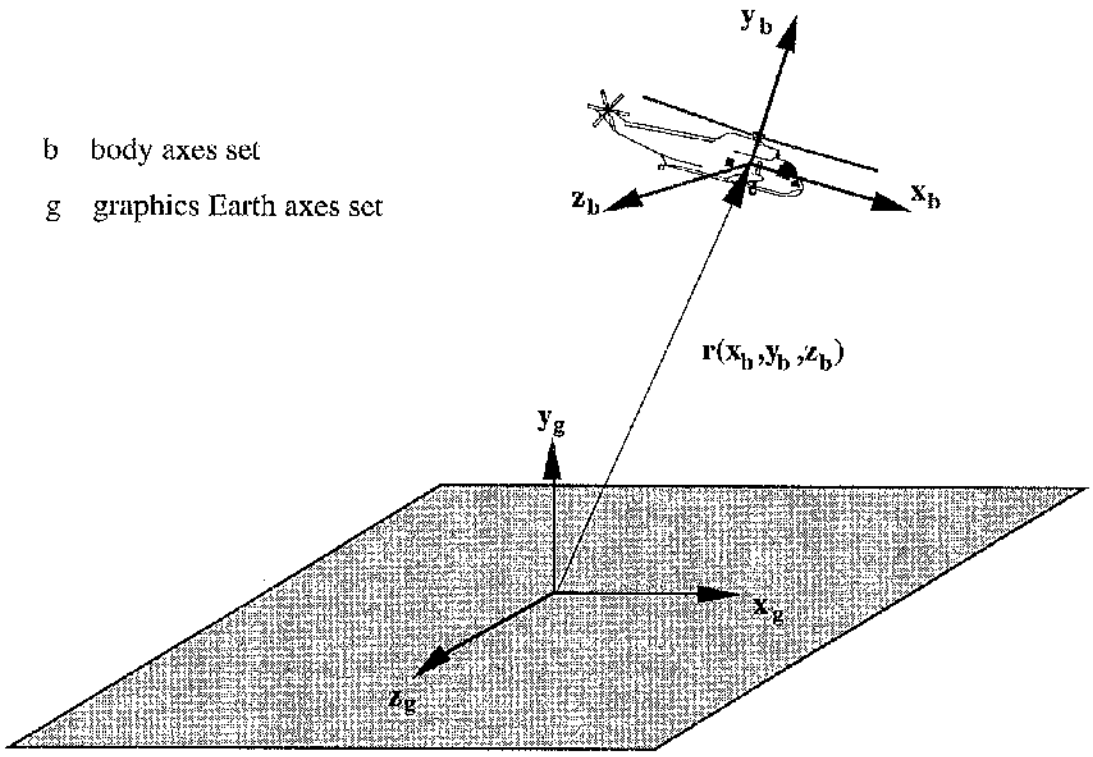

Figure A9.0 : Location of Helicopter In Computer Earth Axes Set

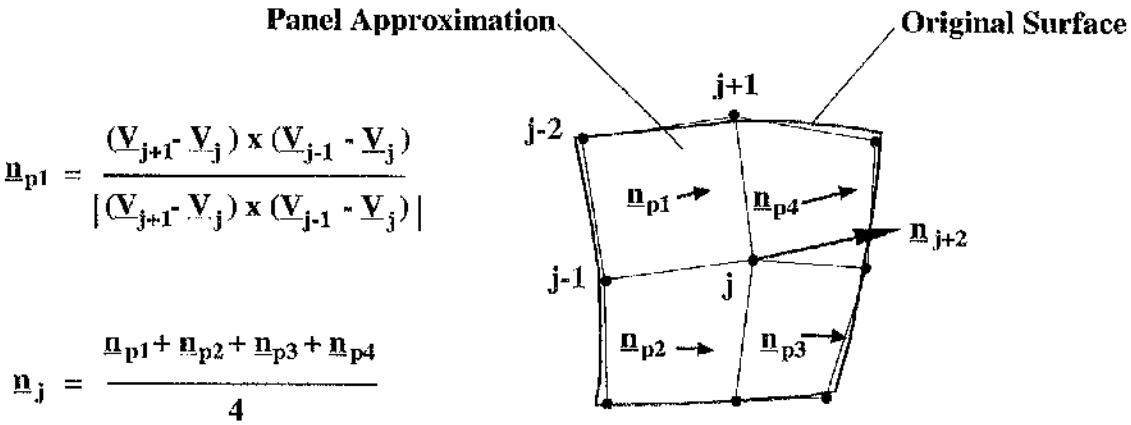

Figure A9.1 : Three Dimensional Panel Generation

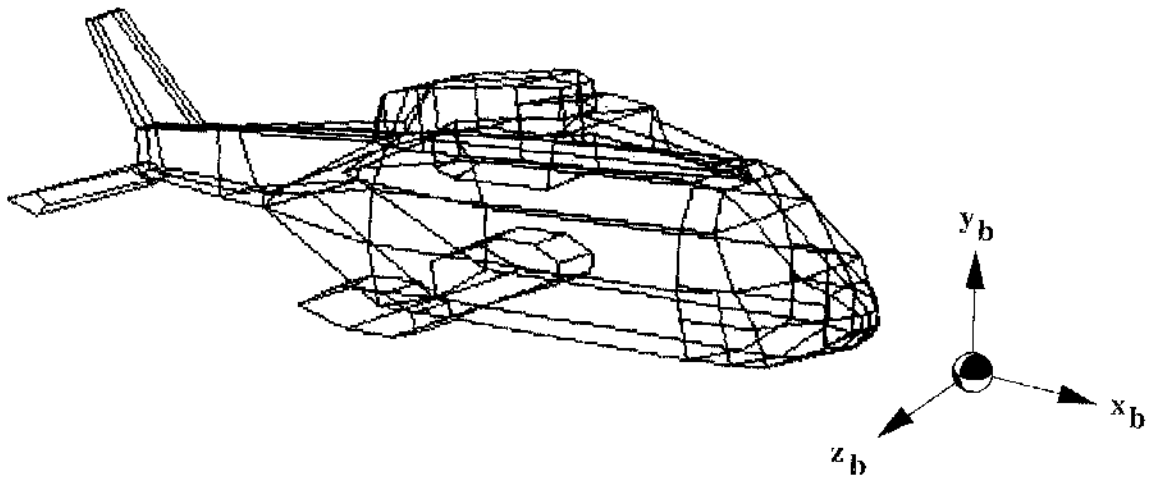

Figure A9.2 : Flat Panel Representation of Complete Helicopter

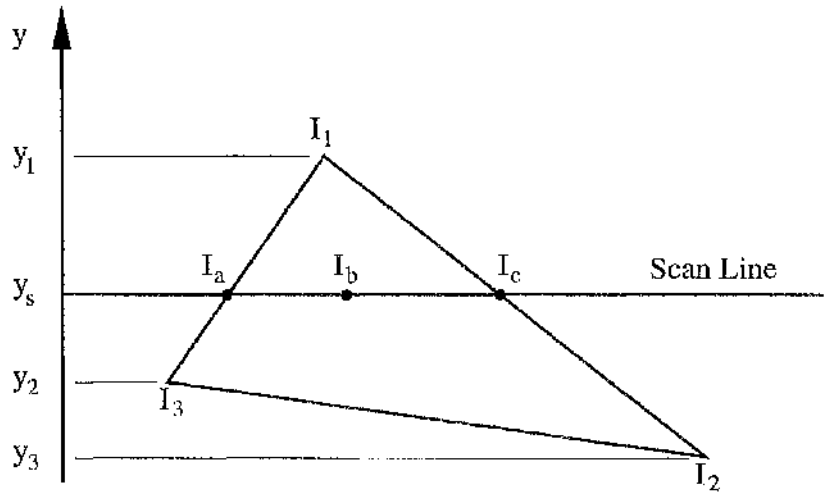

$$I_a = I_1 - (I_1 - I_2)\frac{y_1 - y_s}{y_1 - y_2}$$

$$I_b = I_1 - (I_1 - I_3)\frac{y_1 - y_s}{y_1 - y_3}$$

$$I_p = I_b - (I_b - I_a)\frac{x_b - x_p}{x_b - y_a}$$

Figure A9.3 : Intensity Interpolation Along Polygon Edges And Interior Used In Gouraud Shading (Adapted from Foley, van Dam et. al., 1992)

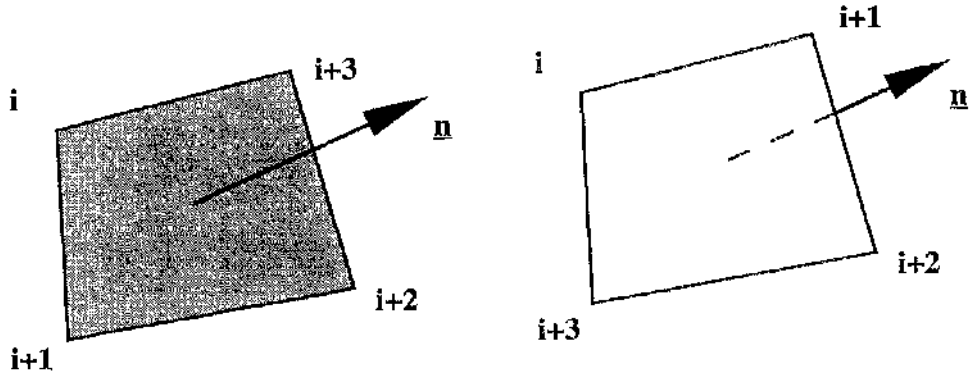

(a) Outward Facing Polygon (b) Rearward Facing Polygon

Figure A9.4 : Polygon Numbering Convention for Back Face Culling

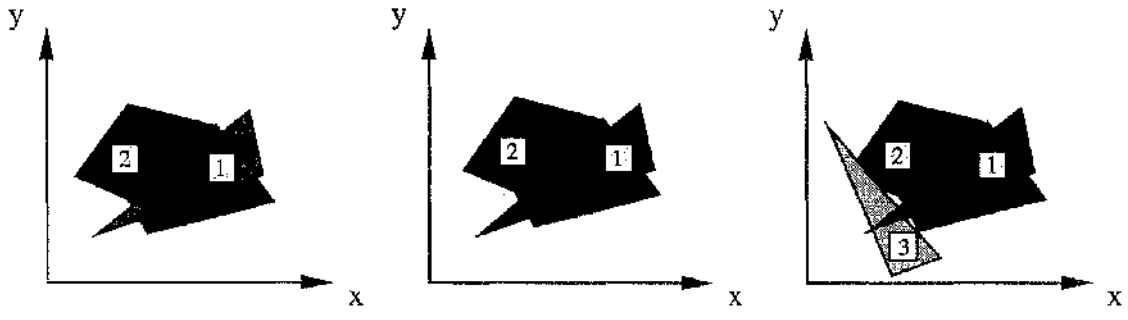

(a) Overlap (b) Penetration (c) Cyclic Sequence

Figure A9.5 : Possible Object Overlap Along Earth z Axis (Adapted from Foley, Van Dam et. al., 1992)

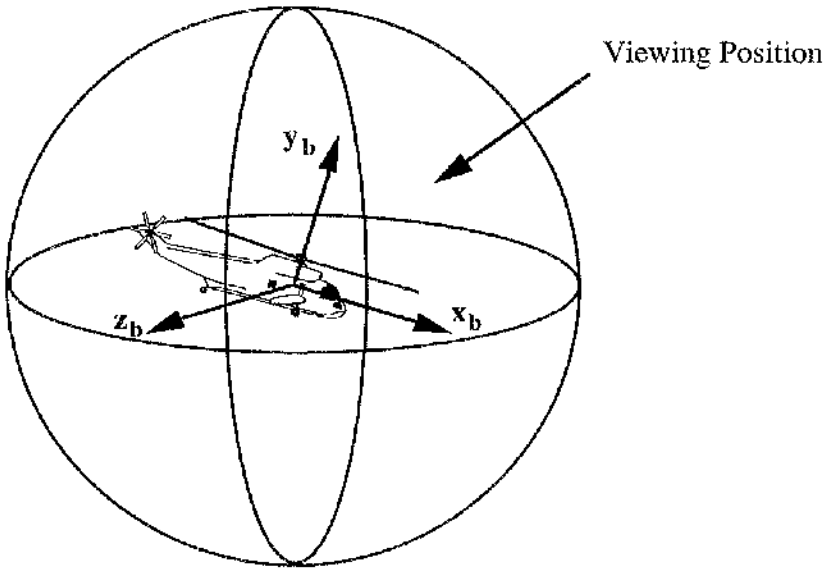

Figure A9.6 : Viewing Attitude Used In Hogs Algorithm